

# **Plant catalases: New insights into targeting and activity**

Yousef Al-Rhoom Al-Hajaya

Submitted in accordance with the requirements for the degree of Doctor of  
Philosophy

The University of Leeds  
Faculty of Biological Sciences  
School of Molecular and Cellular Biology  
April 2021

I confirm that the work submitted is my own and that appropriate credit has been given where reference has been made to the work of others.

## **Acknowledgements**

Foremost, I would like to express my sincere gratitude to my supportive supervisor Professor Alison Baker for taking me through the course of this study every step of the way providing me with the highest standard supervision, valuable guidance, encouragement, and helpful advice throughout my PhD study. Her insightful ideas and encouragement during my PhD study and writing of this thesis turned the dream into reality. My sincere thanks goes to Professor Christine Foyer for her generous advice and very useful feedback.

Special thanks to the University of Leeds for affording me the opportunity to do my PhD study and to be a member of its research activities. Moreover, I would like to offer my special thanks to Dr Chris West for his kindness and help. I am also especially grateful to Professor Changle Ma (Shandong Normal University, China) for kind gifts of CAT2 and CAT3 antibodies. Much thanks goes to all members of the Baker, Foyer and Knox labs for all the emotional support you provided during my presence in the lab. Special gratitude is extended to Dr Elena Zubko for the construction of the CAT2 plasmids and Dr Barbara Karpinska for the generation of transgenic lines.

The research for this thesis would not have been possible without the financial support by a postgraduate studentship from Mu'tah University (Jordan). Last but definitely not the least, I dedicate this thesis to my Mom and Dad who had to live without me for all the time I was studying. I owe them everything I have today.

## Abstract

Reactive oxygen species (ROS) play a key role in both stress responses and developmental pathways in all living organisms. The level of ROS molecules is controlled by different antioxidant enzymes as well as non-enzymatic antioxidants. Peroxisomal catalase is considered as one of the key antioxidant enzymes in the detoxification of hydrogen peroxide (H<sub>2</sub>O<sub>2</sub>), which is generated in peroxisomes as a result of oxidases involved in many processes but especially photorespiration and  $\beta$ -oxidation. In Arabidopsis, catalase exists in three isoforms of which the catalase 2 (CAT2) is the most crucial for photorespiration. The *cat2-1* mutant is a photorespiratory mutant.

Catalase is targeted to peroxisomes by peroxisomal targeting signal type 1 (PTS1) import receptor PEX5, but its carboxy-terminal sequence does not match the normal PTS1 consensus. In Arabidopsis, there is an alternative splicing event that removes the last 18 amino acids of CAT2, and previous studies indicated importance of some amino acids in this region, in particular the last 3 amino acids, for peroxisomal targeting. Transgenic lines in which the *cat2-1* mutant was transformed separately with the wild type CAT2 gene, the alternative splice variant, and a version that has a consensus PTS1 sequence ARL at the C terminus, all under the control of the native CAT2 promoter, were selected. Physiological and biochemical consequences of introducing CAT2 variants with modified C-termini into *cat2-1* mutant background were studied by growing the transgenic lines under short day and long day conditions. The wild type phenotype was largely restored in all of the lines transformed with CAT2 variants, together with catalase activities and redox state. Subcellular fractionation suggests that CAT2 is targeted to the peroxisomes in all cases. To confirm that, the subcellular localisation of CAT2 variants was examined using a self-assembling split superfolder green fluorescent protein (sfGFP<sup>OPT</sup>) system. My results demonstrate that the last 18 amino acids of the CAT2 sequence are required for the targeting of CAT2 to the nucleus but dispensable for peroxisomal targeting, catalase activity and redox homeostasis. These findings provide fundamental new insights into catalase targeting and pave the way for exploration of the mechanism of catalase targeting to the nucleus and its role in non-infected plants.

## Table of Contents

<b>List of Tables</b> .....	<b>i</b>
<b>List of Figures</b> .....	<b>ii</b>
<b>List of Abbreviations</b> .....	<b>vi</b>
<b>Chapter 1 Introduction</b> .....	<b>1</b>
1.1 The eukaryotic cell.....	1
1.2 The peroxisome .....	2
1.3 Peroxisome biogenesis.....	3
1.4 Peroxisome protein import.....	6
1.4.1 Piggyback import.....	12
1.4.2 Peroxisomal targeting signal (PTS3).....	13
1.4.3 The effect of environmental conditions on import into peroxisomes .....	14
1.5 Peroxisome functions .....	14
1.5.1 Metabolic functions .....	16
1.6 Production of reactive oxygen species (ROS) in peroxisomes .....	21
1.6.1 ROS metabolism.....	23
1.7 Glutathione in plants .....	24
1.8 Ascorbate in plants .....	28
1.9 Catalase as antioxidant enzyme .....	30
1.9.1 Catalase history .....	30
1.9.2 Catalase biochemistry.....	31
1.9.3 Classification and structure of catalase.....	34
1.9.3.1 Monofunctional heme-containing catalases.....	34
1.9.4 Catalase genes and isoforms.....	36
1.9.5 Catalase mutants and knockdowns.....	39
1.9.6 Subcellular localisation of catalase .....	42
1.9.7 Catalase import mechanism.....	44
1.9.8 Catalase assembly .....	49
1.10 Autophagy in plants .....	50
1.11 Aims.....	52
<b>Chapter 2 Materials and Methods</b> .....	<b>53</b>
2.1 Materials .....	53
2.1.1 Water .....	53

2.1.2 Reagents.....	53
2.1.3 Restriction and modifying enzymes.....	53
2.1.4 Antibiotics.....	53
2.1.5 Commercial kits.....	53
2.1.6 Basic Medium.....	54
2.1.6.1 Murashige and Skoog medium (MS) .....	54
2.1.6.2 Luria-Bertani medium (LB) .....	54
2.1.6.3 SOC media.....	54
2.1.6.4 Selection media .....	54
2.1.7 Antibodies .....	54
2.1.8 Oligonucleotide primers .....	54
2.1.9 Size markers .....	60
2.1.9.1 DNA size markers.....	60
2.1.9.2 Protein size markers.....	60
2.1.10 <i>Escherichia coli</i> ( <i>E. coli</i> ) strains.....	60
2.2 Methods.....	60
2.2.1 Transgenic lines and CAT2 constructs.....	60
2.2.2 Seed sterilisation.....	62
2.2.3 Plant material and growth conditions .....	62
2.2.3.1 Plant material.....	62
2.2.3.2 Growth conditions and sampling.....	62
2.2.4 Selection on hygromycin .....	63
2.2.5 Photorespiratory test .....	63
2.2.6 Isolation of genomic DNA.....	64
2.2.6.1 Edward's method.....	64
2.2.6.2 DNA extraction kit.....	64
2.2.6.3 Measurement of extracted DNA quality and quantity.....	64
2.2.7 Preparation of plasmid DNA.....	64
2.2.8 Gel purification of DNA fragments.....	65
2.2.9 Polymerase chain reaction (PCR) .....	65
2.2.9.1 Standard PCR .....	65
2.2.9.2 Real-time PCR.....	65
2.2.9.3 Semi-quantitative RT-PCR .....	66
2.2.9.4 Agarose gel electrophoresis .....	66
2.2.9.5 RNA quality .....	66
2.2.10 Protein extraction and measurement .....	67

2.2.10.1 Protein extraction.....	67
2.2.10.2 Preparation of protein samples.....	67
2.2.10.3 SDS-polyacrylamide gel electrophoresis (SDS-PAGE) .....	67
2.2.10.4 Native-PAGE .....	68
2.2.10.5 Staining of the SDS-PAGE gel .....	68
2.2.10.5.1 Coomassie blue staining solution .....	68
2.2.10.5.2 Destain solution.....	68
2.2.10.5.3 Staining method .....	69
2.2.10.6 Western Blotting .....	69
2.2.11 Biochemical assays.....	69
2.2.11.1 Catalase activity assay .....	69
2.2.11.2 Catalase activity using an in-gel activity assay .....	70
2.2.11.3 Ascorbate assay .....	70
2.2.11.3.1 Sample preparation and neutralisation.....	70
2.2.11.3.2 Reagents for ascorbate assay.....	71
2.2.11.3.3 Assay .....	71
2.2.11.4 Glutathione assay.....	71
2.2.11.4.1 Sample preparation and neutralisation.....	71
2.2.11.4.2 Reagents for glutathione assay .....	71
2.2.11.4.3 Assay .....	72
2.2.11.5 Hydroxypyruvate reductase assay.....	72
2.2.11.6 Chlorophyll assay .....	73
2.2.12 Phenotypic analysis .....	73
2.2.12.1 Leaf area .....	73
2.2.12.2 Rosette diameter .....	73
2.2.12.3 Number of leaves and biomass .....	73
2.2.12.4 Primary root length .....	73
2.2.12.5 Seed weight.....	74
2.2.13 Expression of CAT2sfGFP11 plasmids in isolated protoplasts..	74
2.2.13.1 Plant growth conditions .....	74
2.2.13.2 SfGFP11 plasmids preparation.....	74
2.2.13.3 Protoplast isolation .....	74
2.2.13.4 Protoplast transfection assay.....	75
2.2.13.5 Microscopy .....	76
2.2.14 Subcellular localisation.....	77
2.2.14.1 Crude fractionation .....	77

2.2.14.2 Percoll and sucrose density gradient analysis .....	77
2.2.15 Cloning (Construction of vectors) .....	78
2.2.15.1 Generation of CAT2-sfGFP11 constructs .....	78
2.2.15.2 DNA sequencing.....	78
2.2.15.3 DNA ligation reaction.....	79
2.2.15.4 DNA restriction digest.....	79
2.2.15.5 <i>E. coli</i> transformation.....	80
2.2.16 Isolation of RNA from polyribosome pellet .....	80
2.2.17 Statistical analysis.....	81
<b>Chapter 3 Molecular and morphological characterisation of <i>cat2-1</i> mutant and transformants expressing CAT2 C-terminal variants. ....</b>	<b>82</b>
3.1 Background .....	82
3.2 <i>A. thaliana</i> CAT2 transcripts detection using RT-PCR.....	85
3.3 Genomic verification of <i>cat2-1</i> mutant .....	88
3.4 Genomic characterisation of CAT2 derivatives lines.....	90
3.5 No compensatory change in <i>CAT1</i> and <i>CAT3</i> was observed in transgenic lines.....	93
3.6 Using untagged constructs expressed in <i>cat2-1</i> mutant background complement growth phenotype.....	98
3.7 Discussion .....	111
<b>Chapter 4 Restoration of catalase (CAT) activity and redox status by expression of CAT2 variants.....</b>	<b>115</b>
4.1 Background .....	115
4.2 CAT2 expression is restored. No overexpression was observed in <i>CAT3</i> . .....	117
4.3 CAT2 variants are enzymatically active .....	118
4.4 Cell redox state is restored in CAT2 variants.....	124
4.5 Autophagy genes expression ( <i>ATG2</i> and <i>ATG7</i> ).....	130
4.6 Discussion .....	133
<b>Chapter 5 Subcellular localisation of CAT2 variants .....</b>	<b>140</b>
5.1 Background .....	140
5.2 Studying the localisation of CAT2 variants by cell fractionation .....	142
5.2.1 Crude fractionation.....	142
5.2.2 Analysis of CAT2 targeting using percoll and sucrose gradients .....	146
5.2.2.1 Percoll and sucrose gradient analysis .....	148
5.2.3 Location of CAT2 variants using confocal microscopy .....	151

5.2.3.1 Self-assembling split sfGFP <sup>OPT</sup> system to monitor subcellular localisation of CAT2 variants .....	151
5.2.3.2 CAT2 variants localisation using confocal microscopy .....	155
5.2.3.2.1 <i>A. thaliana</i> transgenic lines expressing sfGFP1-10 <sup>OPT</sup> targeted to peroxisomes.....	155
5.2.3.2.2 <i>A. thaliana</i> transgenic lines expressing sfGFP1-10 <sup>OPT</sup> targeted to cytoplasm.....	158
5.2.3.2.3 <i>A. thaliana</i> transgenic lines expressing sfGFP1-10 <sup>OPT</sup> targeted to nucleus.....	160
5.3 Discussion .....	162
<b>Chapter 6 General discussion.....</b>	<b>166</b>
6.1 Summary .....	166
6.2 AtCAT2 lacking the last 18 amino acids produces sufficient activity to maintain growth and cellular redox homeostasis at wildtype levels. ....	170
6.3 AtCAT2 variants are targeted to peroxisomes .....	175
6.3.1 Peroxisomal localisation of AtCAT2 short form. ....	175
6.3.2 Peroxisomal targeting of CAT2ARL. ....	178
6.4 CAT2ARL behaves differently under certain conditions.....	179
6.5 CAT2 variants are assembled within peroxisomes. ....	180
6.6 If not targeting or activity, what is the function of the conserved C terminus? .....	182
6.7 Conclusions .....	183
6.8 Future directions .....	184
<b>References.....</b>	<b>186</b>
<b>Appendix A .....</b>	<b>229</b>
A.1 Selection of T <sub>1</sub> and T <sub>2</sub> generation of PSI, WSQV and ARL on hygromycin plates.....	229
A.1.1 Selection of hygromycin-resistant transformants .....	229
A.1.2 First independent line generation.....	229
A.1.3 Second independent line generation .....	231
A.1.4 Third independent line generation .....	233
A.2 RNA quality .....	237
A.3 Representative image of melting curve for qRT-PCR analysis.....	238
A.4 Semi-quantitative result of 1 <sup>st</sup> independent line.....	239
A.5 Expression level of catalase genes in 2 <sup>nd</sup> independent line using RT-PCR.....	240
<b>Appendix B .....</b>	<b>241</b>

B.1 Morphological characterization of transgenic lines using wild type and <i>cat2-1</i> mutant as a control. ....	241
B.2 Genomic characterisation of transgenic plants.....	244
<b>Appendix C</b> .....	<b>247</b>
C.1 Vector maps.....	247
C.1.1 CAT2variants-sfGFP11 .....	247
C.1.2 Construction of CAT2 variants under the <i>CAT2</i> promoter (by Dr Elena Zubko).....	250

## List of Tables

Table 2.1: Commercial kits used in this work .....	53
Table 2.2: Details of antibodies for western blot analysis.....	55
Table 2.3: List of the primers used in this work. ....	56
Table 2.4: <i>E. coli</i> strains used in this study .....	60
Table 2.5: Transgenic plants and constructs of sfGFP .....	75
Table 2.6: Solutions for protoplast preparation.....	76
Table 2.7 Solutions for RNA isolation from polyribosomal pellet .....	81
Table 3.1: Transgenic lines details.....	90
Table 3.2: The expected product size of the primers.....	91
Table 4.1: Catalase activities. ....	121
Table 5.1: Crude fractionation of plants homogenate.....	143
Table 5.2: Number of protoplasts that show sfGFP signal in different compartments. ....	160
Table 6.1: Plant catalase targeting studies.....	167
Table 6.2: Summary of main findings .....	169

## List of Figures

Figure 1.1: Electron micrograph of <i>A. thaliana</i> peroxisomes. ....	3
Figure 1.2: Models of peroxisomes biogenesis in plants. ....	5
Figure 1.3: A schematic representation of a model for the recognition of PTS1 by PEX5 C-terminal domain. ....	8
Figure 1.4: A schematic model for import of peroxisomal protein in <i>A. thaliana</i> . ....	10
Figure 1.5: PTS1 tripeptides motif in plants. ....	11
Figure 1.6: Diagram demonstrating the piggy-back import of matrix proteins. ....	12
Figure 1.7: Schematic of the fatty acid degradation in <i>A. thaliana</i> . ....	18
Figure 1.8: The prominent role of leaf peroxisomes in photorespiration. ....	20
Figure 1.9: Structure of glutathione. ....	24
Figure 1.10: Glutathione synthesis. ....	25
Figure 1.11: Schematic representation of the ascorbate-glutathione (AsA-GSH) cycle in plants. ....	27
Figure 1.12: The multiple ascorbate biosynthesis pathways. ....	30
Figure 1.13: Classical dismutation reaction of catalase. ....	32
Figure 1.14: The molecular mechanism of the catalase enzyme. ....	33
Figure 1.15: The structure of human catalase. ....	36
Figure 1.16: Location of <i>A. thaliana</i> catalase genes. ....	37
Figure 1.17: Multiple sequence alignment of <i>A. thaliana</i> catalase protein sequences. ....	38
Figure 1.18: A model for translocation of catalase to peroxisomal matrix in plants. ....	44
Figure 1.19: Web-logo image of the C-termini of <i>A. thaliana</i> catalases. ....	47
Figure 1.20: Sequence alignment of <i>A. thaliana</i> CAT2 against number of catalase proteins from different plants. ....	48
Figure 1.21: A proposed model for catalase assembly. ....	49
Figure 2.1: Schematic representation for selecting homozygous transformed plants. ....	61
Figure 3.1: Transcriptional variants of <i>A. thaliana</i> CAT2 ( <i>AtCAT2</i> ). ....	83

Figure 3.2: Schematic diagram of the construction and transformation of <i>CAT2</i> cDNA variants. ....	84
Figure 3.3: A schematic diagram that depicts two splicing variants of <i>AtCAT2</i> gene and primer binding sites. ....	86
Figure 3.4: Detection of <i>A. thaliana</i> catalase 2 gene ( <i>CAT2</i> ) specific transcripts by RT-PCR. ....	87
Figure 3.5: Molecular confirmation of <i>cat2-1</i> mutant. ....	89
Figure 3.6: Molecular characterisation of transgenic lines.....	92
Figure 3.7: Structure and multiple sequence alignment of <i>A. thaliana</i> catalase genes. ....	94
Figure 3.8: A representative image of semi-quantitative RT- PCR of catalase genes. ....	95
Figure 3.9: Transcript abundance of catalase genes of <i>A. thaliana</i> wild type, <i>cat2-1</i> mutant, PSI3, WSQV3 and ARL2.....	97
Figure 3.10: Representative pictures of the rosette appearance of wild type, <i>cat2-1</i> and transgenic lines. ....	99
Figure 3.11: Total number of leaves was counted once a week for plants grown under short-day conditions for four weeks.....	100
Figure 3.12: Rosette diameter (longest diameter) of wild type, <i>cat2-1</i> and transgenic lines grown under short-day conditions for four weeks. ....	102
Figure 3.13: Rosette weight of wild type, <i>cat2-1</i> and transgenic lines grown under short-day conditions for four weeks.....	103
Figure 3.14: Whole plant phenotypes of wild type, <i>cat2-1</i> mutant and transgenic plants. ....	104
Figure 3.15: Rosette diameter (longest diameter) of wild type, <i>cat2-1</i> and transgenic lines. ....	105
Figure 3.16: Rosette weight of wild type, <i>cat2-1</i> and transgenic lines.....	106
Figure 3.17: Number of leaves under long-day-conditions.....	107
Figure 3.18: Average seed weight (expressed as milligrams of weight/ 1000 seeds). ....	108
Figure 3.19: Primary root length (cm) in wild type, <i>cat2-1</i> , PSI, WSQV and ARL plants ten days after germination. ....	109
Figure 3.20: Phenotypical analysis of transgenic lines under photorespiratory conditions. ....	110

Figure 3.21: Comparison of chlorophyll content (Chlorophyll a and b; $\mu\text{g}$ per g fresh weight) of 28-day seedlings of <i>cat2-1</i> mutant and transgenic lines to the wild type. ....	110
Figure 4.1: Immunoblotting analysis of wild type, <i>cat2-1</i> mutant and transgenic lines using antibodies against CAT2 and CAT3.....	117
Figure 4.2: CAT2 with C-terminal truncations is enzymatically active. ....	119
Figure 4.3: Characterisation of catalase isoforms by western blot analysis. ....	123
Figure 4.4: A comparison of rosette ascorbate contents in wild type, <i>cat2-1</i> mutant, PSI, WSQV, and ARL grown under short and long-day conditions. ....	125
Figure 4.5: A comparison of rosette glutathione contents ( $\mu\text{mol g}^{-1}$ FW) in wild type, <i>cat2-1</i> mutant and transgenic lines grown under short and long-day conditions. ....	127
Figure 4.6: RT-qPCR analysis of $\text{H}_2\text{O}_2$ -markers transcripts. ....	129
Figure 4.7: Relative expression levels of autophagy genes ( <i>ATG2</i> and <i>ATG7</i> ).....	131
Figure 5.1: Diagram of self-folding split sfGFP complementation.....	141
Figure 5.2: Diagrammatic representation of the crude fractionation of <i>A. thaliana</i> leaves homogenate. ....	142
Figure 5.3: CAT2 variants are present in the organelle pellet (P2).....	145
Figure 5.4: Diagram illustrating the isolation of leaf peroxisomes from <i>A. thaliana</i> leaves by percoll and sucrose density gradient centrifugation. ....	147
Figure 5.5: Isolation of peroxisomes from wild type, <i>cat2-1</i> mutant, PSI2, WSQV2 and ARL1 leaves on a discontinuous percoll gradient.....	148
Figure 5.6: Subcellular fractionation of mature <i>A. thaliana</i> leaves of wild type, <i>cat2-1</i> mutant, PSI2, WSQV2 and ARL1.....	149
Figure 5.7: Western blot of peak peroxisomal fractions.....	150
Figure 5.8: Construction of CAT2 variants-sfGFP11. ....	152
Figure 5.9: PCR amplification of CAT2 variants to be inserted into PEP109E plasmid.....	153
Figure 5.10: Validation of CAT2 variants ligation into the PEP109E plasmid. ....	154

Figure 5.11: Expression of CAT2-PSI-sfGFP11 and CAT2-WSQV-sfGFP11 in protoplasts with peroxisome targeted sfGFP1-10 leads to peroxisomal GFP fluorescence.....	156
Figure 5.12: CAT2ARL tagged with sfGFP11 is detectable in <i>A. thaliana</i> transgenic plants expressing sfGFP1-10 <sup>OPT</sup> targeted to peroxisomes. ....	157
Figure 5.13: CAT2 variants are not assembled in the cytoplasm. ....	159
Figure 5.14: Nuclear localisation of CAT2-PSI-sfGFP11.....	161
Figure 6.1: Three-dimensional structure of <i>A. thaliana</i> CAT2 (AtCAT2)....	177
Figure 6.2: Proposed model of two targeting pathways.....	182

## List of Abbreviations

AA	Amino acids
AAA	ATPases Associated with diverse cellular Activities
A <sub>230</sub> /A <sub>280</sub>	Absorbance (at 230nm/280nm)
ABA	Abscisic acid
ACX	Acyl-CoA oxidase
APS	Ammonium persulfate
APX	Ascorbate peroxidase
ASC	Ascorbate
ASC-GSH	Ascorbate-glutathione
ATG	Autophagy
ATP	Adenosine 5' triphosphate
BSA	Bovine serum albumin
bp	Base pair
CAT	Catalase
CFP	Cyan fluorescent protein
CFU	Colony forming units
CoA	Coenzyme A
CO <sub>2</sub>	Carbon dioxide
CTS	COMATOSE
C-terminal	Carboxyl-terminal
C°	Degrees Celsius
DHAR	Dehydroascorbate reductase
DMSO	Dimethyl sulfoxide
DNA	Deoxyribonucleic acid
DTNB	5,5'-dithiobis-2-nitrobenzoic acid
DTT	Dithiothreitol
<i>E. coli</i>	<i>Escherichia coli</i>
ECL	Enhanced chemiluminescence
EDTA	Ethylenediaminetetraacetic acid
ER	Endoplasmic reticulum
FACs	Fatty acyl-CoA synthetases
FAs	Fatty acids

GR	Glutathione reductase
<i>g</i>	Relative centrifugal force
GFP	Green fluorescent protein
GSH	Reduced glutathione
GSSG	Glutathione disulphide
H <sub>2</sub> O <sub>2</sub>	Hydrogen peroxide
hr	Hour
HO <sup>•</sup>	Hydroxyl radical
IAA	Indole acetic acid
IBA	Indole -3-butyric acid
JA	Jasmonic acid
kb	Kilobase
kDa	kilodalton
l	Litre
LB	Luria-Bertani
LDH	Lactate dehydrogenase
M	Molar (moles/dm <sup>3</sup> )
MDHAR	Monodehydroascorbate reductase
MDH	Malate dehydrogenase
mg	Milligram
min	Minute
ml	millilitre
mM	millimolar (millimoles/dm <sup>3</sup> )
MW	Molecular weight
MS	Murashige and Skoog
N-terminal	Amino-terminal
NaCl	Sodium chloride
NADPH	Nicotinamide adenine dinucleotide phosphate
ng	nanograms
nm	nanometre
nmol	nanomoles
OD <sub>600</sub>	Optical density at 600 nm
O <sub>2</sub>	Oxygen
O <sub>2</sub> <sup>-</sup>	Superoxide

PBS	Phosphate Buffered Saline
PCR	Polymerase chain reaction
PEG	Polyethylene glycol
pER	Peroxisomal endoplasmic reticulum
PM	Plasma membrane
pMDH	Peroxisomal malate dehydrogenase
PMP	Peroxisome membrane protein
PTS	Peroxisomal targeting signal
PTS1	Peroxisomal targeting signal type 1
PTS2	Peroxisomal targeting signal type 2
PTS3	Peroxisomal targeting signal type 3
PEX	Peroxin
qRTPCR	Quantitative reverse transcription PCR
R	Resistance
RNA	Ribonucleic acid
ROS	Reactive oxygen species
Rubisco	Ribulose-1,5-bisphosphate carboxylase/oxygenase
r.p.m	Revolutions per minute
S	Sensitive
SA	Salicylic acid
sec	Second
SDS	Sodium dodecyl sulfate
SDS-PAGE	Sodium dodecyl sulfate polyacrylamide gel Electrophoresis
<i>S. cerevisiae</i>	<i>Saccharomyces cerevisiae</i>
TAE	Tris-acetate-EDTA
TAGs	Triacyl-glycerides
TE	Tris-EDTA
TEMED	N, N, N-Tetramethylethlenediamine
T-DNA	Transferred deoxyribonucleic acid
UV	Ultra-violet
V	volts
v/v	volume/volume
VPD	2-vinylpyridine

w/w	Weight/weight
w/v	Weight/volume
WT	Wild type
μg	Microgram
μl	Microlitre
μM	Micromolar (micromoles/dm <sup>3</sup> )
α	Alpha
γ-ECS	γ-glutamyl cysteine synthetase
Δ	Delta

## Chapter 1 Introduction

### 1.1 The eukaryotic cell

Eukaryotic cells contain various membrane-bound compartments or organelles. For example, the organelles found in plant cells include chloroplast, vacuoles, mitochondria, nuclei and peroxisomes. These organelles can be distinguished based on their morphological structures, and each hosts a specific set of metabolic activities. Compartmentalisation allows cells to separate, regulate and optimise various metabolic pathways and functions. Although compartmentalisation offers many advantages to the cell, there are also challenges posed by the bounding membranes, which form a barrier. Proteins and other molecules must cross these bounding membranes requiring specific protein targeting signals that direct molecules from their synthesis sites to specific locations. The targeting signals must be both specific and efficient. For instance, peroxisomes, which are present in a range of eukaryotic cells, have no DNA or protein synthesis apparatus. Thus, they import all their proteins from the cytosol via different mechanisms.

Recent studies using various approaches, including proteomics, *in vivo* imaging tools and bioinformatics, shed some light on protein targeting processes. Our understanding of protein import mechanisms is thus gradually increasing, particularly as new mechanisms are discovered. The research presented in this thesis is based on the investigation of the role of amino acid sequences that are suggested to be responsible for the import of catalase, a peroxisomal protein. The findings reported in this thesis provide new insights into the mechanisms of catalase targeting.

## 1.2 The peroxisome

Peroxisomes (also known as microbodies) were first observed in mouse kidney cells using electron microscopy (Rhodin, 1954). They were first isolated from rat liver and characterised by the presence of hydrogen peroxide ( $H_2O_2$ )-producing oxidases and catalase, which degrades  $H_2O_2$  to water and oxygen. Therefore, these organelles were then renamed peroxisomes (De Duve and Baudhuin, 1966). In addition to the  $H_2O_2$  metabolism, the pathway of fatty acid  $\beta$ -oxidation and the glyoxylate cycle were localised in plant peroxisomes (Breidenbach and Beevers, 1967; Cooper and Beevers, 1969; Hutton and Stumpf, 1969). Subsequent studies revealed that peroxisomes are present in all of the major groups of eukaryotes that have been studied (Cavalier-Smith, 1987). In contrast, there is no evidence for the presence of peroxisomes in some species of parasitic eukaryotes such as *Giardia*, *Trichomonas* and *Entamoeba* (Opperdoes et al., 1984; Ding et al., 2000; Hawkins et al., 2007; Žárský and Tachezy, 2015; Jansen et al., 2020).

Peroxisomes are bound by a single membrane. They are usually spherical to elliptical in shape and filled with a granular matrix (Figure 1.1). They are generally small in size, with a diameter of 0.2-1.0  $\mu\text{m}$ . Peroxisomes often contain a dense inner core and they typically have a higher density (1.21-1.25  $\text{gm/cm}^3$ ) than mitochondria (1.18  $\text{gm/cm}^3$ ) (Cavalier-Smith, 1987; Holroyd and Erdmann, 2001; Sparkes et al., 2005; Smith and Aitchison, 2013; Reumann and Lisik, 2017).

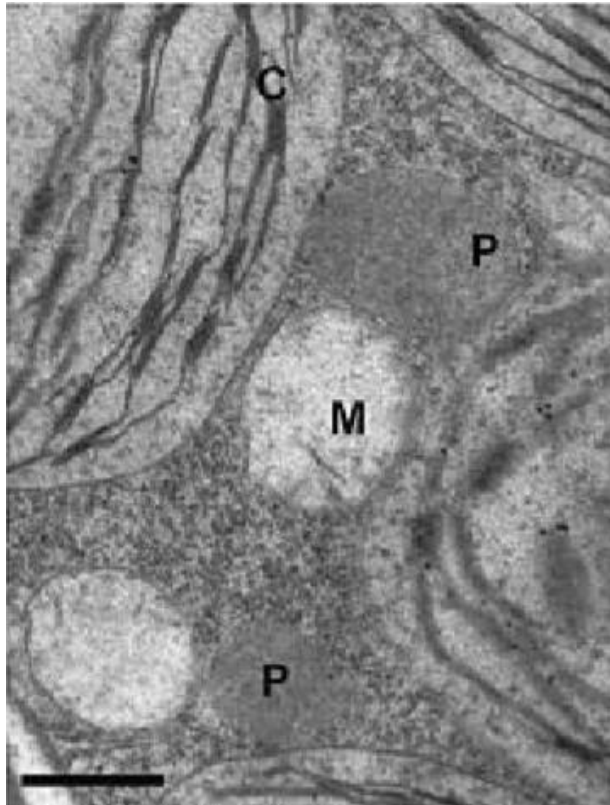


**Figure 1.1: Electron micrograph of *A. thaliana* peroxisomes.**

Transverse electron micrograph section of *A. thaliana* cotyledons (5 days old). The figure also shows the close association between peroxisomes (P), mitochondria (M) and chloroplasts (C), which play a crucial role in ensuring an efficient flow of metabolites between organelles during various metabolic pathways such as photorespiration. Scale bar 500 nm. Image is taken from (Footitt et al., 2002) and reproduced with EMBO permission.

### 1.3 Peroxisome biogenesis

Peroxisome biogenesis encompasses several processes, including peroxisome membrane biosynthesis and assembly, import of proteins into the peroxisomal matrix, proliferation and/ or division (Eckert and Erdmann, 2003; Kaur et al., 2009). The proteins required for peroxisome biogenesis known as “peroxins or *PEX* proteins” (also known as peroxisomal biogenesis factors), are encoded by *PEX* genes [reviewed in (Brown and Baker, 2003; Fujiki et al., 2014; Fujiki et al., 2020)]. To date, 37 *PEX* proteins have been identified (although not all are present in all organisms) and they (all) have been found to have critical roles in the generation of functional peroxisomes (Jansen et al., 2020).

Currently, the nomenclature of PEX proteins causes many issues and inconsistencies when discussing cross-species differences and similarities. For instance, the nomenclature of yeast protein is PexNp, while in plants and mammals is PEXN. To avoid any confusion, plant nomenclature is used in this thesis.

Several models have proposed for the biogenesis of peroxisomes and their relationships to the endoplasmic reticulum (ER). Initially, the “ER-Vesiculation” model was proposed to describe the process of peroxisome biogenesis, as shown in Figure 1.2A (Beevers, 1979; Titorenko and Mullen, 2006; Hu et al., 2012). This model is based on the generation of peroxisomes from specialized and smooth ER regions by vesiculation and budding off after incorporation of nascent soluble peroxisomal proteins and membrane lipids (Hu et al., 2012). In contrast, the “autonomous peroxisome growth and division” model suggests that both the matrix and membrane proteins are sequestered via post-translational mechanisms inside pre-existing peroxisomes, as illustrated in Figure 1.2B (Lazarow and Fujiki, 1985; Lazarow, 2003; Hu et al., 2012). This model proposes that upon import of the proteins, pre-existing peroxisomes grow in size and divide by fission into daughter peroxisomes (Hu et al., 2012). Both of these models have drawbacks. Subsequent studies in the 1990s led to the suggestion of a third model, i.e. the “ER semi-autonomous peroxisome”, which is now widely accepted (Figure 1.2C). In this model, peroxisomes are semi-autonomous and they can be generated by two different routes: de novo biogenesis from ER (ER-derived pre-peroxisomes) and from pre-existing peroxisomes by growth and fission (Mullen and Trelease, 2006; Hu et al., 2012).

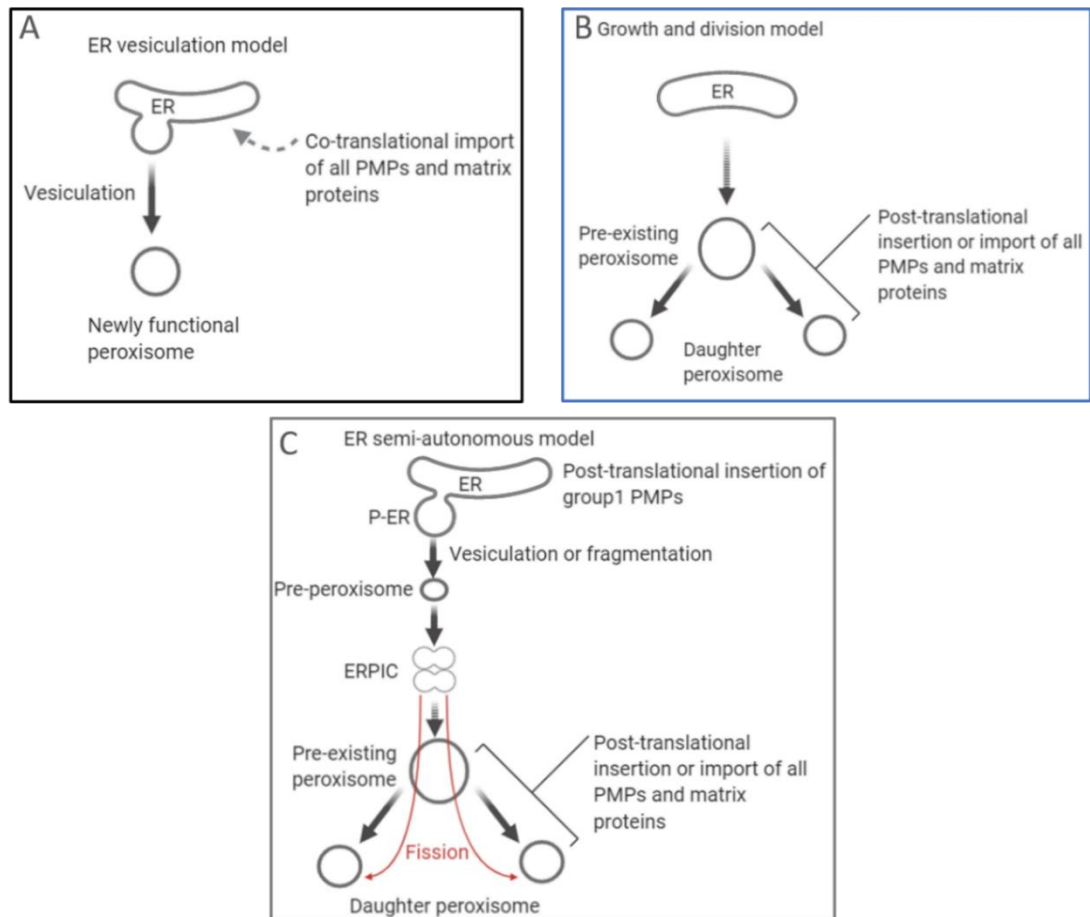


**Figure 1.2: Models of peroxisomes biogenesis in plants.**

In the ER vesiculation model (A), all of the soluble and membrane bound protein constituents of the peroxisome are considered to be synthesized co-translationally on the endoplasmic reticulum (ER) and then sequestered into an expanding vesicle that eventually buds off from the ER to yield nascent, functional peroxisome (Beevers, 1979; Titorenko and Mullen, 2006; Hu et al., 2012). Growth and division model demonstrate that all peroxisome membrane proteins (PMPs) and matrix proteins are synthesized on free polyribosomes in the cytosol and post translationally inserted and transported to pre-existing peroxisomes. It must be noted that the ER in this model serves as the source of membrane lipids that are necessary for peroxisome growth (Lazarow and Fujiki, 1985; Lazarow, 2003; Hu et al., 2012). The current working model for peroxisome biogenesis is the ER semiautonomous model (C). In this model, group I PMPs are inserted post-translationally either directly into a distinct portion of the ER called the peroxisomal ER (pER) subdomain or first to the general reticuloplasm-in-containing ER and then to the pER. Group II PMPs and all matrix proteins are sorted post translationally to pre-existing peroxisomes and (daughter) peroxisomes, and possibly pre-peroxisomes at the ER-intermediate compartment (ERPIC) (Mullen and Trelease, 2006; Hu et al., 2012). Figure was created with BioRender.com.

## 1.4 Peroxisome protein import

Unlike chloroplasts and mitochondria, peroxisomes lack DNA and ribosomes. Consequently, peroxisomal proteins that are encoded by nuclear genes and synthesized on free cytosolic ribosomes are imported into peroxisomes by unique targeting signals, which direct them to their final destination (Lazarow and Fujiki, 1985; Kragler et al., 1993). The proteome of peroxisomes can be divided into matrix proteins, cytosolic receptor proteins and peroxisomal membrane proteins (PMPs) (Hu et al., 2012; Cross et al., 2016; Pan et al., 2020).

To date, two classes of PMPs have been identified (I and II) based on their import pathways. Class I PMPs are directly inserted post-translationally into the peroxisomal membrane after synthesis in the cytosol. This process involves three well conserved peroxins: PEX3, PEX19 and PEX16. PEX19 (PEX19A and PEX19B in *A. thaliana*) is a cytoplasmic chaperone for the Class I PMPs, whereas PEX3 (PEX3A and PEX3B in *A. thaliana*) is required for PEX19 docking at peroxisomes, acting as the membrane anchor for PEX19 and PEX16 (Jones et al., 2004; Fang et al., 2004; Platta and Erdmann, 2007; Hu et al., 2012; Baune et al., 2020). In contrast, Class II PMPs are indirectly targeted to peroxisomes after first being inserted into the ER (Jones et al., 2004; Hu et al., 2012; Reumann and Bartel, 2016; Kao et al., 2018).

Peroxisomal matrix proteins are synthesised on free polyribosomes in the cytosol and targeted directly to the organelle (Goldman and Blobel, 1978; Lazarow and Fujiki, 1985; Baker, 1996; Hua et al., 2015; Walter and Erdmann, 2019). Two distinct targeting pathways have been identified for matrix proteins. Two types of targeting signals have been described at the C-terminus or the N-terminus of the imported protein (Girzalsky et al., 2010; Hu et al., 2012; Smith and Aitchison, 2013; Kim and Hettema, 2015; Walter and Erdmann, 2019; Bürgi et al., 2021). The C-terminal peroxisomal targeting signal is known as PTS1. It consists of tripeptide sequences such as SKL (Ser-Lys-Leu) or related sequences.

Site-directed mutagenesis has been used to generate variants to the SKL tripeptide signal at the carboxy-terminal end. Collectively, such studies have shown that the conserved consensus sequence -(S/A/C)-(K/R/H)-(L/M) is responsible for the import of the majority of peroxisomal matrix proteins (Gould et al., 1989; Hayashi et al., 1997; Lametschwandtner et al., 1998). Our current understanding of this sequence's role has subsequently been expanded by proteomic studies, *in vitro* binding studies and *in silico* analysis (Skoulding et al., 2015; Nötzel et al., 2016).

In contrast to PTS1, the N-terminal peroxisomal targeting signal, which is known as PTS2, is less abundant and found only in a small number of matrix proteins. Unlike PTS1, PTS2 is a nonapeptide and commonly consists of conserved nine amino acids with the consensus sequence [R (L/V/I/Q) XX (L/V/I/H) (L/S/G/A) X (H/Q) (L/A/F)] [reviewed in (Brown and Baker, 2008; Hu et al., 2012; Cross et al., 2016; Pan et al., 2020)]. In some PTS2 proteins, this sequence is cleaved after import into peroxisomes at a conserved cysteine cleavage site in plants and mammals. The plant peroxisomal deg-protease (DEG15) (Helm et al., 2007; Schuhmann et al., 2008) and mammalian trypsin domain containing 1 (Tysnd1) (Kurochkin et al., 2007) are responsible for the removal of the PTS2-containing leader peptide.

The molecular mechanisms involved in recognising and importing the peroxisomal proteins carrying the PTS1 signal at the C-terminus have been intensively studied (Gould et al., 1989; Mullen et al., 1997; Brocard and Hartig, 2006). The targeting process is initiated by the recognition of the PTS1 sequence of the candidate protein by the cytosolic receptor protein called PEX5 (Nito et al., 2002; Williams et al., 2007). All PEX5 orthologs are composed of at least two conserved domains: the PTS1 binding domain located at the C-terminus and the PEX14 binding domain located at the N-terminus (Hu et al., 2012). This short form of PEX5 is known as PEX5S (Dodt et al., 2001). A longer variant of PEX5 (PEX5L) has been identified in human, animals, and plants. This variant was found to have a third domain within the N-terminus that contains a binding site for PEX7 (Dodt et al., 2001). *A. thaliana* has the long variant of PEX5, whereas some plants such as rice contain both PEX5S and PEX5L as splice variants (Lee et al., 2006).

In yeast, second PTS1 receptor has also been characterized and designated PEX9 (Effelsberg et al., 2016; Bürgi et al., 2021). This receptor shares the same C-terminal domain organization with PEX5 and is induced by oleate (see Section 1.4.3).

Studies on PEX5 homologs have revealed that the PTS1-binding domain is composed of seven tetratricopeptide repeats (TPRs). In contrast, the N terminal domain contains several diaromatic WxxxF/Y motifs, which form the binding sites for PEX14, which is the docking factor on the peroxisome membrane (Hu et al., 2012). The molecular basis of PTS1 sequence recognition by PEX5 TPR repeats depends on the arrangement of these seven repeats into two clusters of three units each (TPR1-3 and TPR5-7), with TPR4 forming a hinge region that interconnects the two clusters, creating a groove (Gatto et al., 2002; Stanley et al., 2007; Fodor et al., 2012; Reumann et al., 2016) as illustrated in Figure 1.3. In the presence of the canonical PTS1 sequence, the PEX5 C-terminal end changes from a loose and cargo-free structure to a tightly closed and ring-like conformation (Fodor et al., 2015).

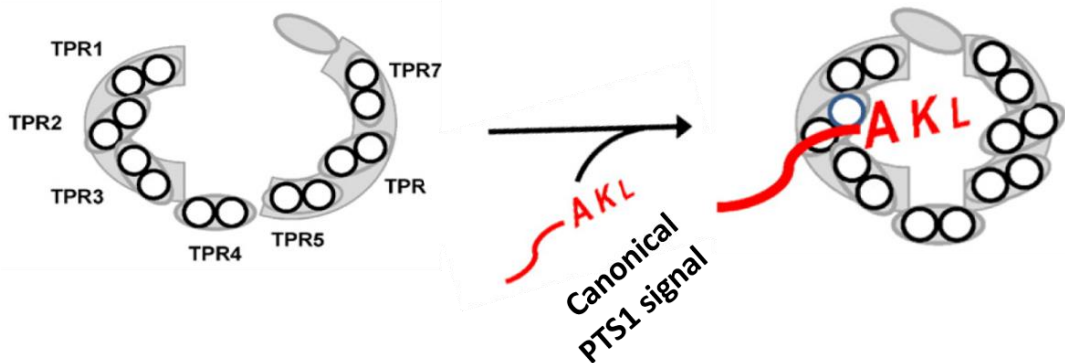


**Figure 1.3: A schematic representation of a model for the recognition of PTS1 by PEX5 C-terminal domain.**

Upon binding of canonical signal like AKL to the formed groove by the arranged clusters of TPRs, this region of PEX5 changes its conformation from cargo-free form to the tightly closed conformation. Figure is adapted from (Reumann et al., 2016).

In general, the import of matrix proteins into peroxisomes is a four-step process, which starts with (1) the recognition of PTS1 by the PEX5 receptor, forming a cargo-receptor complex. This is followed by (2) docking on the peroxisomal membrane and forming a pore through which (3) the cargo passes and is released into the matrix. The receptor itself is then recycled in the cytosol, as illustrated in Figure 1.4 (Kim and Hettema, 2015; Pan et al., 2020). However, the precise molecular mechanism of membrane docking and cargo translocation remains elusive.

The cargo-loaded complex binds a docking complex, which consists of PEX14 and PEX13 (and additionally PEX17 in yeast) (Agne et al., 2003; Brown and Baker, 2008). Binding leads to the formation of a transient and dynamic pore through which the translocation process occurs. Thereafter, the protein is released into the matrix (Meinecke et al., 2010). Later, the receptor is recycled in the cytosol via a ubiquitin-dependent process (Platta et al., 2014; Apanasets et al., 2014). This involves a monoubiquitylation event that is initiated by the ubiquitin-conjugating enzyme PEX4, which is anchored in the peroxisomal membrane via the integral peroxin called PEX22 (Koller, Antonius et al., 1999; Zolman et al., 2005; Rayapuram and Subramani, 2006; Williams et al., 2012b). PEX4 recognizes a conserved cysteine in PEX5 and adds the ubiquitin label by forming a thioester bond (Williams et al., 2007). It must be noted that PEX4 is found in plants, yeast and fungi, whereas mammals use a cytosolic ubiquitin-conjugating enzyme ( $E_2/D1/2/3$ ) [reviewed in (Francisco et al., 2014; Francisco et al., 2017)].

This monoubiquitylation process requires the presence of a conserved RING (Really Interesting New Gene) complex, consisting of the PEX2, PEX10 and PEX12 peroxins, which all have ubiquitin ligase activity (Rayapuram and Subramani, 2006; Williams et al., 2008; Platta et al., 2009; El Magraoui et al., 2012). Finally, the monoubiquitinated receptor is recognized by a heterohexameric complex that acts as a dislocase, which extracts the receptor from the peroxisomal membrane and liberates it into the cytosol in an ATP-dependent manner (Platta et al., 2014). The heterohexameric complex is attached to the membrane protein called PEX15 in yeast (PEX26 human and AEPM9 *A. thaliana*).

It is composed of the AAA (ATPases Associated with diverse cellular Activities) ATPase peroxins PEX1 and PEX6 (Platta et al., 2005; Saffian et al., 2012).

In general, the AAA family assemble into a ring-shaped structure with a central pore. The PEX5 receptor must be deubiquitinated before it can participate in the next import cycle (Platta et al., 2014). The deubiquitination process can be performed by glutathione as well as the deubiquitinating enzymes (Grou et al., 2015). In addition to the RING-finger peroxins, peroxisomal protein import in *A. thaliana* is also modulated by two homologous E3 ubiquitin ligases- SP1 (suppressor of plastid protein import locus 1) and its homolog SPL1 (Figure 1.4). SP1 promotes the degradation of PEX13 and possibly also PEX14 (Pan and Hu, 2017).

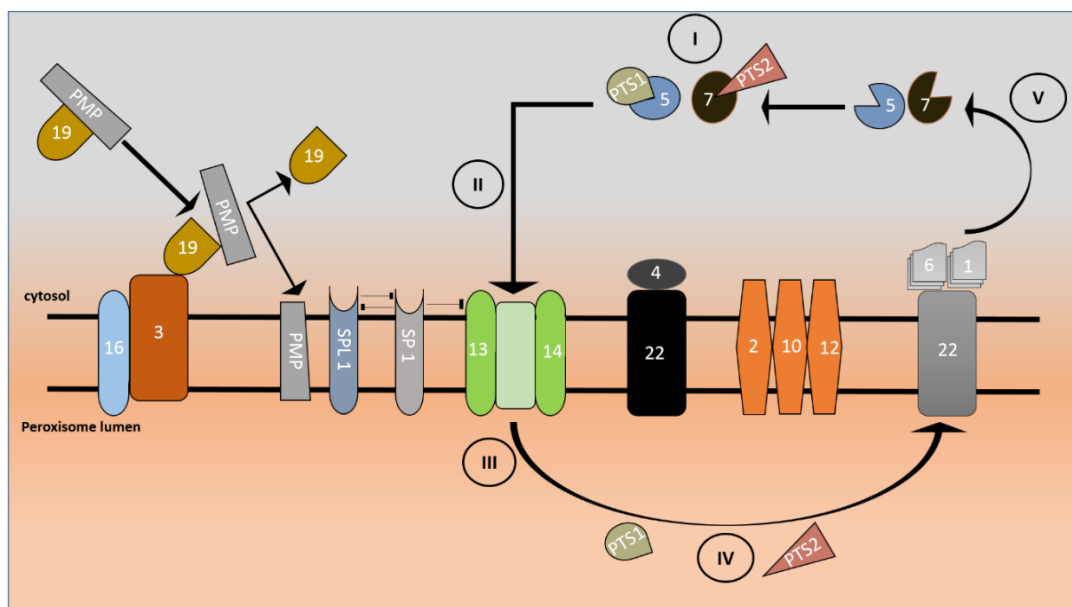


**Figure 1.4: A schematic model for import of peroxisomal protein in *A. thaliana*.**

The import of peroxisomal membrane proteins involves three peroxins: PEX19, PEX3 and PEX16. PEX19 is a chaperone for PMPs, PEX3 is the membrane anchor for PEX19, and PEX16 is involved in the PEX3 recruiting to the endoplasmic reticulum (ER) before the formation of pre-peroxisomes. SP1-suppressor of plastid protein import locus1 and its homologous SPL1 promote matrix protein import. Newly synthesized peroxisomal matrix proteins containing peroxisomal targeting signals PTS1 and PTS2 are recognized in the cytosol by the receptors PEX5 and PEX7, respectively. A protein bearing PTS1 signal is recognized by PEX5 receptor forming a complex (I) which docks the peroxisomal membrane (II) and creates a pore (III) through which the protein is released into the peroxisomal lumen (IV), and the PEX5 receptor is recycled to cytosol again after ubiquitination and subsequent deubiquitinating process (V).

The majority of peroxisomal matrix proteins are sorted via the PTS1 pathway. The PTS1 signal is divided into canonical and non-canonical sequences (Reumann et al., 2016). A typical PTS1 sequence carries the consensus [small, basic, hydrophobic] regions at positions 3, 2 and 1, respectively, considering that position 1 is the last amino acid at the carboxy end (Gatto et al., 2002). Generally, the non-canonical PTS1 sequence can be defined as the replacement of one amino acid, located in the C-terminal tripeptide consensus region with a non-canonical amino acid (Figure 1.5) (Reumann et al., 2016).

Compared to the canonical PTS1 sequence, which confers a stronger binding affinity to the tunnel-shaped pocket of the PEX5 receptor, the non-canonical PTS1 sequence is a weaker signal. To be functional, the non-canonical PTS1 sequence requires the presence of upstream auxiliary residues to enhance the process of targeting (Lingner et al., 2011).

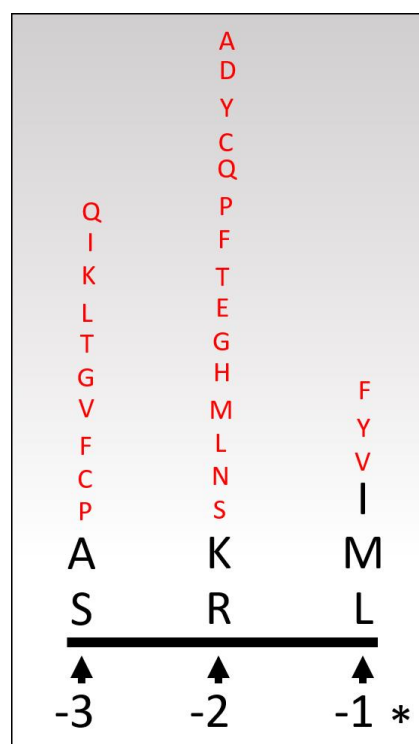


**Figure 1.5: PTS1 tripeptides motif in plants.**

The black letters refer to the canonical residues of the C-terminal consensus whereas, the red letters indicate the possible non-canonical residues which can replace the canonical ones at the corresponding positions. For example, QRL is a non-canonical PTS1 with the amino acid at position three is being replaced with Q instead of S or A residues. (\*) indicates the C terminal end of the protein. Numbers represent the order of the amino acids.

### 1.4.1 Piggyback import

Some matrix proteins that lack an obvious PTS1 or PTS2 sequence can be imported into peroxisomes by piggyback or hitch-hiking onto other systems (Glover et al., 1994; McNew and Goodman, 1994; Lee et al., 1997; Jung et al., 2010; Schueren et al., 2014; Thoms, 2015; Gabay-Maskit et al., 2020). In piggyback import, non-PTS proteins use the PTS proteins as a shuttle factor for import into peroxisomes, as shown in Figure 1.6. The piggyback mechanism was first observed in *Saccharomyces cerevisiae*, where the truncated 3-ketoacyl-CoA thiolase (Thiolase  $\Delta$ PTS2) that was without an important part for the peroxisomal targeting region was shown to be imported into peroxisomes by dimerization with the full-length thiolase subunits (Glover et al., 1994). This type of import has been reported for various proteins, including chloramphenicol acetyltransferase (ChAT) (McNew and Goodman, 1994) and isocitrate lyases (IL) (Lee et al., 1997).

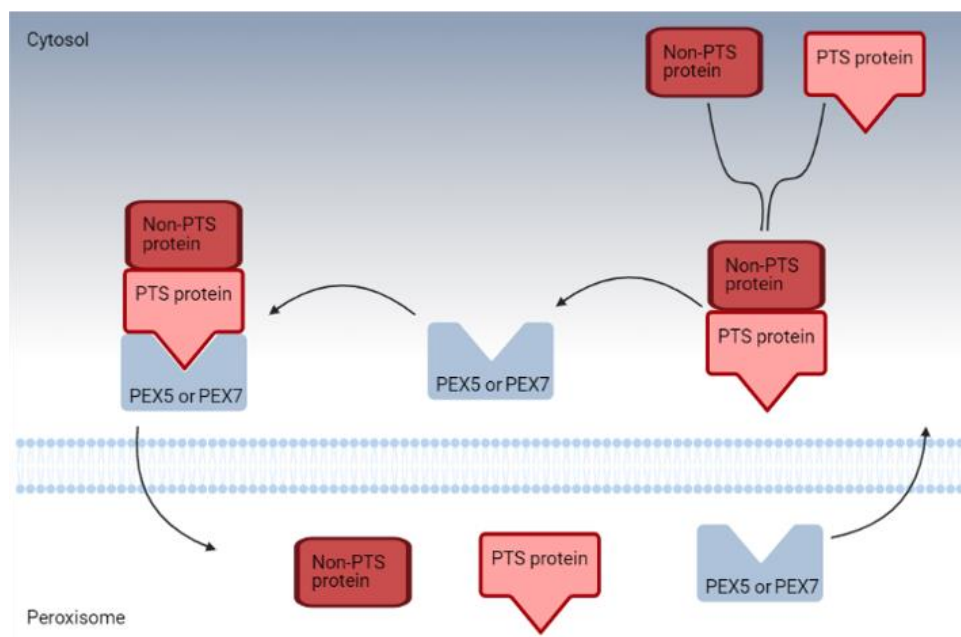


**Figure 1.6: Diagram demonstrating the piggy-back import of matrix proteins.**

Some matrix proteins lacking an obvious peroxisomal targeting signal type 1 or 2 can be imported by piggybacking or hitchhiking on other proteins bearing peroxisomal targeting signals. PTS-protein; peroxisomal protein with a targeting signal, non-PTS protein; peroxisomal protein without a targeting signal, PEX5 or PEX7; PTS-receptors.

In *A. thaliana*, protein phosphatase 2A (PP2A) C and A subunits were shown to be imported into peroxisomes by piggybacking with the B $\theta$  subunit (Kataya et al., 2015). *Saccharomyces cerevisiae* enoyl-CoA isomerase is imported together with the PTS1 enzyme dienoyl-CoA isomerase (Dci1p)(Yang et al., 2001). However, very few examples of naturally occurring piggy-back fashion have been reported thus far. First, a study on mammals by Islinger et al. (2009) showed that the Cu/Zn superoxide dismutase 1 (SOD1) that lacks PTS is imported into peroxisomes using a PTS1-bearing copper chaperone of SOD1 (CCS) as a shuttle (Islinger et al., 2009). Second, piggyback import has been shown for the two subunits (A and B) of lactate dehydrogenase (LDH) (reviewed by Thoms, 2015). Al Saryi and co-workers recently found that nicotinamidase (Pnc1) is imported by piggy-backing onto PTS2-containing enzyme glycerol-3-phosphate dehydrogenase 1, Gpd1 (Al Saryi et al., 2017).

#### **1.4.2 Peroxisomal targeting signal (PTS3)**

In addition to the piggy-back mechanism, a new type of peroxisomal targeting signal has been recently reported, providing an alternative protein import mechanism into the organelles. An example of a protein that is efficiently imported into peroxisomes despite having neither PTS1 nor PTS2 is the budding yeast (*Saccharomyces cerevisiae*) acyl-CoA oxidase (AOx) that is encoded by the POX1 gene (Kempiński et al., 2020). Authors used a random mutagenesis approach combined with a two-hybrid screen that was designed to identify single amino acid residues within the AOx polypeptides that are important for the peroxisomal import, as well as interactions with the N-terminal region of PEX5, suggesting that these amino acids form a signal patch that functions as novel PTS targeting signal. However, in mammals and *Pichia pastoris*, AOx is efficiently imported into peroxisomes via the PTS1 route (Koller, A et al., 1999).

### **1.4.3 The effect of environmental conditions on import into peroxisomes**

The import of some proteins into peroxisomes has been shown to depend on the growth conditions. For example, the presence of oleic acid in the growth medium of *Saccharomyces cerevisiae* induced the expression of PEX9, which contributes to the peroxisomal import of malate synthases, therefore, under strictly defined growth conditions, PEX9 serves as a cytosolic receptor for malate synthase isoenzyme (Effelsberg et al., 2016; Walter and Erdmann, 2019). Unlike PEX5 which is cytosolic, PEX9 is localised in the cytosol and associated with the peroxisomal membrane (Effelsberg et al., 2016).

It has also been shown that the malate synthase is predominantly produced in the cytosol in cells grown on ethanol so that ethanol-derived acetyl-CoA could be processed in the glyoxylate cycle (Kunze et al., 2002; Walter and Erdmann, 2019). Thus, the peroxisomal localisation of malate synthase1 depends on the growth on oleic acid as a sole carbon source.

In *Saccharomyces cerevisiae* and other yeasts, the intracellular localisation of Gpd1p is dependent on the metabolic status of the cells (Jung et al., 2010). Moreover, the subcellular localisation of Gpd1p is altered by osmotic stress, switching from the peroxisomes to the cytosol and nucleus (Jung et al., 2010; Effelsberg et al., 2015). However, the mechanisms, which allow these changes in intracellular localisation are complex and probably as diverse as the peroxisome targeting processes, are not fully understood.

## **1.5 Peroxisome functions**

Peroxisomes carry out a diverse range of metabolic processes, which vary depending on the organism, the cell type and environmental/developmental conditions. These include H<sub>2</sub>O<sub>2</sub> detoxification and  $\beta$ -oxidation, which are the most conserved functions of peroxisomes (Del Río et al., 2002; Heiland and Erdmann, 2005; Nyathi and Baker, 2006; Baker et al., 2006). Peroxisomes are also involved in a variety of specialised functions. For example, they are essential in oil seed germination as they harbour the glyoxylate cycle (Footitt et al., 2002). Additionally, plant peroxisomes house essential steps in the synthesis of several important hormones (Nyathi and Baker, 2006).

In green tissues, peroxisomes take part in the process of photorespiration in conjunction with the mitochondria and chloroplasts. Besides, peroxisomes play an important role in the maintenance of cellular redox homeostasis because they contain several antioxidant enzymes as well as catalases [reviewed in (Hu et al., 2012)]. Various functions linked with plant peroxisomes have also been recently reported, such as sulfite metabolism, isoprenoids, and phyloquinone biosynthesis [ reviewed in (Sandalio et al., 2021), Table 1].

Other organisms such as parasitic protozoa of the genera *Trypanosomes* and *Leishmania* contain glycosomes, which are specialised peroxisomes containing enzymes for glycolysis that are essential for survival (Michels, 1988; Schmidt et al., 2002).

In mammalian cells, peroxisomes are implicated in various catabolic and anabolic processes, such as the  $\beta$ -oxidation of very long chain fatty acids and the biosynthesis of bile acids and phospholipids (plasmalogens) (Van den Bosch et al., 1992; Wanders and Waterham, 2006). In yeasts and plants, peroxisomes are the sole site of fatty acid  $\beta$ -oxidation. They are also involved in the biosynthesis of lysine, degradation of methanol and amino acids (Brown and Baker, 2003). Taken together, the above evidence illustrates the diversity of peroxisomal functions in different organisms. Therefore, it is not surprising that peroxisomes are essential organelles.

The importance of peroxisomes in humans is demonstrated by disorders associated with deficiencies in peroxisomal biogenesis or peroxisomal enzymes. For example, Zellweger's syndrome results a deficiency peroxisomal biogenesis in humans, in which the peroxisomes fail to import some or all proteins. Other peroxisome disorders result from defects in single peroxisomal enzymes: examples are Acatalasemia (catalase deficiency) and X-linked adrenoleukodystrophy (ABCD1 deficiency) (Aebi et al., 1962; Brown and Baker, 2003; Fidaleo, 2010).

Impaired peroxisome biogenesis or peroxisomal functions in plants result in different phenotypes. Peroxisomal mutants such as *ped1/ped1*, which are defective in thiolase (an enzyme involved in fatty acid  $\beta$ -oxidation), are unable to develop expanded green cotyledons or leaves in the absence of exogenous sucrose (Hayashi et al., 1998; Hayashi et al., 2002). These findings demonstrate that the crucial role of glyoxysomal fatty acid  $\beta$ -oxidation in metabolism resulting in the production of respiratory substrates from storage lipids. Loss of the function of the aberrant peroxisome morphology 9 (APEM9) protein, which is involved in peroxisome biogenesis in *A. thaliana*, disrupts plant growth, including embryo development and seed germination (Goto et al., 2011). Similarly, mutations in the *A. thaliana* *PEX10* (Schumann et al., 2003), *PEX10* (Sparkes et al., 2003) and *PEX12* (Fan et al., 2005) genes lead to embryonic lethality. Impaired peroxisomal functions result in decreased pollen fertility and disrupt male-female gametophyte recognition (Boisson-Dernier et al., 2008).

### **1.5.1 Metabolic functions**

Plant peroxisomes carry out a diverse range of metabolic functions, as well as detoxification processes. These include fatty acid  $\beta$ -oxidation, glyoxylate and glycolate metabolism and the detoxification of  $H_2O_2$  (Hu et al., 2012). These pathways are described in more detail below.

Plant peroxisomes are the unique site of fatty acid  $\beta$ -oxidation. Fatty acid  $\beta$ -oxidation is essential for seed development and germination (Baker et al., 2006; Graham, 2008; Hu et al., 2012). In oilseeds such as *A. thaliana*, fatty acids are stored as cytosolic lipid bodies that contain triacylglycerols (TAGs). TAGs are mobilised by oil body-associated TAG lipases such as SUGAR DEPENDENT1 (SDP1) to support post-germinative growth. As a result, free fatty acids are released prior to the commencement of  $\beta$ -oxidation (Eastmond, 2006). Fatty acids or fatty acyl-CoA are then imported to peroxisomes by the peroxisomal ATP binding cassette (ABC) transporter protein (PXA1/ CTS/ PED3) (Footitt et al., 2002; Hayashi et al., 2002; De Marcos Lousa et al., 2009; Lousa et al., 2013) and converted to acyl-CoAs for subsequent catabolism by  $\beta$ -oxidation within the peroxisomes (Cooper and Beevers, 1969; Baker et al., 2006).

Following peroxisomal import, activated fatty acids are degraded and catabolised into acetyl-CoA via several rounds of  $\beta$ -oxidation. The core  $\beta$ -oxidation pathway involves sequential steps of oxidation, hydration, oxidation and thiolysis (Figure 1.7).

These reactions require three proteins/enzymes: acyl-CoA oxidase (ACX), multifunctional protein (MFP) and 3-ketoacylCoA thiolase (KAT), which catalyse oxidation, hydration and thiolytic cleavage, respectively. These reactions produce acetyl-CoA and acyl-CoA shortened by two carbons (Baker et al., 2006; Graham, 2008; Hu et al., 2012). During the first oxidation step, hydrogen peroxide ( $H_2O_2$ ) is produced via acyl CoA oxidase, which is subsequently degraded by catalase (Baker et al., 2006; Graham, 2008) (See section 1.6).

The core  $\beta$ -oxidation pathway metabolises straight-chain saturated fatty acids. However, the metabolism of unsaturated fatty acids with double bonds at both odd and even positions requires additional auxiliary enzyme activities for the removal of the double bonds. These enzymes include enoyl-CoA hydratase, which is encoded by *A. thaliana ECH2*. This enzyme is essential for the degradation of fatty acids with double bonds at the even position. The enzyme dienoyl CoA isomerase encoded by *A. thaliana DCI* is required to metabolise fatty acids with odd double bonds,  $\Delta^{3,5} \Delta^{2,4}$  (Goepfert et al., 2005; Hu et al., 2012; Pan et al., 2020).

Acetyl-CoA derived from fatty acid  $\beta$ -oxidation can enter the glyoxylate cycle, as shown in Figure 1.7, where the peroxisomal citrate synthase (CSY), isocitrate lyase (ICL) and malate synthase (MLS) convert it into 4- carbon compounds that can be consumed by gluconeogenesis and mitochondrial respiration (Baker et al., 2006; Graham, 2008; Hu et al., 2012; Pan et al., 2020) (Figure 1.7).

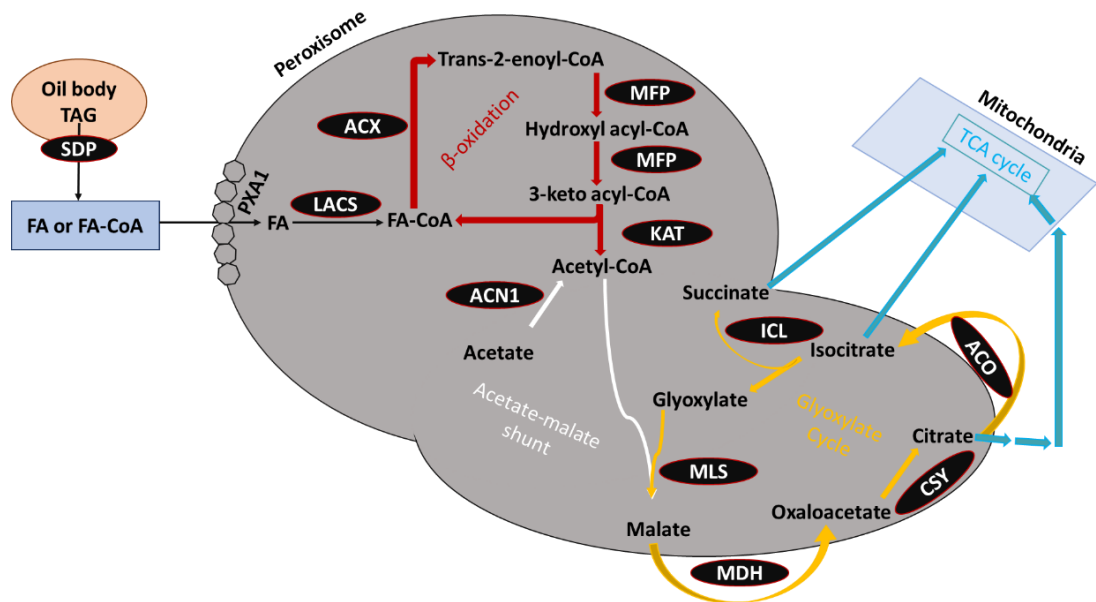


**Figure 1.7: Schematic of the fatty acid degradation in *A. thaliana*.**

Triacylglycerol (TAG) lipase, SUGAR-DEPENDENT (SDP), hydrolyses TAG to fatty acids (FAs). FA or FAcCoA is imported directly into peroxisomes via PXA1 (COMATOSE ATP-binding cassette (ABC) transporter). FAs are activated by a long chain acyl synthetase (LACS) and degraded by the  $\beta$ -oxidation pathway via acyl-CoA oxidase (ACX), multifunctional protein (MFP) and 3-ketoacyl-CoA thiolase (KAT). Each round of  $\beta$ -oxidation releases two carbons as acetyl-CoA. Peroxisomal enzymes isocitrate lyase (ICL) and malate synthase (MLS), in addition to the cytosolic enzymes aconitase (ACO) and malate dehydrogenase (MDH), are essential for the utilisation of acetyl-CoA. MDH also has a peroxisomal isoform (pMDH) to re-oxidise the NADH generated within the peroxisome (Pracharoenwattana et al., 2007). Peroxisomal acetyl-CoA is essential for succinate, isocitrate and citrate production, which can enter the tricarboxylic acid (TCA) cycle. The produced malate is necessary for the malate-oxaloacetate shuttle. In a peroxisomal acetate-male shunt, peroxisomal short-chain acyl-CoA synthetase ACN1 (acetate non-utilising 1) converts free acetate to acetyl-CoA. Figure is adapted from (Pan et al., 2020). A detailed account of this pathway can be found in the following reviews (Baker et al., 2006; Graham, 2008; Hu et al., 2012; Pan et al., 2020).

Leaf peroxisomes play a crucial role in photorespiration. Photorespiration is the salvage process for 2-phosphoglycolate produced by the oxygenase activity of ribulose-1,5-bisphosphate carboxylase/oxygenase (Rubisco). This pathway recycles 2-phosphoglycolate to produce the Calvin-Benson cycle intermediate 3-phosphoglycerate. The photorespiratory pathway involves many enzymatic reactions distributed between chloroplasts, peroxisomes, mitochondria, and the cytosol.

In the peroxisomes, glycolate is oxidised to glyoxylate by glycolate oxidase (GOX), producing  $H_2O_2$  as a by-product (See Section 1.6). Next, the two peroxisomal aminotransferases, glutamate: glyoxylate aminotransferase (GGAT) and serine: glyoxylate aminotransferase (SGAT) transaminate glyoxylate to form glycine. The glycine produced enters the mitochondria and is decarboxylated to serine by the multienzyme glycine decarboxylase complex, which liberates  $CO_2$  and produces  $NH_3$  and NADH as side products. Serine is transported back to the peroxisomes and deaminated by serine: glyoxylate aminotransferase to yield hydroxypyruvate, which in turn is reduced to glycerate by the action of hydroxypyruvate reductase (HPR). The NADH required for this reaction is provided by the peroxisomal malate dehydrogenase (pMDH). Finally, glycerate is shuttled back to the chloroplasts, where it is phosphorylated by the stomatal glycerate kinase (GLYK) to produce 3-phosphoglycerate, as shown in Figure 1.8 [Reviewed in (Hu et al., 2012; Pan et al., 2020; Busch, 2020)].

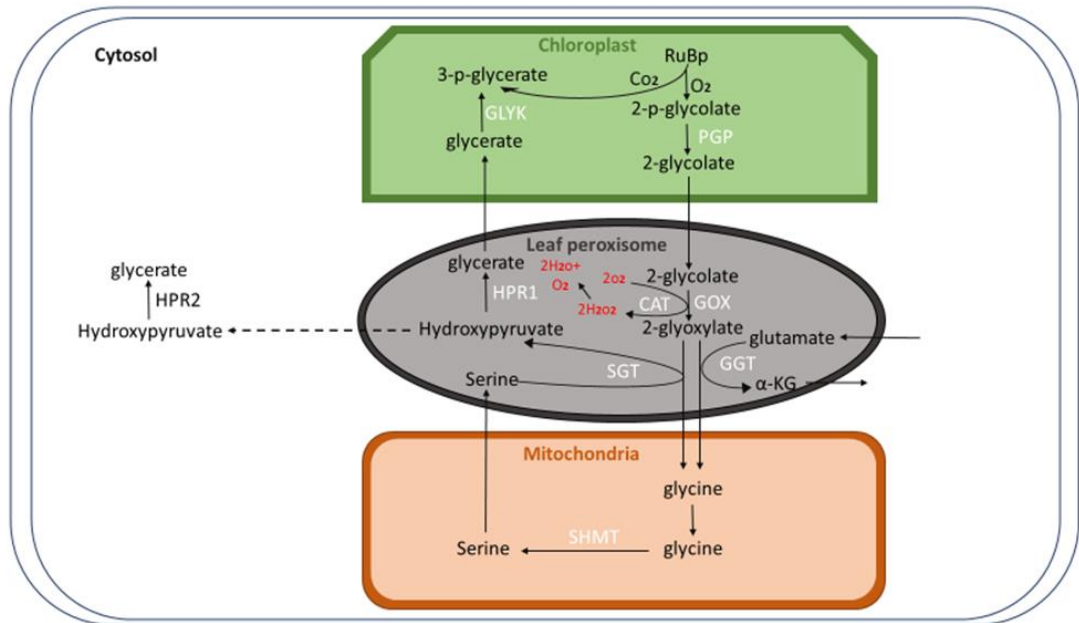


**Figure 1.8: The prominent role of leaf peroxisomes in photorespiration.** Leaf peroxisomes play an integral role in photorespiration. The enzymes involved in photorespiration are PGP-phosphoglycolate phosphatases, GOX-glycolate oxidase, GGT-glutamate: glyoxylate aminotransferase, SHMT-serine hydroxymethyltransferase, HPR-hydroxyypyruvate reductase, SGT-serine: glyoxylate aminotransferase, CAT-catalase (is one of the enzymes indirectly involved). Figure is adapted from (Hayashi and Nishimura, 2006; Hu et al., 2012). A detailed account of this pathway can be found in the following reviews (Hu et al., 2012; Pan et al., 2020; Busch, 2020).

## **1.6 Production of reactive oxygen species (ROS) in peroxisomes**

Between 2.4 and 3.8 billion years ago, molecular oxygen ( $O_2$ ) was most likely introduced into our atmosphere by the evolution of  $O_2$ -evolving photosynthetic organisms (Halliwell, 2006). The  $O_2$  molecule itself is a free radical, with two unpaired electrons that have the same spin quantum number. The electronic structure constrains the reactivity of oxygen so that it cannot accept more than one electron at a time. The univalent reduction of oxygen leads to the generation of reactive oxygen species (ROS) (Apel and Hirt, 2004). The term ROS denotes any oxygen-derived intermediate that is more reactive than  $O_2$  itself. These include superoxide ( $O_2^{\cdot-}$ ), the hydroxyl radical ( $OH^{\cdot}$ ) and the perhydroxy radical ( $HO_2^{\cdot-}$ ), which are free radicals. The term ROS also includes non-radical molecules, such as  $H_2O_2$ , singlet oxygen ( $^1O_2$ ), organic hydroperoxides (ROOH), peroxy radicals ( $ROO^{\cdot}$ ), and the alkoxy radical (RO) (Apel and Hirt, 2004; Foyer et al., 2009; Mittler, 2017). Each type of ROS has specific properties. For example, the estimated lifetime for  $O_2^{\cdot-}$  is 1-4 microseconds in an aqueous solution. Superoxide has a limited reactivity. It can react with ascorbate and the Fe-S groups of proteins. In contrast,  $H_2O_2$  is the most stable form of ROS with a half-life time  $> 1$  milliseconds. It can react with ascorbate, glutathione, the thiol groups of proteins, the heme groups of proteins and nucleic acids (Mittler, 2017; Waszczak et al., 2018).

ROS are produced continuously in plants by the photosynthetic and respiratory electron transport chains, NADPH oxidases, other oxidases, and certain peroxidases. They are also produced as side products of various metabolic pathways that are localised in different cellular compartments such as chloroplast, mitochondria and peroxisomes (Gill and Tuteja, 2010; Sharma et al., 2012; Noctor and Foyer, 2016). Photosynthesis and photorespiration are the major sources of ROS in green tissues (Foyer and Noctor, 2003; Foyer and Noctor, 2005; Foyer, 2018).

ROS formation in chloroplasts is associated with the light-dependent photosynthetic electron transport chain. For example, singlet oxygen is mainly produced within the thylakoid membranes by energy transfer at photosystem (PS) II, whereas  $\text{H}_2\text{O}_2$  is produced from  $\text{O}_2^{\cdot-}$  in a reaction catalysed by superoxide dismutases (SODs) on the stromal side of the thylakoid membrane (Noctor and Foyer, 2016; Foyer, 2018). Mitochondrial ROS production is associated with the respiratory electron transport chain. Complexes I, II, and III have been identified as major sources of  $\text{O}_2^{\cdot-}$  production (Foyer et al., 2009; Waszczak et al., 2018). ROS are also produced in the apoplast via several enzymes such as NADPH-oxidases (also called respiratory burst oxidase homologues, RBOHs) that are localised in the plasma membrane, quinone reductases and amine oxidases (Kärkönen and Kuchitsu, 2015; Considine et al., 2017).

ROS are produced by various metabolic processes in peroxisomes, such as the glycolate oxidase (GOX) reaction of photorespiration and Acyl CoA oxidase in  $\beta$ -oxidation of fatty acids. Two sites of  $\text{O}_2^{\cdot-}$  generation have been identified based on biochemical and electron spin resonance spectroscopy procedures.  $\text{O}_2^{\cdot-}$  is generated in the peroxisomal matrix as a consequence of the oxidation of xanthine and hypoxanthine via xanthine oxidase (XOD). An NADPH-dependent small electron transport chain (composed of flavoprotein NADH: ferricyanide reductase and *Cyt b*) is also responsible for the generation of  $\text{O}_2^{\cdot-}$  in the peroxisomal membrane (Del Río et al., 1998; Del Río et al., 2002; Del Río and López-Huertas, 2016).

Peroxisomes are the primary site of  $\text{H}_2\text{O}_2$  production in the photorespiratory pathway.  $\text{H}_2\text{O}_2$  is generated as a result of the oxidation of glycolate by the action of GOX (see Figure 1.8 (Red), Section 1.5.1). The main enzyme of fatty acid  $\beta$ -oxidation, acyl-CoA oxidase and the enzymatic reaction of flavin oxidases are also responsible for the production of  $\text{H}_2\text{O}_2$  in peroxisomes (Noctor et al., 2002b; Foyer et al., 2009; Baker and Graham, 2013).

It is now well known that ROS are key regulators of a broad range of processes, including metabolism, growth, development, programmed cell death in plants, as well as acclimation responses to abiotic and biotic stresses (Foyer and Noctor, 2005; Baxter et al., 2014; Foyer and Noctor, 2015; Del Río, 2015). ROS act as intracellular signalling molecules that regulate the plant responses to different environmental signals (Foyer and Noctor, 2003). The function of ROS as signalling molecules is achieved through chemical reactions with glutathione and through oxidation of specific groups of target proteins that result in covalent protein modifications (Spadaro et al., 2010). ROS-mediated protein modifications occur via oxidation of thiol groups, particularly cysteine (Cys) residues (Spadaro et al., 2010).

Oxidation of reactive protein Cys residues that possess a low  $pK_a$  results in a formation of a diverse palette of redox-based, post-translational modifications, including S-nitrosylation (Yu et al., 2014), hydrogen sulfide-mediated sulfhydration and ROS-mediated changes (Waszczak et al., 2015).  $H_2O_2$ -mediated thiol-based redox signalling is one of the best-studied cases of ROS-mediated post-translational modifications. These include RNA-binding proteins, proteases and cytosolic kinases (Foyer and Noctor, 2013; Waszczak et al., 2015). ROS signalling is strongly interconnected with responses to phytohormones such as ethylene (ET), abscisic acid (ABA), salicylic acid (SA), jasmonic acid (JA) and auxin (Overmyer et al., 2005; Blomster et al., 2011; Mignolet-Spruyt et al., 2016).

### **1.6.1 ROS metabolism**

ROS generation is increased by various kinds of environmental stresses, such as drought, pathogen attack, salinity, high light, nutrient deficiency and high or low temperatures. Plants have an antioxidant defence system that prevents excessive ROS accumulation. The cellular antioxidant machinery includes enzymatic and non-enzymatic ROS scavenging mechanisms. Non-enzymatic antioxidants include tocopherols, flavonoids as secondary compounds, carotenoids, ascorbate and glutathione (Noctor and Foyer, 1998).

The enzymatic systems include superoxide dismutase (SOD), catalase (CAT), glutathione peroxidase (GPX) and ascorbate peroxidase (APX), as well as the thioredoxin systems. These enzymes can work together with ascorbate, glutathione and thioredoxins to remove H<sub>2</sub>O<sub>2</sub> efficiently (Noctor and Foyer, 1998; Apel and Hirt, 2004). The functions of glutathione, ascorbate and catalase are explained in more detail below.

### 1.7 Glutathione in plants

Glutathione is a tripeptide (GSH;  $\gamma$ -L-glutamyl-L-cysteinyl-glycine, Figure 1.9) that exists in most organisms (Jiménez et al., 1998; Noctor and Foyer, 1998; Noctor et al., 2011). Glutathione exists primarily in its reduced form (GSH) in plant tissues. It is localised in different cellular compartments such as chloroplasts, mitochondria, peroxisomes, cytosol and apoplast, as well as in the vacuole (Mittler and Zilinskas, 1992; Jiménez et al., 1998; Noctor and Foyer, 1998). GSH is oxidised to glutathione disulfide (GSSG) during ROS detoxification. GSSG is rapidly recycled back to GSH by the NADPH-dependent action of glutathione reductases (GRs) (Halliwell and Foyer, 1978; Noctor and Foyer, 1998; Noctor et al., 2012; Hasanuzzaman et al., 2017).

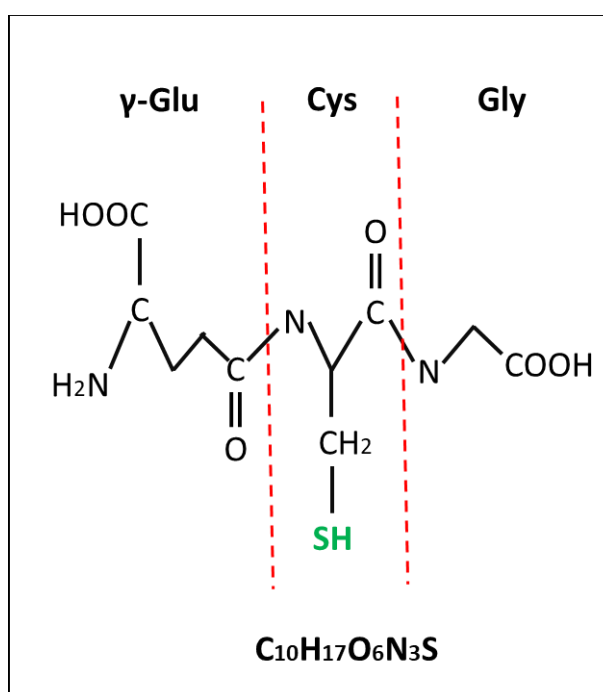


**Figure 1.9: Structure of glutathione.**

Glutathione is a linear tripeptide obtained from the amino acids, glycine (Gly), cysteine (Cys) and glutamate (Glu).

Multiple GSH homologs have been identified in certain plants, in which the C-terminal amino acid glycine is replaced by other amino acids such as  $\beta$ -alanine (homoglutathione;  $\gamma$ -Glu-Cys- $\beta$ -Ala), serine (hydroxymethylglutathione;  $\gamma$ -Glu-Cys-Ser) and  $\gamma$ -Glu-Cys-Glu (Klapheck, 1988; Klapheck et al., 1992) (Meuwly et al., 1993). Oxidized forms of  $\gamma$ -Glu-Cys- $\beta$ -Ala and  $\gamma$ -Glu-Cys-Ser are reduced by the yeast glutathione reductase (Klapheck, 1988; Klapheck et al., 1992), suggesting similar functions to the  $\gamma$ -Glu-Cys-Gly (Noctor and Foyer, 1998).

Reduced glutathione (GSH) is synthesised from the amino acids, glutamate (Glu), cysteine (Cys) and glycine (Gly) in two ATP- dependent steps. In the first step,  $\gamma$ -glutamylcysteine synthetase ( $\gamma$ -ECS) also called  $\gamma$ -glutamylcysteine ligase, catalyses the formation of  $\gamma$ -glutamylcysteine ( $\gamma$ -EC) from Glu and Cys. Glutathione synthetase (GS) catalyses the second step where Gly is added to the  $\gamma$ -EC to yield GSH (Figure 1.10) (Meister, 1988; Noctor and Foyer, 1998; Noctor et al., 2002a; Foyer and Noctor, 2011). The availability of the cysteine or glycine regulates GSH synthesis. GSH synthesis is also regulated by post-translational redox activation of  $\gamma$ -ECS (Noctor et al., 2002a). Knockout  $\gamma$ -ECS mutants are lethal because of impaired GSH synthesis (Cobbett et al., 1998; Ball et al., 2004; Cairns et al., 2006).

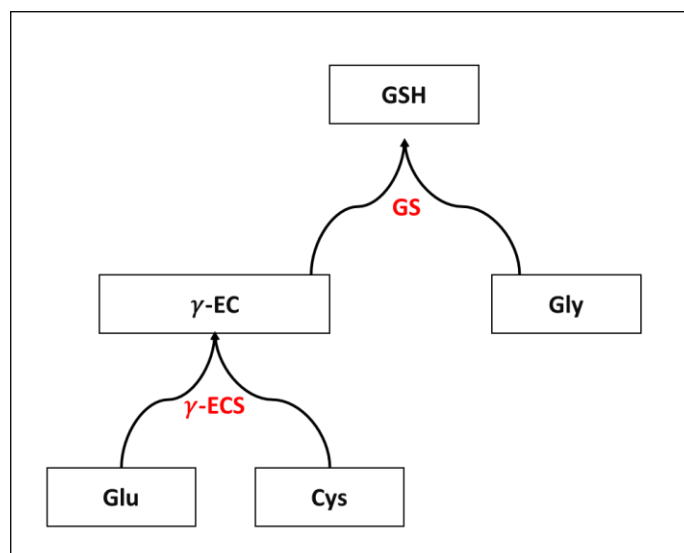


**Figure 1.10: Glutathione synthesis**

Reduced glutathione (GSH) is formed from its constituent amino acids [glutamate (Glu), cysteine (Cys) and glycine (Gly)] in a two-step reaction, which is catalysed by  $\gamma$ -glutamylcysteine synthetase ( $\gamma$ -ECS) and glutathione synthetase (GS).

Glutathione plays an important role in different physiological processes. It acts as a signal that regulates sulphur uptake and metabolism (Herschbach and Rennenberg, 1994; Lappartient and Touraine, 1996; Gigolashvili and Kopriva, 2014). GSH and glutathione S-transferases are involved in the metabolism and detoxification of xenobiotics (Lamoureux and Rusness, 1993; Marrs, 1996; Noctor and Foyer, 1998; Foyer and Noctor, 2011; Del Buono et al., 2020). Phytochelatins ( $\gamma$ -Glu-Cys)<sub>2-11</sub>-Gly are glutathione polymers that are located in the cytosol. They bind heavy metals such as cadmium (Cd) and copper (Cu) to control their free concentrations (Rauser, 1987; Scheller et al., 1987; Grill et al., 1989). Glutathione also plays an important role in redox signalling, for example, in the control of the expression of defence genes, as well as in the regulation of the cell cycle and cell proliferation (Noctor and Foyer, 1998; Foyer and Noctor, 2011; Noctor et al., 2017). Glutathione also plays an important role in the development of flowers and pollen tube growth (García-Quirós et al., 2020).

GSH acts as a redox buffer, which is involved directly in the maintenance of intracellular redox homeostasis. It is accumulated at high concentrations (5-10 mM) in plant cells, in relation to other cellular thiols (Noctor et al., 2011; Noctor et al., 2016). It plays a crucial role in antioxidant defence, which serves to limit the accumulation of ROS in plant cells (Foyer and Noctor, 2011; Noctor et al., 2012; Mittler, 2017). Additionally, GSH is an integral component of the ascorbate (AsA)-glutathione (GSH) cycle. In this cycle, GSH participates in ascorbate regeneration from its oxidised form dehydroascorbate (DHA) as depicted in Figure 1.11 (Foyer and Noctor, 2011; Noctor et al., 2012; Noctor et al., 2015).

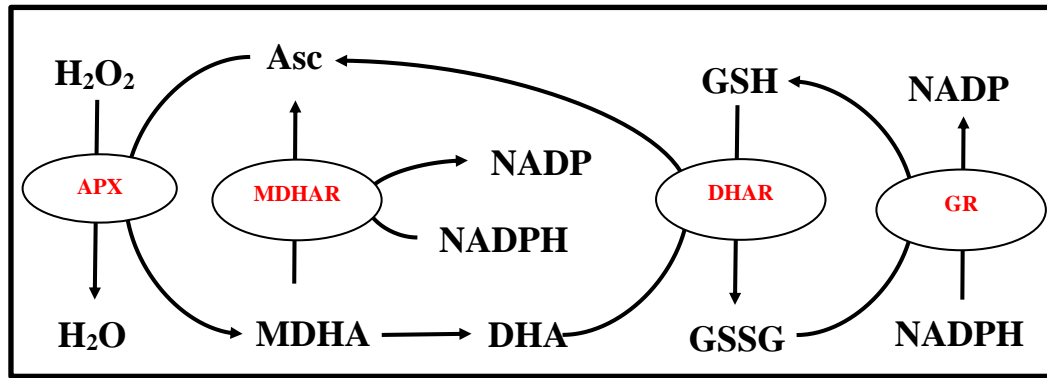


**Figure 1.11: Schematic representation of the ascorbate-glutathione (AsA-GSH) cycle in plants.**

Hydrogen peroxide (H<sub>2</sub>O<sub>2</sub>) is detoxified by ascorbate peroxidase (APX) to produce a water molecule (H<sub>2</sub>O). During this reduction, the reduced form of ascorbate (Asc) gets oxidized into monodehydroascorbate (MDHA). MDHA is either recycled back Asc by the action of monodehydroascorbate reductase (MDHAR) or produces dehydroascorbate (DHA). DHA molecule is reduced to Asc by dehydroascorbate reductase (DHAR). During this reaction, the reduced form of glutathione (GSH) is oxidized to glutathione disulfide (GSSG). GSH is regenerated from GSSG by NADPH-dependent glutathione reductase (GR). Scheme adapted from (Foyer and Noctor, 2011).

Several studies have used GSH and GSSG measurements as markers of oxidative stress, not least because the oxidised and reduced forms can be readily and accurately quantified (Noctor and Foyer, 1998; Foyer and Noctor, 2011; Noctor et al., 2016). An accumulation of glutathione also occurs after exposure plants to stresses such as chilling, pathogen attack and ozone (Gupta et al., 1991; May et al., 1996; Vanacker et al., 2000; Bick et al., 2001; Mou et al., 2003; Gómez et al., 2004). Recently, increased accumulation of glutathione was observed in response to cesium in *A. thaliana* (Adams et al., 2020). The close relationship between intracellular H<sub>2</sub>O<sub>2</sub> availability and the status of the glutathione pool is evidenced by observations made in catalase-deficient *cat2* mutants. The *A. thaliana cat2* mutants exhibit an accumulation of glutathione that is linked to photorespiration (Queval et al., 2007; Mhamdi et al., 2010b; Chaouch et al., 2010; Su et al., 2018). Similar observations were made in barley catalase mutants and tobacco antisense plants (Smith et al., 1985; Willekens et al., 1997).

## 1.8 Ascorbate in plants

Ascorbate is the most abundant low molecular weight cellular antioxidant. It can reach very high concentrations in plants (20-300 mM) (Noctor and Foyer, 1998; Smirnoff, 2000) and is therefore considered to be the most important reducing substrate for ROS detoxification (Nakano and Asada, 1987; Mehlhorn et al., 1996; Noctor and Foyer, 1998). Ascorbate works together with 2-cys peroxiredoxins to keep H<sub>2</sub>O<sub>2</sub> levels low in chloroplasts (Foyer and Shigeoka, 2011).

Ascorbate acts as the primary electron donor in the AsA-GSH cycle for scavenging H<sub>2</sub>O<sub>2</sub> (Figure 1.11) (Foyer and Halliwell, 1976; Foyer and Noctor, 2011). Ascorbate reduces H<sub>2</sub>O<sub>2</sub> to water either directly or in reaction catalysed by APX, as demonstrated in the Asc-GSH cycle (Figure 1.11). Ascorbate is oxidized in the reaction with H<sub>2</sub>O<sub>2</sub>. The reduced form is regenerated by monohydroascorbate reductase (MDHAR) and dehydroascorbate reductase (DHAR), indicating an important recycling role of the Asc-GSH cycle in maintaining cellular ascorbate levels (Foyer and Halliwell, 1976; Foyer, 1997; Noctor and Foyer, 1998).

The important role of ascorbate as an antioxidant in defence against oxidative stresses including ozone, sulfur dioxide and ultraviolet B-radiation has been established using ascorbate-deficient *A. thaliana* mutants such as *vtc1*, which contains 30% of wild type levels of ascorbate (Conklin et al., 1996; Conklin et al., 1997; Conklin and Barth, 2004). Low ascorbate levels are associated with slow growth, increased programmed cell death, premature leaf senescence and the constitutive expression of salicylic acid-mediated defences (Barth et al., 2004; Pavet et al., 2005).

Different functions for ascorbate have also been reported, including preserving the activities of enzymes that contain prosthetic transition metal ions (Padh, 1990), redox regulation and buffering (Horemans et al., 2000) and modulation of lignification of cell walls by scavenging the monolignol radicals that are involved lignin biosynthesis (Takahama, 1993; Otter and Polle, 1994; Schopfer, 1996).

Ascorbate inhibits the activities of the cell wall-bound peroxidases that are responsible for the generation of monolignol radicals (Takahama, 1993; Otter and Polle, 1994; Schopfer, 1996). It is also implicated in the functions of vitamin E ( $\alpha$ -tocopherol) through the reduction of  $\alpha$ -tocopheryl radicals. The  $\alpha$ -tocopheryl radicals that generated when vitamin E is oxidised are recycled back by ascorbate to  $\alpha$ -tocopherol. This reaction participates in the removal of ROS from photosynthetic membranes (Asada, 1999; Davey et al., 2000; Mittler, 2017; Fenech et al., 2019).

Ascorbate functions as an enzyme cofactor, for example, in the xanthophyll cycle, in which the de-epoxidation of violaxanthin to zeaxanthin that is catalysed by violaxanthin de-epoxidase (VDE) is driven by ascorbate oxidation (Eskling et al., 1997). Ascorbate can also serve as a cofactor for other enzymes such as aminocyclopropane-1-carboxylate oxidase, which is crucial for the biosynthesis of the phytohormone ethylene (Smith et al., 1992; Houben and Van de Poel, 2019), as well as prolyl 4-hydroxylase (P4H) and lysyl hydroxylase (LH) (Kivirikko and Pihlajaniemi, 1998; Wojtaszek et al., 1999). P4H and LH catalyse important post-translational modifications in plants and animals. P4H catalyses the formation of 4-hydroxyproline, while LH catalyses the formation of hydroxylysyl residues in proteins that occur during collagen biosynthesis (Hieta and Myllyharju, 2002; Vlad et al., 2007).

Although many ascorbate synthesis pathways have been reported (Figure 1.12), the Smirnoff-Wheeler pathway (also called the D-mannose/L-galactose pathway) is the primary pathway of ascorbate synthesis in leaves. In this pathway, ascorbate is formed from D-glucose via GDP-mannose and L-galactose (Wheeler et al., 1998). A similar pathway with minor differences involves the conversion of GDP-D-mannose to L-glucose instead of L-galactose. L-glucose is then converted to L-gulono-1,4-lactone, which is finally used for ascorbate synthesis (Wolucka and Van Montagu, 2003). Another putative pathway involves cell wall pectins (Smirnoff et al., 2001). Ascorbate synthesis from Myo-inositol has been reported (Valpuesta and Botella, 2004). The different pathways involved in the ascorbate synthesis are presented in Figure 1.12.

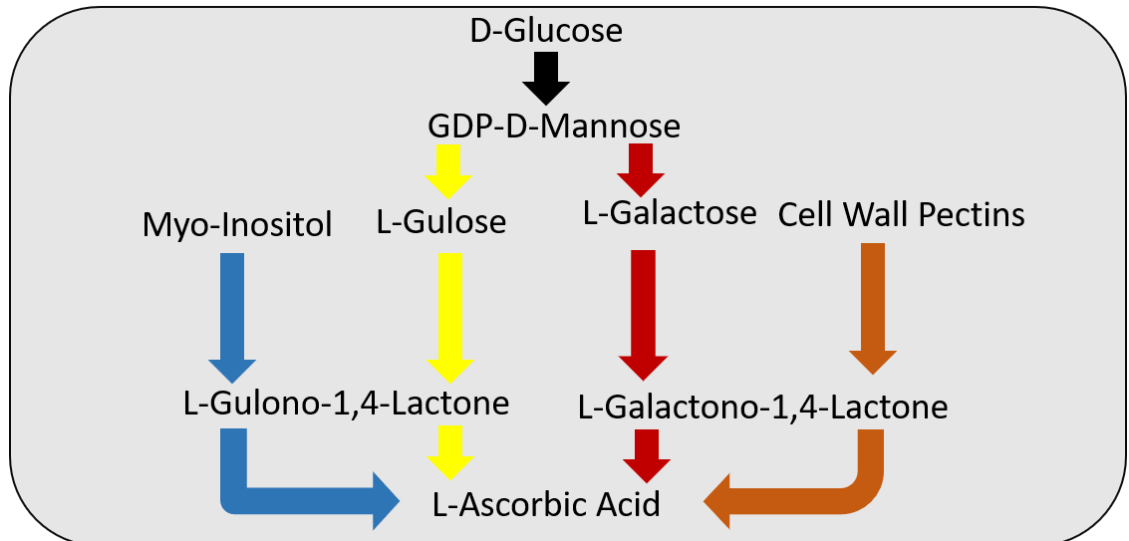


**Figure 1.12: The multiple ascorbate biosynthesis pathways.**  
Figure is adapted from (Akram et al., 2017).

## 1.9 Catalase as antioxidant enzyme

Catalase is one of the most important antioxidant enzymes that plays a key role in the detoxification of  $H_2O_2$ . It converts  $H_2O_2$  to water ( $H_2O$ ) and molecular oxygen ( $O_2$ ) (Alfonso-Prieto et al., 2009).

### 1.9.1 Catalase history

Catalase was the first antioxidant enzyme to be observed and characterized [reviewed in (Kirkman and Gaetani, 2007; Mhamdi et al., 2010b)]. The French chemist Louis Jacques Thénard discovered  $H_2O_2$  in tissues in 1818 and suggested that it was decomposed by an ‘unknown’ substance (Thénard, 1818). In 1863, Schönbein was able to show that the unknown substance can detoxify  $H_2O_2$  (Schönbein, 1863). It was not until 1900 when this enzyme was first named as catalase by the German chemist Oscar Loew. He pointed that “there seems to exist no plant and no animal which is without that particular enzyme” (Loew, 1900).

In the 1920s, Warburg and co-workers demonstrated that the active site of catalase contains an iron porphyrin (Warburg, 1923). A few years later, Stern showed that the hemin group can react with cyanide, sulphides, nitric oxide and fluoride by studying the absorption spectrum of the enzyme (Stern, 1937). In the same year, Sumner and Dounce were able to separate and crystallise catalase from beef liver (Sumner and Dounce, 1937) and then one year later, the molecular weight of the enzyme was determined by Sumner and Gralen (Sumner and Gralén, 1938). In 1969, the bovine catalase gene was first sequenced (Schroeder et al., 1969). The three dimensional structure (3D) of catalase protein was identified in 1981 (Reid et al., 1981).

The first genetic study on catalase was performed by Koltzoff in 1927, who found that the pattern of inheritance of blood catalase follows Mendelian rules in many species [ reviewed in (Feinstein, 1970; Scandalios et al., 1997)]. In 1965, multiple isoforms of maize catalase were shown to be encoded by different structural genes (Scandalios, 1965).

### **1.9.2 Catalase biochemistry**

The monofunctional haem-containing catalase enzyme converts two molecules of  $\text{H}_2\text{O}_2$  to two molecules of  $\text{H}_2\text{O}$  and one molecule of  $\text{O}_2$  (Figure 1.13) through a dismutation or disproportionation reaction (Chelikani et al., 2004), in which one molecule of  $\text{H}_2\text{O}_2$  undergoes oxidation, while the lost electrons are used in the subsequent reduction of the second molecule of  $\text{H}_2\text{O}_2$  (Figure 1.13) (Mhamdi et al., 2010b).

Catalase is one of the most effective enzymes found in nature. Moreover, the enzyme processes  $\text{H}_2\text{O}_2$  at a high rate, equivalent to a turnover number of about  $10^7 \text{ min}^{-1}$  (Scandalios et al., 1997). Despite its very high turnover number, catalase has a very high  $K_m$  for  $\text{H}_2\text{O}_2$  (in the range 40-600 mM) (Chelikani et al., 2004).

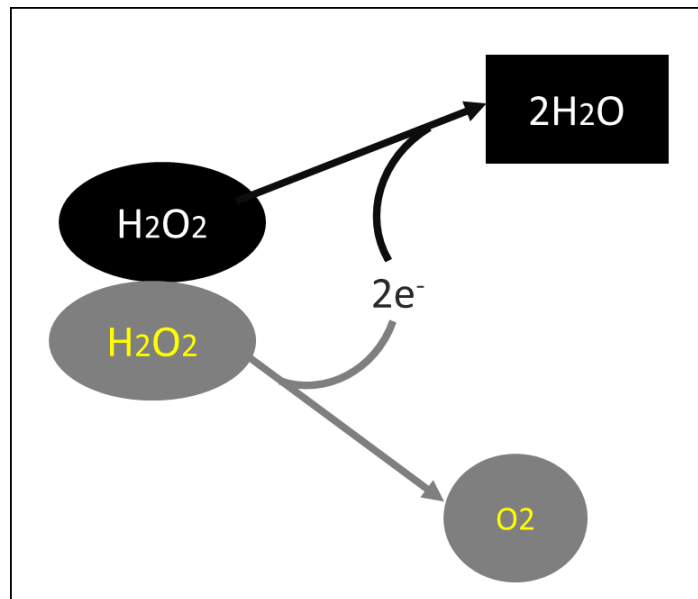


**Figure 1.13: Classical dismutation reaction of catalase.**

Catalase acts through dismutation redox reaction where two molecules of hydrogen peroxide ( $\text{H}_2\text{O}_2$ ) are converted to two molecules of water ( $\text{H}_2\text{O}$ ) and molecular oxygen ( $\text{O}_2$ ). One molecule of  $\text{H}_2\text{O}_2$  is reduced to water ( $\text{H}_2\text{O}$ ) (demonstrated in white), and the second molecule is oxidised to molecular oxygen ( $\text{O}_2$ ), as demonstrated in yellow (Mhamdi et al., 2010b).

Catalase is a tetrameric protein, each monomer bearing a porphyrin ring with an iron atom in the centre (Mhamdi et al., 2010b). Consequently, this enzyme is classed as a heme-containing protein, and its mechanism of action is, therefore heme-dependent (Chelikani et al., 2004; Kato et al., 2004). The iron prosthetic group acts as a cofactor in the redox reaction catalysed by catalase (Zámocký and Koller, 1999).

The mechanism of action of catalase can be generally described in 4 successive steps that are illustrated in Figure 1.14. In the first redox cycle, one molecule of  $\text{H}_2\text{O}_2$  is initially reduced with the concomitant formation of an oxy ferryl intermediate (called compound I) and porphyrin cation radical (Kato et al., 2004). This reduction reaction is mediated by O---O bond splitting releasing the first molecule of water and leaving one oxygen bound to the iron atom (Mhamdi et al., 2010b). In the second redox cycle, the second  $\text{H}_2\text{O}_2$  molecule undergoes oxidation with the electrons lost reducing compound I to the original state from iron (IV) back to iron (III) (Kato et al., 2004). This results in the release of molecular oxygen and a second molecule of water.

The source of the oxygen atom in the second molecule of water is the first  $\text{H}_2\text{O}_2$  molecule. The bound oxygen in compound (I) is released during the second redox cycle, becoming part of the second water molecule (Kato et al., 2004).

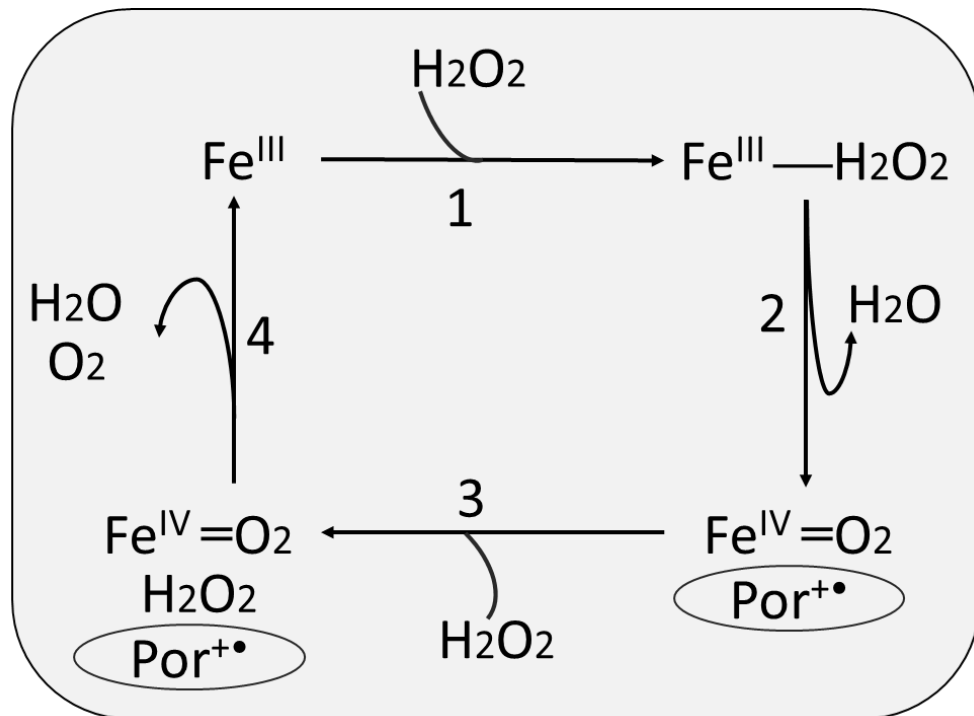


**Figure 1.14: The molecular mechanism of the catalase enzyme.**

One molecule of hydrogen peroxide ( $\text{H}_2\text{O}_2$ ) (1) is reduced to one molecule of water, leaving one oxygen bound to iron atom producing compound I (2). On the other hand, the second  $\text{H}_2\text{O}_2$  molecule (3) is oxidized to molecular oxygen, and another molecule of water with compound (I) is reduced to the original iron III state (4). Roman numbers indicate the oxidation state of the haem iron. The oxidizing equivalent accumulated as porphyrin cation radical, which is indicated by  $\text{Por}^{+\bullet}$  (Mhamdi et al., 2010b).

Mammalian catalases have a tightly bound NADPH molecule, which prevents the formation of the inactive form of the enzyme, known as compound II (Zámocký and Koller, 1999). Compound II is formed as an intermediate during the redox reaction due to the shuttling of electrons between the heme and NADPH molecule (Kirkman et al., 1999). However, comparative structural studies have shown that the NADPH binding site is not present in plant catalases (Chelikani et al., 2004; Zamocky et al., 2008).

### **1.9.3 Classification and structure of catalase**

Catalases were classified into three different types by Goldberg and Hochman (1989) based on selected chemical and physical properties. These are: typical catalases, atypical catalases and catalase-peroxidases (Goldberg and Hochman, 1989). Since then, many catalase genes have been sequenced from different species and the catalases have been reclassified based on sequence homologies (Zámocký and Koller, 1999). The catalases from all living organisms now belong to one of the following subgroups: Monofunctional heme-containing catalases (also known as typical or true catalases), bifunctional heme-containing catalase peroxidases, and manganese catalases (non-heme) (von Ossowski et al., 1993; Zámocký and Koller, 1999; Chelikani et al., 2004; Zamocky et al., 2008; Zámocký et al., 2010; Glorieux and Calderon, 2017). The monofunctional catalases are a more widespread subgroup than the bifunctional ones, and their structures have been well characterized (Chelikani et al., 2004). In contrast, little information is available on the third subgroup, in which manganese acts as a cofactor instead of heme. Notably, this subgroup is present only in bacteria (Zámocký and Koller, 1999; Whittaker, 2012).

#### **1.9.3.1 Monofunctional heme-containing catalases**

Catalases from all aerobic prokaryotes and eukaryotes belong to the category of monofunctional heme-containing catalases, which is considered to be the largest subgroup (Guan and Scandalios, 1995). Generally, the catalases of this subgroup are homotetramers, of between 200 and 340 kDa in size (Quan et al., 1986). As heme-containing proteins, each monomer contains a porphyrin ring with an iron atom at the centre that acts as a prosthetic group during the catalytic redox reaction.

Monofunctional catalases are further subdivided into three main clades (Klotz et al., 1997; Carpena et al., 2003). Clade 1 consists of catalases with small subunits (55-69 kDa) using heme *b* as the prosthetic group, which are present in a subset of bacteria. Clade 2 consists of the large subunit catalases (75-84 kDa), with heme *d* as the prosthetic group and an additional C-terminal flavodoxin domain. Catalases from this subgroup are mainly present in bacteria and fungi.

The most abundant subfamily is clade 3, which contains catalases with a small subunit size (43-75 kDa) containing heme *b*. Clade 3 catalases are found in archaeons, protists, fungi, plants, and animals. Some catalases (e.g. human catalase) that belong to this clade have an additional NADPH cofactor, which is tightly bound to each monomer (Putnam et al., 2000; Chelikani et al., 2004; Zamocky et al., 2008; Zámocký et al., 2012; Glorieux and Calderon, 2017; Karakus, 2020).

Multiple sequence alignments of typical catalases have revealed that the core of the protein consists of a consensus sequence of about 390 amino acids that is conserved, particularly at the distal and proximal sides of the heme group (Zámocký and Koller, 1999).

The structure of monofunctional catalases isolated from various species has been extensively studied (Fita et al., 1986; Melik-Adamyanyan et al., 1986; Klotz et al., 1997; Zámocký and Koller, 1999; Putnam et al., 2000; Carpena et al., 2003; Pena-Soler et al., 2011; Yuzugullu et al., 2013; Glorieux and Calderon, 2017). For example, human catalase forms a tetramer composed of four identical subunits of 62 kDa. Each subunit can be divided into four structural regions and one prosthetic heme group (Zámocký and Koller, 1999; Putnam et al., 2000; Goyal and Basak, 2010; Glorieux and Calderon, 2017). The N-terminal threading arm, which connects two adjacent subunits by hooking through a second domain around another subunit known as a wrapping loop. The N-terminal threading arm contains His81, which is one of the essential amino acids for the catalase reaction. It is known as the distal histidine. In addition, the largest domain is a  $\beta$ -barrel that is comprised of two four-stranded sheets and located at the core of each subunit. This hydrophobic domain is generated by an eight-stranded antiparallel  $\beta$ -barrel ( $\beta 1$ -  $\beta 8$ ). The  $\beta$ -barrel domain is the most conserved region among all typical catalases (Chelikani et al., 2003). Finally, a helical domain consists of eight helices, four of them located at the C-terminus (Figure 1.15).

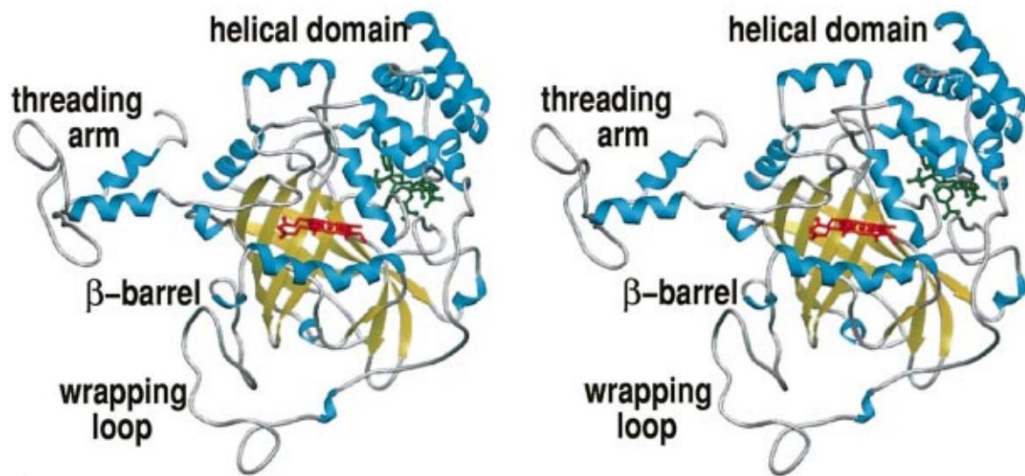


**Figure 1.15: The structure of human catalase.**

Each subunit consists of four domains with a  $\beta$ -barrel (yellow) in the centre surrounded by helices (blue). The heme-containing active site and NADPH cofactor are illustrated in red and dark green, respectively. This figure is taken from (Putnam et al., 2000) and reproduced with permission from Elsevier and Copyright Clearance Center.

#### 1.9.4 Catalase genes and isoforms

The typical “monofunctional” catalases are the most abundant group in plants, animals, fungi, eubacteria, Protista and archaeobacteria (Zamocky et al., 2008). *Escherichia coli* (*E. coli*) produces two catalytically active enzymes, the monofunctional catalase (HPII) and the bifunctional catalase-peroxidase (HPI) that are encoded by the genes KatE and KatG, respectively (Mulvey et al., 1990). In the soil bacterium *Sinorhizobium meliloti*, two typical catalases (KatA and KatC) and a catalase-peroxidase (KatB) have been identified (Jamet et al., 2003). Two typical catalases are found in the yeast *Saccharomyces cerevisiae* (Petrova et al., 2004).

Most plants have more than one catalase gene. Three catalase genes have been identified in tobacco (*Nicotiana plumbaginifolia* Viviana) (Willekens et al., 1994b), *A. thaliana* (Du et al., 2008), maize (*Zea mays* L.) (Guan and Scandalios, 1996), pumpkin (*Cucurbita* Linn.) (Esaka et al., 1997) and rice (*Oryza sativa* L.) (Joo et al., 2014).

Four candidate catalase genes have been identified in cucumber (*Cucumis sativus* L.) (Hu et al., 2016), with two genes in barley (*Hordeum vulgare* L.) (Skadsen et al., 1995) and one in tomato (*Lycopersicon esculentum* Mill) (Drory and Woodson, 1992) and castor bean (*Ricinus communis* L.) (González, 1991).

Based on genome sequencing, the presence of three catalase genes has been confirmed in *A. thaliana* *CAT1* (At1g20630), *CAT2* (At4g35090) and *CAT3* (At1g20620). *CAT1* and *CAT3* are located on chromosome number 1 and *CAT2* is located on chromosome number 4 (Figure 1.16) (Frugoli et al., 1996). Multiple sequence alignments of *A. thaliana* catalases (Figure 1.17) has revealed that the products comprise of 492 amino acids with a high similarity amongst the sequences (Hu et al., 2010). Despite the similarity of the three polypeptides, *CAT1*, *CAT2* and *CAT3*-specific antibodies have been reported in *A. thaliana* (Hu et al., 2010; Su et al., 2018).

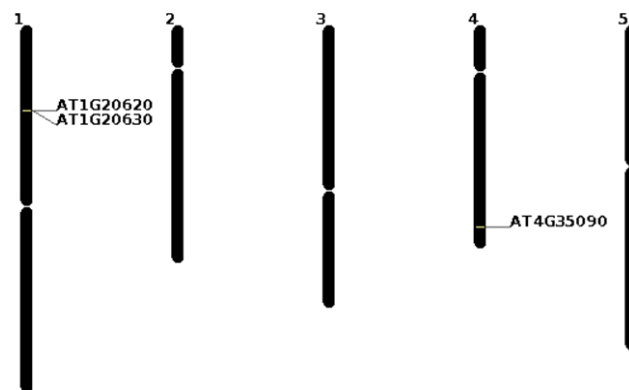


**Figure 1.16: Location of *A. thaliana* catalase genes.**

Two catalase genes located on Chromosome 1 and one located on chromosome 4. *CAT1*, At1g20630; *CAT2*, At4g35090; *CAT3*, At1g20620. Figure is designed using Inter Pro tool. <https://www.ebi.ac.uk/interpro/>.

CAT1	MDPYRVRPSSAHDSPFFTTNSGAPVWNNSSSLTVGTRGFILLEDEYHLLKLANFDRERIP	60
CAT2	MDPYKYRPASSYNSPFFTTNSGAPVWNNSSMTVGGPRGFILLEDEYHLVEKLANFDRERIP	60
CAT3	MDPYKYRPSSAYNAPFYTTNGGAPVSNNISLTIIGERGEVLLLEDYHLIEKVANFTRERIP	60
CAT1	ERVVHARGASAKGFFEVTHTDITQLTSADFLRGPVQTPVIVRFSTVIHERGSPETLRDPR	120
CAT2	ERVVHARGASAKGFFEVTHTDISNLTCADFLRAPGVQTPVIVRFSTVIHERGSPETLRDPR	120
CAT3	ERVVHARGISAKGFFEVTHTDISNLTCADFLRAPGVQTPVIVRFSTVVHERASPETMRDIR	120
CAT1	GFAVKFYTREGNFDLVGNFFVFFVIRDMGKFPDMVHALKPNPKSHIQENWRILDFSSHHP	180
CAT2	GFAVKFYTREGNFDLVGNFFVFFIRDMGKFPDMVHALKPNPKSHIQENWRILDFSSHHP	180
CAT3	GFAVKFYTREGNFDLVGNNTPVFFIRDMGKFPDMVHALKPNPKSHIQENWRILDFSSHHP	180
CAT1	ESLHMFSFLFDDLGIPQDYRHMEGAGVNTYMLINKAGKAHYVKFHWKPTCGIKLSDEEA	240
CAT2	ESLNMFTFLFDDIGIPQDYRHMDGSGVNTYMLINKAGKAHYVKFHWKPTCGVKSLEEDA	240
CAT3	ESLLTWCWMFDDVIGIPQDYRHMEGFGVHTYTLIAKSGKVLVFKFHWKPTCGIKNLTDEEA	240
CAT1	IRVGGANSHATKDLYDSIAAGNYPQWNLFVQVMDPAHEDKDFDPLDVTKIWPEDILPL	300
CAT2	IRVGGTNHSHATQDLYDSIAAGNYPEWKLFIQIIDPADEKDFDPLDVTKIWPEDILPL	300
CAT3	KVVGGANSHATKDLHDALIASGNYPEWKLFIQITMDPADEKDFDPLDVTKIWPEDILPL	300
CAT1	QPVGRLVNLKNIDNFFNEEQIAFCPALVVPGLHYSDDKLLQTRIFSYADSQRHRLGPNY	360
CAT2	QPVGRMVLNKNIDNFFAENEQLAFCPAIIVPGLHYSDDKLLQTRVFSYADTQRHRLGPNY	360
CAT3	QPVGRLVNLNRTIDNFFNETEQLAFNGLVVPGLIYSDDKLLQCRIFAYGDTQRHRLGPNY	360
CAT1	LQLPVNAPKCAHHNNHHDGFMNFMHRDEEVNYFPSRLDPVRHAEKYPTPIVCSGNREKC	420
CAT2	LQLPVNAPKCAHHNNHHEGFMNFMHRDEEVNYFPSRYDQVRHAEKYPTPPAVCSGKRERC	420
CAT3	LQLPVNAPKCAHHNNHHEGFMNFMHRDEEINYYPKFDVPRCAEKVPTPTNSYTGIRTKC	420
CAT1	FTGKENNFKQPGERYRSDSDRQERFVKRFVEALSEPVTHEIRSIWISYWSQADKSLGQ	480
CAT2	IIEKENNFKEPGERYRTFTPERQERFIQRWIDALSDPRITHEIRSIWISYWSQADKSLGQ	480
CAT3	VIKENNFKQAGDRYRSWAPDRQDRFVKRWVEILSEPRLTHEIRGIWISYWSQADRSLGQ	480
CAT1	KLATRLNVRPNF	492
CAT2	KLASRLNVRPSI	492
CAT3	KLASRLNVRPSI	492

**Figure 1.17: Multiple sequence alignment of *A. thaliana* catalase protein sequences.**

The protein sequences of CAT1, CAT2 and CAT3 were aligned using Clustal Omega software (Sievers et al., 2011). The grey colour illustrates the identical amino acids among the three catalases.

Three catalases are classified into three classes depending on their expression properties: Class I, Class II and Class III. Several literature studies support the classification of catalases. It was found that the three catalases of *A. thaliana* are identical to three classes. *CAT1* corresponds to Class III and is primarily expressed in pollen and seeds, whereas the *CAT2* corresponds to Class I and is strongly expressed in photosynthetic tissues but also seeds and roots. Finally, *CAT3* is related to Class II, and is mainly expressed in vascular tissues and young leaves (Mhamdi et al., 2010b). The expression of *CAT2* and *CAT3* is controlled by a circadian rhythm, with a morning-specific phase of *CAT2* expression and an evening-specific phase of *CAT3* expression (Zhong et al., 1994).

In addition, day/night variations in expression are less marked in CAT1 than the other forms (McClung, 1997). CAT1 plays an important role in the removal of H<sub>2</sub>O<sub>2</sub> produced under different abiotic stresses (Du et al., 2008). CAT2 and CAT3 are the major isoforms in rosette tissues (Mhamdi et al., 2010b). These forms detoxify H<sub>2</sub>O<sub>2</sub> and contribute to peroxisomal H<sub>2</sub>O<sub>2</sub> homeostasis in the light and in darkness, respectively (Du et al., 2008). The expression profiles and activities of *A. thaliana* CAT2 and CAT3 have been analyzed under various environmental stresses such as cold, drought and oxidative stress. CAT2 is induced by cold and drought, while CAT3 is mainly induced by abscisic acid and oxidative treatments (Du et al., 2008).

### **1.9.5 Catalase mutants and knockdowns**

Catalase deficiency, which was first identified in humans in 1948 by Takahara (Takahara, 1948), leads to the genetic disease known as Acatlasemia or Takahara disease. Patients with Acatlasemia suffer from increased mouth ulcers leading to oral gangrene as a result of soft tissue death (Zamocky et al., 2008). In contrast, catalase deficiency in mice leads to various disorders that differ from tissue to tissue (Ho et al., 2004).

Catalase is particularly important in plants that have the C<sub>3</sub> pathway of photosynthesis. Photorespiration is a major pathway of metabolic H<sub>2</sub>O<sub>2</sub> production in C<sub>3</sub> plants. The crucial role of catalase in photorespiratory metabolism has been demonstrated using sense and antisense technology. For example, transgenic tobacco lines that are deficient in *cat1* (Cat1AS) show necrotic lesions on the leaves when grown at high irradiance (300-1000  $\mu\text{mol}/\text{m}^2/\text{s}$  photosynthetic photon fluence rates) (Chamnongpol et al., 1998; Willekens et al., 1997). At low light intensities (< 100  $\mu\text{mol}/\text{m}^2/\text{s}$  PPFR), the same mutants did not show any leaf phenotypes. It should be noted that the Cat1 isoform in tobacco accounts for 80% of leaf catalase activity. Cat1 therefore plays a pivotal role in H<sub>2</sub>O<sub>2</sub>-scavenging during photorespiration in tobacco leaves (Willekens et al., 1994a).

Catalase-deficient barley mutants have also been characterised (Kendall et al., 1983). These catalase-deficient mutants have only about 10% of the catalase activity of the wild type plants and they are unable to grow well in air (Kendall et al., 1983). The barley mutants show growth abnormalities when grown in air including tissue oxidation and leaf bleaching. However, the growth retardation could be avoided by growth at high (0.2%) CO<sub>2</sub> (Kendall et al., 1983; Smith et al., 1985).

Analysis of *A. thaliana* T-DNA mutants confirmed that *CAT2* encodes the major leaf isoform of catalase in this species. *CAT2* is responsible for a large part of the leaf catalase activity and its functions are closely linked to photorespiration (Queval et al., 2007). Thus, the functions of the photorespiratory *CAT2* form cannot be replaced by the other isoforms (Hu et al., 2010). Growth of *A. thaliana cat2* mutants in air resulted in decreased rosette biomass accumulation, but the mutants grow normally under high CO<sub>2</sub>, which suppresses photorespiration (Queval et al., 2007).

The *cat2* mutants showed specific growth phenotypes under different growth conditions (i.e., dependent on the growth CO<sub>2</sub> level and day length), which are considered to be associated with specific alterations in redox signalling (Queval et al., 2007). Under short day growth conditions in air, the mutants showed slow growth and an altered cellular redox state, with increases in the total leaf glutathione pool and changes in the expression of genes involved in oxidative signalling. The *cat2* mutant leaves showed lesions under long-day conditions but not under short day growth conditions (Queval et al., 2007). Moreover, aphid fecundity was decreased in the *cat2* mutants compared to the wild type grown under moderate light (250 μmol m<sup>-2</sup> s<sup>-1</sup>) (Rasool et al., 2020). These findings point to the important role of *CAT2* in redox signalling. The *cat2* mutants also display a constitutive induction of salicylic acid (SA) and jasmonic acid (JA)-dependent pathways with constitutive upregulation of pathogen defence responses and resistance (Chaouch et al., 2010).

In addition to the well-known roles of *CAT2* in photorespiration, other non-photorespiratory functions of *CAT2* are possible although these have not been fully characterised. For example, *A. thaliana cat2* RNAi lines were more sensitive to ozone (Vandenabeele et al., 2004; Vanderauwera et al., 2005). Similarly, *A. thaliana cat2* mutants showed altered monovalent cation homeostasis and enhanced lithium tolerance (Bueso et al., 2007). The latter finding may be related to decreases in root catalase activity (Bueso et al., 2007). *CAT2* has also been shown to affect seedling growth by altering H<sub>2</sub>O<sub>2</sub> accumulation (Liu et al., 2017; Yang et al., 2018). It also plays an important role in plant defence against pathogens (Yuan et al., 2017). The authors demonstrated that *CAT2* promotes *AXC2/3* activity to increase jasmonic acid accumulation during pathogenic infection.

The generation of *cat2 cat1* and *cat2 cat3* double mutants is not difficult because the *CAT2* gene is located on a different chromosome from *CAT3* and *CAT1* genes (Figure 1.16). The catalase activity in *cat1* leaves was similar to wild type, whereas catalase activity was decreased by about 20% in *cat3* leaves (Mhamdi et al., 2010b). Catalase activity was also decreased by about 95% and 88% in the *cat2 cat3* and *cat2 cat1* double mutants, respectively (Mhamdi et al., 2010b). These findings confirm that *CAT1* expression is not significant in leaves. Moreover, the largest part of leaf catalase activity is determined by the expression of the *CAT2* gene.

In earlier studies, *cat1 cat2* and *cat2 cat3* double mutants were obtained by crossing the individual T-DNA knockout mutant lines. It is difficult to obtain the *cat1 cat2 cat3* triple mutants or the *cat1 cat3* double mutants using the same approach because of the short distance between the *CAT1* and *CAT3* genes, which are located in the same chromosome. However, *cat1cat3* double mutants and *cat1cat2cat3* triple mutants were recently generated using CRISPR/Cas9 technology (Su et al., 2018). Interestingly, deletion of all of the catalase genes was not lethal. However, the growth was severely affected and the redox state of the leaves was greatly changed (Su et al., 2018).

The phenotypes of the *cat1* and *cat3* single mutants and the double mutants have been measured under growth light conditions that allow about 50% of the maximal rates of photosynthesis (Mhamdi et al., 2010b; Hu et al., 2010). No phenotypic differences were observed in the *cat3* and *cat1* *single* mutants and the wild type. In contrast, the *cat2 cat3* and *cat2 cat1* double mutants showed a *cat2* rosette phenotype (Mhamdi et al., 2010b; Hu et al., 2010).

### **1.9.6 Subcellular localisation of catalase**

Catalase is present in all plant and most animal cells. It has also been found in some prokaryotic cells (Singh, 1996). In contrast, most anaerobic and some aerobic bacteria lack catalase (Welinder, 1992; Singh, 1996). The subcellular localization of catalase has been studied in different organisms. The yeast *Saccharomyces cerevisiae* contains two catalase genes (*CTA1* and *CTT1*), one of which encodes a cytosolic isoform, while a second encodes a major peroxisomal enzyme (Petrova et al., 2004). More interestingly, it has also been demonstrated that the yeast catalase A (Cta1p) can enter mitochondria, a phenomenon that is dependent on the nature of the carbon source in the growth medium (Petrova et al., 2004). However, the mechanisms that control the distribution of Cta1p between mitochondria and peroxisomes remain to be elucidated.

In mammals, catalase is localised in peroxisomes. Interestingly, a biochemical and immunocytochemical study demonstrated that catalase is also localised in rat heart mitochondria (Radi et al., 1991). While no other studies have supported this observation, studies on transgenic mice in which the catalase was overexpressed in cardiac tissues showed that the enzyme is localized in peroxisomes, with some extra peroxisomal sites such as the nuclei and sarcoplasm but not mitochondria (Zhou and Kang, 2000). Immune gold labelling of the cardiac tissues revealed that catalase is exclusively localized to peroxisomes of the wild-type tissues. The differences in subcellular localization between the transgenic and control tissues were explained by the overexpression of catalase, where the amount of catalase protein produced exceeded the capacity of peroxisomal accommodation, and consequently, excess catalase remained in the cytosol (Zhou and Kang, 2000).

Unlike most animals, the nematode *Caenorhabditis elegans* was reported to contain two forms of catalase. One encodes a cytosolic enzyme (CTL-1) while a second encodes a major peroxisomal enzyme (CTL-2) (Taub et al., 1999; Togo et al., 2000; Petriv and Rachubinski, 2004). Knockout of the peroxisomal catalase form caused a progeric phenotype, developmental abnormalities and restricted lifespan (Petriv and Rachubinski, 2004).

Plant peroxisomes contain high levels of catalase activity. Subcellular localisation of plant catalases has been performed using various techniques, including subcellular fractionation, electron-microscopic detection using cytochemical staining with 3,3'-diaminobenzidine (DAB) based on the peroxidative activity of catalase, and immunogold labelling (Novikoff and Goldfischer, 1969; Drumm et al., 1970; Scandalios et al., 1980; Tenberge and Eising, 1995; Mullen et al., 1997). It was estimated that catalase comprises 10-25% of the total peroxisomal proteins (Reumann et al., 2004). Therefore, catalase is widely used as a marker for plant peroxisomes.

Although subcellular fractionation techniques have shown that catalase is present in different plant cell compartments, cross contamination artefacts and other effects cannot be ruled out. Therefore, in the past decade, computational prediction methods and fluorescent protein fusion approaches have been used to examine the subcellular localisation of catalase in plant cells. Fusions with a green, yellow or cyan fluorescent protein (GFP, YFP and CFP) have extensively used because of their speed and reliability in protein localisation (Chalfie et al., 1994; Palm et al., 1997; Nagai et al., 2002). However, such fusions are not problem-free because they can alter protein properties and/or localisation. For example, some GFP variants are able to dimerise at very high concentrations, which in turn lead to unspecific artificial localisations (Falter et al., 2019). Nevertheless, questions remain concerning the nature of the catalase import mechanism.

### 1.9.7 Catalase import mechanism

Unlike chloroplast and mitochondrial proteins, newly synthesized peroxisomal proteins may fold or assemble into oligomers and form the active and mature conformation in the cytosol prior to their import to peroxisomes (Kim and Hettema, 2015; Reumann et al., 2016). However, for proteins like catalase, it is still not clear whether the heme group is added and the protein folded before peroxisomal import, or alternatively if the disassembly of the cytosolic protein is a prerequisite for translocation into peroxisomes (Lazarow and De Duve, 1973; Walton et al., 1995; Mhamdi et al., 2012).

Some studies have shown that catalase monomers are first translocated into the peroxisomes before assembly, and hence the peroxisomal matrix (rather than the cytosol) is the site of cofactor association and oligomerization (Figure 1.18) (Lazarow and De Duve, 1973).

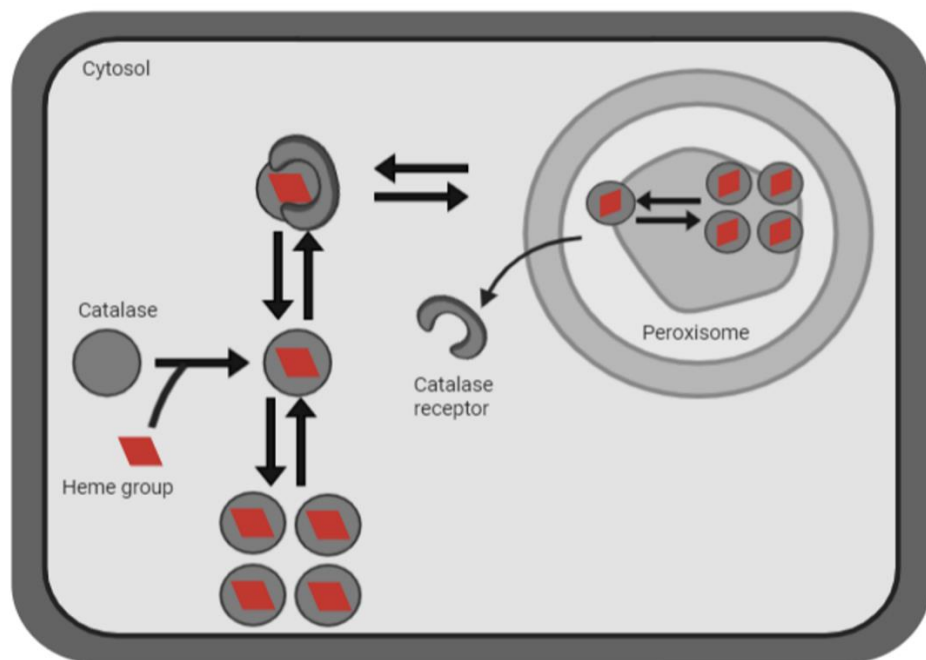


**Figure 1.18: A model for translocation of catalase to peroxisomal matrix in plants.**

Dark grey circles represent catalase monomers or subunits and red rhombus represents the heme group. In this model, only heme-containing subunits are transported via PEX5 to peroxisomes, where they assemble to the active protein in peroxisomal matrix. Cytosolic catalase found in the active and mature conformation should disassemble prior to peroxisomal import (Mhamdi et al., 2012). Created with BioRender.com.

Work in yeast has suggested that if catalase is imported too quickly, it does not acquire a haem group in the cytosol, and it is therefore not functional (Williams et al., 2012a). One explanation of such results is that the regulation of catalase assembly may occur in different locations within the cell dependent on growth conditions (See Section 1.4.3).

In mammals, PEX5 was found to inhibit the tetramerization of catalase. PEX5 interacts with monomeric mammalian catalase form more strongly than the tetrameric catalase form (Freitas et al., 2011). This finding suggests that mammalian catalase is imported into the peroxisomes in its monomeric state. The monomeric forms may therefore be the preferred substrates for peroxisomal import (Freitas et al., 2015). It should be mentioned that the amount of PEX5 in the cytosol may determine whether or not catalase forms tetramers prior to import into the organelles. If cells contain an excess amount of PEX5, then, monomeric catalase will be imported into the peroxisome (Freitas et al., 2011; Mhamdi et al., 2012).

In all species studied to date, catalases were sorted into peroxisomes via non-canonical PTS1 sequences. A tetrapeptide sequence –KANL at the C-terminus of human catalase was shown to be sufficient for peroxisomal targeting (Purdue and Lazarow, 1996). The presence of the uncharged residue asparagine (N) at position 2 instead of a basic amino acid is necessary for the targeting process (Purdue and Lazarow, 1996). While the role of the lysine (K) at position 4 is critical, the tripeptide –ANL alone is not a functional PTS1 signal. Work in mammalian cells has also pointed to a role for cellular redox regulation in catalase targeting (Koepke et al., 2007). PTS1 import and the activity of PEX5 are controlled by the redox state of the cytosol. In this scenario, PEX5 (Cys 11) acts as a redox switch under oxidative stress conditions (Apanasets et al., 2014; Walton et al., 2017).

The tripeptide sequence SKI is found in the methylotrophic yeast *Hansenula polymorpha* (Didion and Roggenkamp, 1992), but the catalase from *Candida boidinii* carries the non-canonical –NKF signal at the C-terminus (Horiguchi et al., 2001).

Analysis of the *Hansenula polymorpha* catalase showed that replacing the non-canonical PTS1-SKI by the SKL resulted in reduced enzyme activity and also lead to the formation of catalase protein segregates in the peroxisomal matrix (Williams et al., 2012a). Moreover, studies using isothermal titration microcalorimetry have shown that the affinity of PEX5 to a C-terminal -SKI is eight-fold lower than a peptide with SKL (Williams et al., 2012a). In addition to the C-terminal PTS hexapeptide -SSNSKF, the *Saccharomyces cerevisiae* catalase has a second internal peroxisomal sorting signal found in the N-terminal (Kragler et al., 1993). Both are sufficient to import protein to peroxisomes.

The PSI sequence was necessary for the import of a cottonseed catalase (Ccat) into tobacco (*Nicotiana tabacum*) BY-2 cell peroxisomes (Mullen et al., 1997). In contrast, the Pumpkin catalase (cat1) tripeptide at the C-terminal is not necessary for import (Kamigaki et al., 2003). It also contains an internal PTS1-like tripeptide (QKL) at a position 13 to 11 from the C-terminal, which is required for import (Kamigaki et al., 2003). This study was performed using a green fluorescent protein (GFP)-fusion protein, in which the GFP was fused to a Cat1 cDNA. This construct was stably expressed in *A. thaliana* and tobacco (*Nicotiana tabacum*) Bright Yellow 2 (BY-2 cells). However, the interpretation of such data is complicated because of the large size of the GFP protein. The presence of the large GFP protein may restrict or inhibit catalase assembly.

Additionally, the recognition of the PTS1 requires a free carboxyl group at the C terminus. Therefore, the internal QKL may not function as a classic PTS1 signal. Contradictory results have been obtained in studies involving the import of fusion proteins. For example, the last 3 amino acids were found to be required for import using a transient expression system (Kamigaki et al., 2003). However, the level of expression of the different constructs may explain some of the differences found in published results. Additionally, such studies rarely take the 3D structure of the receptor/cargo complex into account. However, these interactions are functionally important.

The three *A. thaliana* catalases have a non-consensus PTS1 targeting signal [ reviewed in (Mhamdi et al., 2012)]. Web-logo analysis of the last tripeptide of the C-terminus of the three *A. thaliana* catalases revealed the presence of a non-canonical PTS1 targeting signal (Figure 1.19). The C-terminal peptides also differ from the mammalian consensus sequence (-KANL). A multiple sequence alignment using a number of catalase proteins from different species revealed that the C-terminal residues are highly conserved (Figure 1.20).

Finally, catalase import is dependent on PEX5 and other import machinery components. In addition to the PTS1 consensus sequence, which interacts with the C-terminal TPR domain, catalase can be imported into peroxisomes via interactions with the N terminal domain of PEX5 (Oshima et al., 2008).



**Figure 1.19: Web-logo image of the C-termini of *A. thaliana* catalases.** The C-terminal 22 amino acids sequences of three catalases, including the non-canonical peroxisomal targeting signal type1; PNF, PSI, PSI for CAT1,2 and 3, respectively, are presented. Figure is designed using a sequence logo generator [WebLogo,(Crooks et al., 2004)].

```

P      MDPYKYPSSAYNTPFCTTNSGAPIWNNNTAVMSVGERGFI LLEDYQLIEKIIATFTTRERIE 60
M      MDPYKHRPSSAFNAPYWTNSGAPVWNNDSSTLVGARGPILLEDYHC-EKLANFDRERIE 59
R      MDPYKHRPSSSFNGPLWSTNSGAPVWNNNSLTVGSRGPILLEDYHLVEKLANFDRERIE 60
T      MDPYKYPSSAFNSTFCTTNSGAPVFNNSLTVGARGPV LLEDYHLVEKLANFDRERIE 60
At     MDPYKYPASSYNSPFFTTNSGAPVWNNNSMTVGP RGPILLEDYHLVEKLANFDRERIE 60

P      ERVVHARGASAKGFFEVTHTDVS DLS CADFLRAPGVQTPVIVRFSTVIHERVSPETVRDRP 120
M      ERVVHARGASAKGFFEVTHTDITHLT CADFLRAPGVQTPVIVRFSTVIHERGSPETLRDRP 119
R      ERVVHARGASAKGFFEVTHTDITHLT CADFLRAPGVQTPVIVRFSTVIHERGSPETLRDRP 120
T      ERVVHARGASAKGFFEVTHTDITHLT CADFLRAPGVQTPVIVRFSTVIHERGSPETLRDRP 120
At     ERVVHARGASAKGFFEVTHTDISNLT CADFLRAPGVQTPVIVRFSTVIHERGSPETLRDRP 120

P      GFAVKFYTREGNFDLVGNFPVFFV RDAMQFPDVIRAFKPNPKSHLQESWRFLDFCSYHE 180
M      GFAVKFYTREGNFDLVGNFPVFFV IRDGKIFPDMVHALKPNPRTHIQDNWRILDFFSHHP 179
R      GFAIKFYTREGNFDLVGNFPVFFV IRDGKIFPDMVHSLKPNPKSHVQENWRILDFFSHHP 180
T      GFAVKFYTREGNFDLVGNFPVFFV IRDGKIFPDMVHALKPNPKSHIQENWRVLDFFSHVP 180
At     GFAVKFYTREGNFDLVGNFPVFFV IRDGKIFPDMVHALKPNPKSHIQENWRILDFFSHHP 180

P      ESLLSEAWFYDDVGIPI NYRHMEGFVQAYSLINKAGKARLVKFWKPTCGVKSMLEEEA 240
M      ESLHMFSLFDDVGI PADYRHMDGSGVHTYTLVSRAGTVTVKFWWRPTCGVRS LMDDEA 239
R      ESLHMTFLFDDIGIPADYRHMDGSGVNTYTLVNRAGKSHYV KFWKPTCGVKSLDDEA 240
T      ESLHMTFLFDDIGIPQDYRHMDGSGVHTFTLINKAGKSTYV KFWKPTCGVKSLLEDEA 240
At     ESLNMTFLFDDIGIPQDYRHMDGSGVNTYMLINKAGKAHYV KFWKPTCGVKSLLEEDA 240

P      IRVGGSNHSHATQDLYES IAAGNFPEWRLYIQTIDYEDQNNY-DFEPLDTTIAWPEDVVE 299
M      VRC-GANHSHATKDLTDAIAAGNFPEWTLYIQTMDPEMEDRLD DLDPLDVTKTWPEDTFE 298
R      VTVGGTNHSHATQDLYDS IAAGNFPEWKLFIQTIDPDHEDRF-DFDPLDVTKTWPEDIVE 299
T      ARVGGANHSHATQDLYDS IAAGNFPEWKLFIQTMDPDHEDRF-DFDPLDVTKTWPEDILE 299
At     IRVGGTNHSHATQDLYDS IAAGNFPEWKLFIQI IDPADEKDF-DFDPLDVTKTWPEDILE 299

P      LRPVGRVLV LNKNI DNFFAENEMLAFSMS-LVPGIHYSDDKMLQARSFAVADTQRHRLGPN 358
M      LQPVGRVLV LNRNIDNFFAENEQLAFCPGLIVPGIYYSDDKLLQTRIFSYSDTQRHRLGPN 358
R      LQPVGRMVLNRNIDNFFSENEQLAFCPGIIVPGIYYSDDKLLQTRIFSYSDTQRHRLGPN 359
T      LQPVGRVLV LNKNI DNFFNENEQLAFCP SIVVPGVYYSDDKMLQTRIFSYSDTQRYRLGPN 359
At     LQPVGRMVLNRNIDNFFAENEQLAFCPAII VPGIHYSDDKLLQTRVFSYADTQRHRLGPN 359

P      YLQLFVNAPKCPHNNHHEGF MFMHRDEEVNYFPSRYDACRHA EKYPMPNVLSGKRER 418
M      YLLL PANAPKCAHNNHYDGS MNFMHRHEEVDFPSRYDAVRNAPRYPIPTAHIAGRREK 418
R      YLLL PPNAPKCAHNNHYDGS MNFMHRDEEVDFPSRYDPAKHAPRYPIPSATLTGRREK 419
T      YLQL PANAPKCAHNNHYDGS MNFMHRDEEIDYFPSRYDPVRHA EKYPPIPTMCTGKRER 419
At     YLQLFVNAPKCAHNNHHEGF MFMHRDEEVNYFPSRYDQVRHA EKYPTEPAVCSGKRER 419

P      CVIIPKENHNFQAGDRYRSWAPDRQERFVNRFVEALS DSKVTHEVRNIWISYWTQADRSL 478
M      TVISKEN-NFKQPGERYRAMD PARQERFITRWVDALSDPRLTHEIRTIWLSNWSQADRSL 477
R      VVIAKEN-NFKQPGERYRSWD PARQERFIKRWIDALSDPRLTHEIRSIWLSYWSQADRSL 478
T      CVIQKEN-NFNQPGERYRSFT PDRQERFIRRWEALS DPRITYEIRSIWISYWSQADKSL 478
At     CIIEKEN-NFEKPGERYRTFT PERQERFIQRWIDALSDPRITHEIRSIWISYWSQADKSL 478

P      GQKIASRMNARPNM 492
M      GQKLASRLSAKPSM 491
R      GQKLASRLSAKPSM 492
T      GQKLASRLNVRPSI 492
At     GQKLASRLNVRPSI 492

```

**Figure 1.20: Sequence alignment of *A. thaliana* CAT2 against number of catalase proteins from different plants.**

The amino acid sequences of different plant catalases were aligned using Clustal Omega software (Sievers et al., 2011). The numbers indicate the end of each segment in the corresponding sequence. Regions of identical amino acids are shown in grey. P, Pumpkin (*Cucurbita pepo*) CAT2; M, Maize (*Zea mays*) CAT2; R, Rice (*Oryza sativa subsp. Japonica*) CATC; T, Tobacco (*Nicotiana tabacum*) CAT1; At, *A. thaliana* CAT2.

### 1.9.8 Catalase assembly

The above discussion has shown that catalase assembly from its heme and polypeptide components in living cells is poorly understood (Prakash et al., 2002; Díaz et al., 2012; Nicholls, 2012). A model for catalase biogenesis has been proposed based on structural considerations as well as radioactive labelling studies in yeast and mammalian cells (Ruis, 1979; Zámocký and Koller, 1999; Nicholls et al., 2000). This model suggests that hemylation (heme insertion), apoprotein monomer folding and oligomerisation are extremely interconnected processes. The heme prosthetic group is thought to be inserted into the catalase apoprotein monomers, leading to the formation of a dimer, which finally oligomerizes into an enzymatically-active holo-tetramer (Baureder et al., 2014). Active catalase can be obtained *in vitro* by mixing purified apocatalase from *Enterococcus faecalis* catalase (KatA) with heme (Baureder et al., 2014). KatA is a small subunit (54-kDa) monofunctional catalase that is very similar to the mammalian catalase (Zámocký et al., 2012; Díaz et al., 2012). These results obtained are consistent with the proposed model for catalase biogenesis that is illustrated in Figure 1.21. However, little is known about how the heme prosthetic group is recognized by apocatalase or how it is trafficked. The *Enterococcus faecalis* catalase is able to assemble with (metal-free) protoporphyrin IX (Brugna et al., 2010). Hence, the initial association between apo-catalase and heme prosthetic group probably does not include the iron atom of the heme prosthetic group.

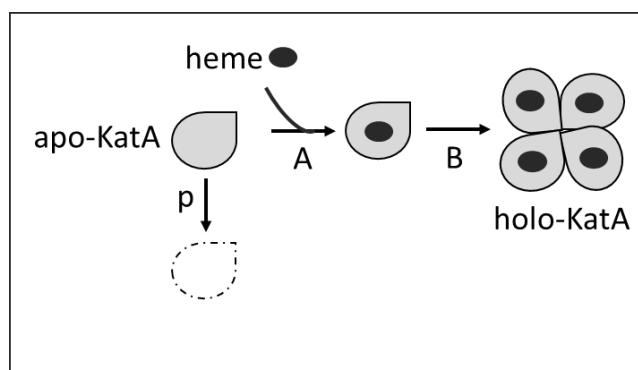


**Figure 1.21: A proposed model for catalase assembly.**

A schematic diagram displays the main steps of catalase biogenesis suggested by Baureder and co-workers (Baureder et al., 2014). Heme prosthetic group is acquired by catalase polypeptide (apo-KatA) (step A), followed by oligomerisation of hemylated monomers to form holo-tetramer (holo-KatA), which is enzymatically active (step B) (Baureder et al., 2014).

The mechanisms of catalase assembly and/or import could affect quality control in peroxisomes. For example, catalase inactivation triggers an accumulation of H<sub>2</sub>O<sub>2</sub>, which induces peroxisomal aggregation. These aggregates are degraded through the process known as pexophagy which is a form of autophagy.

### **1.10 Autophagy in plants**

The term autophagy originates from the Greek words “auto” meaning self and “phagy” meaning eating. Autophagy (self-eating) is a highly conserved mechanism that is found in all eukaryotic cells [reviewed in (Su et al., 2020)]. This important process maintains cellular homeostasis under most conditions by degrading protein complexes, aggregates and organelles via the action of lysosomes (in animals) or the vacuole (in plants and yeast) (Bassham et al., 2006; Bassham, 2007; Rabinowitz and White, 2010; Marshall and Vierstra, 2018; Qi et al., 2020). Autophagy in plants is often divided into three major types: microautophagy, macroautophagy, and mega-autophagy. Of these, macroautophagy is perhaps the best characterised [Reviewed in (van Doorn and Papini, 2013; Marshall and Vierstra, 2018; Su et al., 2020)].

The proteins that are responsible for the autophagy process (ATG proteins) are encoded by the autophagy-related genes (ATGs). More than 40 ATG genes have been identified in plants, most of which are homologous with animal and yeast ATGs [Reviewed in (Marshall and Vierstra, 2018; Su et al., 2020)]. In addition to general autophagy (nonselective degradation), highly selective mechanisms are present that ensure cellular quality control and stress responses [Reviewed by (Yoshimoto and Ohsumi, 2018)]. Pexophagy is a specialised selective autophagy mechanism that is involved in quality control of peroxisomes. It degrades excess and/or damaged peroxisomes [Reviewed by (Young and Bartel, 2016)]. The occurrence of pexophagy in plants was first postulated in the 1970s (Vigil, 1970). This study involved a castor bean endosperm that was isolated by sucrose density-gradient centrifugation and examined by electron microscopy. The image of peroxisomes surrounded by a double membrane suggested the possible existence of pexophagy in plants (Vigil, 1970).

However, since then accumulating evidence has demonstrated the presence of pexophagy in plants (Farmer et al., 2013; Kim et al., 2013; Shibata et al., 2013; Yoshimoto et al., 2014b; Yoshimoto and Ohsumi, 2018).

H<sub>2</sub>O<sub>2</sub> is generated as a byproduct of various metabolic pathways that are localised in various cellular compartments as described in Section 1.6. However, the accumulation of H<sub>2</sub>O<sub>2</sub> in the peroxisomal matrix may lead to oxidation of peroxisomal proteins and loss of the functional integrity of the peroxisomes (Van den Bosch et al., 1992; Eastmond et al., 2000; Adham et al., 2005; Fahnenstich et al., 2008). Several studies have shown that pexophagy actively clears damaged peroxisomes. For example, the peroxisome unusual positioning 1 (*peup1*), *peup2* and *peup4* mutants show accumulation of oxidised peroxisomal proteins (Shibata et al., 2013). Three lines contain mutations that are identical to three of the genes that are involved in the autophagy system (*ATG2*, *ATG18a* and *ATG7*). Hence, autophagy (pexophagy) plays an important role in the degradation of peroxisomes.

The accumulation of inactive catalase aggregates was also observed in the peroxisomes of *A. thaliana atg*-knockout mutant leaves (Yoshimoto et al., 2014a). This finding provides further evidence that accumulated peroxisomes are degraded by autophagy. Peroxisomal aggregation has also been observed in the *cat2* knockout mutants (Shibata et al., 2013), demonstrating that H<sub>2</sub>O<sub>2</sub> accumulation results in peroxisomal aggregation.

## 1.11 Aims

Taken together, there is little consensus in the literature regarding the importance of C terminal amino acids in catalase targeting. Previous studies have often used unphysiological levels of expression driven by the 35S promoter or transient expression systems. Moreover, studies using heterologous systems involve fusion of catalase to large reporter proteins, which may disturb catalase folding. The aim of the following studies was therefore to characterise CAT2 targeting in *A. thaliana* in a system that avoids these problems. The plan is to study these processes in a completely homologous system, in which catalase will be expressed under the control of the native promoter. It was noticed that there was an alternative splice variant of CAT2 in the TAIR database in which the last 18 amino acids were absent. The differential expression of this variant was examined under photorespiratory and cold stresses. The properties of this form will therefore be compared with wild type catalase and also a mutant in which the C terminal '3 last amino acids' have been replaced with a consensus PTS1 sequence (ARL).

The following objectives were designed to achieve the overall aim of gaining a more detailed mechanistic knowledge of CAT2 targeting in *A. thaliana*.

1. To introduce three CAT2 variants with modified C-termini into the *cat2-1* mutant background in order to define the role of the terminus in activity and import. This includes investigating the physiological and biochemical consequences of introducing CAT2 variants with modified targeting signals into the *cat2-1* mutant background.
2. To determine catalase location in the lines expressing each of the CAT2 variants using subcellular fractionation and split GFP techniques.
3. To use this information to determine the overall importance of C terminal amino acids in catalase targeting.

## Chapter 2 Materials and Methods

### 2.1 Materials

#### 2.1.1 Water

Sterilised distilled water and RNase-DNase free water were used in this study.

#### 2.1.2 Reagents

Reagents were obtained from a variety of sources, but routinely these included: Alfa-Aesar, Axygen, Badrilla, Bio-Rad, Bioline, Cayman, GE-Healthcare Amersham, Integrated DNA Technologies (IDT), Millipore, Qiagen, Seven Biotech Ltd and Sigma Aldrich.

#### 2.1.3 Restriction and modifying enzymes

Restriction enzymes DNA ligase were obtained from New England Biolabs and used with their relevant buffer system supplied by the manufacturer.

#### 2.1.4 Antibiotics

Hygromycin B (Hygromycin B, Alfa Aesar Catalog # j60681) and Kanamycin stock solutions (50 mg/ml) were prepared as follows: 0.5 g was dissolved with 10 ml of sterile distilled water. The stock solutions were sterilised using 0.22 µm syringe filter and kept at -20°C.

Chloramphenicol (25 mg/ml) stock solution was prepared as follows: 0.25g of chloramphenicol was dissolved with 10 ml of 95% EtOH. The stock solution was sterilised using 0.22 µm syringe filter and kept at -20°C. They were diluted as required, prior to usage.

#### 2.1.5 Commercial kits

Commercial kits used in this study are listed in Table 2.1.

**Table 2.1: Commercial kits used in this work**

Commercial kit	Source
DNeasy Plant Mini Kit	Qiagen, Germany
QIAprep® Spin Miniprep Kit	Qiagen, Germany
QIAGEN plasmid midi kit	Qiagen, Germany
RNeasy plant mini kit	Qiagen, Germany
TURBO DNA-free kit	Invitrogen, UK

QuantiTect reverse transcription kit	Qiagen, Germany
QIAquick gel Extraction Kit	Qiagen, Germany

### **2.1.6 Basic Medium**

All media were made up in distilled water and then autoclaved at 121°C for 20 minutes unless otherwise stated.

#### **2.1.6.1 Murashige and Skoog medium (MS)**

One litre of ½ MS was prepared according to the following protocol: 2.2g/L Murashige and Skoog Basal Medium, 0.1 g/L Myo-inositol, 0.5g/L MES, 10g/L sucrose, the pH was adjusted to 5.7 with 1 M potassium hydroxide (KOH). For plates agar (10 g) was added.

#### **2.1.6.2 Luria-Bertani medium (LB)**

One litre of LB medium was prepared as follows: 10g/L tryptone, 5g/L yeast extract, 10g/L NaCl. 5 N NaOH was used to adjust the pH to 7.0 prior to autoclaving. For solid media, 15 g/L bacto agar was added.

#### **2.1.6.3 SOC media**

Tryptone (2% w/v), Yeast extract (0.5% w/v), NaCl (10mM), KCl (2.5 mM), MgCl<sub>2</sub> (10 mM), MgSO<sub>4</sub> (10 mM), glucose (20 mM).

#### **2.1.6.4 Selection media**

The following antibiotics were added, when appropriate, to autoclaved media (hand hot) at the final concentration given: Hygromycin (50 µg/ml), kanamycin (50 µg/ml) and chloramphenicol (25 µg/ml).

### **2.1.7 Antibodies**

All antibodies used in this study are listed in Table 2.2.

### **2.1.8 Oligonucleotide primers**

Table 2.3 presents oligonucleotides used in this study.

**Table 2.2: Details of antibodies for western blot analysis.**

Primary antibody	Primary antibody dilution	Primary antibody manufacture catalogue #	Secondary antibody	Secondary antibody dilution	Secondary antibody manufacture catalogue #
Catalase	1: 1000	Agrisera (AS09501)	Goat anti-rabbit (HRP)	1:5000	Jackson ImmunoResearch Europe LTD. Product code #: 111-035-003
Catalase 2	1: 20,000	(Su et al., 2018)	Goat Anti-Mouse IgG H&L (HRP)	1:10000	Abcam (ab6789)
Catalase 3	1: 2000	(Su et al., 2018)	Goat Anti-Mouse IgG H&L (HRP)	1:10000	Abcam (ab6789)
UBQ11*	1: 10,000	Agrisera (AS08307)	Goat anti-rabbit (HRP)	1:5000	Jackson ImmunoResearch Europe LTD. Product code #: 111-035-003
RbcL**	1: 10,000	Agrisera (AS03037)	Goat anti-rabbit (HRP)	1:5000	Jackson ImmunoResearch Europe LTD. Product code #: 111-035-003
AtpB ***	1: 5000	Agrisera (AS05085-10)	Goat anti-rabbit (HRP)	1:5000	Jackson ImmunoResearch Europe LTD. Product code #: 111-035-003
GFP	1: 5000	Abcam (ab6556)	Goat anti-rabbit (HRP)	1:5000	Jackson ImmunoResearch Europe LTD. Product code #: 111-035-003
<p>* Ubiquitin                      ** Rubisco large subunit, form I and form II                      *** Beta subunit of ATP synthase (chloroplastic + mitochondrial)</p>					

**Table 2.3: List of the primers used in this work.**

All primers were prepared at 100 µM in sterilised distilled H<sub>2</sub>O and stored at -20°C.

<b>N°</b>	<b>Name</b>	<b>primer sequence (5' to 3')</b>	<b>Application</b>	<b>Source</b>	<b>Manufacture</b>
1	Cat2-1 RP	TCATGTGCCTTTTGACTTGTG	Forward primer for amplification of CAT2 in wild type	This thesis	Sigma Aldrich
2	cat2-1LP	AGAGGCAAGATATCCTCAGGC	Reverse primer for amplification of CAT2 in wild type	This thesis	Sigma Aldrich
3	LBb1.3	ATTTTGCCGATTTTCGGAAC	Specific primer for T-DNA insertion	T-DNA primer Design	Sigma Aldrich
4	Cat2-F	CGAGGTATGACCAGGTTTCGT	Genomic characterisation of transgenic lines	This thesis	Sigma Aldrich
5	Cat2-R	GATGCTTGGTCTCACGTTCA	Genomic characterisation of transgenic lines	This thesis	Sigma Aldrich
6	Cat2-1R	GACTTATCAGCCTGAGACCA	Genomic characterisation of transgenic lines	This thesis	Sigma Aldrich
7	Cat2-2R	GAACGAGACAATGACAGTAACAG A	Genomic characterisation of transgenic lines	This thesis	Sigma Aldrich
8	Cat2-11R	TTCTGTCCCAAAGACTTATCAGCC TG	Genomic characterisation of transgenic lines	This thesis	Sigma Aldrich
9	Cat2- ARL	GTACAAGAAAGCTGGGTCTTAGA AGTCT	Genomic characterisation of transgenic lines	This thesis	Sigma Aldrich
10	ACT2up2	TTCCCTCAGCACATTCCAGCAG	RT-qPCR	Queval <i>et al.</i> 2007	Sigma Aldrich

11	ACT2do	TTAACATTGCAAAGAGTTTCAAGG	RT-qPCR	Queval <i>et al.</i> 2007	Sigma Aldrich
12	qPCRact2 up	CTGTACGGTAACATTGTGCTCAG	RT-qPCR	Queval <i>et al.</i> 2007	Sigma Aldrich
13	qPCRact2do	CCGATCCAGACACTGTACTTCC	RT-qPCR	Queval <i>et al.</i> 2007	Sigma Aldrich
14	qPCRcat1up	CTTCGATCCGCTTGATGTCAC	RT-qPCR	Queval <i>et al.</i> 2007	Sigma Aldrich
15	qPCRcat1do	GGAACCACAAGAGCAGGACAG	RT-qPCR	Queval <i>et al.</i> 2007	Sigma Aldrich
16	qPCRcat2up	TGCTGGAAACTACCCTGAATGG	RT-qPCR	Queval <i>et al.</i> 2007	Sigma Aldrich
17	qPCRcat2do	TCAACACCATACGTCCAACAGG	RT-qPCR	Queval <i>et al.</i> 2007	Sigma Aldrich
18	qPCRcat3up	CCACTTGATGTGACCAAGATCTG	RT-qPCR	Queval <i>et al.</i> 2007	Sigma Aldrich
19	qPCRcat3do	GTAGATTCCAGGAACCACAAGAC C	RT-qPCR	Queval <i>et al.</i> 2007	Sigma Aldrich
20	qPCRgpx6up	GATGTTAACGGTGACAAAGCTG	RT-qPCR	Queval <i>et al.</i> 2007	Sigma Aldrich
21	qPCRgpx6do	TTGGTGCGAAACGATCG	RT-qPCR	Queval <i>et al.</i> 2007	Sigma Aldrich
22	qPCRgstF8up	CGAAGGTAAGCTCCAGAAAGTC	RT-qPCR	Queval <i>et al.</i> 2007	Sigma Aldrich
23	qPCRgstF8do	AGAGTCAAAGAGCACCTTGGAG	RT-qPCR	Queval et al 2007	Sigma Aldrich
24	qPCRhsp17up	GGAGAAAGAAGATAAGAATGACA CG	RT-qPCR	Queval et al 2007	Sigma Aldrich
25	qPCRoxi1up	GTTGAGGAAATCAAGGGTCATG	RT-qPCR	Queval et al 2007	Sigma Aldrich

26	qPCRoxi1do	TGGACGATATTCTCCACATCC	RT-qPCR	Queval et al 2007	Sigma Aldrich
27	ATG2 F	GGCTAGTGAAGGGAGTCCAA	RT-qPCR	This thesis	Sigma Aldrich
28	ATG2 R	GGGGTTGTGGCAATGATGG	RT-qPCR	This thesis	Sigma Aldrich
29	ATG7 F	GTACCGCTTGCTCTGAAACC	RT-qPCR	Wang et al. 2015	Sigma Aldrich
30	ATG7 R	GTCTTCCCAGTCGAGGTTGA	RT-qPCR	Wang et al. 2015	Sigma Aldrich
31	CTSPF2	CTTACAACCTCTCCCTTCTTCACCA CCAACCT	C-terminal sequencing	This thesis	IDT
32	CTSPR2	TGTTTGAACGATCGGGGAAATTC GA	C-terminal sequencing	This thesis	IDT
33	CTSPR3	ACCCGCCAATATATCCTGTCAAA CAC	C-terminal sequencing	This thesis	IDT
34	CAT1RT F	ACCGTCTTGGACCAAACCTATCTG	Semi-quantitative-RT-PCR	Hu <i>et al.</i> 2010	Sigma Aldrich
35	CAT1RT R	GAAACCAAACCGTAAGAGGAGCA	Semi-quantitative-RT-PCR	Hu <i>et al.</i> 2010	Sigma Aldrich
36	ForRTCAT2	CTCCAAGCTCTCTTCTCATCAAAC C	Semi-quantitative-RT-PCR	This thesis	IDT
37	RevRTCAT2	TCAGGGAACCTTCATCCCATCGC	Semi-quantitative-RT-PCR	This thesis	IDT
38	CAT3RTF	GCCTTGGACCGAATTATTTGCAG	Semi-quantitative-RT-PCR	Hu <i>et al.</i> 2010	Sigma Aldrich
39	CAT3RTR	GACAAGAAACAACAACACATGTG	Semi-quantitative-RT-PCR	Hu <i>et al.</i> 2010	Sigma Aldrich
40	CAT2PSIF	TGGGTTGGTACCGATCCTTACAA GT ATCGTCCAGCTAGTTC	C-terminal PCR product	This thesis	IDT

<b>41</b>	CAT2PSIR	GGTCCACTAGTTTGATGCTTG GTCTCACG TTCAGAC	C-terminal PCR product	This thesis	IDT
<b>42</b>	CAT2WSQVR	GGTCCACTAGTTTCACCTGAGA CCA GTAAGAGATCCAG	C-terminal PCR product	This thesis	IDT
<b>43</b>	CAT2ARLR	GGTCCACTAGTTTAGAGTCTTG CT CTCACG TTCAGAC	C-terminal PCR product	This thesis	IDT

## 2.1.9 Size markers

### 2.1.9.1 DNA size markers

Gene ruler 1kb DNA ladder (Thermo Scientific, UK) was used according to the manufacturer's instructions. Aliquots were prepared and stored at -20°C.

### 2.1.9.2 Protein size markers

CSL-BBL prestained protein ladder (Cleaver Scientific, UK) is ranged from (10- 245kDa) was used. Aliquots were prepared and stored at -20°C.

## 2.1.10 *Escherichia coli* (*E. coli*) strains

*E. coli* strains used in this study are listed in Table 2.4.

**Table 2.4: *E. coli* strains used in this study**

<i>E. coli</i> strain	Genotype	Purpose	Source
One Shot® TOP10 Chemically Competent cells	F- mcrAΔ( mrr-hsdRMS-mcrBC) Φ80lacZΔM15 Δ lacX74 recA1 araD139 Δ( araleu)7697 galU galK rpsL (StrR) endA1 nupG.	Plasmid transformation	Lab stock
XL-10 gold ultra competent cells	TetrD(mcrA)183 D(mcrCB-hsdSMR-mrr)173 endA1 supE44 thi-1 recA1 gyrA96 relA1 lac Hte [F' proAB lacIqZDM15 Tn10 (Tetr) Amy Camr].	Plasmid transformation	Lab stock
Library Efficiency DH5a Competent Cells	F- Φ80lacZΔM15 Δ(lacZYA-argF)U169 recA1 endA1 hsdR17(r <sub>k</sub> m <sub>k</sub> <sup>+</sup> ) phoA supE44 thi-1 gyrA96 relA1 λ <sup>-</sup>	Plasmid transformation	Invitrogen CAT# 18263012

## 2.2 Methods

### 2.2.1 Transgenic lines and CAT2 constructs

Plasmids corresponding to 971 [cat2promoter-CAT2-PSI-3UTR-nos], 972 [cat2promoter-CAT2-WSQV-3UTR-nos], and 973 [cat2promoter-CAT2-ARL-3UTR-nos] were generated by Dr Elena Zubko (Appendix C.1.2). Briefly, they were generated by cloning the *CAT2* cDNA under the control of *CAT2* promoter with a native C-terminus, an alternative splice variant and a version that has a consensus PTS1 sequence ARL at the C terminus. These constructs were then transformed into *cat2-1* mutant background by Dr Barbara Karpinska. The generated lines were termed PSI, WSQV and ARL for simplicity (PSI, WSQV and ARL containing constructs 971,972 and 973, respectively). Transgenic plants were available at the start of the project.

Dr Barbara Karpinska provided one independent homozygous line of the transgenic plants, whilst the other lines were obtained from T1 during the course of this study (T1 seeds were also provided by Dr Barbara Karpinska). T3 seeds were used for experiments (Figure 2.1). More details are provided in appendix A.

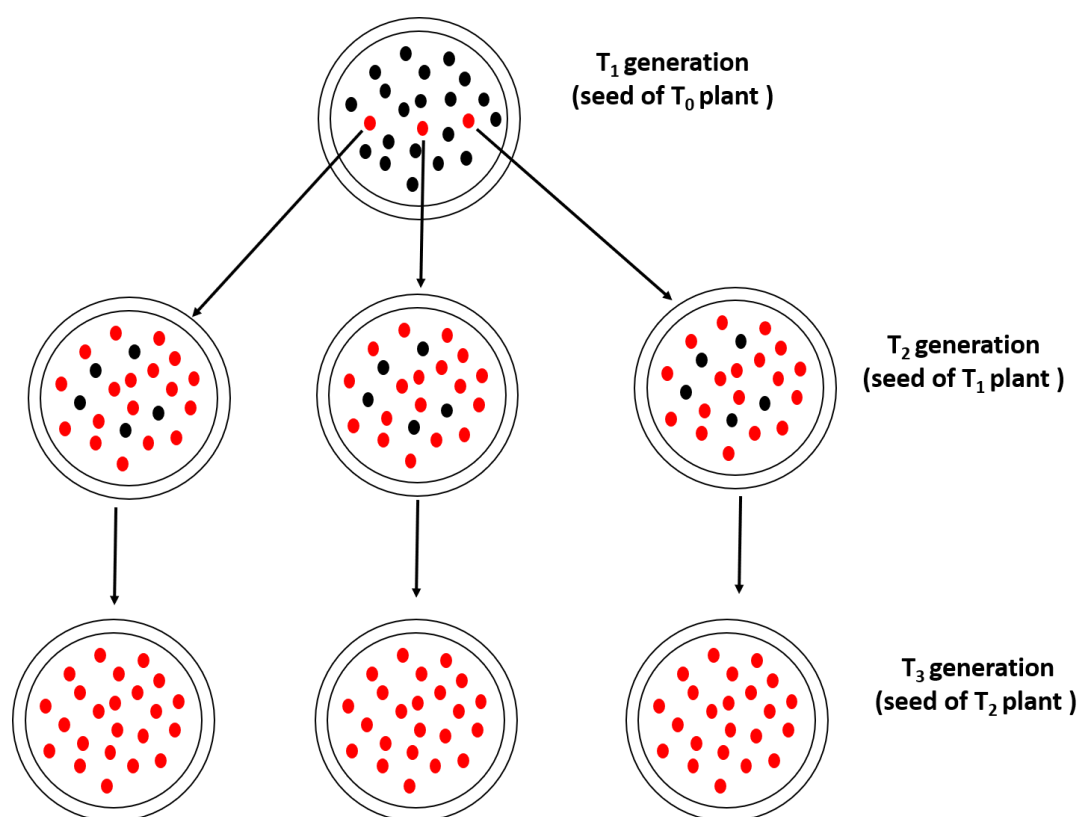


**Figure 2.1: Schematic representation for selecting homozygous transformed plants.**

Red colour shows resistant seeds, whereas black colour represents sensitive seeds. Resistant seeds undergo another round of selection on  $\frac{1}{2}$  MS containing hygromycin to find a plate with a 3:1 ratio of resistant plants (T<sub>2</sub> generation, single insert). Seeds were then collected from these plants and then used to find a plate with 100 resistance (T<sub>3</sub> generation ,homozygous plants).

## **2.2.2 Seed sterilisation**

All seeds were sterilised to prevent contamination on the agar plates using a bleach solution and hydrogen chloride (HCl). In a fume hood, the seeds of each line were placed in open Eppendorf tubes in a dessicator jar containing a beaker of 100ml of bleach. Prior to sealing the dessicator jar, 3ml of concentrated HCl was added to the bleach. The seeds were sterilised using the chlorine gas from this solution for 3-6 hours.

## **2.2.3 Plant material and growth conditions**

### **2.2.3.1 Plant material**

*Arabidopsis thaliana* wild type lines (Col-0) were provided by Dr Barbara Karpinska (Prof. Christine Foyer's lab, University of Leeds, UK). The T-DNA catalase mutant was obtained from Nottingham Arabidopsis Stock Centre, Nottingham University, UK. The *cat2-1* mutant was previously described (Queval et al., 2007) with an accession number SALK\_057998.55.00 which carries the T-DNA in the third exon from the 5' end of the *CAT2* (At4g35090) gene. In contrast, the SALK\_076998 was characterised and named as *cat2-1* (Bueso et al., 2007), and this nomenclature has been adopted by TAIR. Therefore, the mutant published as *cat2-1* by Queval corresponds to *cat2-2* according to TAIR. In this work, the original nomenclature of Queval et al. (2007) is used.

### **2.2.3.2 Growth conditions and sampling**

For all experiments, wild type and *cat2-1* mutant seeds were sterilised (Section 2.2.2) and sown on ½ MS, while the transgenic seeds were sown on ½ MS containing 50 µg/ml hygromycin. Seeds were then stratified for two days in the dark at 4°C. After stratification, seeds were transferred to a growth chamber (16hr light) and incubated for 6 hours at 20°C in continuous white light (150-200 µmol m<sup>-2</sup> s<sup>-1</sup>) to stimulate germination. The plates were then wrapped in aluminium foil and incubated for two days at room temperature. The foil was removed, and plates were placed for five days in a 16 hours light. Then, seedlings (i.e. same size) were transferred into the soil.

After transplanting the seedlings, they were covered with a plastic dome for the first week to maintain humidity and kept in a controlled environment growth chamber (Day length: 8 hrs, Day and night temperature 20°C, lights on: 10.00, lights off: 18.00, humidity 60 %) for four weeks. After that, they were moved to long-day conditions (Day length: 16 hrs, day and night temperature 21°C, lights on: 6.00, lights off: 22.00, humidity 60 %) for further one week. All samples were collected and rapidly frozen in liquid nitrogen and stored at -80°C.

#### **2.2.4 Selection on hygromycin**

Seeds were sterilised and sown as described in sections 2.2.2 and 2.2.3.1, respectively. Following the light treatment, hygromycin resistant seedlings were then transferred onto soli. Hygromycin resistant seedlings were standing tall like normal dark grown seedlings with long hypocotyls and closed cotyledons. In contrast, hygromycin sensitive seedlings were lying on medium with very short hypocotyls and open cotyledons (Appendix A, Figure A1).

#### **2.2.5 Photorespiratory test**

To study the phenotype under photorespiratory conditions, seeds of wild type, *cat2-1* mutant and transgenic lines were sterilised as described in section 2.2.2 and grown in Petri dishes on ½MS at 22°C and long-day conditions (16h light/8h dark; light intensity [ $100\mu\text{mol m}^{-2} \text{s}^{-1}$ ]) following the protocol described by (Waszczak et al., 2016). Each plate was divided into five parts, each part contained 6-8 seedlings. After 21 day of growth, the Micropore tape which sealed the round plates was replaced by two layers of parafilm (PM-992, Neenah, WI 54956, USA). Plates were then transferred to continuous light conditions (24h/light, 22°C day and night temperature, 60% humidity and light intensity [ $100\mu\text{mol.m}^{-2}.\text{s}^{-1}$ ]) for 7 days. Plates were photographed using a Nikon D5100 digital camera. Samples were collected and used for chlorophyll assay.

## **2.2.6 Isolation of genomic DNA**

### **2.2.6.1 Edward's method**

This method is modified from (Edwards et al., 1991). Leaf samples were ground in liquid nitrogen and DNA was extracted in 400µl of extraction buffer prepared as follows: 200 mM Tris-HCl pH 7.5, 250 mM NaCl, 25 mM EDTA, 0.5 % (w/v) SDS. The mixture was centrifuged for 5 min at 14000 rpm and 4°C in a microcentrifuge. 350µl of the supernatant was transferred to a new Eppendorf tube contain 350µl of ice-cold isopropanol. The mixture was then centrifuged for 5 min at 4°C and 14000 rpm. Following the centrifugation, the supernatant was removed, and the pellet was washed twice with 1 ml of 80 and 70 % (v/v) ethanol, respectively. The ethanol was then removed and then any residual ethanol allowed to evaporate. Following the evaporation of the ethanol, DNA was resuspended in 100 µl of sterile distilled water.

### **2.2.6.2 DNA extraction kit**

100 mg of 4-week-old tissues were ground into a fine powder using liquid nitrogen. DNA was isolated using the DNeasy Plant Mini Kit following the manufacturer's instructions.

### **2.2.6.3 Measurement of extracted DNA quality and quantity**

DNA concentrations were determined using Thermo Scientific Nano Drop™ 1000 Spectrophotometer. Initially, 1.5µl of sterilised water was used as a blank. Subsequently, 1.5µl of each DNA sample was used to measure the concentration of DNA in ng/µl. To determine the quality of the extracted DNA in each sample and to measure the purity, absorbance was measured at 260nm and 280 nm, and the ratio of 260/280 was used to determine the presence of proteins and other impurities in the sample.

## **2.2.7 Preparation of plasmid DNA.**

5 ml LB media supplemented with appropriate antibiotic were incubated with a single colony and grown overnight at 37°C on a shaker at 200 rpm. The cell suspension was centrifuged using 13,000 rpm for 10 min. Plasmid DNA was isolated using QIAprep® Spin Miniprep Kit, which is based on alkaline lysis of bacterial cells, followed by adsorption and elution of plasmid DNA using a specific membrane (silica) in the presence of high-salt and low-salt buffer to

certify that the only DNA will be adsorbed, while the other substances will be found in the flow-through. DNA was eluted from the spin column using 50  $\mu$ l sterile distilled water.

### **2.2.8 Gel purification of DNA fragments**

A gel slice containing the DNA band was excised from the agarose gel using a clean, sharp scalpel. The gel slice was weighed in an Eppendorf tube. The purification steps were then proceeded using the gel extraction kit (QIAquick gel Extraction Kit, Qiagen) in accordance with the manufacturer's instructions.

### **2.2.9 Polymerase chain reaction (PCR)**

#### **2.2.9.1 Standard PCR**

PCR for amplification of DNA fragments was performed using BioMix™ Red (Bioline, London, UK) with a 1x final working concentration. PCR was performed in 0.2 ml PCR tubes with 20 $\mu$ l of final volumes of the reaction mix. The reaction mixture consists of 2  $\mu$ l of each forward and reverse primers (0.5  $\mu$ M final concentration), 2  $\mu$ l DNA (100 ng/ $\mu$ l), 10  $\mu$ l BioMix and 6  $\mu$ l sterilised ultrapure water. Reactions were run in a thermal cycler with the following conditions: an initial denaturation step was performed at 94°C for 45 seconds, followed by (30-40) cycles of amplification consisting of a denaturation step at 94°C for 10 seconds, an annealing step at (56.0-60.0) °C for 30 seconds, and an extension step at 72°C for 40 seconds. This was followed by a final extension step at 72°C for 5 minutes. The annealing temperature was occasionally changed depending on the melting temperature ( $T_m$ ) of the primers. It was typically 5°C below the  $T_m$ .

#### **2.2.9.2 Real-time PCR**

Total RNA was extracted from leaves of 4-week -old *Arabidopsis thaliana* wild type, *cat2-1*, PSI, WSQV and ARL with RNeasy plant mini kit (QIAGEN) and treated with TURBO DNA-free kit (Invitrogen) to remove the remaining genomic DNA prior to RT-qPCR, according to the manufacturer's instructions. 1 $\mu$ g RNA was used for cDNA synthesis. Reverse transcription was performed using QuantiTect reverse transcription kit (QIAGEN). Real-time PCR reactions were assayed using a CFX connect real-time PCR system (Bio-Rad Laboratories, Hercules, CA, USA).

The 20 µl reaction volume was comprised of 10 µl 2X Brilliant<sup>®</sup> II SYBR<sup>®</sup> Green qPCR master Mix (Agilent, CAT#600828-51), 2 µl (1/50 dilution) cDNA, 6 µl H<sub>2</sub>O, 2 µl of each forward and reverse primer (0.5 µM final concentration).

Real-time cycler conditions were as follows: incubation 95°C for 5 min; 39 cycles of amplification consisting of 95°C for 10 sec and 30 sec at 60°C. Three biological replicates of each sample were processed and per sample two-three technical replications were performed. Reactions were performed in low-profile 96 well PCR plates (Axygen, Cat #: 19117002, Mexico). All transcripts were normalised to independent constitutive gene, which was *ACTIN2* (see melting curve, Appendix A.3). In all cases, catalase transcripts were quantified in samples taken at the same times of day as samples for the other experiments.

#### **2.2.9.3 Semi-quantitative RT-PCR**

The isolated RNA was used to generate cDNA (method described above). This cDNA (1/10 dilution) was used as a template in semi-quantitative RT-PCR reactions using catalase gene specific primers. Transcripts of the catalase genes in wild type, *cat2-1* and *cat2-1* transformed with PSI, WSQV and ARL variants were analysed after 20, 30 and 40 cycles on 1 % (w/v) agarose gel.

#### **2.2.9.4 Agarose gel electrophoresis**

Agarose gel intended for electrophoresis was prepared by dissolving 1g Agarose in 100ml of 1x Tris-acetate-EDTA (TAE) buffer. 1X TAE buffer was prepared as follows: 40 mM Tris, 20 mM acetic acid, and 1 mM EDTA by heating. Once cooled, 2 µl of 1x SYBR<sup>®</sup> safe DNA gel stain (Qiagen NV, Hilden Germany) was added to allow visualisation of DNA under ultraviolet (UV) light. Electrophoresis was conducted at a constant voltage of 100 V in 1X TAE buffer for 40 min.

#### **2.2.9.5 RNA quality**

RNA quality was assessed using Agilent 2100 bioanalyser (G29388, serial # DE24802242) or gel electrophoresis. RNA samples were prepared and analysed according to the instrument's manual. Some RNA samples were also analysed by gel-electrophoresis.

To assess the quality of RNA by gel electrophoresis, gel tank was washed with DEPC treated water (1ml of Diethyl Pyrocarbonate was mixed with 1 litre of distilled water. Incubated and autoclaved). RNaseZap<sup>®</sup> (Sigma, R2020-250ml, 069K0661) was used for pipettes and tools decontamination. 2 µl of RNA with 2 µl of GelPilot loading dye (5X, Lot No. 163030905) and 8 µl RNase free water were mixed together and loaded into 1% agarose gel (1g agarose in 100ml 1 XTAE in DEPC-water). Gel was run for 40 min at 70V. The representative images of bioanalyser and gel electrophoresis results are shown in Appendix A.2.

## **2.2.10 Protein extraction and measurement**

### **2.2.10.1 Protein extraction**

100 mg of wild-type (Col-0), *cat2-1* mutant and transgenic lines leaf tissues were ground with liquid nitrogen using chilled pestle and mortars. 1 ml extraction buffer (2% (w/v) LDS, 10mM Tris pH 8.5, 0.5 mM EDTA, 10 % (v/v) glycerol, 2mM(w/v) DTT, 2µl (w/v) protease inhibitors (Pierce<sup>™</sup> protease inhibitor tablets, Thermo scientific, Prod# A32963, one tablet was dissolved in 50ml of buffer) was added into each extract. The soluble protein was vortexed then centrifuged at 14000 rpm at 4°C for 10 min. The supernatants were removed and quantified using BCA assay (Thermo scientific, Pierce<sup>™</sup> BCA protein assay reagent A and B with prod # 23223 and 23224, respectively).

### **2.2.10.2 Preparation of protein samples**

Total protein concentrations of wildtype, *cat2-1*mutant and transgenic lines were determined using BCA assay, leaf extract containing 5-20µg of protein were mixed with 1X of loading buffer (4x Laemmli sample buffer, prod# 1610747, Bio-Rad). The samples were heated for 5 min at 90°C to denature the proteins.

### **2.2.10.3 SDS-polyacrylamide gel electrophoresis (SDS-PAGE)**

12 % gel was prepared for separation. This was prepared with separating buffer (2.6 ml ddH<sub>2</sub>O, 3.2 ml 30 % (w/v) acrylamide (Severn Biotech Ltd, prod# 20-2100-05), 2.0 ml 1.5 M Tris pH 8.8, 0.08 ml 10 % (w/v) SDS, 0.08ml 10% (w/v) ammonium persulphate (APS), 0.008ml Tetramethylethylenediamine (TEMED) (Sigma, prod#101125341).

This solution was transferred into the cast and was kept for 20 min. After that, 4 % stacking gel was prepared as follows: 3 ml ddH<sub>2</sub>O, 0.67 ml 30 % (v/v) acrylamide, 1.25 ml 0.5 M Tris pH 6.8, 0.05 ml 10 % (w/v) SDS, 0.05 ml 10% APS and 0.005 ml TEMED.

The stacking gel was immediately added into the separating gel and the comb was inserted into the stacking gel solution. This was left for 20 min, and then the gel comb was removed carefully. Afterwards, the gel was placed in the gel tank, and it was filled with running buffer (25 mM Tris base, 192 mM Glycine, 0.1 % SDS (w/v), pH 8.3). 18 µl of lysates were loaded into the gel wells. The electrophoresis was performed at 100V for 60 min. Bio-Rad Mini protean 3 electrophoresis system was used.

#### **2.2.10.4 Native-PAGE**

100 mg tissues of leaves of 4-weeks wild type, *cat2-1*, PSI, WSQV and ARL were ground to a powder in liquid nitrogen and then homogenised in native extraction buffer [100 mM Tris-HCl, pH 8.0, 20% glycerol and 30 mM dithiothreitol (DTT)]. After centrifugation at 14000 rpm for 30 min at 4 °C, the supernatant was recovered, and protein concentration was determined using Nanodrop (protein A280). 20 µg of total protein was separated by 7.5% native gel (Bio-Rad) 5h (70 V) at room temperature in electrophoresis buffer (192 mM glycine, 25 mM Tris-HCl, pH 8.3).

#### **2.2.10.5 Staining of the SDS-PAGE gel**

##### **2.2.10.5.1 Coomassie blue staining solution**

The stain was prepared by mixing 2.5g Coomassie brilliant blue R (0.25% w/v), 500ml methanol (50% v/v), 100ml acetic acid. 400ml of dH<sub>2</sub>O was added to obtain a final volume of 1 Litre. (Kept in the dark at room temperature).

##### **2.2.10.5.2 Destain solution**

The destain solution was prepared by mixing 150ml of methanol (15% v/v), 100ml acetic acid (10% v/v). 750ml of dH<sub>2</sub>O was added to obtain a final volume of 1 Litre. (Kept in the dark at room temperature).

### **2.2.10.5.3 Staining method**

Coomassie stain was used to visualise proteins separated by SDS-PAGE. Following electrophoresis, the gel was stained with 25ml of Coomassie stain (Section 2.2.10.5.1) and incubated for 60 min at room temperature with shaking. The gel was then destained several times with a de-staining solution (Section 2.2.10.5.2) and incubated overnight with agitation. After that, the gel was washed with dH<sub>2</sub>O. The washing step was performed several times to remove any background staining and enable the visualisation of protein bands.

### **2.2.10.6 Western Blotting**

Proteins were transferred from the SDS-gel to nitrocellulose membranes (GE-Healthcare Amersham™ Protran™ NC Nitrocellulose Membranes) for 60 min at 100 V in transfer buffer (25 mM Tris base, 192mM Glycine, 20 % methanol; pH 8.3) to enable the following immunodetection. Blots were blocked with 5 % (w/v) low fat dried milk in Tris-Buffered with Tween (20mM Tris-HCl, 150 mM NaCl, 0.1 % (v/v) Tween 20 pH 7.6) for (60-30) min at room temperature (RT) with shaking. The membranes were incubated with primary antibodies overnight at 4°C with agitation. The primary antibodies were decanted, and the blots were washed three times with TBS-T for 5-15 minutes each time at RT. Blots were incubated in secondary antibodies for 1 hour at RT with shaking. The blots were washed three times for 5-15 minutes each time and developed in a dark room for 1-5 min using chemiluminescence substrate (super signal west Dura, USA). All antibodies used in this study are listed in Table 2.2.

## **2.2.11 Biochemical assays**

### **2.2.11.1 Catalase activity assay**

Catalase activity assay was performed according to (Veljovic-Jovanovic et al., 2001; Noctor et al., 2016). Briefly, 100 mg of leaf material of wildtype, *cat2-1* mutant and transgenic lines were ground in liquid nitrogen. 1.5 ml 0.1 M NaH<sub>2</sub>PO<sub>4</sub>, 1mM EDTA was added to the extract. The homogenates were centrifuged for 10 min at 4°C, and the supernatants were used for the assay.

Catalase was determined by the decrease in absorbance at 240 nm ( $\epsilon_{M40} M^{-1} cm^{-1}$ ) following the addition of 10 $\mu$ l extract to a mixture containing 0.1 M NaH<sub>2</sub>PO<sub>4</sub>, 1mM EDTA and 2M H<sub>2</sub>O<sub>2</sub> (initial concentration). Additionally, different amounts of extract were assayed to ensure that the assay was linear with respect to the amount of extract added.

#### **2.2.11.2 Catalase activity using an in-gel activity assay**

Analysis of catalase using in-gel activity assay was carried out using the protocol described in (Weydert and Cullen, 2010). Briefly, after protein separation (Section 2.2.10.4), the gels were rinsed twice with dH<sub>2</sub>O (10 min each), incubated for 10 min in a 0.003% H<sub>2</sub>O<sub>2</sub> solution (by mixing 10 $\mu$ l of H<sub>2</sub>O<sub>2</sub> 30% solution (v/v) with 100 ml dH<sub>2</sub>O) and rinsed again twice with dH<sub>2</sub>O (5 min each). The staining was performed in a solution containing 2% ferric chloride (w/v) and potassium ferricyanide (w/v) until achromatic bands became visible. The reaction was stopped by extensively rinsing with dH<sub>2</sub>O.

#### **2.2.11.3 Ascorbate assay**

##### **2.2.11.3.1 Sample preparation and neutralisation**

Ascorbate was measured following the protocol described in (Queval and Noctor, 2007; Noctor et al., 2016) with minor modifications. 100mg of frozen leaves of wildtype, *cat2-1* mutant and transgenic lines were ground to a fine powder in liquid nitrogen using pre-cooled pestles and mortars. 1ml of perchloric acid (HClO<sub>4</sub>) was added to the sample while it was still frozen. The homogenates were centrifuged at 14000 rpm and 4°C for 3 min and then the supernatants were transferred to a new tubes. 100 $\mu$ l 0.2 M phosphate buffer pH5.6 was added to 0.2 ml supernatant, then 15-16  $\mu$ l of 5 M potassium carbonate (K<sub>2</sub>CO<sub>3</sub>) was added to the extract to adjust the pH. The pH was determined using pH strips (pH Test Strips 0.0-6.0, SIGMA, P-4661) which had been divided to ½ the original strip to reduce loss of extract. The pH of the extract was 6.0 after adjusting. Following the pH adjusting, the mixture was centrifuged, and the supernatant was transferred to a new tube. The final supernatant was used for the assay.

### **2.2.11.3.2 Reagents for ascorbate assay**

A stock solution of ascorbate oxidase (AO) (Ascorbate Oxidase, *Cucurbita* sp. Cat: 189724-1000U, Millipore) was prepared by dissolving 1 KU of the enzyme in 25ml of 0.2 M NaH<sub>2</sub>PO<sub>4</sub> pH 5.6 to obtain a final concentration of 40 U.mL<sup>-1</sup>. This stock was divided into aliquots and stored in the freezer (-20°C), until use.

### **2.2.11.3.3 Assay**

Reduced ascorbate (AsA) and total ascorbate [AsA plus oxidised form dehydroascorbate (DHA)] were determined by decrease in absorbance (the difference between endpoint and starting point until the absorbance became stable) at 265 nm at 25°C on a FLUOstar Omega microplate reader (BMG Labtech) using Greiner F-bottom 96-well UV-transparent plates. For AsA, 0.005ml (0.2 Unit) of AO was added to a mixture mix containing 40 µl extract, 100 µl 0.2 M phosphate buffer pH 5.6 and 55 µl H<sub>2</sub>O.

For total ascorbate, the DHA was reduced to ascorbate by incubating the extract with dithiothreitol (DTT) as follows: 100 µl of neutralised sample was incubated with 140 µl 0.2 M phosphate buffer pH 7.5 and 10 µl 25mM DTT at room temperature for 30 min. After that, total ascorbate was assayed in the reaction mixture of the AsA. The amount of DHA was calculated by subtraction of AsA from total ascorbate. The amount of ascorbate was calculated using the extinction coefficient ( $A_{265}=14000\text{mol/L}$ ; 0.014 nmol/ml).

### **2.2.11.4 Glutathione assay**

#### **2.2.11.4.1 Sample preparation and neutralisation**

Samples were prepared and neutralised, as described in section 2.2.11.3.1.

#### **2.2.11.4.2 Reagents for glutathione assay**

10mM NADPH and 12mM 5,5`-dithiobis-2-nitrobenzoic acid (Ellman's reagent, DTNB) reagents were prepared fresh in 0.2M NaH<sub>2</sub>PO<sub>4</sub> (pH 7.5), 10mM EDTA reaction buffer. After that, aliquots were made from NADPH and stored in freezer (-20°C), whereas the DNTB solution was kept in the dark at 4°C.

Moreover, glutathione reductase (GR) was prepared by centrifuging 0.100 ml of GR stock (Glutathione Reductase, From Baker's Yeast. SIGMA, G3664-2.5KU) and resuspending the pellet in 2.3 ml of 0.2M NaH<sub>2</sub>PO<sub>4</sub> (pH 7.5), 10mM EDTA to achieve a final concentration of 20U.

#### **2.2.11.4.3 Assay**

Total glutathione (GSH and GSSG) and oxidised glutathione (GSSG) were determined as the Glutathione reductase (GR)-dependent reduction of DTNB. Change in absorbance at 412 nm was measured on a FLUOstar Omega microplate reader (BMG Labtech) using Greiner F-bottom 96-well UV-transparent plates.

To distinguish between both forms of oxidised (GSSG) and reduced (GSH), GSSG is measured by treating the extracts with GSH-complexing reagent; 2-vinylpyridine (VPD). Total glutathione is measured without pre-treatment the extract.

For total glutathione, the reaction mixture contained 20 µl extract, 100 µl 120mM NaH<sub>2</sub>PO<sub>4</sub> pH 7.5, 50 µl H<sub>2</sub>O, and 10 µl 10mM NADPH, 10 µl 12mM DTNB. The reaction was started by adding 10 µl 0.2 U of GR to the wells. For oxidised glutathione, 200 µl of extracts were treated with 3 µl VPD at room temperature for 30 min. Following the incubation, the mixtures were centrifuged twice at 4°C for 10 min. 140 µl of supernatants were transferred to new tubes and then centrifuged again. 20 µl of supernatants were measured using the same reaction mixture used for total glutathione assay.

The total and oxidised glutathione in all leaves were calculated from the equations derived from the linear part of its standard curves. Moreover, the concentration of reduced glutathione was calculated from the formula: GSH = total glutathione - (2\* GSSG).

#### **2.2.11.5 Hydroxypyruvate reductase assay**

Hydroxypyruvate reductase (HPR) activity was measured by monitoring the NADH oxidation at 340 nm (Cooper and Beevers, 1969). The reaction mixture (1 ml total volume) contained 200 mM KH<sub>2</sub>PO<sub>4</sub> / K<sub>2</sub>HPO<sub>4</sub> (pH 6.7), 2.8 mM NADH, 100 mM HPR and plant extract.

### 2.2.11.6 Chlorophyll assay

Chlorophyll quantification was conducted spectrophotometrically. The absorbance of the samples was measured at 646.6nm, 663.6nm and 750nm in a glass cuvette. Chlorophyll content was calculated according to the extinction coefficients described in (Porra *et al.*, 1989) as follows:

$$Chl\ a\ (\mu g/ml) = \frac{12.25 E_{663.6} - 2.55 E_{646.6}}{sample\ volume(ml)}$$

$$Chl\ b\ (\mu g/ml) = \frac{20.31 E_{646.6} - 4.91 E_{663.6}}{sample\ volume(ml)}$$

$$Chl\ a + b\ (\mu g/ml) = \frac{17.76 E_{646.6} + 7.34 E_{663.6}}{sample\ volume(ml)}$$

Where  $E_{663.6}$  and  $E_{646.6}$  represent absorbances at 663.6 nm and 646.6 nm minus absorbance at 750 nm, respectively.

### 2.2.12 Phenotypic analysis

#### 2.2.12.1 Leaf area

Leaf area was measured on wildtype, *cat2-1* mutant and transgenic lines. Measurements involved 6-24 plants per genotype per experiment. In all cases, photographs were taken using a Nikon D5100 digital camera. A ruler was used for scaling and all images were analysed by ImageJ 1.48 V programme.

#### 2.2.12.2 Rosette diameter

Rosette diameter was determined using ImageJ 1.48 V programme. The longest diameter was measured, and the mean was determined.

#### 2.2.12.3 Number of leaves and biomass

Measurements of the number of leaves and rosette biomass (fresh weight) were performed for plants grown under short- and long-day conditions. Measurements involved a minimum of 6-12 plant per genotype analysed per experiment.

#### 2.2.12.4 Primary root length

Plants were grown on ½ MS to the age of 10 days after germination in long-day conditions (16 hr) at an irradiance of 200  $\mu\text{mol.m}^{-2}.\text{s}^{-1}$  light intensity. Measurements of the primary root length were performed by analysing photographs of individual plants for each genotype using ImageJ 1.48 V programme.

### **2.2.12.5 Seed weight**

Seed weight was determined by weighing 1000 seed. Seeds were counted using a digital hand tally counter (RelX).

## **2.2.13 Expression of CAT2sfGFP11 plasmids in isolated protoplasts**

### **2.2.13.1 Plant growth conditions**

Transgenic *Arabidopsis thaliana* lines that express sfGFP1-10<sup>OPT</sup> targeted to peroxisomes, nucleus and cytoplasm were obtained from Arabidopsis Biological Resource Centre(ABRC) (Table 2.5). Seeds of the transgenic lines were sterilised as described in section 2.2.2 and sown on ½MS plates containing hygromycin at a final concentration of 50 µg/mL. Seedlings were then transplanting into soil and kept in long-day conditions (Light intensity: 180 µmol. m<sup>-2</sup>. s<sup>-1</sup>, 16hr light and 8 hr dark, 22°C) for 4-6 weeks.

### **2.2.13.2 SfGFP11 plasmids preparation**

Organelle targeted mCherry-sfGFP11 constructs were also obtained from ABRC (Table 2.5B). Plasmid DNA was extracted using a QIAGEN plasmid midi kit, according to the manufacturer's instruction. DNA pellet was resuspended using 50 or 100 µl of sterile distilled water.

### **2.2.13.3 Protoplast isolation**

*Arabidopsis* protoplasts were transfected by a method described previously (Wu et al., 2009). Solutions used for isolation and transformation are described in Table 2.6. Briefly, leaves were collected from 4 to 6- week-old plants grown under long-day conditions. Using the Tape-*Arabidopsis* Sandwich method, the upper epidermal surface was stabilised by affixing a strip of time tape whereas the lower surface was affixed to a strip of magic tape. Then, the magic tape was pulled away from the time tape, peeling away the lower epidermal surface cell layer. The peeled leaves which are adhering to the time tape were incubated with 10 ml of enzyme solution for 60 min with gentle shaking.

After incubation, the protoplast suspension was centrifuged at 100 g for 3 min. The pelleted protoplasts were washed twice with 25 ml of pre-chilled W5 solution, incubated on ice for 30 min.

At this step, protoplasts were counted using a haemocytometer using a light microscope. Finally, the protoplasts were then centrifuged and resuspended in MaMg solution to a final concentration 2 to 5 x 10<sup>5</sup> cells/ ml.

**Table 2.5: Transgenic plants and constructs of sfGFP**

<b>(A) Organelle targeted sfGFP1-10OPT transgenic lines</b>		
Stock number	Name	ABRC Stock Number
PEP101P	CYTO-sfGFP1-10	CS69831
PEP102P	NU-sfGFP1-10	CS69832
PEP105P	PX-sfGFP1-10	CS69835
<b>(B) Organelle targeted mCherry-sfGFP11 construct</b>		
Stock number	Name	ABRC Stock Number
PEP109E	CYTO-mCherry-11	CD3-2430
PEP110E	NU-mCherry-11	CD3-2431
PEP113E	PX-mCherry-11	CD3-2434

#### **2.2.13.4 Protoplast transfection assay**

Approximately 5 x 10<sup>4</sup> protoplasts in 200 µl MaMg were mixed with plasmid DNA (20-40 µg) at room temperature followed by addition of a freshly prepared solution of 40% (w/v) PEG (MW 4000; Fluka) with 0.1 M CaCl<sub>2</sub> x2H<sub>2</sub>O and 0.2 M mannitol. The mixture was incubated for 5 min at RT. After incubation, 3 mL of W5 solution was added slowly, the solution was mixed, and the protoplasts were pelleted by centrifugation at 100 g for 1 min. The W5 wash step was repeated twice, and the protoplasts were recovered in 1 mL of W5 solution and incubated (6-well plates coated with 1% BSA) at RT for 16hr in the light. The expression of proteins was examined at different time points after transformation.

**Table 2.6: Solutions for protoplast preparation**

<b>Solution</b>	<b>Contents concentrations</b>	<b>Volume</b>	<b>Molar mass (g/mol)</b>	<b>Weights (g)</b>	<b>Sterilisation</b>
<b>Enzyme</b>	1% Cellulase 'Onozuka' R10 0.25% macerozyme 'Onozuka' R10 0.4 M mannitol 10 mM CaCl <sub>2</sub> x2H <sub>2</sub> O 20 mM KCl 0.1% BSA 20 mM MES pH 5.7	200 ml	- - 182.17 111 147.02 - 195.24	2 0.5 14.5736 0.222 0.15 0.2 0.78096	Sterile filter
<b>W5</b>	154 mM NaCl 125 mM CaCl <sub>2</sub> x2H <sub>2</sub> O 5 mM KCl 5 mM glucose 2 mM MES, pH 5.7	1000 mL	58 147.02 74.54 180 195.24	8.932 18.38 0.3727 0.9 0.39048	Autoclave
<b>MaMg</b>	0.4M mannitol 15 mM MgCl <sub>2</sub> 4 mM MES, pH 5.7	50 ml	182.17 95.21 195.24	3.6434 0.167 0.039	Sterile filter
<b>PEG</b>	0.2M Mannitol 0.1M CaCl <sub>2</sub> x2H <sub>2</sub> O 40% Poly ethylene glycol (PEG)		182.17 147.02 4000	0.36 0.15 4	Sterile filter

**2.2.13.5 Microscopy**

Protoplasts were observed with a Zeiss 700 laser scanning confocal microscope using EC Plan-Neofluar 20x/0.5 M27. Excitation wavelengths and emission filters were 8.5% of 488-nm diode laser /band-pass 300-531nm to detect sfGFP. Controls were carried out to check for and prevent bleed through of fluorescence between the channels.

## **2.2.14 Subcellular localisation**

### **2.2.14.1 Crude fractionation**

Extraction buffer was prepared as follows: Tricine (170 mM), KCl (10 mM), MgCl<sub>2</sub> (1 mM), EDTA (1 mM), Sucrose (1mM), and DTT (5mM). The pH was adjusted to 7.0 with 5M KOH and stored immediately at -20°C. For crude fractionation, 2g of four weeks-old wild type, *cat2-1*, PSI, WSQV and ARL leaves were harvested and homogenised using a parsley chopper. Following cell disruption, three fractions were prepared as follows: The first fraction, the homogenate fraction (S1 supernatant), was obtained by centrifugation of the homogenate (10 min, 4°C; rotor 11186, 2000g). The second fraction, the cytosolic fraction (S2), was obtained by centrifugation of 1 ml of the S1 supernatant (12154-H rotor, 12000g, 20 min, 4°C). Finally, the S2 pellet (organelle fraction) was suspended in 0.1ml of the homogenisation buffer.

### **2.2.14.2 Percoll and sucrose density gradient analysis**

Three to five weeks-old *Arabidopsis* plant leaves were harvested and leaf peroxisomes were isolated as described previously (Reumann et al., 2007). The isolation procedure was performed in a cold-room (4°C).

*Arabidopsis* leaves (5-10 g) were harvested at the end of a dark period and ground in grinding buffer (170 mM Tricine-KOH, pH 7.5, 10 mM KCl, 1 mM MgCl<sub>2</sub>, 1 mM EDTA, 1 mM Sucrose, 5 mM DTT and 0.3% (w/v) BSA) supplemented with protease inhibitors using a mortar and a pestle. The homogenate was filtered through three muslin layers and centrifuged at 7000g (1 min, F21-8X50Y). The supernatant was applied to the top of a 21ml Percoll density gradient prepared in TE buffer (20 mM Tricine-KOH, pH 7.5, 1 mM EDTA) supplemented with 0.75 M sucrose and 0.2% (w/v) BSA (top to bottom: 3mL of 15% Percoll, 9mL of 38% Percoll, 2mLmixture of 38% Percoll, and 36% [w/w] sucrose at a ratio of 2:1 and 1:2, and 3 mL of 36% (w/w) sucrose in TE buffer). The gradient was centrifuged for 12 min at 13,000g and 20 min at 27,000g (F21-8X50Y rotor). Then, the peroxisome fraction at the bottom of the percoll gradient was diluted in 36% (w/w) sucrose and centrifuged for 30 min, 39,000g (F21-8X50Y rotor). The supernatant was then removed, and the washed leaf peroxisomes fraction was homogenised by slow strokes using a potter homogeniser.

Then, the peroxisome fraction carefully was applied on the top of a 7.5 ml discontinuous sucrose density gradient (1mL 41%[w/w], 1mL 44%[w/w], 1mL 46%[w/w], 2mL 49%[w/w], 0.5mL 51% [w/w], 1 mL 55% [w/w], and 1 mL 60% [w/w] in TE buffer) and centrifuged (40 min, 25,000 rpm; Beckman SW40). The gradient was fractionated for top to bottom into 1 ml aliquots. The fractions were analysed for catalase, hydroxypyruvate reductase, protein concentration and chlorophyll content.

## **2.2.15 Cloning (Construction of vectors)**

### **2.2.15.1 Generation of CAT2-sfGFP11 constructs**

To generate CAT2-sfGFP11 fusion constructs (Appendix C, C.1.1), CAT2 plasmids (971, 972 and 973, section 2.2.1 and Appendix C.1.2) were isolated from glycerol stocks (Section 2.2.6). Isolated plasmids were used as a template with CAT2PSIF, CAT2PSIR, CAT2WSQVR and CAT2ARLR primers (Table 2.3, #40, #41, #42, #43, respectively) to produce CAT2PSI, CAT2WSQV and CAT2ARL, respectively. These PCR products contain *KpnI* and *SpeI* restriction sites. The PCR products were gel purified and digested with *KpnI* and *SpeI* (described in sections 2.2.8 and 2.2.15.4, respectively) and then ligated (Section 2.2.15.3) into the PEP109E plasmid (Table 2.5B) (Park et al., 2017), which was digested (Section 2.2.15.4 ) with *KpnI* and *SpeI* to remove the Cyto-mCherry-11 fragment and dephosphorylated to ensure that the PEP109E vector does not re-circularise during ligation. Following the ligation, *E. coli* transformation was performed (Section 2.2.15.5). Following transformation, plasmid DNA was extracted from putative clones and sequenced using the primers CTSPF2, CTSPR2 and CTSPR3 (Table 2.3, # 31,32 and 33, respectively) to confirm the cloning. Plasmids isolated from positive clones were also amplified using catalase specific primers (CAT2F and CAT2R, Table 2.3, #4 and #5) to confirm the presence of CAT2 insert.

### **2.2.15.2 DNA sequencing**

The obtained constructs used in this study were sequenced by GENEWIZ. Sequencing results were analysed using the SNAPGENE programme.

### 2.2.15.3 DNA ligation reaction

(50-100 ng) vector with a different molar ratio of insert was used in a 20  $\mu$ l reaction volume. Volume adjusted to 10  $\mu$ l with nuclease-free water. Then, 10  $\mu$ l of 2X Quick ligation buffer was added and mixed. 1  $\mu$ l of Quick ligase was added and mixed thoroughly. Centrifuged briefly and incubated at room temperature for 5 minutes. Chilled on ice and 5  $\mu$ l was used for *E. coli* transformation according to the manufacturer's instructions.

### 2.2.15.4 DNA restriction digest

For the C-terminal, CAT2PSI, CAT2WSQV and CAT2ARL PCR products and PEP109 plasmids were double digested with *KpnI* (NEW ENGLAND BioLabs, R0142S) and *SpeI* (NEW ENGLAND BioLabs, R0133S). The reaction (50  $\mu$ l) was set up as follows:

DNA	1 $\mu$ g
NEB buffer (10X)	5 $\mu$ l
<i>SpeI</i>	1 $\mu$ l
<i>KpnI</i>	1 $\mu$ l
Nuclease- free water	Up to 50 $\mu$ l

The reaction was then incubated at 37°C for 1 hour. Followed by heat inactivation (65 °C for 15 minutes). Confirmation of restriction digests was processed by agarose gel electrophoresis. DNA samples were mixed with 6X loading buffer (NEB) and loaded into agarose gel consisting of 1% (w/v) agarose melted in 1x TAE and 1:10000 diluted SYBR® Safe (Qiagen NV, Hilden Germany). A 1 kb ladder was loaded as a DNA marker. Samples were separated by electrophoresis in 1X TAE buffer at 100V for 60 min and visualised using a gel imager (syngene).

### **2.2.15.5 *E. coli* transformation**

50-100 µl competent *E. coli* cells were removed from -80°C and thawed on ice. 1-5 µl ligation reaction was added to the cells and mixed by swirling for a few seconds. Cells were incubated on ice for 30 minutes. The cells were subsequently heat-shocked at 42°C for 30 seconds without shaking and incubated on ice for 2 minutes. For each transformation reaction, 900 µl SOC medium was added and incubated for 60 minutes at 37°C with shaking at 250 rpm. 20-200 µl was plated onto LB agar plates containing Kanamycin. Plates were then incubated overnight at 37°C.

### **2.2.16 Isolation of RNA from polyribosome pellet**

Solutions used for isolation and recovery are described in Table 2.7. Six-day-old seedlings (300 mg) grown on ½ MS were harvested and ground with liquid nitrogen using a precooled and sterilised mortar and pestle. 5ml PXB was added to the tissue powder and homogenised.

The homogenate was centrifuged at 18,000 rpm (Sorvall SS-34 rotor) for 20 minutes at 4°C. The supernatant was carefully overlaid on the 5 ml SCB and ultracentrifuged at 28,000 rpm (SW28 rotor) for 3 hours at 4°C. Following the ultracentrifugation, the supernatant and cushion were removed, and the pellet was resuspended in 0.5ml 1X PRB.

RNA was recovered from the resuspended polyribosome pellet as follows: 10mM EDTA and 0.1% SDS were added as a final concentration to the resuspended pellet. An equal volume of phenol-chloroform was added and centrifuged for 5 minutes at 10,000 rpm (Sorvall H-6 rotor) to separate the phases. The upper aqueous phase was transferred into a clean tube and 1/10 volume of 3M Na-acetate, pH 5.5 and 2 volumes of ethanol were added and allowed to precipitate at 20°C for 30 minutes. Following the precipitation, the pellet was recovered by centrifugation (Sorvall HB-6 at 10,000 rpm) for 5 minutes. The supernatant was then removed, and the pellet washed twice with 2 ml 80% ethanol. 50 µl sterile distilled H<sub>2</sub>O was used to dissolve the pellet. RNA recovery was checked using a nanodrop spectrophotometer and agarose gel.

**Table 2.7 Solutions for RNA isolation from polyribosomal pellet**

<b>Buffer</b>	<b>Contents concentrations</b>	<b>Sterilization/storage</b>
Polysome extraction buffer (PXB)	200mM Sucrose 200mM Tris-Cl, pH 8.5 60mM KCl 30mM MgCl <sub>2</sub> 1% (v/v) Triton X-100 2mM DTT	Autoclaved Stored at 4°C
Sucrose cushion buffer (SCB)	1M Sucrose 40mM Tris-Cl, pH 8.5 20mM KCl 10mM MgCl <sub>2</sub>	Autoclaved Stored at 4°C
Polysome resuspension buffer (PRB)	20mM Tris-Cl, pH 8.5 20mM KCl 10mM MgCl <sub>2</sub>	Autoclaved Stored at 4°C
5X PRB	100mM Tris-Cl, pH 8.5 100mM KCl 50mM MgCl <sub>2</sub>	Autoclaved Stored at 4°C
Sucrose gradient buffer (SGB)	7.5g sucrose 10ml 5X PRB H <sub>2</sub> O to 50ml	Autoclaved Stored at 4°C

### 2.2.17 Statistical analysis

All the statistical analysis and calculations were done using Windows® Microsoft Excel. The asterisks indicate statistically significant differences compared with the wild type by Student's *t* test as follows: \*\*\**p* < 0.001, \*\**p* < 0.01. The error bars represent SE. The means are determined from different biological replicates.

## Chapter 3

### Molecular and morphological characterisation of *cat2-1* mutant and transformants expressing CAT2 C-terminal variants.

#### 3.1 Background

Peroxisomes are single membrane-bound organelles that are present ubiquitously in the cytoplasm of eukaryotic cells. These organelles contribute to the detoxification of ROS (Lazarow and Fujiki, 1985). H<sub>2</sub>O<sub>2</sub> is one of the major ROS and mainly generates during photorespiration in peroxisomes (Noctor et al., 2002b; Foyer and Noctor, 2009). Peroxisomes contain a tetrameric iron porphyrin enzyme known as catalase that catalyses the dismutation of photorespiratory H<sub>2</sub>O<sub>2</sub>, generated during photorespiration, to water and oxygen (Mullen et al., 1997; Queval et al., 2007; Mhamdi et al., 2012).

Peroxisomal proteins are encoded by nuclear genes and synthesized on free cytosolic polyribosomes before being transported to peroxisomes (Goldman and Blobel, 1978; Lazarow and Fujiki, 1985; Baker, 1996; Lametschwandtner et al., 1998). The peroxisomal matrix proteins are targeted to their destination by PTS1 (Gould et al., 1989; Hayashi et al., 1997) and PTS2 (Swinkels et al., 1991; Kato et al., 1996; Girzalsky et al., 2010) which are recognised in the cytosol by a shuttling receptors, PEX5 and PEX7, respectively (Nito et al., 2002). Plant catalase appears to have neither a typical PTS1 nor PTS2, and there are conflicting data in the literature as discussed in Chapter 1, Section 1.9.7 (also see Chapter 6, Table 6.1). Because of the uncertainties and contradictions, the catalase import mechanism remains unclear.

*A. thaliana* has *CAT2* that plays an important role in photorespiration; the *cat2-1* mutant is a photorespiratory mutant, and several studies have been conducted to investigate the phenotype of *cat2-1* mutant lines (Bueso et al., 2007; Queval et al., 2007; Hu et al., 2010; Yang et al., 2018). Therefore, the *cat2-1* mutant offers a well-characterised background to investigate the role of the CAT2 C terminal sequence on plant growth.

According to the Arabidopsis Information Resource (TAIR) database, there are two variants of *CAT2* gene. *AT4g35090.1* describes the transcript that encodes the normal protein sequence ending PSI-COOH while *AT4g35090.2* describes the alternative spliced form, which removes the last 18 amino acids of the coding sequence (Figure 3.1). This variant is supported by cDNA evidence which raises the possibility that alternative splicing could generate catalase variants with different C termini with potential to modulate targeting to peroxisomes. Therefore, cDNA of both variants and a variant that has the PSI sequence replaced by ARL have been cloned under the control of the native *CAT2* promoter and terminator and then transformed into *cat2-1* mutant (Figure 3.2). ARL fits the consensus PTS1 targeting sequence. The constructs and transformation were performed by previous group members and details are provided in (Chapter 2, section 2.2.1) and (Appendix C.1.2.1). Three independent transgenic lines of each construct were selected for this study (appendix A.1).

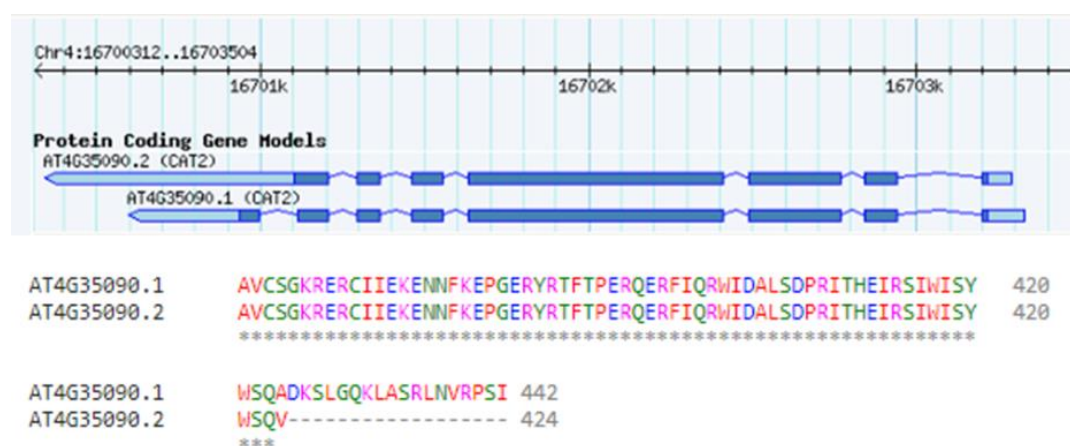


**Figure 3.1: Transcriptional variants of *A. thaliana* *CAT2* (*AtCAT2*).**

*AtCAT2* C-terminal alignment and TAIR proposed protein coding gene model indicate the difference between the two variants. (Top) The *AtCAT2* variant 1 (AT4G35090.1) represents the fully spliced version, whereas variant 2 (AT4G35090.2) indicates the second splice variant, which arises from the last intron. Exons are presented by dark blue boxes, while the light ones depict the untranslated region. For comparison, the sequence alignment of the C-terminal last 82 and 64 residues of variant 1 and 2 is shown (bottom). Clustal Omega software (Sievers et al., 2011) was used to align the sequences.

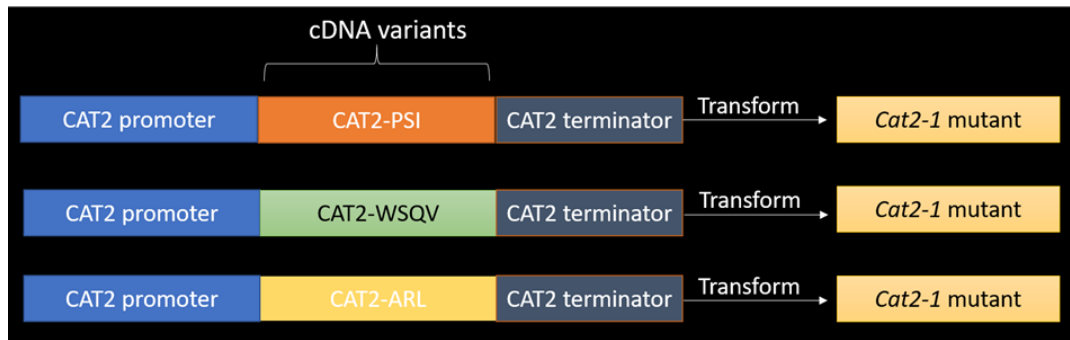


**Figure 3.2: Schematic diagram of the construction and transformation of *CAT2* cDNA variants.**

Native C-terminus variant (PSI), an alternative splice variant (WSQV) and a variant where the C-terminal three amino acids PSI of *CAT2* were replaced with ARL, which is a consensus peroxisomal targeting signal, were cloned under the control of the native *CAT2* promoter and terminator and introduced into the *cat2-1* mutant background.

**This chapter presents a number of experiments that were designed to detect and confirm the presence of the short form of the *CAT2* gene. PCR analysis was carried out to verify that *cat2-1* mutant is the correct mutant and to confirm presence of transgene in different transgenic lines. Also presented in this chapter is work conducted to study the morphological consequences of introducing *CAT2* variants with modified C termini into the *cat2-1* mutant background under different conditions.**

### **3.2 *A. thaliana* CAT2 transcripts detection using RT-PCR**

It has been shown that the *CAT2* gene has an alternative spliced variant with the accession number At4g35090.2 (Figure 3.1) which arises from non-splicing of the last intron and, if translated, it could produce an 18aa shorter protein with a C-terminal sequence which would not be expected to conform to the requirements for recognition by the PEX5 TPR domain. In order to test if the At4g35090.2 splice variant is present on ribosomes and translated, specific primers (see Materials and Methods, Table 2.3) were designed to amplify both transcripts (Figure 3.3). RNA was recovered from a polyribosome pellet prepared from six-day-old seedlings of *A. thaliana* wild type Columbia plants grown under long-day conditions (16h/8h light/dark photoperiod). Samples were harvested after 4.30hr relative to the start of the light period since catalase transcription is circadian regulated. In this section, the full variant and the short form are termed CAT2-1 and CAT2-2, respectively.

PCR1 using primers *CAT2-F* and *CAT2-R* will amplify both transcripts with an expected band from *CAT2-2* cDNA of 407bp and 293bp from *CAT2-1* cDNA (Figure 3.3). PCR2 using primers *CAT2-F* and *CAT2-1R* will amplify only the *CAT2-1* transcript as this primer spans the spliced intron as shown in (Figure 3.3) with a 246bp expected band size. PCR3 using primers *CAT2-F* and *CAT2-2R* will amplify only *CAT2-2* transcript (i.e. specific for *CAT2-2* cDNA) with expected band 276bp (Figure 3.3).



As shown in (Figure 3.4A, star), only one band (293 bp), which is specific for *CAT2-1* transcripts, was detected in PCR1 after 35 cycles. *CAT2-1* specific transcripts were also detected in PCR2 after 25 and 30 cycles (star, Figure 3.4 B and C, respectively). On the other hand, *CAT2-2* specific transcripts represented by 276 bp were detected after 40 cycles (star, Figure 3.4 D). However, additional bands were also amplified after 40 cycles. The triangle denotes a band that could correspond to another un-spliced variant, and the circle represents an unspecific band as it was previously sequenced with the same primer.

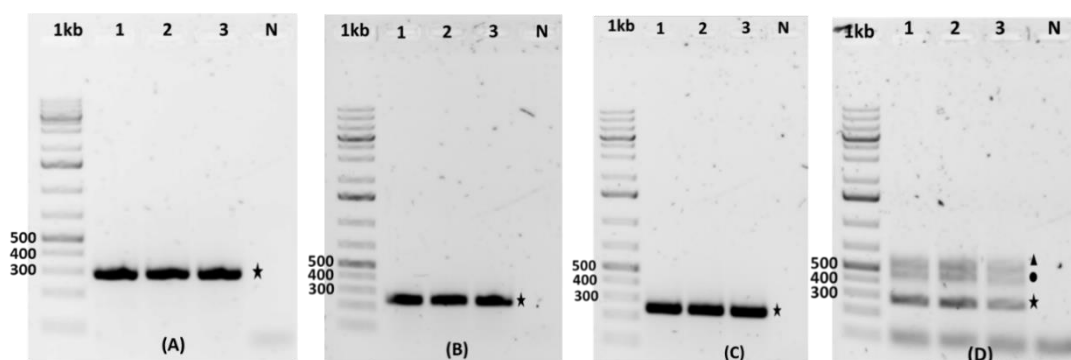


**Figure 3.4: Detection of *A. thaliana* catalase 2 gene (*CAT2*) specific transcripts by RT-PCR.**

RT-PCR analysis to detect *CAT2* specific transcripts from polysomal RNA of wild type *A. thaliana*. (A) In PCR1, *CAT2-F* and *CAT2-R* primer pair was used to amplify both *CAT2* transcripts. As a result, only one band (star, 293 bp), corresponding to the At4g35090.1 transcript, was detected at 35 cycles. (B) and (C) presented PCR2 at 25 and 30 cycles, respectively. In PCR2, one band (star, 246 bp), which is also specific to the At4g35090.1 transcript, was detected using *CAT2-F* and *CAT2-1R* primer pair. (D) PCR3 at 40 cycles where is the At4g35090.2 specific transcript was detected (star, 276bp) using *CAT2-F* and *CAT2-2R* primer pair. 1kb, DNA molecular weight markers; positions of markers (base pair) are shown on the left. Lanes (1-3), three different preps. H<sub>2</sub>O was included as a negative control of the PCR reaction (N). Additional bands are indicated by triangle and circle. Triangle (D) shows a band that is suggested to be another-un spliced variant. An unspecific band (confirmed by sequencing) is shown (circle, D).

The presence of the non-spliced variant in polysomal RNA (Figure 3.4) supports the idea that it is translated, although likely at a low level compared to the fully spliced version. Therefore, to determine whether this C terminally truncated form has any biological activity and function, the ability of this variant and a variant with a consensus PTS1ARL to correct the reported phenotypes of the *cat2-1* mutant was examined. In order to verify this, *cat2-1* mutant was used as a control. Consequently, it was crucial to confirm the presence of T-DNA insertion in *cat2-1* mutant lines.

### **3.3 Genomic verification of *cat2-1* mutant**

The *cat2-1* mutant described by Queval et al. 2007 is used as a control in this study. To confirm the presence of the T-DNA insertion and therefore verify this is the correct mutant, crude genomic DNA was isolated from wild-type and *cat2-1* mutant leaves (see Material and Methods, Section 2.2.5). Leaf DNA was amplified by PCR using specific primers for *CAT2* gene and T-DNA insertion. T-DNA insertion was confirmed by PCR amplification of DNA using *cat2-1* right primer (RP) with T-DNA left border primer (LBb1.3), whereas *cat2-1* RP with *cat2-1* left primer (LP) was used for wild-type (Figure 3.5A). As can be seen in (Figure 3.5 B) upper gel, the combination of *CAT2-1* LP with *cat2-1* RP should give an 1132 bp product size and should be amplified only with wild-type (lanes A and B) but not with the *cat2-1* T-DNA line (Lanes 1-4). On the other hand, the combination of *cat2-1* RP with LBb1.3 should give the fragment of a 774 bp size and exclusively with DNA from the *cat2-1* line (Figure 3.5B lower gel).

The result presented so far (Figure 3.5) has indicated that the *cat2-1* mutant was homozygous for the T-DNA inserted in exon three as described by Queval et al. 2007. According to that, *cat2-1* mutant was used as a control to study the morphological characterisation of the *CAT2* variants. However, it was first necessary to confirm the presence of the transgene in the *CAT2* variants.

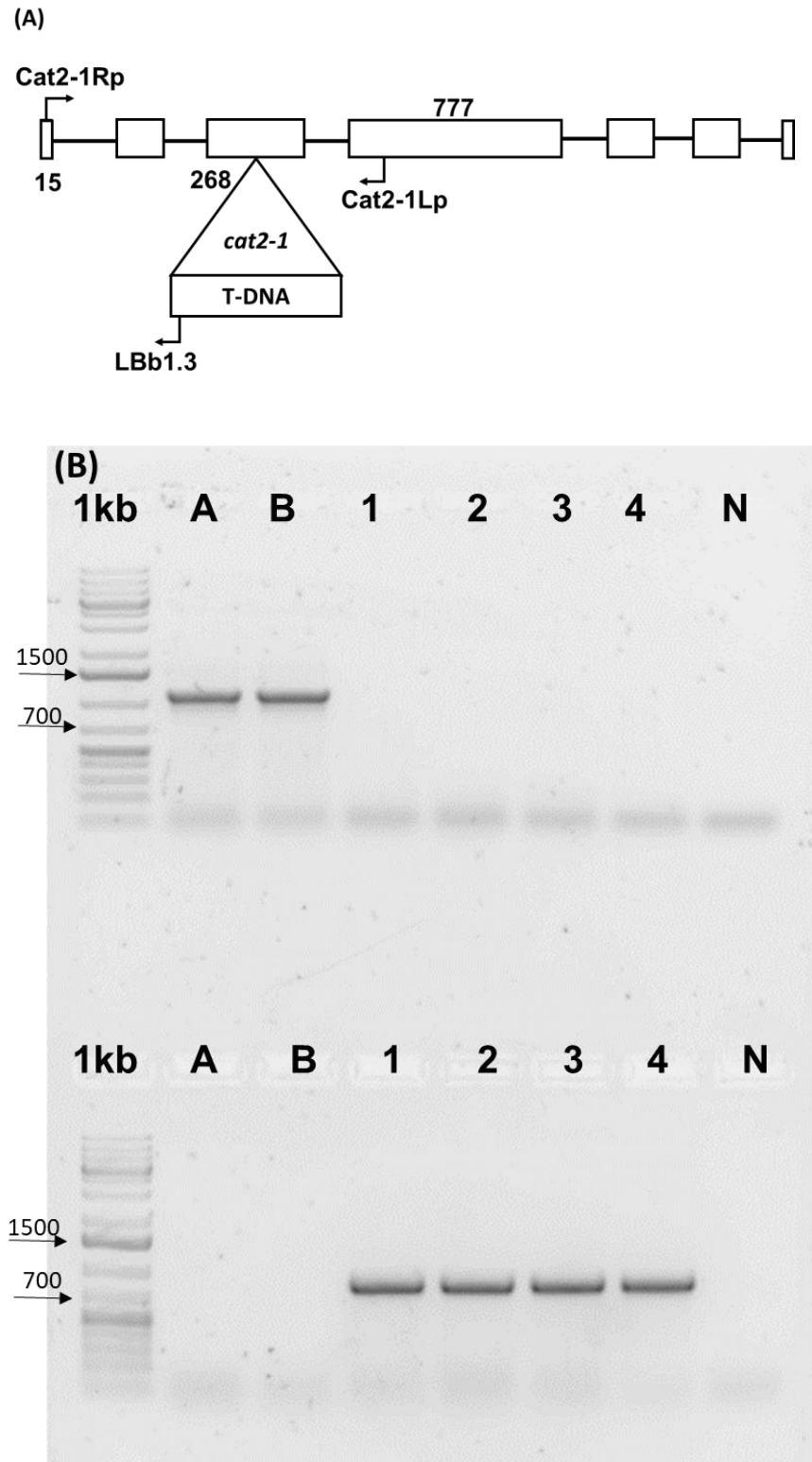


**Figure 3.5: Molecular confirmation of *cat2-1* mutant.**

(A) *CAT2* gene structure with the insertion site of the T-DNA and combinations of primers. Blocks correspond to exons and nucleotide positions are numbered. Introns are indicated by lines. (B) Verification of the *cat2-1* mutant by PCR. A and B represent wild-type DNA samples from 2 different plants. The numbers indicate the *cat2-1* mutant DNA samples from 4 different plants. (N) is a negative (no DNA, H<sub>2</sub>O) control.

### 3.4 Genomic characterisation of CAT2 derivatives lines

As previously described in (Chapter 2, Section 2.2.1), transgenic lines were generated by previous group members. Before using these lines to investigate the ability of the different catalase variants to complement the morphological, physiological, and biochemical defects of the *cat2-1* mutant, it was necessary to validate the available lines and identify additional independent transgenic lines.

One line for each PSI, WSQV and ARL had been selected and taken to homozygous T3 prior to the start of this project (Dr Barbara Karpinska). In this line, WSQV and ARL plants were mixed up due to mislabelling. Thus, I re-confirmed the WSQV lines using specific primers and sequencing. However, I also selected two additional independent homozygous T3 lines (for more details, see Appendix A). Different independent lines were generated and numbered as 1, 2, and 3, as shown in (Table 3.1). Three independent lines of WSQV and PSI and two independent lines of ARL were confirmed separately for the presence of transgene using specific primers.

**Table 3.1: Transgenic lines details.**

The first independent line of PSI and WSQV had been selected before the start of the project, whereas new independent lines were selected during this study. T2 generations are segregating 3:1, and T3 lines are 100% resistant. Numbers represent different independent lines. For example, (PSI1) is the first independent line of PSI plants that contain CAT2 with native C-terminal tripeptide sequence (-PSI). This line was generated from T3 plant # 2. (PSI2), the 2<sup>nd</sup> independent line of PSI plants, produced from T2 generation plant # 6 and T3 generation plant # 6.

Transgenic lines	Source
PSI1	PSI T3 plant # 2
PSI2	PSI T2 plant # 6 T3 plant # 6
PSI3	PSI T2 plant # 5 T3 plant # 3
WSQV1	WSQV T3 plant # 6
WSQV2	WSQV T2 plant # 4 T3 plant # 4
WSQV3	WSQV T2 plant # 2 T3 plant # 7
ARL1	ARL T2 plant # 1 T3 plant # 1
ARL2	ARL T2 plant # 3 T3 plant # 5

The presence of the transgene was confirmed using catalase specific primers and genomic DNA prepared from the transgenic lines. One independent line genotyping is presented here, while the results of the other lines are presented in appendix A, Figures A.3, A.8 and A9. All product sizes are listed in Table 3.2, and the primer sequences can be seen in (Chapter 2, Materials and Methods, Table 2.3). The primer binding sites are presented in appendix B.2, Figure B.4. Although the three constructs are all in the *cat2-1* mutant background, the primers used here are 3' to the site of the T-DNA insertion.

**Table 3.2: The expected product size of the primers.**

Primer pair	PSI	WSQV	ARL
Pair 1 ( <i>CAT2-F/CAT2-R</i> )	597bp (genomic) 293bp (cDNA)	597bp (genomic) 407bp (cDNA)	597bp (genomic) 293bp (cDNA)
Pair 2 ( <i>CAT2-F/CAT2-2R</i> )	466bp (genomic) ----- (cDNA)	466bp (genomic) 276bp (cDNA)	466bp (genomic) ----- (cDNA)
Pair 3 ( <i>CAT2-F/CAT2-11R</i> )	563bp (genomic) 259bp (cDNA)	563bp (genomic) 373bp (cDNA)	563bp (genomic) 259bp (cDNA)
Pair 4 ( <i>CAT2-F/CAT2-ARL</i> )	----- (genomic) ----- (cDNA)	----- (genomic) ----- (cDNA)	----- (genomic) 308bp (cDNA)

As can be seen in (Figure 3.6), primer pair 1 (*CAT2-F* + *CAT2-R*) amplifies the genomic *CAT2* locus with 579bp product size in all three transgenic lines (PSI, WSQV and ARL) (arrow, Figure 3.6). Additionally, the same primer pair amplifies PSI, WSQV and ARL construct with a product size of 293bp, 407bp and 293bp, respectively (star, Figure 3.6) because the *CAT2-F* primer lies in an exon that is common to both splice variants.

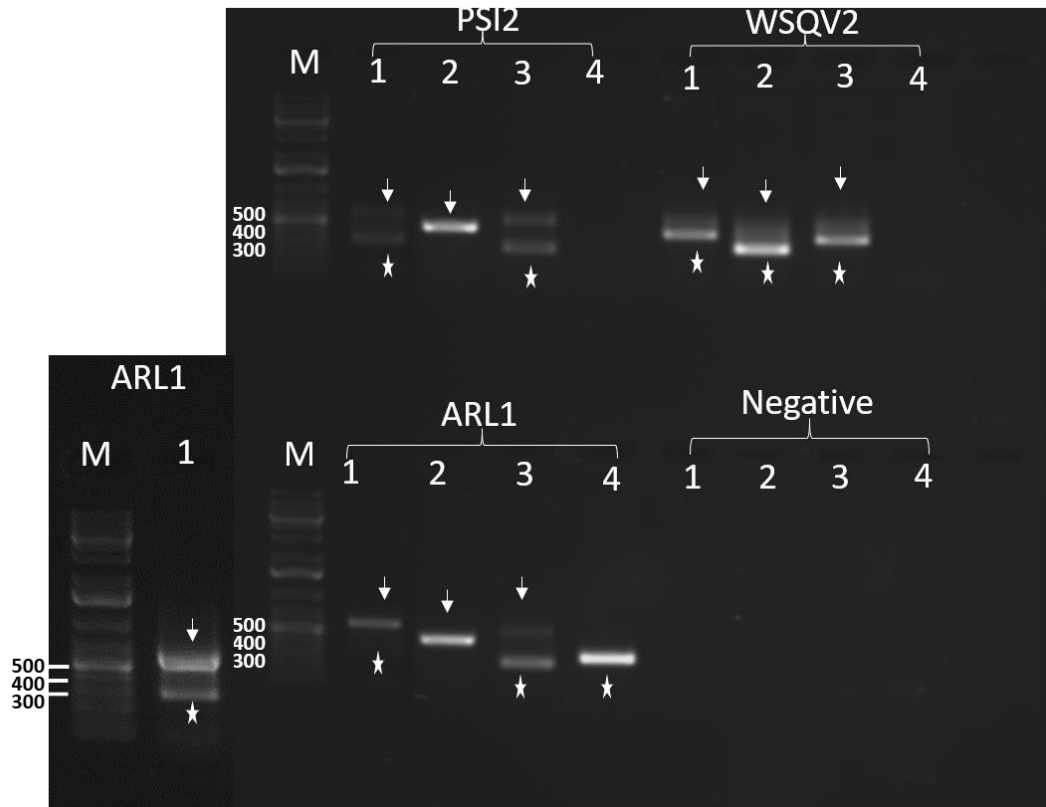


**Figure 3.6: Molecular characterisation of transgenic lines.**

1% of agarose gel electrophoresis of PCR products of genomic DNA of PSI2, WSQV2 and ARL1 plants. 1kb ladder was used in this gel (M). The numbers represent the primer pairs (1-4). Negative: negative control (no DNA). Specific bands are indicated as arrows and stars. The extra panel shows the confirmation of the amplification result of primer pair 1 with ARL1 lines DNA.

As presented in Appendix B.2, Figure B.4, *CAT2-2R* lies in an intron where the intron is not spliced out. Therefore, it is amplifying the *CAT2* genomic locus in all the lines, but only the WSQV construct will contain this sequence in addition to the genomic copy (Appendix B2, Figure B4 A and B). Based on that, primer pair 2 (*CAT2-F* and *CAT2-2R*) was also used to amplify genomic DNA of PSI, WSQV, and ARL with 466 bp product size (arrow, Figure 3.6) and WSQV construct with 276 bp product size (star, Figure 3.6).

Using primer pair 3, *CAT2-11R* amplifies PSI, WSQV and ARL genomic DNA with 563 bp product size (arrow, Figure 3.6). It also amplifies PSI, WSQV and, ARL constructs with 259bp, 373bp and 259 bp, respectively (star, Figure 3.6) (Appendix B2, Figure B4 A and B).

Finally, primer pair 4 was used to recognise the lines with ARL. *CAT2*-ARL extends beyond the stop codon into the region that differs between the genomic DNA and the construct because of the gateway recombination site (Appendix B2, Figure B4 C). Consequently, primer pair 4 (*CAT2*-F + *CAT2*-ARL) was used as a specific primer for ARL construct with 308bp product size (star, Figure 3.6). However, all previous primers were used with H<sub>2</sub>O as a template to confirm the absence of any contamination (Negative, Figure 3.6).

Taken together, these results confirmed the presence of the transgene in the transformed plants. Although the constructs were driven by the native *CAT2* promoter, it could not be certain that all essential regulatory elements had been captured and that copy number and position of insertion could also affect the expression level. Also, there could potentially be compensating changes in the expression of the other catalases. Therefore, the expression levels of the *CAT* gene family in the transgenic lines were analysed.

### **3.5 No compensatory change in *CAT1* and *CAT3* was observed in transgenic lines.**

The expression level of catalase genes (*CAT1*, *CAT2* and *CAT3*) was assessed by semi-quantitative RT-PCR using total RNA isolated from the leaves of wild type, *cat2-1* mutant and the transgenic lines grown under short-day conditions (8hr photoperiod) for four weeks. Leaves were harvested 4-4.5hr after the beginning of illumination. RT-PCR analysis was performed using two independent lines of PSI and WSQV and one line of ARL. One independent line is presented in this section, while the 2<sup>nd</sup> line result is presented in Appendix A.4, Figure A.12. Similar results were obtained with another line.

Specific primers were designed for each *CAT* gene. Their sequences can be found in Table 2.3 Materials and Methods, and the location of the primers on their respective sequences can be seen in the multiple sequence alignment shown in (Figure 3.7). However, the primers either spanned intron/exon junctions meaning that they would not amplify any contaminating genomic DNA or included at least one intron so that any PCR product arising from contaminating genomic DNA would be easily distinguished.

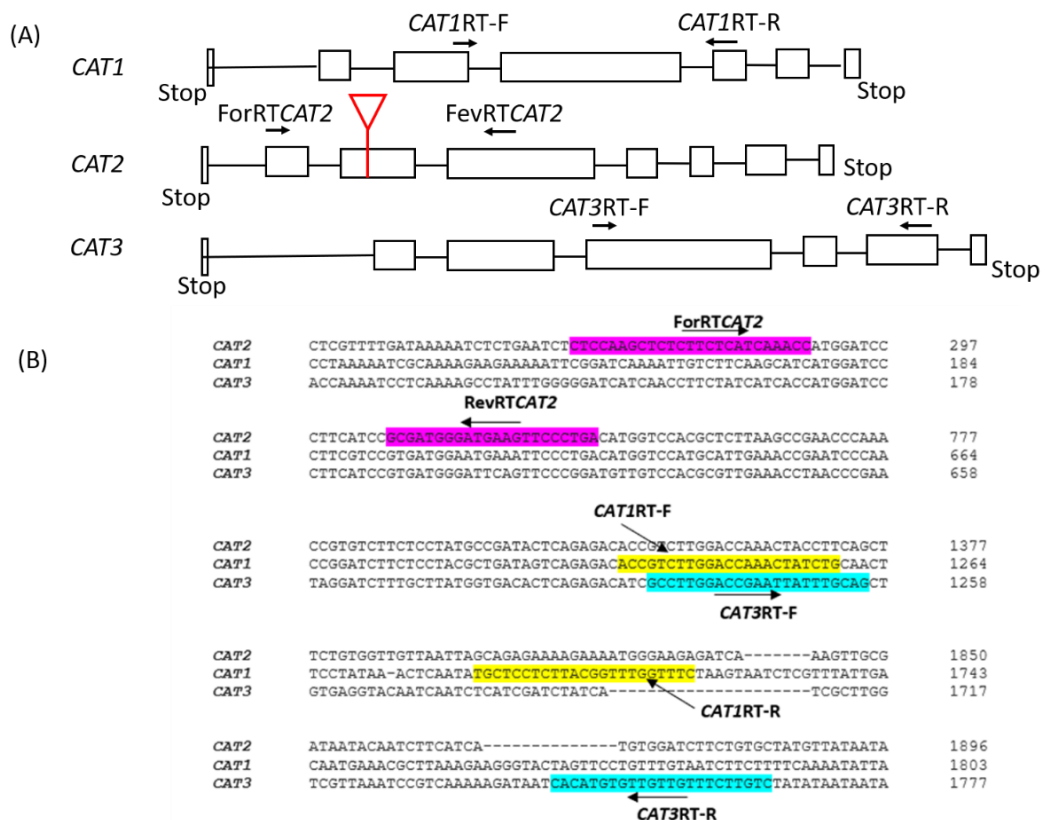


**Figure 3.7: Structure and multiple sequence alignment of *A. thaliana* catalase genes.**

(A) Structures of genes *CAT1*, *CAT2* and *CAT3* are shown with the insertion site (Red tag) of T-DNA in *CAT2*. (B) Primer binding sites are shown; *CAT1* specific primers highlighted yellow with arrow in a 5'-3' direction. *CAT2* primers highlighted purple. While *CAT3* highlighted turquoise. All primers underlined with arrow in a 5'-3' direction. Nucleotide positions are numbered. Clustal Omega software (Sievers et al., 2011) was used to perform the multiple sequence alignment.

As indicated in Figure 3.8A, the *CAT1* primer pair amplifies a product of 487bp at 40 cycles, and the level of expression is similar in all the lines. *CAT2* primer pair (star, Figure 3.8B) amplifies a product size 483bp from the lines except for *cat2-1* mutant due to the presence of T-DNA insertion (Figure 3.7A and 3.8B). Transcripts levels of *CAT3* were also detected in all lines at 40 cycles (532bp band, star, Figure 3.8C) using specific primers with no obvious changes. Faint bands were also detected at 30 cycles during the amplification of *CAT2* and *CAT3* transcripts, indicating that they are expressed in leaves.

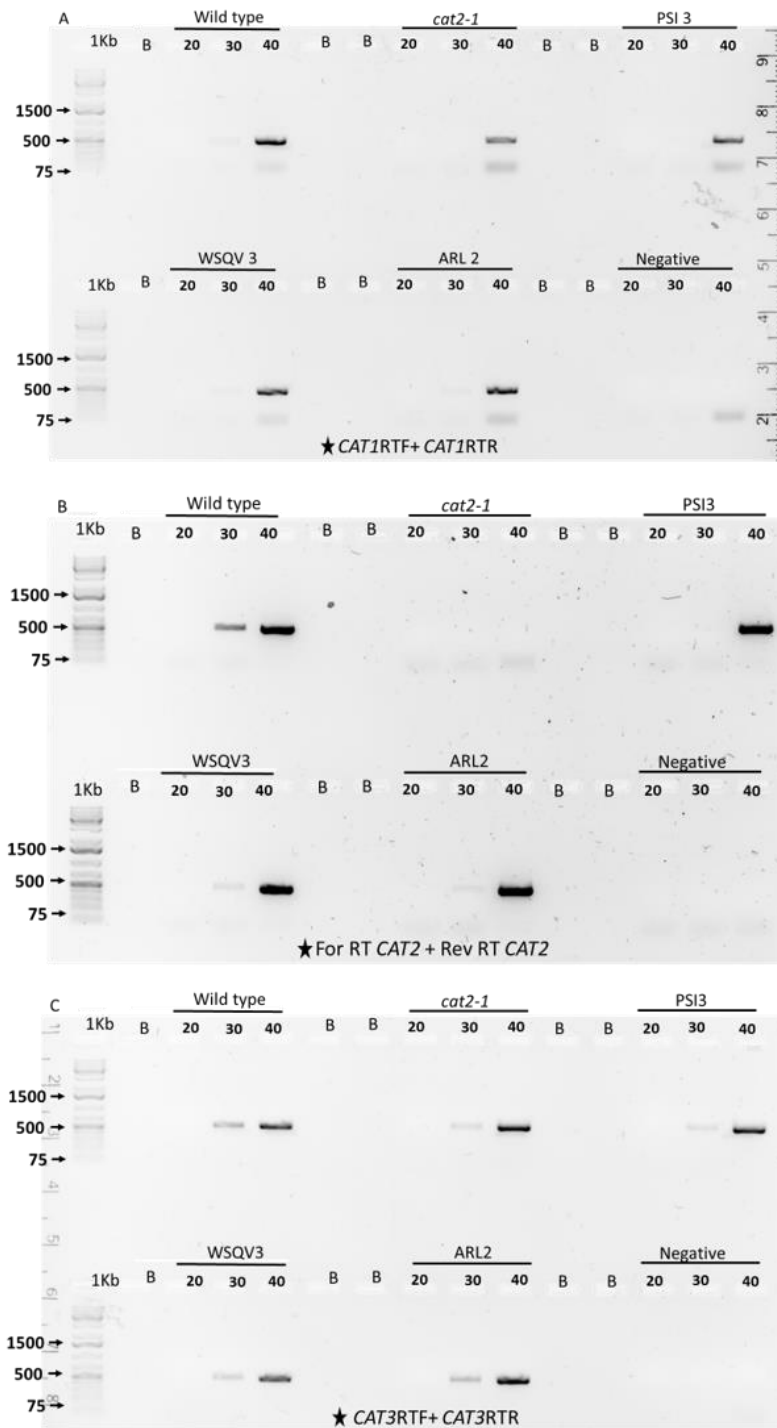


**Figure 3.8: A representative image of semi-quantitative RT-PCR of catalase genes.**

The expression level of *CAT1*(A), *CAT2* (B), and *CAT3* (C) was measured in wild type, *cat2-1*, PSI3, WSQV3 and ARL2 using a different number of cycles (20, 30 and 40). Total RNA was isolated from wild type, *cat2-1*, PSI3, WSQV3 and ARL2 and reversed transcribed to cDNA. All reactions were performed with 1/10 dilution cDNA samples. The PCR cycles (20, 30 and 40) were determined to ensure that the results are produced from the exponential phase of PCR amplification. H<sub>2</sub>O was used as a negative control. Primer pairs are shown at the bottom of each gel (star).

However, semi-quantitative RT-PCR provided a quick overview of the expression level. Thus, quantitative RT-PCR was conducted to examine the transcript levels of three catalases. For that, wild type, *cat2-1* mutant and transgenic lines grown in short-day conditions for four weeks were used to extract total RNA. Leaves were harvested 4-4.5hr after the beginning of illumination as it has been shown that the *CAT2* transcripts show a circadian rhythm that has peak expression at the night/day transition (Zhong et al., 1994). Three biological replicates and nine technical replicates were used for RT-qPCR analysis. In this section, RT-qPCR results of one independent line are presented whereas, 2<sup>nd</sup> independent line results are shown in Appendix A.5, Figure A.13. The results of the two independent lines are similar.

The RT-qPCR analysis revealed that the expression level of *CAT1* in PSI3, WSQV3 and ARL2 was similar to wild type level whereas, the expression level of *CAT1* in the *cat2-1* mutant was notably lower than the wild type level (A, Figure 3.9). *CAT2* transcript level was not detected in the *cat2-1* mutant, whereas, in PSI3, WSQV3 and ARL2 was clearly detected but lower than the wild type level (B, Figure 3.9). On the other hand, *CAT3* transcripts analysis showed no obvious change in the level of *CAT3* transcripts in PSI3, WSQV3 and ARL2 compared to wild type (C, Figure 3.9). These results are in agreement with the results of semi-quantitative RT-PCR presented in the previous section.

These findings confirmed that despite the absence of *CAT2* function, no compensatory induction of *CAT1* or *CAT3* transcripts were observed in the *cat2-1* mutant. They also confirmed that the *CAT2* is expressed in transgenic lines, and no overexpression of *CAT1* and *CAT3* was observed.

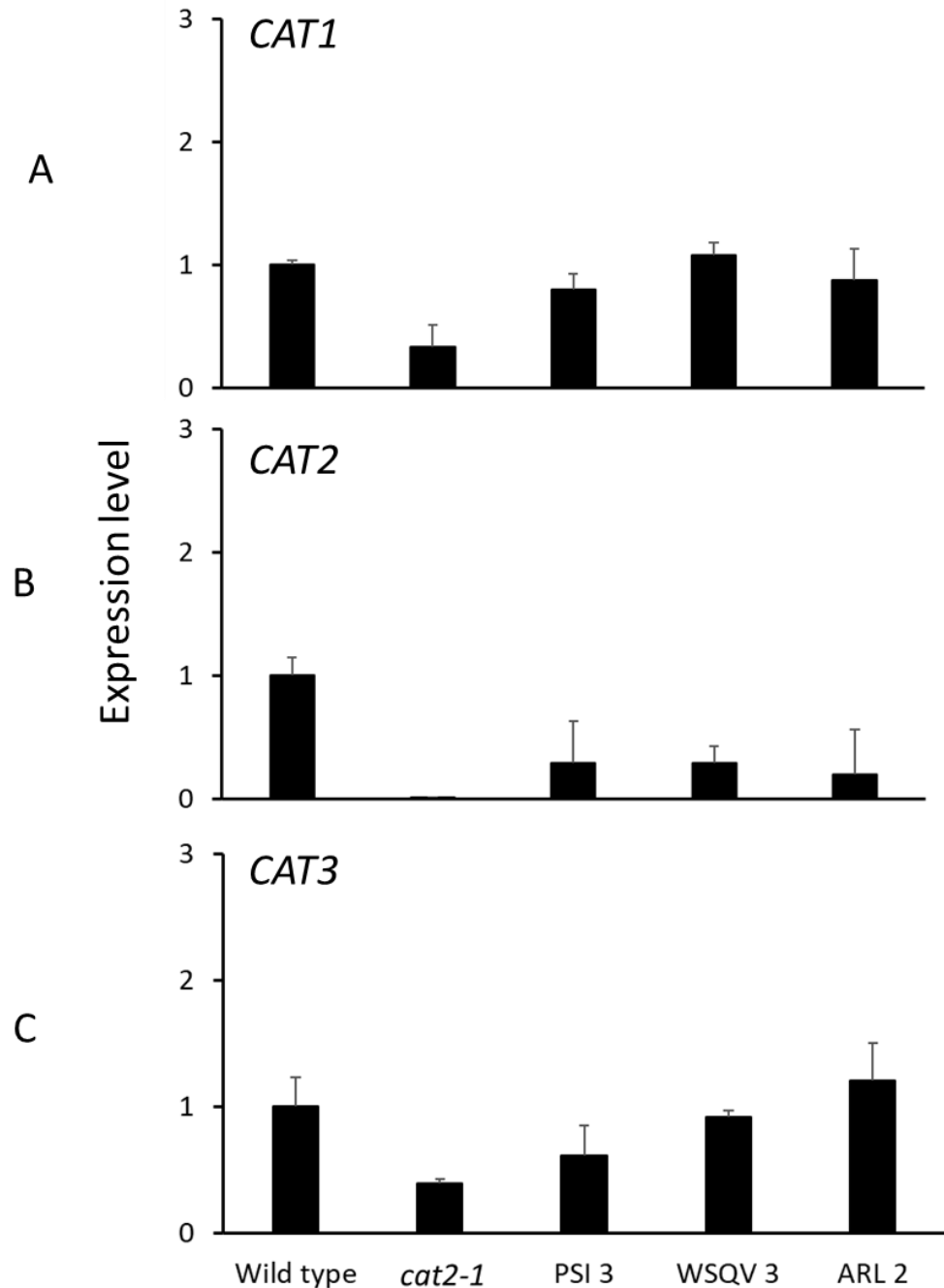


**Figure 3.9: Transcript abundance of catalase genes of *A. thaliana* wild type, *cat2-1* mutant, PSI3, WSQV3 and ARL2.**

RT-qPCR was performed using gene-specific primers (see Chapter 2, Table 2.3) and cDNA obtained from triplicate RNA extracts of plants grown in 8h/16 h light/dark conditions for four weeks. A; *CAT1* transcripts level, B; *CAT2* transcripts level. C; *CAT3* transcripts level. Independent lines of transgenic lines are numbered; 2<sup>nd</sup> independent line of ARL and 3<sup>rd</sup> independent line of PSI and WSQV. Wild type and *cat2-1* mutant grown in parallel with the transgenic lines. All experiments were repeated with a different independent line with similar results. The expression level was quantified by RT-qPCR and are relative to *ACTIN 2*.

The results presented earlier confirmed the presence of transgenes, and there is no compensating change in the expression of the other *CAT* isoforms. Accordingly, morphological analysis of the transgenic lines was performed using *A. thaliana* wild type and *cat2-1* mutant as controls, as presented in the next section.

### **3.6 Using untagged constructs expressed in *cat2-1* mutant background complement growth phenotype**

To investigate the growth phenotypes of the different lines, wild-type, *cat2-1* mutant, three independent lines of PSI, WSQV and two independent ARL lines were grown in short-day conditions (8h light/16h dark regime) for four weeks. Plants of the *cat2-1* mutant grown under short day conditions have several morphological alterations, such as reduced growth and pale-green colour compared to the wild type (2<sup>nd</sup> column, Figure 3.10). The growth observations of the *cat2-1* mutant are similar to those of *cat2-1* mutant plants previously described (Queval et al., 2007), which verify that CAT2 plays an important role as an antioxidant enzyme by detoxification of H<sub>2</sub>O<sub>2</sub> accumulated in leaf peroxisomes.

Transgenic lines were grown together with wild type and *cat2-1* mutant under identical growth conditions. Compared to the wild type, PSI lines had no obvious differences (3<sup>rd</sup> column, Figure 3.10). This is explained by the reconstruction of the wild type native gene. Surprisingly, the WSQV and ARL lines were indistinguishable from wild-type plants (4<sup>th</sup> and 5<sup>th</sup> columns, respectively, Figure 3.10). These interesting results suggest that the WSQV and ARL variants encoded by the transgene complement the growth phenotype of the *cat2-1* mutant. The results of other independent lines were similar to those presented here (Appendix B.1, Figures B1 and B2).

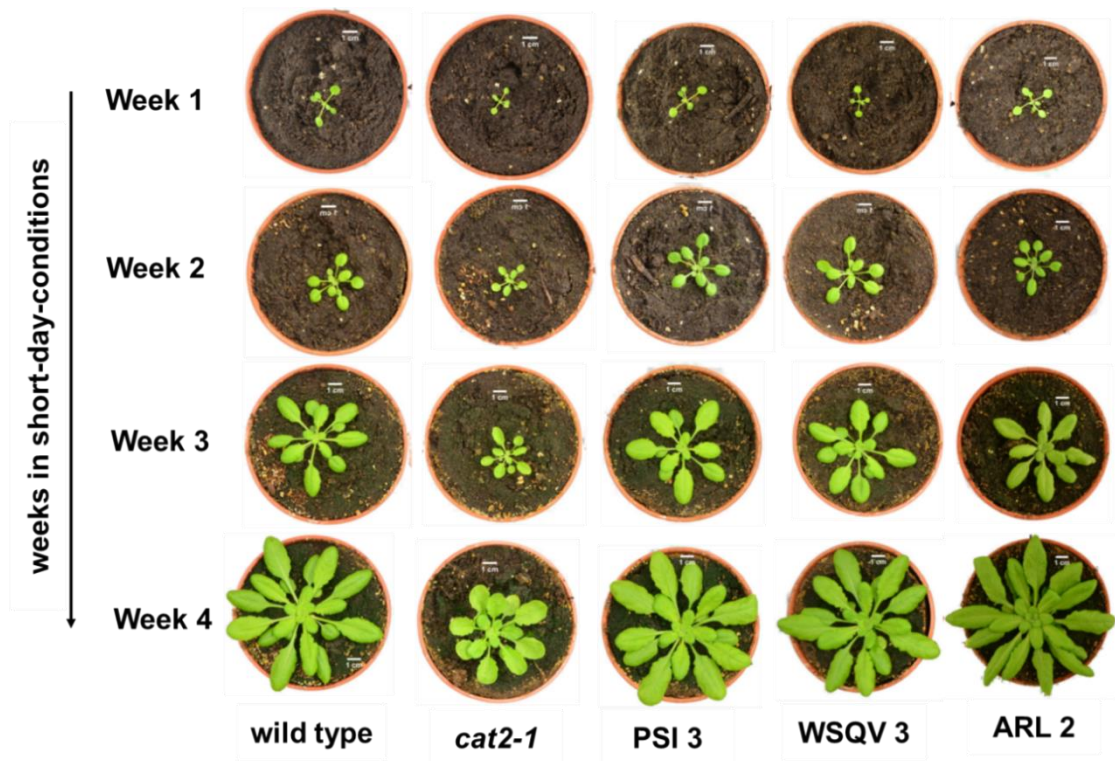


**Figure 3.10: Representative pictures of the rosette appearance of wild type, *cat2-1* and transgenic lines.**

2-3-4- and 5-week-old plants of wild type, *cat2-1*, 3<sup>rd</sup> independent line of PSI3 and WSQV3, and 2<sup>nd</sup> independent line of ARL2 grown under short-day conditions (Light intensity: 190  $\mu\text{mol. m}^{-2} \text{ s}^{-1}$ , 8hr light and 16hr dark, 20°C, 60% humidity) for four weeks. Scale bars represent 1cm. All plants photographed at the same magnification once a week for four weeks. Plants photographed at the 1<sup>st</sup>, 2<sup>nd</sup>, 3<sup>rd</sup>, 4<sup>th</sup> week (indicated as week 1, week 2, week3 and week 4, respectively). The experiment was repeated three times (three independent lines) with similar results.

To confirm the visual observations, the number of rosette leaves was counted once a week for four weeks in wild type, *cat2-1* mutant and two independent transgenic lines (A, B, C and D, Figure 3.11). Wild type and *cat2-1* mutant were grown in parallel with each independent experiment. The two independent experiments are indicated in black and white bars. As can be seen in Figure 3.11, two independent lines of PSI, WSQV and ARL produced wild type number of rosette leaves (Black and white bars, Figure 3.11), while that of the *cat2-1* mutant was significantly decreased as compared to the wild type (Black and white bars, Figure 3.11) Moreover, both sets of lines behaved similarly. These results confirmed the findings shown in (Figure 3.10).

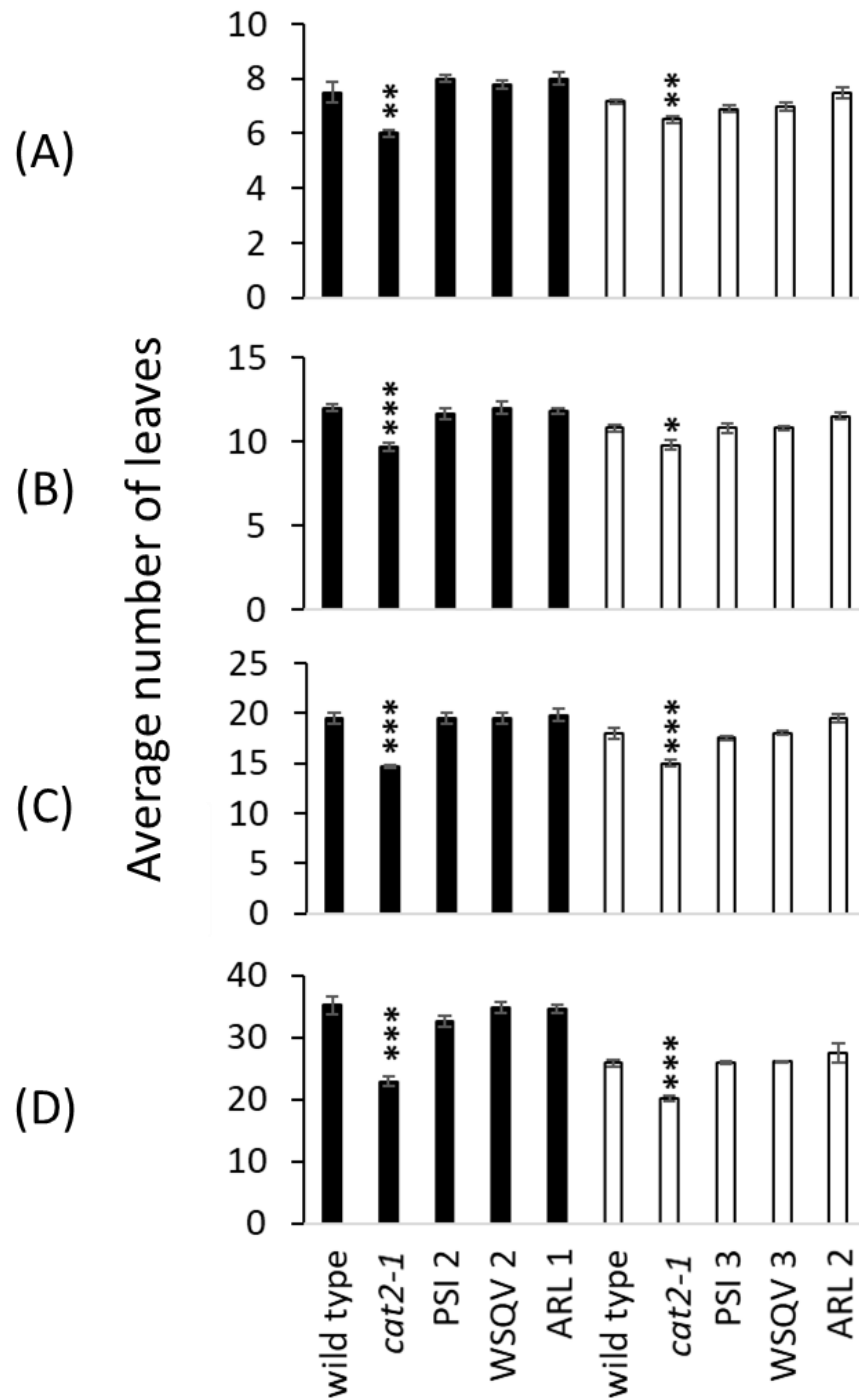


**Figure 3.11: Total number of leaves was counted once a week for plants grown under short-day conditions for four weeks.**

Wild type and *cat2-1* mutant lines were grown in parallel with each independent line of PSI, WSQV and ARL. Black bars show the number of leaves of the 2<sup>nd</sup> independent lines of PSI and WSQV and the 1<sup>st</sup> independent ARL line. White bars represent the number of leaves of the 3<sup>rd</sup> independent lines of PSI and WSQV and 2<sup>nd</sup> independent line of ARL. Measurements were taken at 4 points; first week (A), second week (B), third week (C) and fourth week (D). Values are presented as means obtained from 12 different plants per genotype in two independent lines. \* P < 0.05, \*\* P < 0.01 and \*\*\* P < 0.001, compared with wild type plants (Student's *t* test).

The rosette size was examined in three independent lines by measuring the diameter of the rosette of each genotype. Three experiments were performed, presented by black, white and grey bars in Figure 3.12. In each experiment, the transgenic lines being examined were grown alongside the *cat2-1* mutant and wild type plants. Similar to the situation of rosette leaves number, the diameter of rosette was only significantly reduced in *cat2-1* mutant, compared to wild type plants (A, B, C and D, Figure 3.12). It's necessary to mention that the rosette diameter of the first independent lines of PSI and WSQV was taken at three and four weeks (C and D, Figure 3.12) whereas, the rosette diameter of 2<sup>nd</sup> and 3<sup>rd</sup> independent lines of PSI and WSQV, in addition to the two independent ARL lines of was taken once per week for four weeks under short-day conditions (A, B, C, D Figure 3.12). Two independent lines of ARL were grown in parallel with the 2<sup>nd</sup> independent line of WSQV and PSI. These findings confirm no difference between wild type and any of the transgenic lines, whereas *cat2-1* mutant is consistently smaller.

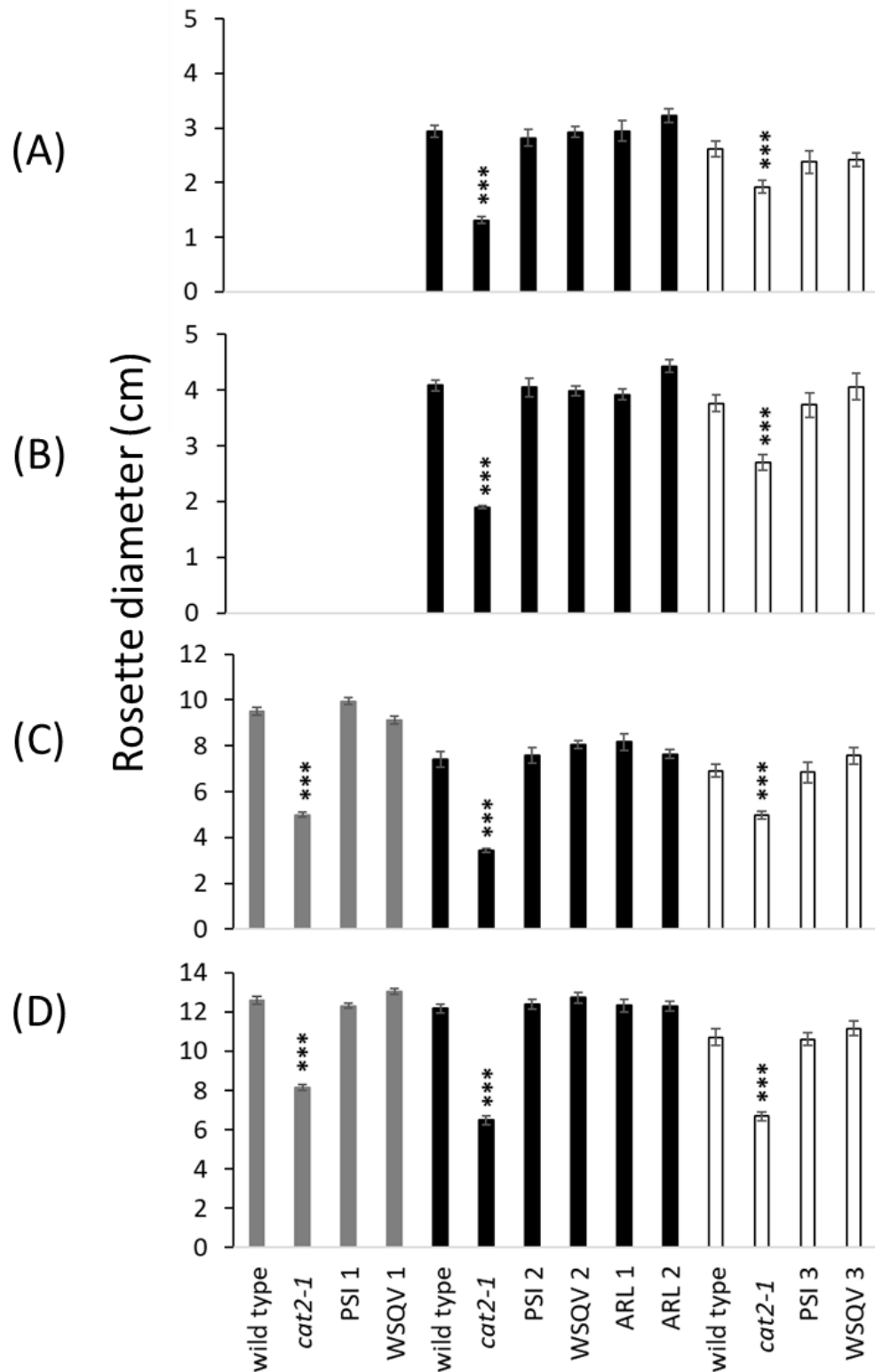


**Figure 3.12: Rosette diameter (longest diameter) of wild type, *cat2-1* and transgenic lines grown under short-day conditions for four weeks.** Means and SE were calculated from 6 plants of each line. Rosette diameter was determined using ImageJ 1.48V programme. Measurements involved six plants per genotype per experiment per independent line. Asterisks indicate statistically significant differences compared with wild type by Student's *t* test (\*\*\*)  $P < 0.001$ ).

Following the growth for four weeks under short-day conditions, some plants were collected for further analysis (see Chapter 4). At this point, fresh weight was examined in the different lines (grey, black and white bars, Figure 3.13). The fresh weight of the *cat2-1* mutant was significantly decreased compared to the wild type (grey, black and white bars, Figure 3.13). The first and 3rd independent line of PSI and WSQV fresh weights were similar to the wild type (grey and white bars, Figure 3.13). Surprisingly, the fresh weight of the 2<sup>nd</sup> independent lines of WSQV and the two independent ARL lines was significantly increased compared to the wild type (black bars, Figure 3.13).

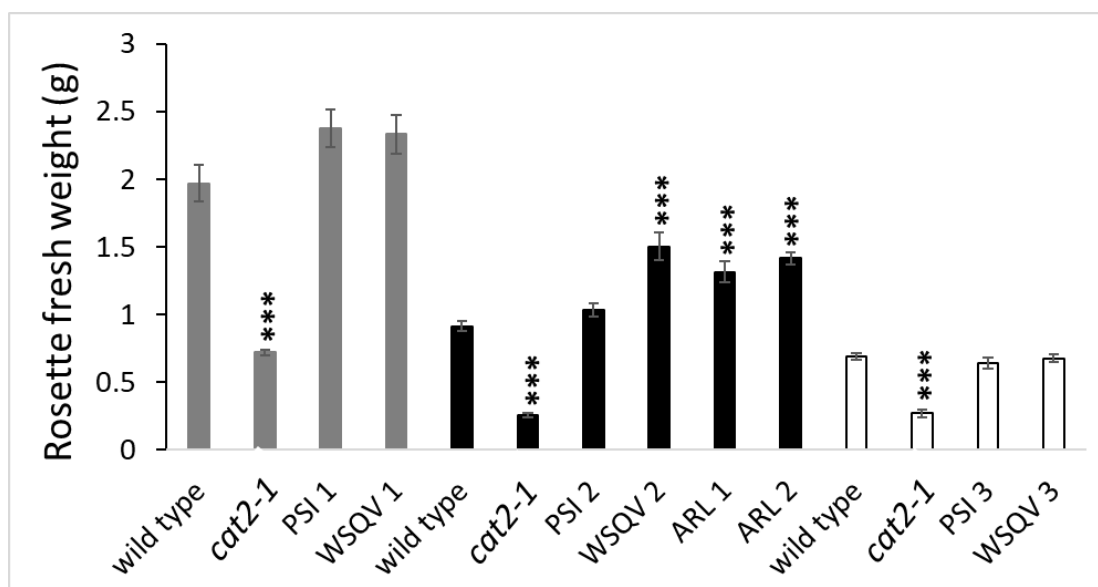


**Figure 3.13: Rosette weight of wild type, *cat2-1* and transgenic lines grown under short-day conditions for four weeks.**

Three independent lines are presented (grey, black and white bars). With each independent line, wild type and *cat2-1* mutant were also grown under identical growth conditions. Plants presented by black and white bars are 5-week-old. In comparison, plants presented by grey bars are six weeks old. Rosette fresh weight was determined using ImageJ 1.48V programme. Means were calculated from six plants per experiment. Asterisks indicate statistically significant differences compared with wild type by Student's *t* test (\*\*\*)  $P < 0.001$ ).

The significant increase of rosette fresh weight in WSQV plants is a peculiarity of this one line. In contrast, it was significant in two independent lines of ARL. To fully confirm these results, lines were grown twice in identical growth conditions (Appendix B.1, Figure B3) with similar results. A slight variation in growth conditions could explain these results as photosynthetic rate, and stomatal conductance could be affected.

Plant phenotype was also examined under long-day conditions. For this, wild-type, *cat2-1* mutant and transgenic lines grown for four weeks in short-day conditions (8h light – 16h dark) were transferred to a long day condition (16h light – 8h dark). Growth of plants was monitored for a further one week after the transfer. This analysis showed that the rosette of the *cat2-1* mutant was visibly smaller than those of the wild type (Figure 3.14). It is worth mentioning that the first independent lines were kept for five weeks in short-day conditions then moved to long-day conditions for one-week.

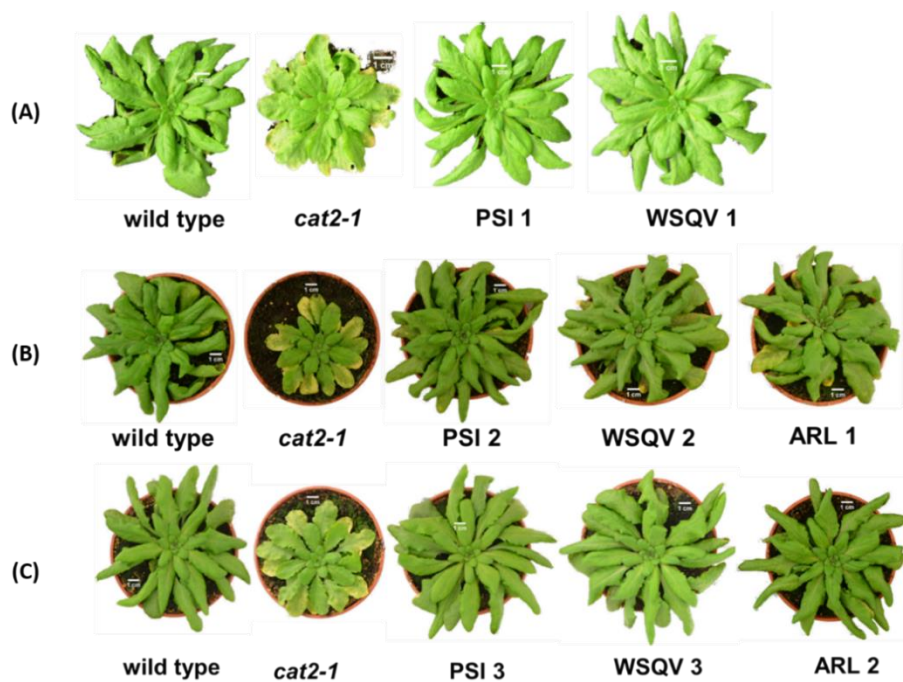


**Figure 3.14: Whole plant phenotypes of wild type, *cat2-1* mutant and transgenic plants.**

Wild type and *cat2-1* mutant grown in parallel with each independent line. Plants grown for four-five weeks under short-day conditions and then transferred to long-day conditions (Light intensity:  $187 \mu\text{mol} \cdot \text{m}^{-2} \cdot \text{s}^{-1}$ , 16hr light and 8hr dark,  $20^{\circ}\text{C}$ , 60% humidity) for one week. Each set of plants were photographed at the same magnification. Scale bars represent 1cm. Numbers indicate different independent lines. Images involved 24 plants (A) and six plants per genotype (B + C).

In contrast, phenotypic observations showed that the different independent lines had comparable growth and development to the wild type, and no abnormal phenotypes were detected under the growth condition (A, B and C, Figure 3.14). These results confirm that introducing CAT2 variants under the control of the *CAT2* promoter and terminator into the *cat2-1* mutant background fully rescue the growth phenotype of the *cat2-1* mutant.

The rosette diameter of the transgenic lines was also analysed. All the WSQV and PSI independent lines and the two independent lines of ARL showed no obvious differences in comparison with the wild type (grey, black and white bars, Figure 3.15). In contrast, the *cat2-1* mutant had a smaller rosette diameter (Figure 3.15).

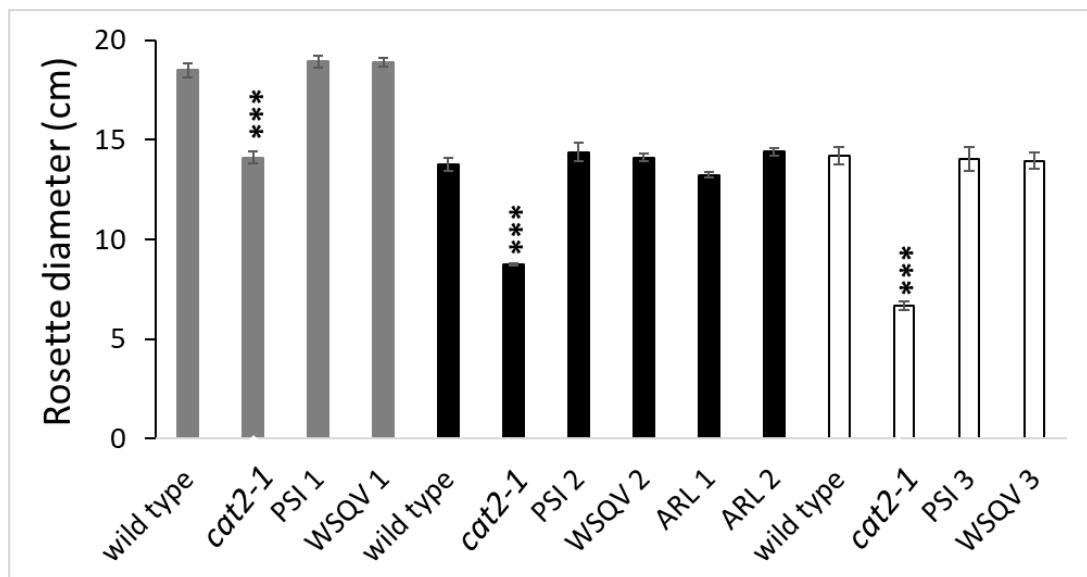


**Figure 3.15: Rosette diameter (longest diameter) of wild type, *cat2-1* and transgenic lines.**

Mean were calculated from 24, 6 and 6 plants per each genotype (grey, black and white, respectively). Rosette diameter was determined using ImageJ 1.48V programme. \*\*\*  $P < 0.001$ , compared with wild type plants (student's *t* test).

Rosette fresh weight was also examined after a one-week transfer in plants of transgenic lines, *cat2-1* mutant and wild type (Figure 3.16). At this stage, three independent PSI lines had a similar fresh weight to the wild type (black bars, Figure 3.16). One line of WSQV and two ARL lines had significantly greater fresh weight than the wild type, while the other lines of WSQV presented no significant differences (grey and white bars, Figure 3.16). However, when these experiments were repeated, there was an indication of an increased fresh weight of this line. It is not clear why such differences were observed; however, it appears that the developmental stages and a slight variation in growth conditions affected the rosette biomass. On the contrary, the *cat2-1* mutant had smaller rosette biomass (Figure 3.16).

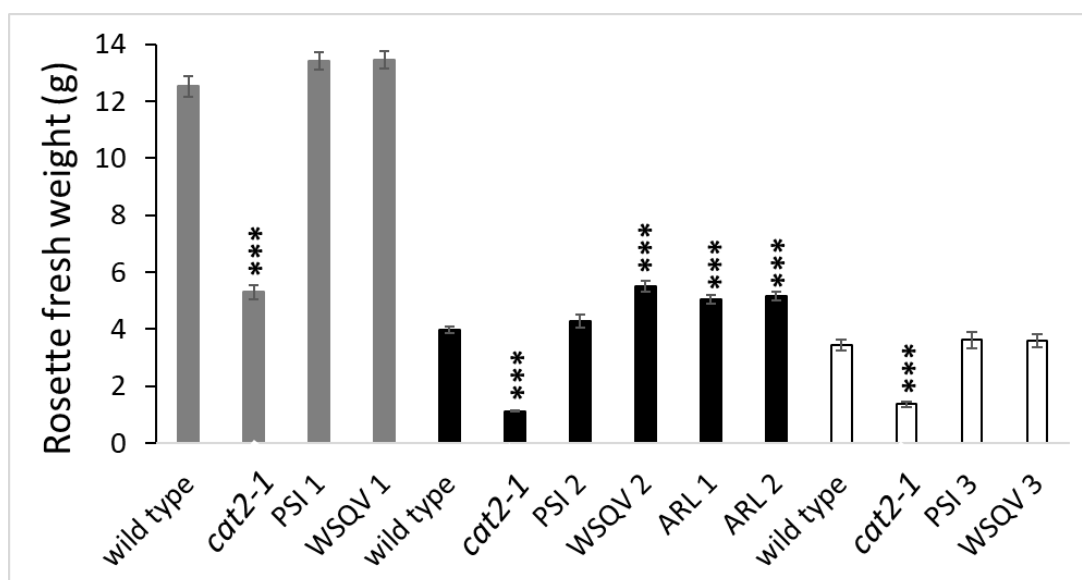


**Figure 3.16: Rosette weight of wild type, *cat2-1* and transgenic lines.** Grey bars represent the rosette diameter of 1st independent lines of PSI and WSQV. Two independent lines of ARL were grown in parallel with the 2nd independent lines of WSQV and PSI (black bars) whereas, 3rd independent lines of PSI and WSQV are shown as white bars. With each set of experiment, wild type and *cat2-1* mutant grown in parallel. \*\*\*  $P < 0.001$ , compared with wild type plants (student's t test). Rosette fresh weight was determined using ImageJ 1.48V programme.

The number of leaves in the rosette of the different lines was counted compared with those of the wild type after one-week transfer under long-day conditions (16h light/8h dark photoperiod). This analysis showed that the number of leaves of one independent line of PSI, WSQV and ARL was similar to that of the wild type (Figure 3.17). In contrast, the *cat2-1* mutant showed a significant decrease in the number of leaves.

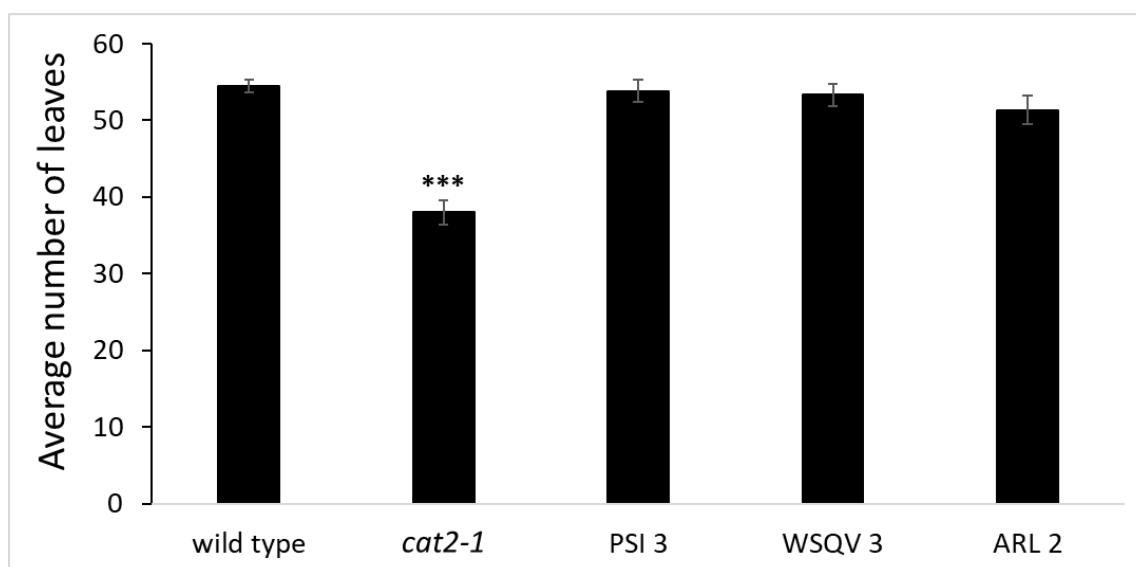


**Figure 3.17: Number of leaves under long-day-conditions.**

The total number of leaves was counted for 6 -week-old wild type, *cat2-1* mutant and CAT2 derivatives (3<sup>rd</sup> independent line of PSI and WSQV; 2<sup>nd</sup> independent line of ARL) grown under long-day conditions (16h light/8 h dark regime) for one week. Data are the mean values (n= 6) of one independent line. Asterisks indicate statistically significant differences compared with wild type by Student's *t* test (\*\*\*) P< 0.001).

All previous experiments were undertaken to explore the morphological effect of introducing different CAT2 variants into the *cat2-1* mutant background. Through morphological characterisation, it was shown that the rosette phenotypes are largely similar in all genotypes, except for the *cat2-1* mutant, which shows significant growth retardation. Additionally, these results imply that the removal of the C terminus of CAT2 does not affect the growth phenotypes.

Following the phenotypic characterisation of wild type, *cat2-1* mutant and the transgenic lines, seeds were collected from one independent transgenic line and wild type and *cat2-1* mutant. Collected seeds were analysed to evaluate the effect of *CAT2* deficiency and the C-terminal alteration on seeds production. To achieve this, the weight of seeds was analysed, as shown in Figure 3.18. This analysis revealed that the seed weight of the *cat2-1* mutant and the transgenic lines was similar to that of the wild type.

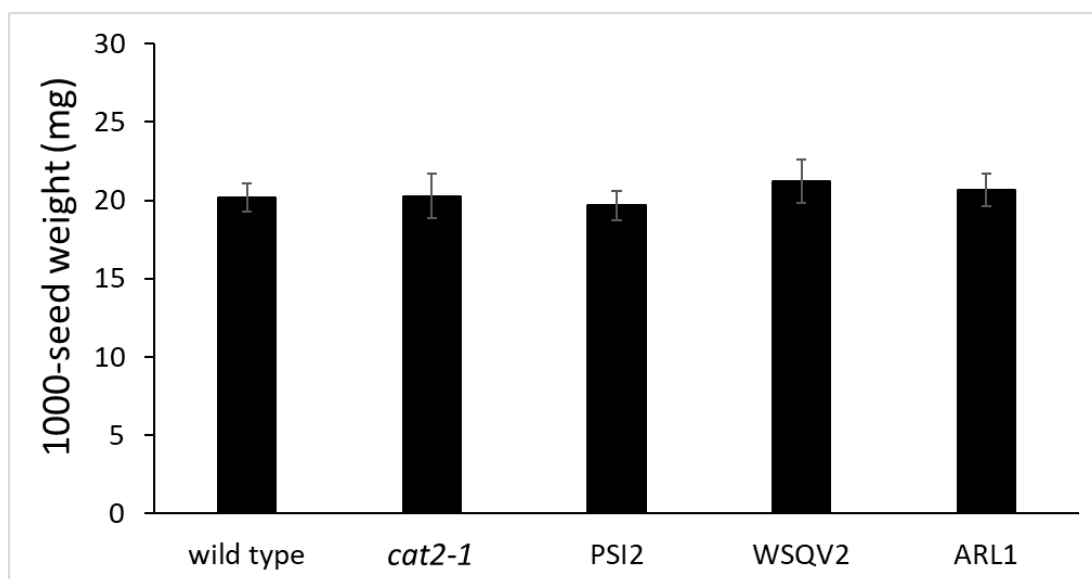


**Figure 3.18: Average seed weight (expressed as milligrams of weight/ 1000 seeds).**

Seeds collected from wild type, *cat2-1* mutant, 2<sup>nd</sup> independent line of PSI and WSQV, as well as 1<sup>st</sup> independent line of ARL. Plants were grown under short-day conditions (8h light/16 dark photoperiod).

Although *cat2* mutation had no impact on seed weight, *cat2* had a substantial effect on root length. Based on that, primary root length was analysed in wild type, *cat2-1* mutant, three independent lines of PSI and WSQV and two independent ARL lines (Figure 3.19). Consistent with previous reports for growth analysis (Yang et al., 2018), the *cat2-1* mutant showed a significant decrease in root length. Transgenic lines root length measurements showed no difference.

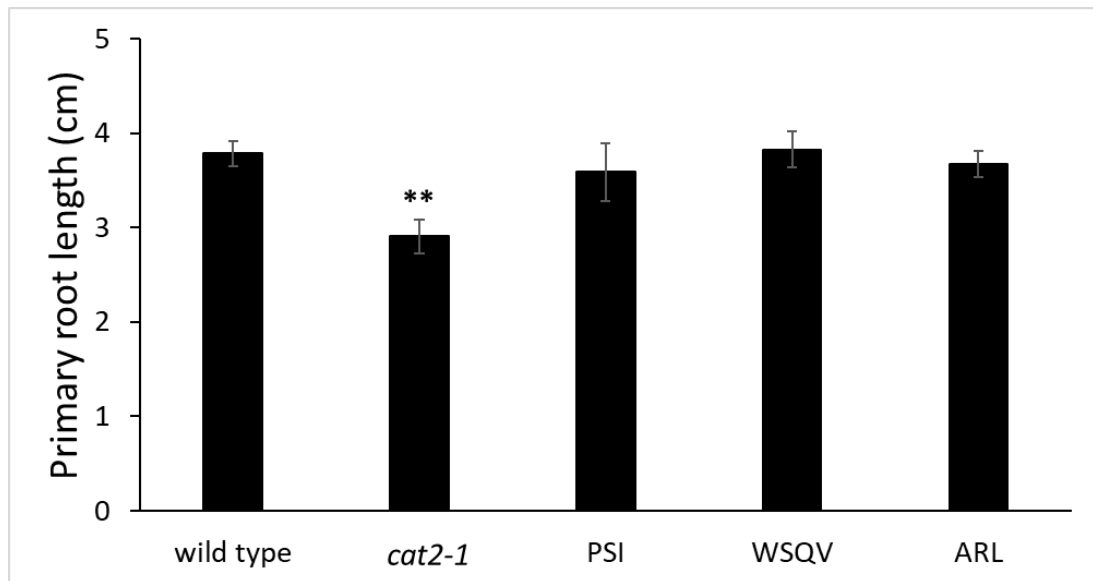


**Figure 3.19: Primary root length (cm) in wild type, *cat2-1*, PSI, WSQV and ARL plants ten days after germination.**

Wild type, *cat2-1* mutant and transgenic lines were sown on ½ MS plates (supplemented with Hygromycin for the transgenic lines) and kept in the cold room for two days. After cold treatment, plates were moved into the light for 6hrs, then kept for two days in the dark. Plates were then moved into 16hr photoperiod. Ten days after germination, plates were photographed using a Nikon D5100 digital camera. Image J 1.48 V programme was used to analyse the images. Data shown are means of 11 plants. ‘\*\*’ significant difference from wild type at  $p < 0.01$ .

All previous results showed clearly that the transgenic lines restored the wild type phenotype in the air. In order to investigate the phenotype of different lines under environmental conditions that enhance the photorespiratory flux, the photorespiration was promoted by artificially restricting gas exchange to *in vitro* grown plants (by sealing the Petri dishes with two layers of Parafilm) and grew them under continuous light to avoid the influence of night respiration on gas homeostasis. As a result, the CO<sub>2</sub> levels in the plates decreased rapidly, enhancing the oxygenase activity of Rubisco and subsequently higher flux through the photorespiratory pathway (Vanderauwera et al., 2012; Kerchev et al., 2015; Waszczak et al., 2016). Under these conditions, *cat2-1* mutants were visually chlorotic after seven days of photorespiratory stress (Figure 3.20). In contrast, no obvious phenotypic differences were observed between PSI and WSQV lines and wild type whereas the ARL lines were slightly chlorotic. These observations were confirmed by the Chlorophyll assay (Figure 3.21).



**Figure 3.20: Phenotypical analysis of transgenic lines under photorespiratory conditions.**

Representative image of wild type, *cat2-1* mutant and transgenic (PSI, WSQV and ARL) plants grown under controlled environmental conditions (16h/light, 22°C day and night temperature, 60% humidity) for 21 day before transfer to photorespiratory conditions (24h/light, 22°C day and night temperature, 60% humidity) for seven days.

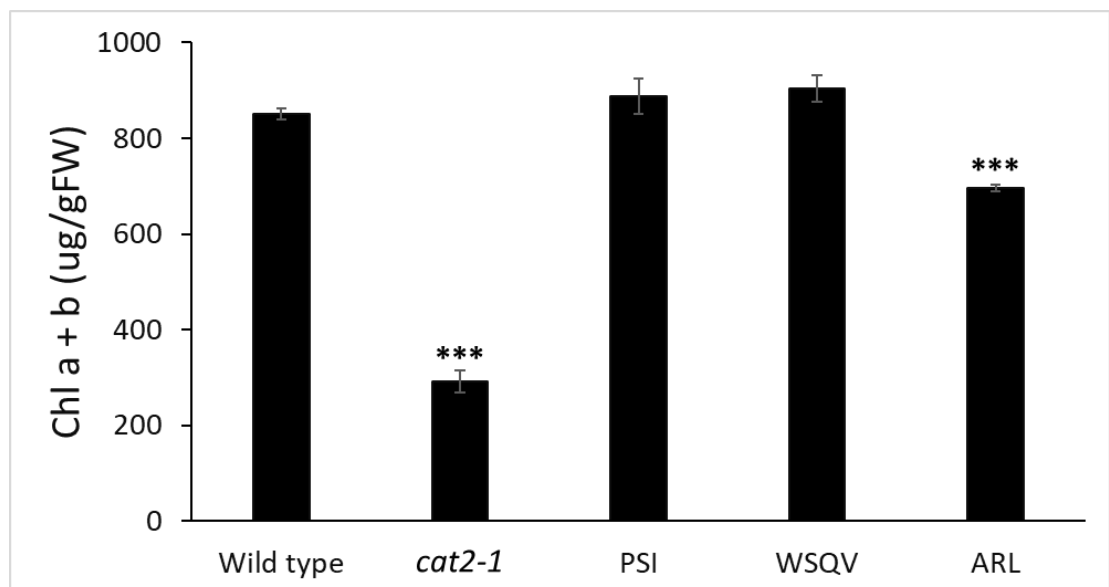


**Figure 3.21: Comparison of chlorophyll content (Chlorophyll a and b; µg per g fresh weight) of 28-day seedlings of *cat2-1* mutant and transgenic lines to the wild type.**

All plants that used to test the phenotype under photorespiratory conditions were collected and used for chlorophyll assay. Data shown are means of 9 plants. '\*\*\*' significant difference from wild type at  $p < 0.001$  by Student *t* test.

### 3.7 Discussion

The studies that are described in this chapter were undertaken to study the morphological consequences of introducing CAT2 variants into the *cat2-1* mutant background. The phenotype of the PSI, WQSV and ARL lines was studied in plants grown under two different growth conditions, short and long-day conditions, as well as conditions that enhance the photorespiratory pathway using wild type and *cat2-1* mutant as a control. However, the data presented in this chapter allows drawing several conclusions.

The T-DNA of the *cat2-1* mutant was inserted within the third exon of the *CAT2* (At4g35090) gene. PCR analysis verified the presence of T-DNA insertion (Figure 3.5) and RT-PCR analysis showed that the level of *CAT2* expression is undetectable (B, Figures 3.8 and 3.9). The *cat2-1* mutant was previously characterised as a photorespiratory mutant under normal growth conditions ( $200 \mu\text{mol m}^{-2} \text{s}^{-1}$ ), which is about 50% saturating for photosynthesis in the Columbia ecotype of *A. thaliana* cultivated in a controlled environment growth chamber (Veljovic-Jovanovic et al., 2001; Queval et al., 2007; Hu et al., 2010) and, accordingly, the *cat2-1* mutant showed severely decreased growth relative to the wild type (Figure 3.10). The number of leaves (Figure 3.11) and rosette diameter (Figure 3.12) confirmed the growth alteration. Additionally, the fresh plant weight was approximately 30% of wild-type fresh weight (Figure 3.13). These observations were consistent with previous findings (Queval et al., 2007; Bueso et al., 2007; Hu et al., 2010; Yang et al., 2018).

Based on the analysis of RNA-sequencing of a normalised cDNA library made from *A.thaliana* seedlings and flowers, over 61% of intron-containing genes undergo alternative splicing under normal growth conditions (Marquez et al., 2012). Differential expression of *CAT2* variants was examined under different stress conditions. For example, both variants of the *CAT2* gene seem 2-fold induced under photorespiratory stress; however, the full spliced version is by far the dominant transcript. The expression level of the fully spliced version is approximately 100-fold higher than the short variant (Dr Frank Van Breusegem and Dr Patrick Willems, personal communication).

Additionally, RNA-seq data from John Brown group are also supporting the existence of the alternative splice variant but at low levels under cold stress compared to the *At4g35090.1* transcript (Dr John Brown, unpublished). In agreement with that notion, RT-PCR results confirmed experimentally that the *At4g35090.2* transcript exists but at a low level compared to the *At4g35090.1* transcript (Figure 3.4). It should be noted that the current study showed that this variant is present in polysomal RNA so is presumable translated whereas the previous experiments are RNAseq.

Variations in the position and the basic structure of the transgene locus may affect the expression levels of the transgene. Additionally, the overexpression of the wild type genes can cause identical phenotypes. In this chapter, it was shown that no overexpression issues that could result from isoforms (Figure 3.8 and 3.9). Additionally, it was also shown that the *CAT2* transcripts were detected in transgenic lines with lower levels than that in the wild type (B, Figure 3.9). Possible explanations: 1) not all regulatory elements are captured in the promoter fragment used in the constructs, 2) cDNA was used so if introns play any regulatory role they are absent in the transgene constructs.

In this study, PSI lines exhibited the wild type phenotype under short-day conditions (Figure 3.10). The number of leaves, rosette diameter, and fresh weight confirmed the growth observations (Figure 3.11,3.12 and 3.13, respectively). The growth observations were also similar under long-day conditions (Figure 3.14,3.15, 3.16 and 3.17). Indeed, it is not surprising that the PSI lines restore the wild type phenotype since the PSI variant was made by reconstructing the native *CAT2* gene under its promoter and terminator. Thus, it became apparent that the expression of the *CAT2* gene under its promoter restores the wild type growth phenotype. In agreement with this, it was previously revealed that the expression of *CAT2* from the *CAT2* promoter, but not *CAT2* under the control of the *CAT1* or *CAT3* promoter, restored the wild type phenotype in a *cat2-1* mutant (Hu et al., 2010).

Surprisingly, expression of an alternative splice variant in the *cat2-1* mutant background under *CAT2* promoter and terminator complements *cat2-1* mutant for growth (Figure 3.10). It is surprising as this variant describes a transcript that fails to remove the last intron, introducing an in-frame stop nearly removing the last 18 amino acids comprising the terminal peripheral alpha-helix and the C terminal targeting determinant. Thus, it was expected that this variant does not behave like the wild type. However, it is essential to note that no studies have been devoted to characterising this variant to date. Fresh weight, diameter and number of leaves in the WSQV lines were also examined under short-day conditions. The number of leaves and rosette diameter showed that WSQV lines were similar to the wildtype (Figure 3.11 and 3.12). Similar observations were observed in the plants transferred from short to long days (Figure 3.14, 3.15,3.16 and 3.17). Additionally, no apparent difference between the WSQV and wild type rosette fresh weight under both growth conditions (Figure 3.13 and 3.16), suggesting that the short form of CAT2 is responsible for complementing the growth.

It is also surprising that the variant which has a robust peroxisomal targeting signal ARL complements *cat2-1* mutant for growth (Figures 3.10-3.17). It is surprising because the native variant of catalase contains non-canonical C-terminal tripeptide. Additionally, peroxisomal catalase does not have a canonical PTS1 sequence in any of the organisms studied so far (Williams et al., 2012a). It has also been shown by the same authors that introducing a consensus PTS1 on yeast catalase interfered with maturation, suggesting that the mechanisms may be different between plant and yeast.

It was reported previously that the *cat2* mutation causes a decrease in root growth (Queval et al., 2007; Bueso et al., 2007; Yang et al., 2018). In this chapter, primary root length results are largely consistent with these earlier reports. Interestingly, the primary root length in all of the lines transformed with CAT2 variants appears to be restored.

Since the *cat2* mutant is a photorespiratory mutant, study the phenotype under photorespiratory conditions was important. Thus, a previously published approach (Kerchev et al., 2015; Waszczak et al., 2016) was applied to study the phenotype of different lines under photorespiratory conditions. *Cat2-1* mutant phenotype (Figure 3.20) was consistent with previous observations (Kerchev et al., 2015; Waszczak et al., 2016). Surprisingly, the introduction of the CAT2 with modified C termini largely restored the wild type phenotype. Interestingly, ARL lines showed a slight sensitivity to these conditions. This was confirmed by measuring the chlorophyll content in all previous lines (Figure 3.21). ARL lines had about 82% of the wildtype chlorophyll content, which means that they largely restored the chlorophyll content compared to the *cat2-1* mutant, which only had 34% of wild type chlorophyll content. These results indicate that PSI, WSQV and ARL lines are able to complement the *cat2-1* phenotype even under photorespiratory conditions.

According to the results of this chapter, CAT2 with C-terminal truncations can recover the growth deficiency of the *cat2-1* mutant, which could indicate that these forms can produce sufficient activity and act as antioxidant enzymes that detoxify the peroxisomal H<sub>2</sub>O<sub>2</sub>. Therefore, it is necessary to perform a biochemical analysis for all previous lines to examine the catalase activity, redox buffer and quantification of the expression level of H<sub>2</sub>O<sub>2</sub>-marker genes.

## Chapter 4

### Restoration of catalase (CAT) activity and redox status by expression of CAT2 variants

#### 4.1 Background

The results presented in Chapter Three demonstrated that the expression of the CAT2 variants in the *cat2-1* mutant background restored the wild type growth phenotype. This raises an important question of whether the biochemical defects of the *cat2-1* mutant including, catalase activity reduction, cellular redox state perturbation and upregulation of H<sub>2</sub>O<sub>2</sub> marker genes (Queval et al., 2007) are restored. Accordingly, wild type, *cat2-1* mutant and transgenic lines were used in this study to examine the catalase activity, ascorbate, and glutathione levels under short and long-day conditions. CAT protein levels were also assessed by western blotting. Besides, H<sub>2</sub>O<sub>2</sub> marker and autophagy genes were analysed to explore the cellular redox status at the molecular level.

Several studies have reported that *cat2* mutations reduce leaf catalase activity by about 80% compared to the wild type and accumulate H<sub>2</sub>O<sub>2</sub> under photorespiratory conditions (Queval et al., 2007; Mhamdi et al., 2010b; Hu et al., 2010; Gao et al., 2014; Su et al., 2018; Yang et al., 2018). Therefore, it plays an important role in the breakdown of H<sub>2</sub>O<sub>2</sub> produced in peroxisomes during photorespiration. However, catalase is not the only H<sub>2</sub>O<sub>2</sub>-scavenging enzyme in peroxisomes. H<sub>2</sub>O<sub>2</sub> levels may also be controlled by different peroxidases such as ascorbate peroxidase with the aid of various low molecular weight reductants such as ascorbate and glutathione (Jiménez et al., 1998; Del Río et al., 2002; Mhamdi et al., 2012; Del Río and López-Huertas, 2016). Plant cells contain very large quantities of ascorbate (10-100mM) and glutathione (0.2-10 mM) to counteract high fluxes of ROS production (Foyer and Noctor, 2003).

*A. thaliana* plants that are deficient in peroxisomal catalase exhibit symptoms of oxidative stress. For example, when *cat2* knockout mutants are grown in air redox homeostasis is perturbed, such that the leaves accumulate high glutathione levels and sometimes decrease ascorbate levels (Queval et al., 2007; Mhamdi et al., 2010b). In addition to ascorbate and glutathione, The levels of H<sub>2</sub>O<sub>2</sub> marker transcripts (*OXI1*, *HSP17.6*, *GSTF8*) are increased in the *cat2* mutants relative to the wild type (Queval et al., 2007; Su et al., 2018).

The *cat2* mutants do not show excessive H<sub>2</sub>O<sub>2</sub> accumulation because of these responses in antioxidants and gene expression. However, one important consequence of low CAT2 activity is peroxisome aggregation (Shibata et al., 2013; Yoshimoto et al., 2014b). The peroxisomes aggregates are selectively degraded by a process called pexophagy, a form of organelle specific autophagy that maintains cellular homeostasis (Veenhuis et al., 1983; Burkhart et al., 2013; Farmer et al., 2013; Bartel et al., 2014; Young and Bartel, 2016; Su et al., 2020; Pan et al., 2020). The autophagic (self-eating) process is mediated by a set of genes known as autophagy-related genes (*ATGs*) (Li and Vierstra, 2012; Avin-Wittenberg and Fernie, 2014). Disruption of *ATG* genes such as *ATG2* and *ATG7*, which are the major genes involved in the autophagic process has been shown to promote the aggregation of peroxisomes (Shibata et al., 2013; Yoshimoto et al., 2014b; Yamauchi et al., 2019; Su et al., 2020).

**The study of this chapter aims to determine whether the expression of the different CAT2 variants can correct the changes in redox homeostasis observed in the *cat2* mutants.**

## 4.2 CAT2 expression is restored. No overexpression was observed in CAT3.

It has been shown that CAT2 and CAT3 are the major isoforms in *A. thaliana* rosette leaves (Frugoli et al., 1996; Zimmermann et al., 2006). In agreement with that notion, the expression of *CAT2* and *CAT3* was studied at the protein level in the leaves of *A. thaliana* wild type, *cat2-1* mutants, PSI, WSQV and ARL plants grown under short-day conditions (8/16 h light/dark regime). After four weeks, leaves were harvested, and protein extracts were subjected to SDS-PAGE and western blotting. Using specific anti-CAT2 antibody, the presence of the CAT2 protein was observed in the leaf extracts of the wild type, PSI, WSQV and ARL plants (Figure 4.1, top). The absence of CAT2 in the *cat2-1* mutant leaves indicates that the antibody is specific for CAT2. This finding is also consistent with a recent study by Su et al. (2018), who used the same antibodies to detect CAT2 in catalase-deficient mutants and wild type.

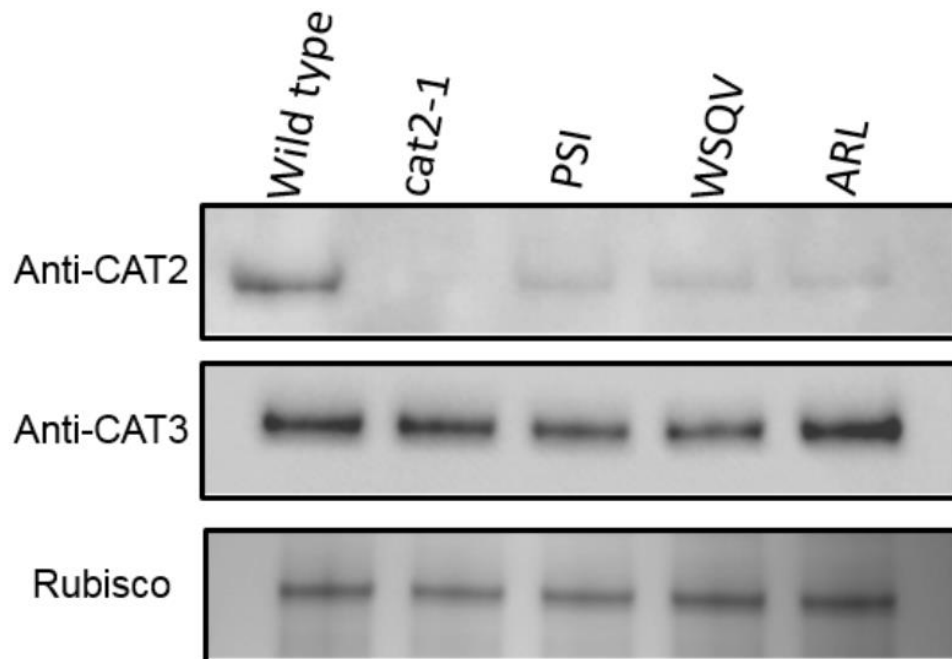


**Figure 4.1: Immunoblotting analysis of wild type, *cat2-1* mutant and transgenic lines using antibodies against CAT2 and CAT3.**

Western blot analysis of SDS-PAGE of protein extract (20 µg protein per lane) from wild type, *cat2-1* and transgenic leaves grown under short-day conditions for 4-weeks. CAT2 and CAT3 were detected using specific antibodies against CAT2 (Top) and CAT3 (Middle). Coomassie blue staining of the rubisco protein was used as the loading control (bottom). All SDS-PAGEs were run under the same conditions. All the experiments were repeated twice always showing the same results.

It should be noted that the level of the CAT2 protein in all of the transgenic lines was lower than that of the wild type, which is consistent with the lower level of *CAT2* transcripts detected by qRT-PCR analysis (Chapter 3, Figure 3.9B).

As presented in Figure 4.1, the middle lane, the CAT3 protein was detected in all lines using a specific antibody against CAT3. The specificity of this antibody for CAT3 was recently shown by a lack of immunodetection in *cat3* mutants (Su et al., 2018). Thus, this result clearly indicates that there were no detectable changes in the amount of the CAT3 protein in the transgenic lines relative to the wild type and *cat2-1* mutants. However, to assess the potential problems associated with differences in protein loading, rubisco large subunit protein was used as a loading control (Figure 4.1, bottom).

According to the western blot analysis, expression of the CAT2 protein is restored in the CAT2 variants but at levels that are lower than the wild type. Therefore, given this interesting observation, the determination of CAT activity in the different lines was the next crucial step to determine whether the CAT2 variants produce an enzymatically active protein.

### **4.3 CAT2 variants are enzymatically active**

To establish whether the transgenes restore CAT activity, the CAT activity of wild type, *cat2-1* mutant and transgenic lines was determined in plants that had been grown under short-day conditions for four weeks and then transferred to long-day conditions for a further week. Since *CAT2* expression shows a circadian rhythm, all samples were collected at the same time point, i.e. after 4-4.5h in the light period.

Leaf CAT activity was only 19-31% in the *cat2-1* mutant leaves of the activity measured in the wild type plants (Figure 4.2A). It should be noted that in Figure 4.2A, grey, black and white bars represent different experiments. Moreover, in order to make easy comparisons between the lines, the wild type CAT activity for each experiment was set at 100%. Notably, I chose to express the values as % to aid comparison between three experiments. However, the actual data is also presented in Table 4.1.

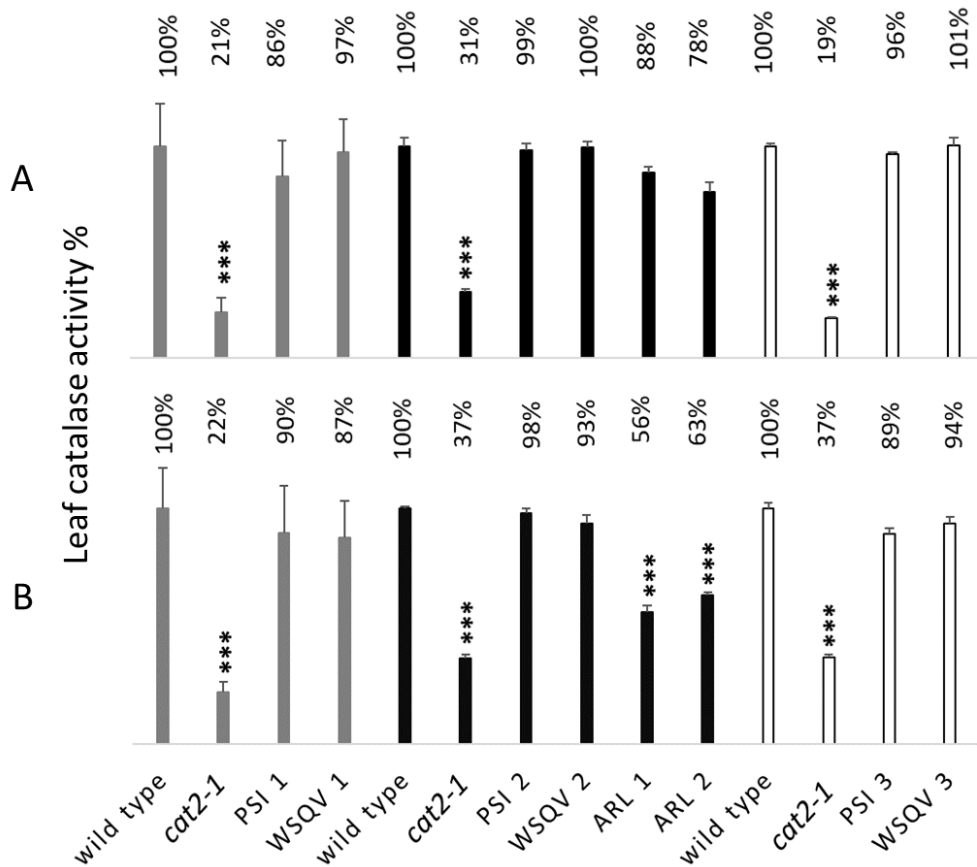


**Figure 4.2: CAT2 with C-terminal truncations is enzymatically active.**

Catalase activity was measured in leaf extracts from wild type, *cat2-1* mutant and different independent lines of transgenic grown under short and long-day conditions. Plants in each experiment were sampled at the same time. Percentage of catalase activity relative to wild type in each experiment is indicated at the top of the graph. (A) The activity of three independent lines of PSI and WSQV, in addition to the activity of two independent lines of ARL, was measured for plants grown under short-day conditions (8h-photoperiod) for 4 weeks. Plants were then transferred for one week to long-day conditions (16-h photoperiod), and the catalase activity was measured again (B). Grey bars represent the 1<sup>st</sup> line of WSQV and PSI. Black bars show the 2<sup>nd</sup> independent line of PSI and WSQV. The catalase activity of two independent lines of ARL is also indicated by black bars. White bars show the activity of the 3<sup>rd</sup> line of PSI and WSQV. Grey, black, and white bars are data from separate experiments. Wild type and *cat2-1* mutant grown in parallel with each experiment. Error bars represent the SE. \*\*\*P < 0.001 in significance given from analysis by Student's *t*-test. \*\*\* indicates significantly lower catalase activity compared to the control (wild type). Means were determined from three biological replicates (9 technical replicates).

The observed decrease in CAT activity in *cat2-1* mutant leaves confirms that *CAT2* is responsible for a large part of the leaf CAT activities. CAT activity was also examined in the different PSI lines (PSI1; grey bar, PSI2; black bar and PSI3; white bar) grown under short-day conditions. This analysis showed that the PSI lines retained about 86%, 99% and 96% (PSI1, PSI2 and PSI3, respectively) of wild type CAT activity, respectively (Grey, black and white, Figure 4.2A). Surprisingly, it was found that the CAT activity in the leaves of the three independent WSQV lines was similar to that measured in the leaves of wild type plants (grey, white and black, Figure 4.2A). These lines have about 97%, 100% and 101 % of the wild type CAT activity. These results suggest that the introduction of the short form of *CAT2* under the control of the *CAT2* promoter into the *cat2-1* mutant background can restore leaf CAT activity. This, in turn, provides strong evidence that the last 18 amino acids of *CAT2* sequence are not essential for the correct assembly of the CAT protein and hence CAT activity.

I also sought to determine whether the CAT activity was restored in the ARL transformants. This analysis revealed that both independent ARL lines had 78-88% of the wild type CAT activity (black, Figure 4.2A). This finding suggests that the replacement of the non-canonical PTS1 with a canonical form can also restore the wild type CAT activity under short-day conditions.

When plants were grown under long-day conditions (16h light/ 8h dark regime), as shown in Figure 4.2B, *cat2-1* mutants had only approximately 22-37% of the wild type CAT activity, in agreement with previous reports. CAT activity was restored to wild type levels in the PSI and WQSV lines under these growth conditions. However, leaf CAT activity was only about 56-63% of the wild type in the ARL lines (Figure 4.2B).

The results presented in this section, when taken together, provide evidence that these variants produce an enzymatically active CAT protein. The PSI and WSQV lines have similar activities to the wild type, with a small decrease in the ARL leaves under long-day conditions, which suggest that replacement of the non-canonical PTS1 with canonical PTS1 may affect the activity level under certain conditions.

The full restoration of CAT activity in the transgenic lines was surprising given that the levels of the CAT2 protein were lower in these lines. This discrepancy may be explained by the actions of post-translational regulation of the CAT2 protein. However, these results are consistent with the morphological characteristics of the different lines shown in chapter three.

**Table 4.1: Catalase activities.**

Values unit : ( $\mu\text{mol H}_2\text{O}_2 \text{ mg}^{-1} \text{ protein min}^{-1}$ ), SD; short-days, LD; long days, SE; standard error.

	SD	SE	LD	SE
Wild type	171	20.3	198	17.1
<i>Cat2-1</i>	37	6.8	44	4.4
PSI1	148	16.7	178	19.9
WSQV1	167	16.1	173	15.8
Wild type	60	4.6	84	0.6
<i>Cat2-1</i>	19	1.0	31	1.3
PSI2	59	2.9	82	2.1
WSQV2	60	2.4	78	3.7
ARL1	53	2.8	47	2.7
ARL2	47	4.8	53	1.0
Wild type	111	1.9	81	2.4
<i>Cat2-1</i>	21	0.8	30	1.1
PSI3	107	0.01	73	2.2
WSQV3	112	0.04	76	2.8

Based on previous observations, in-gel activity assay and characterisation of CAT subunits were necessary to detect the native form of CAT2 subunit, to examine whether CAT2 was properly assembled and active and if there is any evidence for the formation of hetero-oligomeric enzymes since catalase is a tetramer protein that can be built by any combination of CAT2 and CAT3 (Mhamdi et al., 2010b).

Native-PAGE analysis has been extensively used to analyse different CAT isoforms (Frugoli et al., 1996; Orendi et al., 2001; Zimmermann et al., 2006; Du et al., 2008; Hu et al., 2010). To this end, analysis of CAT isoforms was performed using non-denaturing gel electrophoresis where 20µg total protein isolated from wild type, *cat2-1* and transgenic leaves was separated using Native-PAGE, followed by western blotting with an anti-catalase antibody that recognises all three catalases. Then, the activity of isoforms was analysed using an in-gel activity assay.

CAT2 isoform was clearly detected in wild type and transgenic lines, whereas it was not detected in the *cat2-1* mutant, suggesting that the CAT2 was properly assembled (circle, Figure 4.3A). A shifted band in ARL, deemed to represent CAT2 (arrow, Figure 4.3A), indicating that the migration could be affected by adding an extra positive charge to the protein (Arginine; R). The upper band observed in Figure 4.3 (triangle) is likely to be an unrelated cross-reacting protein (possibly RUBISCO) (Appendix B, Figure B5). The band denotes rubisco was observed when SDS-PAGE of *cat2-1* mutant was blotted with this antibody. It was also confirmed by using a specific antibody against rubisco (i.e. same band with the same size was detected). Thus, the band presented by the triangle denotes rubisco (triangle, Figure 4.3A).

This result was also supported by the in-gel activity assay, which revealed that the activity was detected in wild-type and transgenic lines. In contrast, the activity was not detected in *cat2-1* mutant, suggesting CAT3 is below detection level in this assay (Figure 4.3B). Interestingly, the higher band in the ARL line also showed the activity, indicating that this band clearly represents CAT2 (arrow, Figure 4.3B). It was also clear that the activity was not detected in the upper band that denotes rubisco (triangle, Figure 4.3A).

Both the western blot and the activity assay reveal clear single bands for each of the constructs. Therefore, these results provide an independent line of evidence that the introduced transgene products are active and assemble into homo-oligomers.

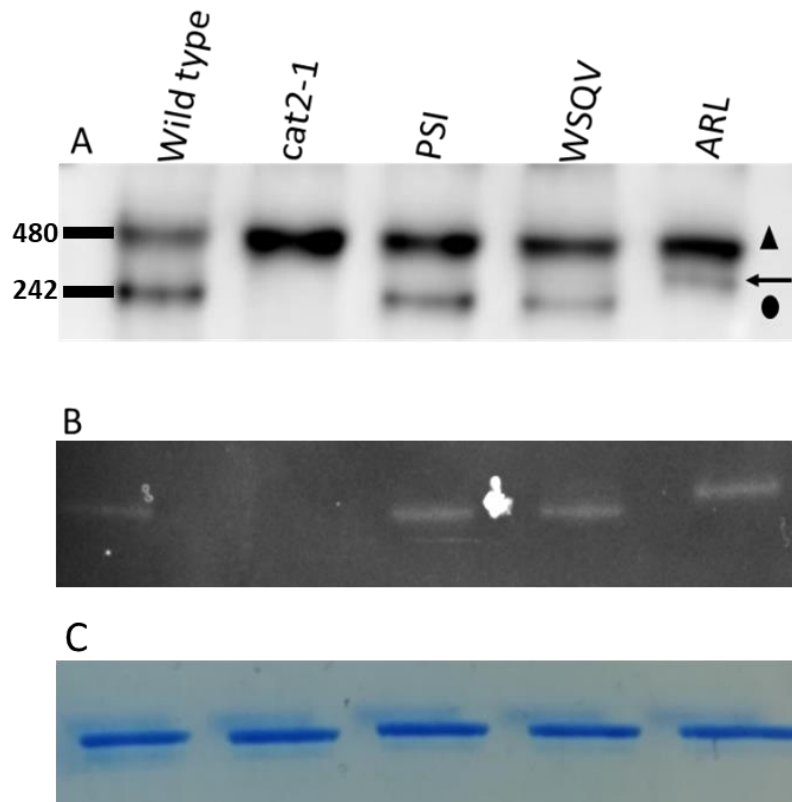


**Figure 4.3: Characterisation of catalase isoforms by western blot analysis.**

Total protein (20 µg per line) extracted from leaves of wild type, *cat2-1*, PSI, WSQV and ARL was separated on Native-PAGE and blotted on nitrocellulose membrane with catalase antibody, which recognises the three catalases and rubisco. Rubisco (Triangle) and CAT2 (Circle). A shifted band of ARL CAT2 is presented by an arrow (B) Native-PAGE, followed by an in-gel activity assay to define the CAT2 band in wild type, PSI, WSQV and ARL. All native-PAGEs were run under the same conditions. (C) Coomassie blue staining of the rubisco protein was used as the loading control

In conclusion, CAT2 protein is expressed in all transgenic lines but at a lower level than the wild type. SDS and native-PAGE analysis showed that CAT2 is clearly detected in PSI, WSQV and ARL transgenic lines. After separation of leaf protein extracts of wild type, *cat2-1* mutant and transgenic lines on native PAGE, it was confirmed that the activity of CAT2 protein is detected in all transgenic lines relative to the wild type. Importantly, no overexpression was observed. It was also shown that the presence of arginine in the 'ARL', which adds an extra positive charge to the protein, affects the protein migration on the native gel.

Although the previous results showed that the transgenic lines are fully functional and in accordance with the fact that the *CAT2* plays an important role in leaf redox homeostasis, it was necessary to explore if any redox perturbation occurs in the transgenic lines.

#### **4.4 Cell redox state is restored in CAT2 variants.**

Catalase deficiency generally results in an imbalance of cell redox status due to the accumulation of H<sub>2</sub>O<sub>2</sub>. This leads, in turn, to an imbalance of cell redox status, which results in an increase in the synthesis of non-enzymatic antioxidants such as ascorbate and glutathione. Ascorbate and glutathione (see Chapter 1, Sections 1.7 and 1.8) are key players in determining the cellular redox status due to their central role in H<sub>2</sub>O<sub>2</sub> detoxification (Noctor and Foyer, 1998).

To analyse the cell redox buffers; ascorbate and glutathione, wild type, *cat2-1* mutant, two independent lines of PSI, WSQV and one line of ARL were grown for 4 weeks in short-day conditions (8-h photoperiod) (Figures 4.4A and 4.5A) and then transferred to long-day conditions (16-h photoperiod) for one week (Figures 4.4B and 4.5B). Grey and black columns represent two separate experiments. In the first experiment, total ascorbate was measured, whereas the oxidised and reduced forms of ascorbate were analysed in the second experiment. The oxidized form of ascorbate (dehydroascorbate) is presented by red bars, while the reduced form is shown by black bars (Figure 4.4).

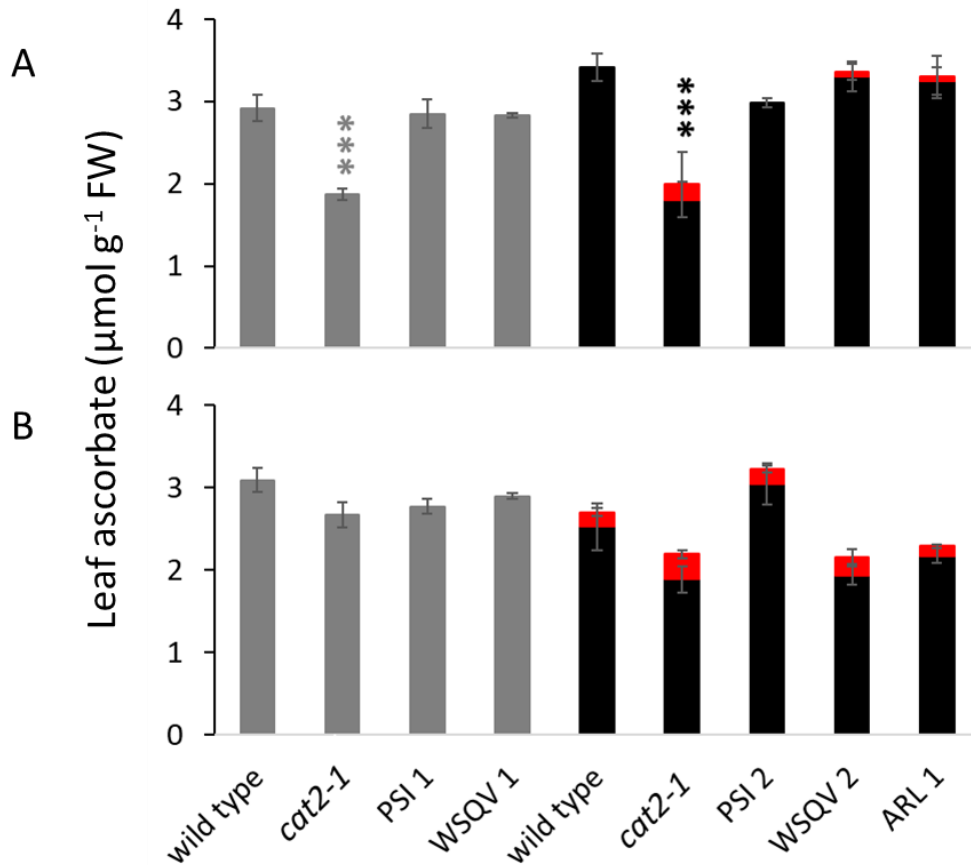


**Figure 4.4: A comparison of rosette ascorbate contents in wild type, *cat2-1* mutant, PSI, WSQV, and ARL grown under short and long-day conditions.**

Grey bars show total ascorbate as a separate experiment. In a different experiment, black blocks show the reduced form of ascorbate, whereas red blocks show the oxidized form of ascorbate (dehydroascorbate). (A) Ascorbate level ( $\mu\text{mol g}^{-1}$  FW) in leaves of the wild type, *cat2-1* mutant, one independent line of ARL and two independent lines of PSI and WSQV after growth under short-day conditions (8h light/16h dark) for 4 weeks. For comparison, the level of ascorbate under long-day conditions (16h light/ 8h dark), ascorbate contents of the same lines grown one week after transfer from 8-h to 16-h photoperiods is shown (B). Different independent lines are indicated by numbers. Wild type and *cat2-1* mutant grown in parallel with each experiment. Grey bars show the total ascorbate of the first independent line of WSQV and PSI, whereas the black with red bars represent the reduced and oxidized form of ascorbate of the 2<sup>nd</sup> line of WSQV, PSI and 1<sup>st</sup> line of ARL. Grey bars show the data of means of (6) independent extracts of different plants. In contrast, black bars indicate the data of means of (3) independent extracts of different plants. Each independent extract was run with three technical replicates. \*\*\* P < 0.001. Statistical analysis by Student's *t*-test showed that the ascorbate level of *cat2-1* mutant decreased compared with the wild type under short-day conditions. Error bars represent the SE. Significant differences between *cat2-1* mutant and wild type are indicated by grey and black asterisks (contents of the reduced form).

As can be seen in Figure 4.4A, total ascorbate was decreased significantly in *cat2-1* mutant grown under short-day conditions for four weeks. This is consistent with previous reports by others (Queval et al., 2007; Mhamdi et al., 2010b), pointing out that the decreases in ascorbate levels are sometimes observed in catalase-deficient plants. Remarkably, no significant differences were observed in the level of total ascorbate in PSI and WSQV lines compared to the wild type (grey, Figure 4.4A). In order to further explore the redox status in all lines, reduced and oxidized forms of the ascorbate were quantified in wild type, *cat2-1* mutant, ARL, and second line of PSI and WSQV grown under similar conditions (black, Figure 4.4A). This analysis revealed that the reduced ascorbate was significantly decreased only in *cat2-1* mutant whereas, both forms of ascorbate were not affected in PSI, WSQV and ARL lines (black, Figure 4.4A). It must be noted that the total ascorbate was recovered in all the lines compared to the *cat2-1* mutant, but that ratio of reduced to oxidised in WSQV and ARL was still lower, nonetheless, higher than in the *cat2-1* mutant.

When transferred to long-day conditions for a further one week, *cat2-1* mutant showed no significant difference in the total, reduced and oxidized ascorbate compared with the wild type. Interestingly, total, reduced, and oxidized ascorbate contents in PSI, WSQV and ARL were not significantly changed by the transfer (grey and black, Figure 4.4B). However, the oxidised form that was hardly detected in short days, it was detected in long days, indicating that the pool should be more oxidised in long-day conditions. Interestingly, that seems to be true for the other lines.

In conclusion, ascorbate content analysis suggested that the transgenic lines largely restored the ascorbate levels. However, it has been shown that the amount of glutathione can sharply change to maintain the redox state (Queval et al., 2007; Mhamdi et al., 2010b; Su et al., 2018). Thus, the reduced form of glutathione (GSH) in addition to the disulphide form (GSSG) were examined in wild type, *cat2-1* mutant, one independent line of ARL and two independent lines of WSQV and PSI grown under short-day condition and then transferred to long-day conditions for a further one-week. Grey and black bars show the reduced form of two independent experiments, whereas the oxidised form of each experiment represented by red bars (Figure 4.5).

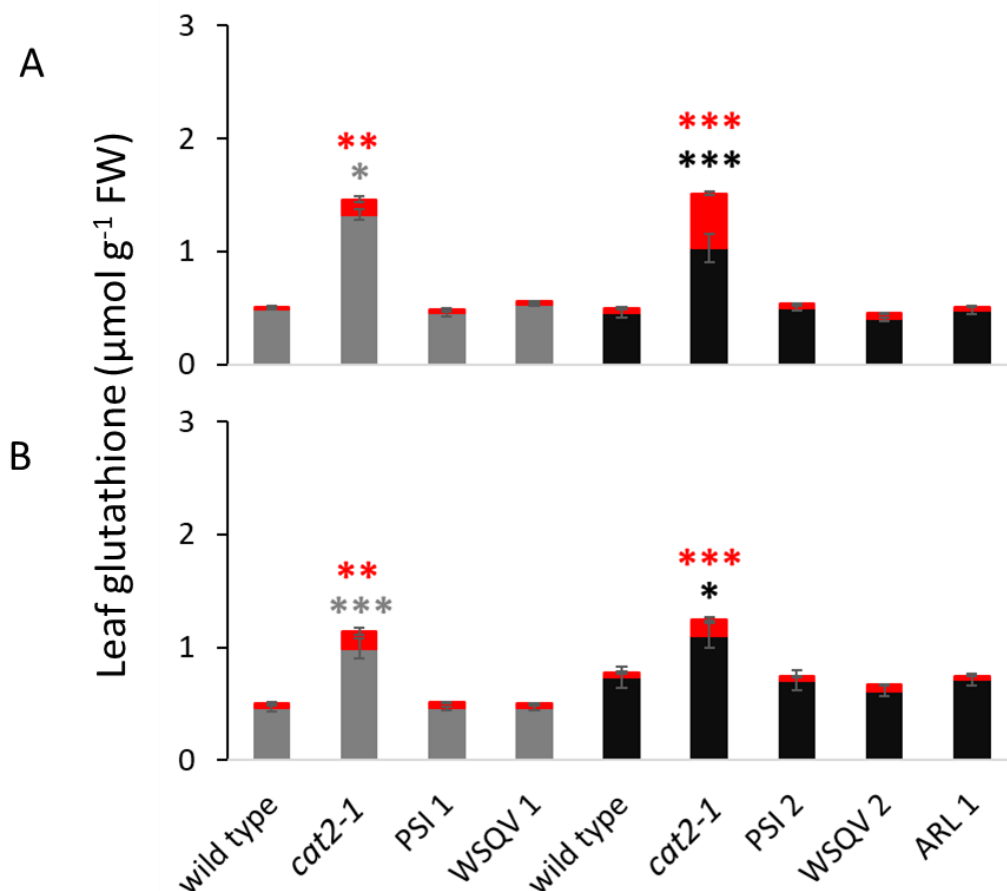


**Figure 4.5: A comparison of rosette glutathione contents ( $\mu\text{mol g}^{-1}$  FW) in wild type, *cat2-1* mutant and transgenic lines grown under short and long-day conditions.**

Grey and black blocks show the reduced form of glutathione (GSH) of different experiments, while the oxidized form of glutathione (GSSG) is presented by red blocks. (A) Glutathione measurements of wild type, *cat2-1* mutant, two independent lines of PSI and WSQV, one independent line of ARL grown under short-day conditions (8hrs photoperiod) for 4 weeks. (B) Glutathione contents of the same lines grown under long-day conditions (16 hrs photoperiod) for one week after transfer from short-day conditions. 1<sup>st</sup> independent line of PSI and WSQV is presented by grey with red bars. Black with red bars indicate the 2<sup>nd</sup> independent line of PSI, WSQV and 1<sup>st</sup> independent line of ARL. Wild type and *cat2-1* mutant grown in parallel with each set of experiment. Data are means of three independent extracts of different plants (i.e. three biological replicates and nine technical replicates). Error bars represent the SE. (\*  $P < 0.05$ ) (\*\*  $P < 0.01$ ) (\*\*\*)  $P < 0.001$ ) in significance given from analysis by Student's *t*-test compared to the wild type. Different independent lines are indicated by numbers. Significant differences from wild type are indicated above *cat2-1* mutant bars by grey and black asterisks (contents of GSH) or red (contents of GSSG).

Under short-day conditions, the level of the GSH and GSSG was dramatically increased in the *cat2-1* mutant compared with the wild type (Figure 4.5A). This is consistent with previous studies and explained by the increased availability of photorespiratory H<sub>2</sub>O<sub>2</sub> in leaves (Queval et al., 2007; Mhamdi et al., 2010b). On the other hand, no significant change in both forms of glutathione occurred in PSI lines compared with the wild type (Figure 4.5A). Similarly, no change in the level of glutathione forms was observed in two WSQV lines and ARL lines (Figure 4.5A), supporting the earlier observations (Figure 4.4).

Similar results were observed when plants transferred to long-day conditions, where the most dramatic changes occurred in only *cat2-1* mutant glutathione which is consistent with the previous studies (as above), whereas the glutathione in transgenic lines was not changed in all transgenic lines with respect to wild type (Figure 4.5B). Taken together, these data suggest that the biochemical markers of redox status are not affected in all transgenic lines and not influenced by the photoperiod in which plants are growing, supporting the idea that no redox perturbation occurred in transgenic lines. However, in order to obtain further information in regards to the cell redox status at the molecular level, H<sub>2</sub>O<sub>2</sub> marker genes were examined using RT-qPCR and specific gene primers, particularly, the misregulation of these transcripts has been extensively shown to occur under oxidative stress (Vanderauwera et al., 2005; Queval et al., 2007; Noctor et al., 2016). For this effect, RT-qPCR analysis of H<sub>2</sub>O<sub>2</sub>- marker genes (*HSP17.6*, *GSTF8*, and *OXI1*) was performed using cDNA samples of wild type, *cat2-1* and transgenic lines grown under short-day conditions for four weeks. This analysis was performed twice using different independent lines with similar results. Results of one independent line are presented here.

As indicated in Figure 4.6, the *cat2-1* mutant showed upregulation of *HSP17.6*, *OXI1* and *GSTF8* transcripts. The upregulation of H<sub>2</sub>O<sub>2</sub>-marker transcripts is consistent with decreased ascorbate and accumulation of glutathione (Figure 4.4 and 4.5). This result is also consistent with previous findings, suggesting that the redox perturbation linked to *CAT2* deficiency affected gene expression (Queval et al., 2007; Mhamdi et al., 2010b; Noctor et al., 2016).

H<sub>2</sub>O<sub>2</sub> marker genes were examined under short-day conditions because it has been well documented that these genes are strongly induced in *cat2* leaves under short-day conditions (Queval et al., 2007; Noctor et al., 2016).

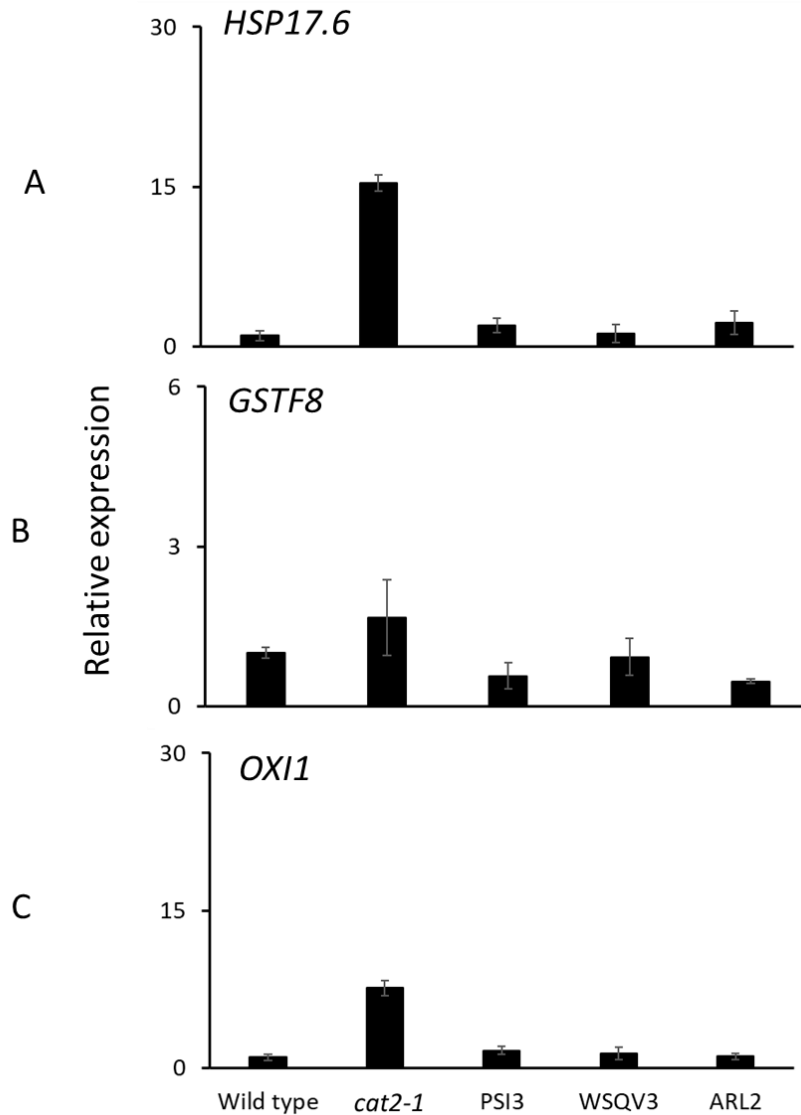


**Figure 4.6: RT-qPCR analysis of H<sub>2</sub>O<sub>2</sub>-markers transcripts.**

Wild type, *cat2-1* mutant, PSI, WSQV and ARL were grown under short-day conditions (8h light/16h dark) for 4 weeks. The mean value of three replicate was normalized using *ACTIN 2* as the internal control. AGI codes for the gene encoding marker transcripts: (A) At2g29500 (*HSP17.6*). (B) *GSTF8*, At2g47730. (C) At3g25250, *OXI 1*. Independent lines of transgenic lines are numbered; 2<sup>nd</sup> independent line of ARL and 3<sup>rd</sup> independent lines of PSI and WSQV. Wild type and *cat2-1* mutant grown in parallel with the transgenic lines. Expression level relative to *ACTIN 2*. The expression level in the wild type was assigned a value of 1. The expression level was calculated using the  $2^{-\Delta\Delta CT}$  method. Error bars represent the SE.

Under short-day conditions, PSI transgenic lines *HSP17.6*, *GSTF8* and *OXI1* transcripts level analysis showed that they have similar expression level to those in the wild type (A, B and C, Figure 4.6). When *HSP17.6*, *GSTF8* and *OXI1* transcripts examined in WSQV lines under short-day conditions, no difference in wild type and WSQV was apparent (A, B and C, Figure 4.7). Furthermore, analysis of H<sub>2</sub>O<sub>2</sub> marker transcripts in ARL lines showed no obvious change compared to the wild type (A, B and C, Figure 4.6). Taken together, these results confirmed the previous experiments (Figure 4.4 and 4.5), which correctly conclude that there is no evidence for any redox perturbation in all transgenic lines.

In conclusion, the findings of the biochemical redox status markers and H<sub>2</sub>O<sub>2</sub>-marker transcripts data provide a good indication of the cellular redox homeostasis in the three variants, and they are considered a reliable proxy for H<sub>2</sub>O<sub>2</sub> metabolism. Therefore, no evidence for an accumulation of H<sub>2</sub>O<sub>2</sub>. However, several studies have shown that the accumulation of H<sub>2</sub>O<sub>2</sub> (particularly the photorespiratory H<sub>2</sub>O<sub>2</sub> generated during photorespiration in peroxisomes) cause oxidative damage which in turn induce peroxisome aggregation. Plants degrade peroxisomes through a process known as pexophagy, a form of specialized autophagy (Chapter 1, Section 1.10). Consistent with that notion, it was worth analysing the expression level of autophagy marker transcripts (*ATG2* and *ATG7*) in *cat2-1* mutant and all transgenic lines.

#### **4.5 Autophagy genes expression (*ATG2* and *ATG7*)**

As discussed in Chapter 1, Section 1.10, it has been demonstrated that H<sub>2</sub>O<sub>2</sub> accumulated in *cat2* mutant is one of the peroxisome aggregation inducers, therefore, the autophagy marker genes (*ATGs*) have been reported to colocalise with peroxisome aggregates, indicating that the damaged peroxisomes are selectively degraded by autophagy to maintain peroxisome quality control (Veenhuis et al., 1983; Shibata et al., 2013; Bartel et al., 2014; Kao et al., 2018). For that, the expression level of two autophagy-marker genes was examined in wild type, *cat2-1* mutant, PSI, WSQV and ARL grown under short-day conditions for four weeks using RT-qPCR.

Under short-day conditions, RT-qPCR analysis of *ATG2* and *ATG7* transcripts showed induction in *cat2-1* mutant compared to the wild type, indicating that the pexophagy induced by that the H<sub>2</sub>O<sub>2</sub> accumulation. However, analysis of autophagy genes in the PSI lines revealed that no obvious difference in the level of *ATG2* and *ATG7* transcripts were observed (Figure 4.7A and B).

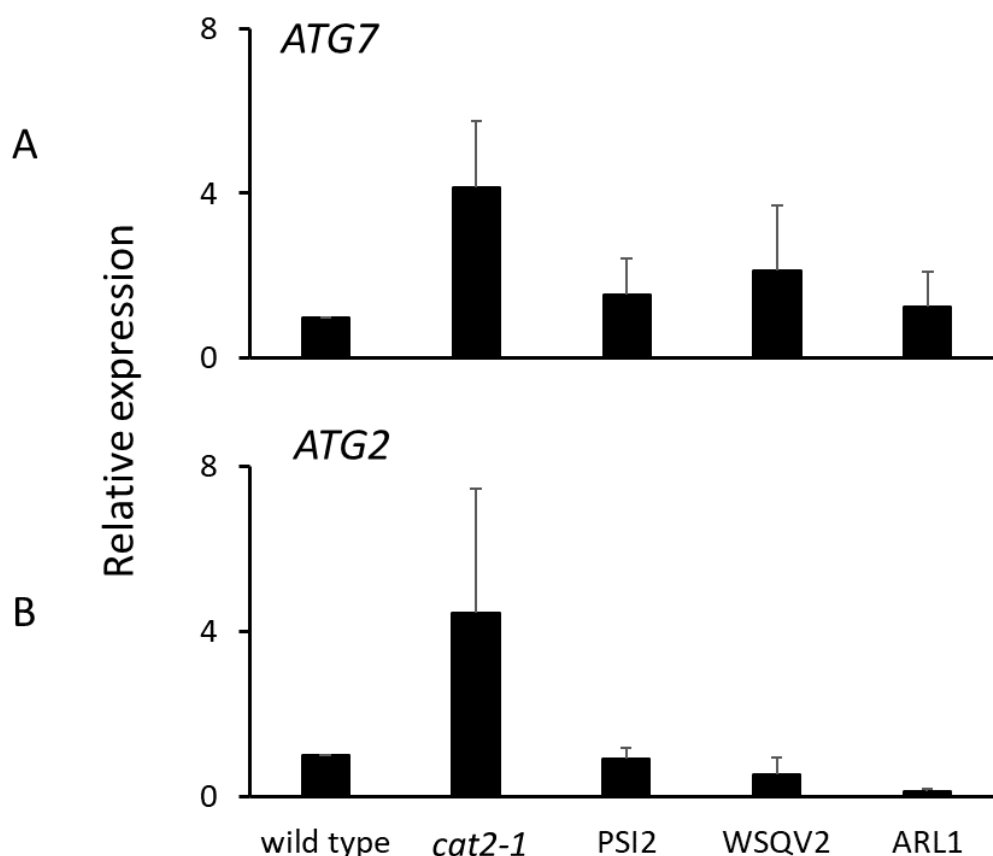


**Figure 4.7: Relative expression levels of autophagy genes (*ATG2* and *ATG7*).**

Wild type, *cat2-1*, PSI, WSQV and ARL plants were grown under short-day conditions for 4 weeks. The mean value of two replicates was normalized using *ACTIN 2* as the internal control. 1<sup>st</sup> independent line of ARL (ARL1) and 2<sup>nd</sup> independent line of PSI (PSI2) and WSQV (WSQV2) were used. Wild type and *cat2-1* mutant grown in parallel with the transgenic lines. Expression level relative to *ACTIN 2*. The expression level in the wild type was assigned a value of 1. The expression level was calculated using the  $2^{-\Delta\Delta CT}$  method. Error bars represent the SE.

Expression analysis of two autophagy transcripts revealed that no induction in WSQV lines ( Figure 4.7A and B). When autophagy transcripts of ARL lines were analysed, no induction was revealed compared to the wild type (A and B, Figure 4.7). These results, when taken together, suggested that the presence of catalase in transgenic lines prevents the H<sub>2</sub>O<sub>2</sub> accumulation and any aggregation that may occur in peroxisomes.

The results presented in this chapter indicated that the catalase activity of PSI WSQV and ARL lines were fully restored under short-day conditions. Similar results were observed under long-day conditions except for ARL lines which showed a reduction in the activity. The findings presented here also confirmed that the CAT2 expression of the transgenic lines was restored. It was also shown that transgenic lines were largely restored the redox status. Additionally, it was confirmed that the transgenic lines had corrected the levels of H<sub>2</sub>O<sub>2</sub> and autophagy marker genes where these genes were clearly upregulated in the *cat2-1* mutant.

## 4.6 Discussion

The studies described in this chapter were performed to investigate the metabolic consequences of introducing CAT2 variants into a *cat2-1* mutant background, as well as to understand the role of the conserved C-terminal sequence in CAT functions. Measurements were made on plants grown either for four weeks under the short-day conditions or for four weeks under the short-day regime followed one week of long-day conditions. The data provide new information concerning the CAT activity, redox status, and gene expression in the transgenic lines compared to the wild type and *cat2-1* mutants. H<sub>2</sub>O<sub>2</sub> and autophagy marker transcripts were analysed in the lines grown under short-day conditions. The data presented here clearly show that the CAT2 variants restore CAT enzyme activity and cellular redox status to levels observed in the wild type. The implications of these results are discussed in more detail below.

Using specific anti-CAT2 and anti-CAT3 antibodies, the data presented here show that the level of the CAT2 protein in the leaves of the transgenic lines was restored to levels that were slightly lower than those measured in the wild type (Upper blot, Figure 4.1). This finding was surprising given that the levels of *CAT2* transcripts were lower than the wild type (chapter 3, Figure 3.9B). These findings may be explained by post-translational regulation of the CAT protein (discussed in more details below). The levels of the CAT3 protein were similar in all lines, including the wild type and *cat2-1* mutant (Middle blot, Figure 4.1). This finding is consistent with the data presented in chapter 3 (Figure 3.8 and 3.9C), which show that there is no overexpression of CAT3 in any of the lines. The specificity of the antibodies used in the present studies was reported by Su et al. (2018). They used these antibodies to detect the expression of CAT2 and CAT3 in *cat* mutants (*cat1/3* double mutants). These results demonstrate that the CAT2 protein is expressed in all the lines and that there is no evidence for altered expression of CAT3.

CAT3 and CAT2 have been shown to mainly expressed in leaves (McClung, 1997; Frugoli et al., 1996). Therefore, the formation of mixed oligomers of the two proteins might be possible. No evidence to suggest the presence of hetero-oligomers was found in the present study (Figure 4.3). This finding is consistent with previous suggestions that the formation of hetero-oligomeric proteins from more than one CAT gene product is a minor phenomenon *in vivo* (Zimmermann et al., 2006; Mhamdi et al., 2010b).

In this study, it was shown that the leaves of the *cat2-1* mutant exhibit low CAT activity under both short and long-day conditions (Figure 4.2A and B), pointing to a greater contribution of the *CAT2* isoform to total leaf CAT activity. This result is consistent with the rosette phenotypes of *cat2-1* mutants (Chapter 3). Moreover, these findings complement literature data (Bueso et al., 2007; Queval et al., 2007; Du et al., 2008; Hu et al., 2010; Yang et al., 2018), showing that *cat2* mutants exhibit a much great reduction in leaf CAT activity than the *cat3* mutants. In agreement with the fact that the *CAT2* is the major leaf CAT isoform, the data presented here show that the PSI lines exhibited wild type CAT activity levels. This evidence suggests that the CAT activity measured in the lines transformed with the PSI construct produces an active *CAT2* enzyme (Figure 4.2A and B). Indeed, this result was predicted because the native *CAT2* variant was introduced into the *cat2-1* mutant background under the control of the *CAT2* promoter, similar to the wild type gene.

In chapter 3 (Figure 3.4), it was shown that the alternative splice variant of *CAT2* is present and presumably translated. However, the functions of this variant have not been elucidated. In this chapter, it was shown that the lines transformed with the alternative splice variant (WSQV construct) restored the wild type CAT activity in plants grown under both short- and long day-conditions (Figure 4.2A and B). This finding demonstrates that the short form of *CAT2* is enzymatically active. The levels of *CAT2* transcripts and protein were lower in the WSQV lines than the wild type, indicating that changes in transcript abundance do not necessarily reflect changes in enzyme activity.

A possible explanation for this finding is that the activity of the CAT protein is regulated by posttranslational modifications. Several studies have reported post-translation modifications, such as succinylation and acetylation of the CAT protein (i.e. lysine acylations). For example, it has been demonstrated that succinylation has a profound effect on the CAT activity of recombinant CAT(CATA) protein in rice (*Oryza sativa*) leaves (Zhou, H. et al., 2018).

Moreover, protein phosphorylation has also been shown to regulate CAT activity, for example, CAT activity in mammals is regulated by the c-Abl and Arg protein kinases (Cao et al., 2003). Plant catalase activity is enhanced by calmodulin (CaM) in the presence of calcium (Ca<sup>2+</sup>) to regulate H<sub>2</sub>O<sub>2</sub> homeostasis. Recently, rice catalase (CatC) is phosphorylated mainly at Tyr-210 and is activated by salt tolerance receptor-like kinase 1 (STRK1) (Zhou, Y.B. et al., 2018).

Numerous proteins have been described to interact with catalase and affect its activity, including calmodulin, salt overly sensitive 2 (SOS2), nucleoside diphosphate kinase 1 (NDK1) and triple gene block protein 1 (TGBp1) and LESION SIMULATING DISEASE1 (LSD1) (Yang and Poovaiah, 2002; Fukamatsu et al., 2003; Verslues et al., 2007; Mathioudakis et al., 2013; Li et al., 2013). In addition, the chaperone protein activity of NO CATALASE ACTIVITY1 (NCA1) is required for full CAT activity (Hackenberg et al., 2013; Li et al., 2015). Hsp17.6CII, a peroxisomal small heat shock protein and chaperon, have also been shown to interact with *At*CAT2 to increase catalase activity (Li et al., 2017). It was recently found that *A. thaliana* natriuretic peptide (AtPNP-A) plays a critical role in modulating the activity of CAT2 (Turek et al., 2020). However, the interaction mechanism is still not well understood.

Higher CAT activity of the WSQV lines suggests that the conserved C-terminus (i.e. The C-terminal sequence on monocot and dicots CAT proteins is highly conserved based on the sequence alignment analysis) is not important for protein folding or activity. There have been no previous reports showing that the effect of the C-terminal removal on the CAT activity. It should be noted that the structural information on plant catalases is limited and the structure of the *A. thaliana* CAT has not been established.

However, based on the predicted 3D structural model of *A. thaliana* CAT (see Chapter 6, Figure 6.1), the C-terminal domain is predicted to be lying on the external side of the protein. Thus, it is very unlikely to affect protein folding and activity. In agreement with this conclusion, the data presented in this study clearly shows that the C-terminal is not important for activity.

The lines transformed with ARL constructs had wild type levels of CAT activity when plants were grown under short-day conditions (Figure 4.2A). Strikingly, following transfer from short- to long-day conditions (for one week), a lower level of CAT activity was observed in the ARL lines relative to the wild type (Figure 4.2B). Therefore, changing the C-terminus sequence to ARL has an influence on CAT activity under these specific day-length conditions. Williams et al. (2012) reported that the CAT activity of *H. polymorpha* was decreased by replacing the non-canonical PTS1 by the canonical PTS1 tripeptide-SKL. These results showed that the CAT-SKL protein was present as inactive aggregates. In this study, adding a consensus PTS1-ARL sequence resulted in a slightly lower CAT activity than the wild type. However, in this case, there was no change in the levels of transcripts encoding proteins involved in autophagy (Figure 4.7). Further investigations using this variant are required, for example, using confocal microscopy to detect the presence of protein aggregates. This aspect will be covered in chapter 5.

The plant antioxidant defence system includes enzymatic and non-enzymatic components. Non-enzymatic antioxidants such as ascorbate and glutathione play a crucial role in plant defences against oxidative stress (Apel and Hirt, 2004). Ascorbate and glutathione are major molecules that form an integral part of the ascorbate-glutathione cycle that functions to detoxify H<sub>2</sub>O<sub>2</sub> (Foyer and Halliwell, 1976; Foyer and Noctor, 2011). It has previously been shown that an accumulation of glutathione occurs in response to exposure to different environmental stresses. For example, the antioxidant system is increased in response to cold stress in maize leaves by Gomes and co-workers (Gómez et al., 2004).

The redox perturbations occurring in CAT-deficient *A. thaliana* plants have been extensively studied, and evidence provided for altered levels of ascorbate and glutathione (Queval et al., 2007; Mhamdi et al., 2010b; Su et al., 2018). Moreover, studies on CAT-deficient barley and tobacco lines, have shown that H<sub>2</sub>O<sub>2</sub> processing is impaired in the *cat2* mutants, such that greater amounts of H<sub>2</sub>O<sub>2</sub> are scavenged by alternative mechanisms, including glutathione and ascorbate (Willekens et al., 1997; Smith et al., 1985; Milla et al., 2003; Davletova et al., 2005).

The present study shows that the absence of the CAT2 protein leads to greater glutathione accumulation and decreased levels of ascorbate, compared to the wild type (Figures 4.4 and 4.5). The increased amounts of reduced glutathione (GSH) and glutathione disulphide (GSSG) observed in the *cat2-1* mutants may be explained by oxidative activation of the pathway of GSH synthesis and that GSSG accumulates due to higher levels of GSH oxidation than GSSG reduction in the *cat2* mutants (Mhamdi et al., 2010b). Therefore, it is clear that the *cat2-1* mutants experience redox perturbations, which were detected as decreased ascorbate and increased glutathione levels. Thus, restoration of the wild type levels of ascorbate and glutathione in the transgenic lines could provide strong evidence of restored cellular redox status (Figures 4.4 and 4.5).

In order to provide evidence that cellular redox status is restored in the transgenic lines, the expression of H<sub>2</sub>O<sub>2</sub> marker transcripts was analysed in the transgenic lines. Several studies have investigated the expression patterns of the *A. thaliana* heat shock proteins *HSP17.4* and shown that *HSP17.4* is expressed in response to oxidative stress (Sun et al., 2001; Sun et al., 2002; Li et al., 2017). The expression of *HSP17.4* was enhanced in the *cat2-1* mutants, suggesting that these plants experience oxidative stress (Queval et al., 2007; Sewelam et al., 2019). Therefore, any change in the levels of *HSP17.4* expression transcripts may indicate the presence of oxidative stress.

In this study, it was shown that the expression level of *HSP17.4* was dramatically increased in the *cat2-1* mutants. In contrast, no significant differences in the level of *HSP17.4* expression were observed in the transgenic lines compared to the wild type (Figure 4.6A). These findings suggest that the transgenic lines are experiencing a similar level of the oxidative stress as the wild type.

It has previously been shown that the *A.thaliana* glutathione S-transferase called PHI8 (*GSTF8*) is specifically expressed in response to oxidative stress in the *cat* mutants (Queval et al., 2007; Rahantaniaina et al., 2017). In agreement with these published results, the data presented in Figure 4.6B show that the levels of *GSTF8* transcripts are increased in the *cat2-1* mutants compared to the wild type. On the contrary, the expression of *GSTF8* is similar in the transgenic lines to the wild type (Figure 4.7B), indicating that the introduction of the CAT2 variants into the *cat2-1* mutant background was able to correct the oxidative stress perturbation in the *cat2-1* mutants and restore the levels of *GSTF8* transcripts to those observed in the wild type.

*OXI<sub>1</sub>* (OXIDATIVE SIGNAL INDUCIBLE 1) is a protein kinase that has been shown to be differentially expressed in response to oxidative stress (Wang et al., 2010). As shown by Queval et al. (2007) and Su et al. (2018), the expression of *OXI<sub>1</sub>* was significantly increased in the *cat* mutants. In this study, it was shown that the level of *OXI<sub>1</sub>* transcripts was markedly increased in the *cat2-1* mutants, whereas, it was not significantly different in the wild type and transgenic lines (Figure 4.6C). This indicates that the presence of CAT2 in the transgenic lines corrects the perturbation that leads to elevated expression of *OXI<sub>1</sub>*. In conclusion, these results clearly demonstrate that H<sub>2</sub>O<sub>2</sub>-marker transcripts are increased in the *cat2-1* mutants and that these changes are reversed by introducing different CAT2 variants into the *cat2-1* mutant background.

It has been demonstrated that autophagy plays an important role in the regulation of metabolism that occurs in response to oxidative stress (Xiong et al., 2007; Yoshimoto et al., 2014b; Yamauchi et al., 2019). The *A. thaliana atg2* mutant is an autophagy defective mutant that exhibits enhanced accumulation of H<sub>2</sub>O<sub>2</sub> even in the absence of stress (Yoshimoto et al., 2009). H<sub>2</sub>O<sub>2</sub> accumulation is an inducer of peroxisome aggregate formation.

H<sub>2</sub>O<sub>2</sub> accumulates in peroxisomes in response to CAT inactivation, which triggers clusters of damaged peroxisomes (Shibata et al., 2013). Pexophagy facilitates peroxisome degradation (Burkhart et al., 2013; Farmer et al., 2013; Bartel et al., 2014; Young and Bartel, 2016; Pan et al., 2020; Su et al., 2020). Mutants with aggregated peroxisomes have been identified by Shibata et al. (2013), who showed that the *atg2* and *atg7* mutations cause aggregation. These findings suggest that there is a selective degradation of peroxisomes via autophagy. In this study, the expression levels of *ATG2* and *ATG7* were analysed in plants grown under short-day conditions. The results shown in Figure 4.7A and B show that the expression levels of autophagy genes were markedly increased in the *cat2-1* mutants. In contrast, there was no induction of the expression of autophagy genes in the transgenic lines (Figure 4.7A and B), suggesting that the *CAT2* variants are able to maintain cellular redox status at similar levels to the wild type. This conclusion is strongly supported by the data on ascorbate and glutathione, as well as the expression of H<sub>2</sub>O<sub>2</sub> marker genes.

In summary, the evidence presented in this study on the consequences of introducing different *CAT2* variants into the *cat2-1* mutant background under the control of the *CAT2* promoter shows that all the variants produced fully functional proteins. However, it remains to be established whether these variants are correctly targeted to the peroxisomes. This will be explored in the next chapter. To this end, the isolation and characterisation of leaf peroxisomes will be presented to determine the intracellular location of *CAT2* variants.

## Chapter 5 Subcellular localisation of CAT2 variants

### 5.1 Background

Results presented in Chapters Three and Four indicated that introducing CAT2 variants that contain different C-termini into the *cat2-1* mutant background restores most of the morphological and biochemical features which are altered due to CAT2 deficiency in the *cat2-1* mutant. Consequently, it was concluded that the highly conserved C terminal 18 amino acids of CAT2 are dispensable for growth, redox status, and activity. These findings led to an important question regards the subcellular localisation of CAT2 variants since the mechanism of catalase targeting is still unclear (see Chapter 1, Section 1.9.6, for more detail about the catalase targeting). For this effect, this chapter presents an extensive series of experiments that were designed to investigate the subcellular localisation of CAT2-PSI, CAT2-WSQV and CAT2-ARL variants.

Isolation of pure organelles and /or tagging proteins with a suitable reporter such as a fluorescent protein can effectively demonstrate protein localisation. To this end, firstly, peroxisomes were isolated by cellular fractionation techniques. However, peroxisome isolation is complicated because they are highly fragile organelles and relatively similar in density to mitochondria. Moreover, they are usually adhering to chloroplasts in photosynthetic tissues, which results in contamination by these organelles (Hajra and Wu, 1985; Reumann and Singhal, 2014). Consistent with this notion, various techniques were tested for their ability to isolate reasonably pure peroxisomes, as free as possible from contamination in order to detect whether the CAT2 variants are present in peroxisomes or not.

Secondly, CAT2 variants were fused to a green fluorescent protein (GFP), and their subcellular localisation was examined using confocal laser microscopy. A self-assembling split GFP system (Van Engelenburg and Palmer, 2010) was used in this study. GFP is an 11-stranded  $\beta$ -barrel protein which can be split into two fragments, 1-10  $\beta$  strands (GFP1-10) and the 11  $\beta$  strands with 16 amino acids (GFP 11) neither of which are fluorescent on their own, but which combine to produce a fluorescent signal (Figure 5.1).

GFP1-10 was engineered for GFP1-10<sup>OPT</sup> to enhance solubility and fluorescence intensity (Cabantous et al., 2005; Cabantous et al., 2013; Park et al., 2017). In this system, a protein of interest is fused to sfGFP11, and when delivered into transgenic lines expressing GFP1-10<sup>OPT</sup>, the two fragments can assemble and emit fluorescence if they are in the same compartment. (Figure 5.1).

The self-assembling split GFP system has been extensively used as a tool to study the subcellular localisation of various proteins. For example, it has been used to visualize *Agrobacterium tumefaciens* VirE2 delivered through type-IV secretion system (T4SS) into plant cells (Li et al., 2014) and to study the subcellular localisation of human proteins (Leonetti et al., 2016). It has recently been used to monitor the subcellular localisation of type III effector proteins (T3Es) delivered from *Pseudomonas syringae* into plant cells (Park et al., 2017). Park et al. (2017) generated transgenic *A. thaliana* plants that express the improved sfGFP1-10<sup>OPT</sup> in different cellular compartments. They also generated various organelle-targeted sfGFP11 constructs. Seeds and plasmids were obtained from the ABRC (See Chapter 2, Table 2.5). CAT2 variants were fused to sfGFP11 and the generated constructs were transfected into protoplasts isolated from different lines expressing sfGFP1-10<sup>OPT</sup> and scanned using confocal microscopy.



**Figure 5.1: Diagram of self-folding split sfGFP complementation.**

An sfGFP11 (11  $\beta$  strands) is fused to a protein of interest (X) either at C or N-terminal domain. The complementary GFP1-10<sup>OPT</sup> fragment (1-10  $\beta$  strands) is expressed separately, and fluorescence occurs upon protein interaction.

## 5.2 Studying the localisation of CAT2 variants by cell fractionation

The localisation of the CAT2 variants was examined by crude fractionation of cellular contents and then a more detailed analysis by fractionating the cellular contents on a percoll and sucrose gradient.

### 5.2.1 Crude fractionation

Peroxisome enriched pellets were prepared from 4-week-old rosette leaves of wild type, *cat2-1* mutant, PSI2, WSQV2 and ARL1 complementing lines grown under short-day conditions. Three fractions were generated as described in (Chapter 2, Section 2.2.14.1). Figure 5.2 summarises the crude fractionation process, including the preparation of three fractions. Homogenate fraction (S1), cytosolic fraction (S2) organelle pellet fraction (P2) were used for the analysis.

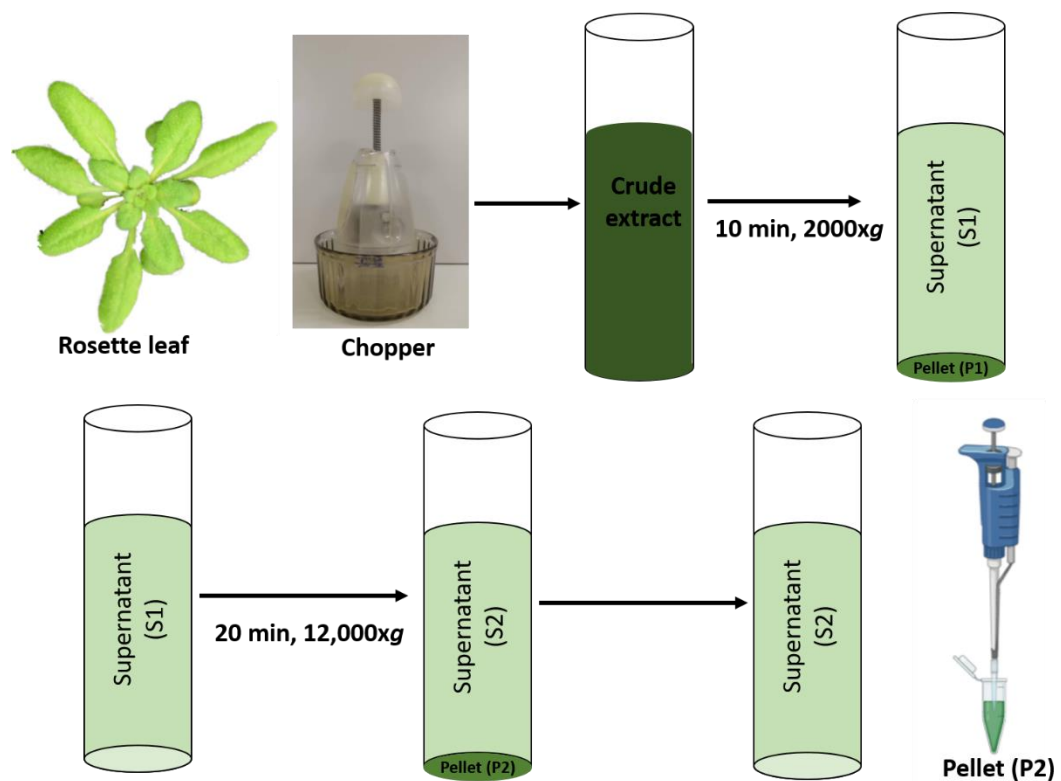


Figure 5.2: Diagrammatic representation of the crude fractionation of *A. thaliana* leaves homogenate.

Protein concentration, catalase and hydroxypyruvate reductase (HPR) activities were measured in each S1, S2 and P2 fractions (Table 5.1). As shown in Table 5.1, S1 fraction of wild type, *cat2-1* mutant, PSI2, WSQV2 and ARL1 had the higher amount of protein, while only a small amount of protein was detected in P2 fractions. Preparation of the peroxisome enriched pellet (P2) was correlated with getting rid of a higher amount of protein. Clearly, the amount of protein of S1 fraction was distributed between S2 and P2 in which the P2 fraction contains the lower amount of protein. The recovery of protein was about 88-108%. To determine if peroxisomes had been pelleted in the P2 fraction, the peroxisomal marker enzyme hydroxypyruvate reductase (HPR) activity was measured. HPR activity was detected in the P2 fraction but with some organelle breakage allowing leakage into the S2 fraction. The overall recovery of HPR activity was 85-102%.

**Table 5.1: Crude fractionation of plants homogenate.**

Four weeks-old rosettes of *A.thaliana* wild type, *cat2-1* mutant, PSI2, WSQV2 and ARL1 lines were homogenised in extraction buffer (see Chapter 2, Section 2.2.14.1) and fractionated into a homogenate (S1), cytosolic (S2) and organelle (P2) fraction (Figure 5.2). The amount of protein, catalase activity, hydroxypyruvate reductase (HPR) activity, total recovery of each enzyme and protein are given.

Fraction	WT	<i>Cat2-1</i>	PSI2	WQSV2	ARL1
Protein S1 (mg)	96	45	90	122	99
Protein S2 (mg)	79	34	87	100	85
Protein P2 (mg)	10	6	10	10	12
Protein Recovery (%)	92	88	108	90	98
Catalase S1 ( $\mu\text{mol}/\text{min}$ )	876	194	640	645	573
Catalase S2 ( $\mu\text{mol}/\text{min}$ )	515	91	386	393	436
Catalase P2 ( $\mu\text{mol}/\text{min}$ )	355	81	505	419	234
Catalase recovery (%)	99	89	135	126	113
Catalase % in P2	41	42	77	65	50
HPR S1( $\mu\text{mol}/\text{min}$ )	3799	1372	3571	4243	4665
HPR S2( $\mu\text{mol}/\text{min}$ )	2932	1037	2287	3051	3380
HPR P2 ( $\mu\text{mol}/\text{min}$ )	848	363	1506	530	1232
HPR recovery %	100	102	101	85	99
HPR % in P2	22	26	30	13	26
Catalase: HPR ratio	0.42	0.22	0.34	0.75	0.19

Catalase activity was measured in three fractions. The recovery of the total catalase activity was 89-135%, indicating that most of the catalase activity was recovered as evidenced by the distribution of the activity between fractions where the amount of activity in S2 and P2 of all lines was approximately similar to the amount of the activity in S1 fraction.

As previously shown in the previous chapter, *cat2-1* mutant had only ~30% of wild type activity, emphasizing the importance of the *CAT2* gene in determining high leaf catalase activities, however half of this activity was detected in peroxisomes and is presumably due to the *CAT3* isoform. In the transgenic lines catalase activity was restored to closer to wild type levels and a similar percentage of the activity was recovered in P2 compared to wild type, suggesting that the *CAT2* variants are localised into peroxisomes. The transgenic lines ARL1 had higher activity than that in *cat2-1* mutant but less than the wild type, although the proportion of activity in the P2 pellet was similar. The ratio of catalase and HPR was then calculated (catalase activity/HPR activity) for wild type, *cat2-1*, PSI2, WSQV2 and ARL1, suggesting that PSI2 and WSQV2 are efficiently targeted whereas ARL1 much less so.

Next, samples from the P2 fraction were separated by native PAGE and a western blot was carried out using anti-catalase antibody that recognises all three catalase isoforms (*CAT1*, *CAT2* and *CAT3*) (See Chapter 2, Table 2.2). *CAT2* isoform subunit (~ 240 kDa) was detected in P2 fraction of wild type, PSI and WSQV (Star, Figure 5.3). *CAT2* isoform of ARL is detected as a higher band (arrow, Figure 5.3), supporting the results presented in Figure 4.3, Chapter 4. The experiment was repeated three times using different protein concentration with a similar result. It must be noted that although the antibody should recognise all three catalases, the absence of a band in the *cat2-1* mutant reinforce the notion that *CAT2* is the main isoform in the leaf tissue and gives assurance that the bands that are seen in PSI2, WSQV2 and ARL1 undoubtedly are *CAT2* isoforms expressed from the transgene. Additionally, it must be noted that the same antibody also recognised Rubisco and this upper band running at ~480 kDa acts as a loading control.

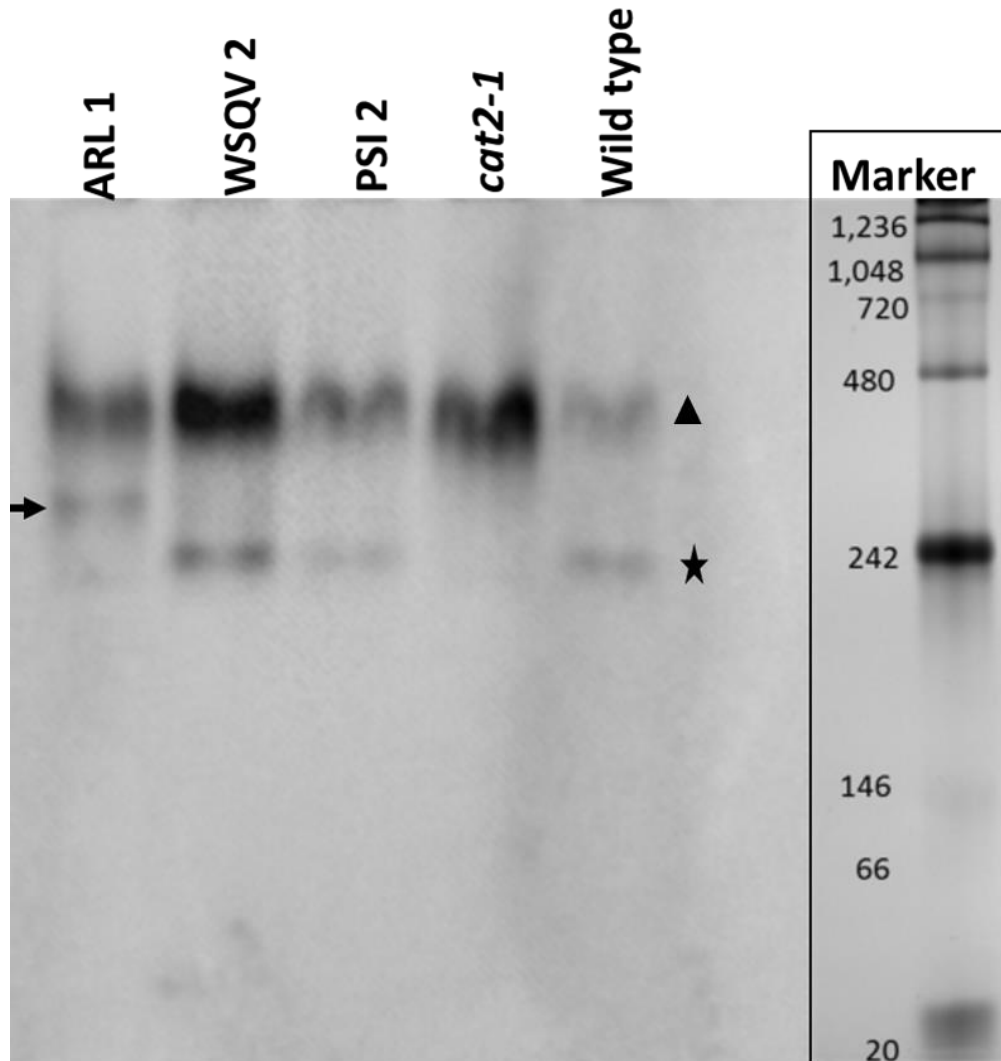


**Figure 5.3: CAT2 variants are present in the organelle pellet (P2).**

The fraction corresponding to the P2 was separated by native-PAGE in 7.5% gels (5 µg protein per lane) and immunoblotted with a CAT- antibody that recognises three catalases (CAT1, CAT2 and CAT3) followed by goat anti-mouse IgG antibody conjugated to HRP (Antibodies details can be found in Chapter 2, Table 2.2). The antibody was detected using ECL. The 240 kDa CAT2 is indicated (star and arrow).

When taken together, these results suggest that the PSI2 and WSQV2 variants are present clearly in the peroxisome-enriched pellet, with the evidence being a little uncertain for ARL1. However, the P2 pellet also contains mitochondria so to confirm the peroxisomal localisation unambiguously purified peroxisomes were prepared using percoll and sucrose gradients.

### **5.2.2 Analysis of CAT2 targeting using percoll and sucrose gradients**

The previous findings should be interpreted with some caution since the P2 pellet is peroxisomes that are contaminated with other organelles. Therefore, for a more detailed analysis of the localisation of CAT2 variants, the homogenate was fractionated on percoll and sucrose gradient. However, different methods were tested for their ability to isolate pure peroxisomes.

After some trial experiments (not shown), percoll and sucrose gradients were found to give the best preparations of pure peroxisomes. To this end, 4-week-old wild type, *cat2-1* mutant, PSI2, WSQV2, and ARL1 rosette leaf plants were harvested and ground in peroxisomes extraction buffer (Chapter 2, Section 2.2.14.2). After differential centrifugation, the supernatant was laid on top of a discontinuous percoll density gradient (Top, Figure 5.4). Following the gradient centrifugation, the percoll gradient was fractionated, and the fractions representing the intact peroxisomes were homogenised and washed. The resuspension was laid on top of a discontinuous sucrose density gradient (Bottom, Figure 5.4). Different fractions obtained from the gradients were assayed for protein concentrations, chlorophyll content, catalase and HPR activities.

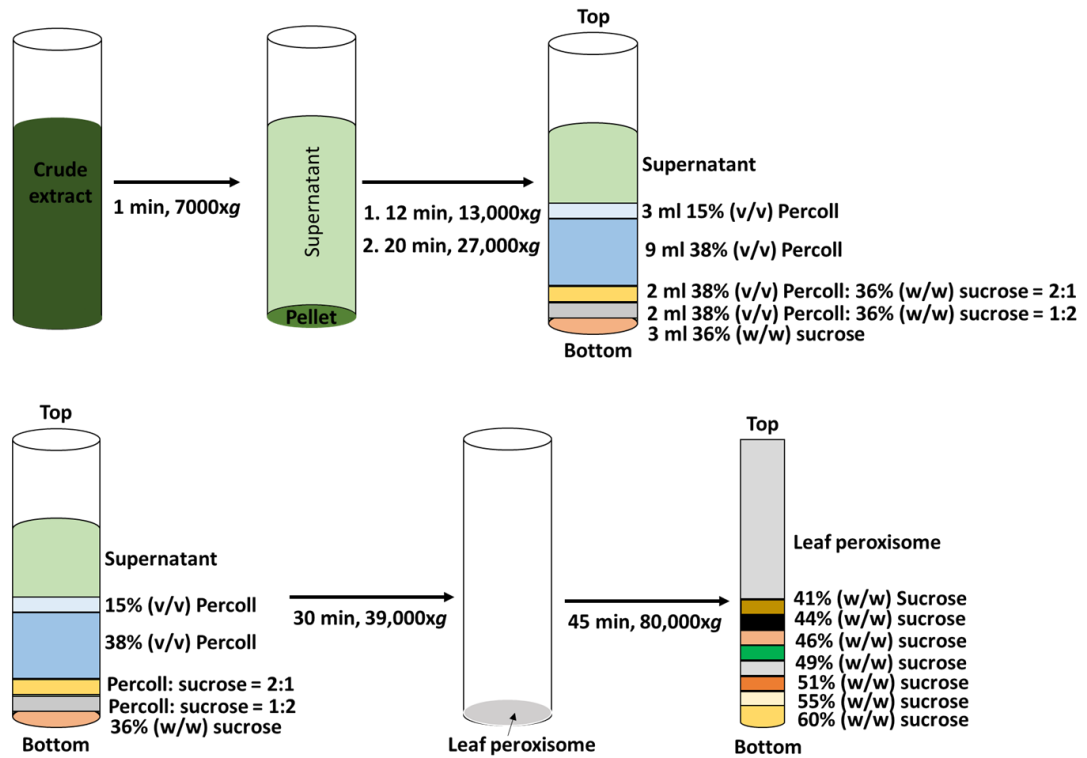


**Figure 5.4: Diagram illustrating the isolation of leaf peroxisomes from *A. thaliana* leaves by percoll and sucrose density gradient centrifugation.**

(Top). The crude extract was centrifuged at 7000xg for 1 min to sediment the chloroplasts. The supernatant was then loaded onto a percoll density gradient which consists of two different percoll fractions. The percoll gradient then centrifuged for 12 min at 13,000xg and then the speed was increased to 27,000 xg for another 20 min. Then, about 2 ml 36% (w/w) sucrose which includes the leaf peroxisomes, was resuspended and diluted with 36% (w/w) sucrose. Diluted peroxisomes were then centrifuged at 39,000 xg for 30 min. Finally, the homogenate fraction was loaded on top of the sucrose gradient (bottom) and ultracentrifuged for 45 min at 80,000 xg (See section 2.2.14.2, Chapter 2 for detail).

### 5.2.2.1 Percoll and sucrose gradient analysis

Fractions obtained from the percoll gradient were analysed for chlorophyll content. As indicated in Figure 5.5, chloroplasts were retained mainly in the 15 and 38 % (v/v) percoll fraction. Whereas, peroxisomes were passed the percoll layer and recovered at the bottom, suggesting good separation of these organelles. It must be noted that the catalase activity was measured in two lines to confirm that the intact peroxisomes are recovered at the bottom.

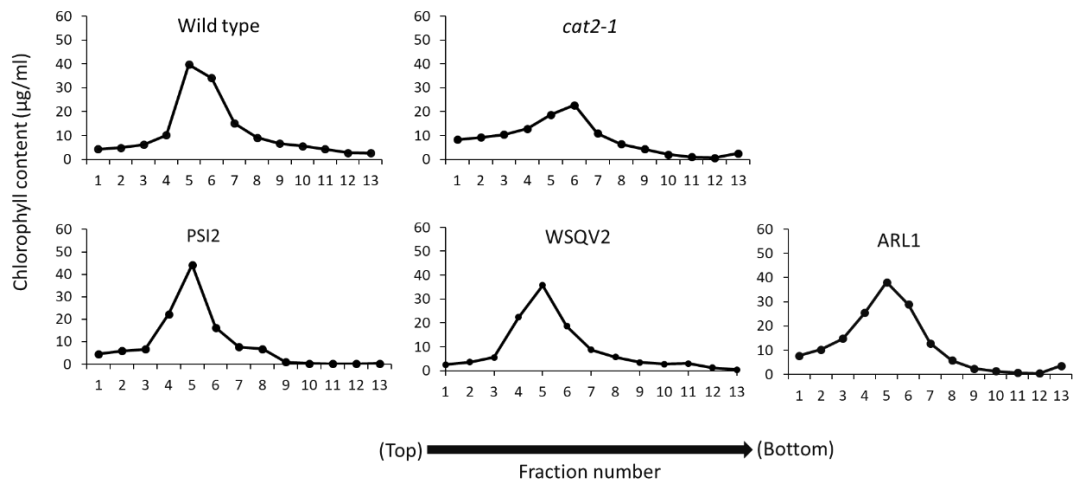


**Figure 5.5: Isolation of peroxisomes from wild type, *cat2-1* mutant, PSI2, WSQV2 and ARL1 leaves on a discontinuous percoll gradient.**

After separation of intact chloroplasts (Figure 5.4), the supernatant was loaded on top of a discontinuous percoll density gradient. After differential centrifugation, the percoll gradient was fractionated from top to bottom (Figure 5.4) into 13 fractions and analysed for chlorophyll content.

After centrifugation of percoll gradient, peroxisome fractions were washed (Chapter 2, Section 2.2.14.2). After washing, the peroxisome fraction was homogenised and laid on top of a discontinuous sucrose gradient (Bottom, Figure 5.4). Following ultracentrifugation, gradients were fractionated and assayed for chlorophyll content, catalase and HPR activities and protein concentration (Figure 5.6). No peak for chlorophyll content was detected in wild type, *cat2-1* mutant, PSI2, WSQV2 and ARL1 fractions, suggesting no peroxisomal contamination of the chloroplasts at all. A higher amount of total protein was detected at the bottom, indicating good separation of peroxisomes. To determine if the catalase activity is really in peroxisomes, HPR activity was measured in all fractions. The highest activity of the

peroxisomal enzyme HPR was found in fraction 7, identifying this as the peroxisomal fraction.

Interestingly, the distribution of catalase followed that of HPR, providing strong evidence for peroxisomal location. Isolation of peroxisomes was repeated with similar results.

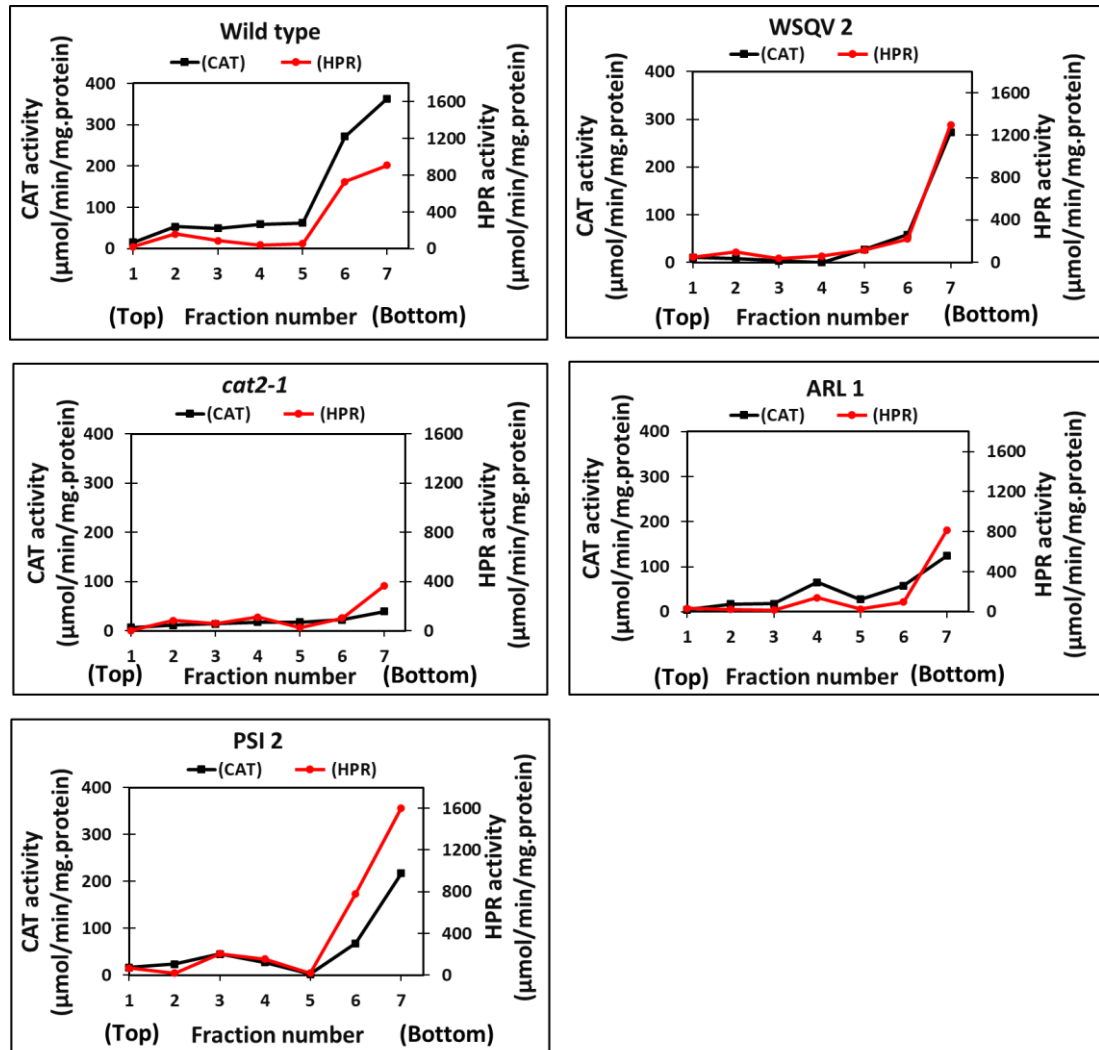


**Figure 5.6: Subcellular fractionation of mature *A. thaliana* leaves of wild type, *cat2-1* mutant, PSI2, WSQV2 and ARL1.**

A crude peroxisome pellet (Figure 5.4, lower panel, middle tube) was washed and laid on top of a discontinuous sucrose density gradient. Following ultracentrifugation, sucrose gradient was fractionated from top to bottom using 1 ml micropipette into 1 ml fractions. Hydroxypyruvate reductase (HPR, red) and catalase (black) activities were determined in the last 7 fractions.

To assess the degree of separation between the mitochondrial and peroxisomes, 10µg protein of peroxisomal fractions (#7) were analysed by SDS-PAGE followed by western blot analysis using antibodies against CAT2 and Atpβ (Beta subunit of ATP synthase, a mitochondrial marker). CAT2 was detected in peroxisomal fractions of all lines except the *cat2-1* mutant. The wild type peroxisome fraction showed only very minor contamination of mitochondria as judged by the level of cross-reaction with the ATPβ antibody. Importantly, no detectable contamination was observed in the peroxisomes from the transgenic lines, suggesting that the CAT2 variants are localised in peroxisomes. The *cat2-1* peroxisome fraction shows a higher degree of contamination which may reflect altered density of peroxisomes lacking their most abundant protein (Figure 5.7).

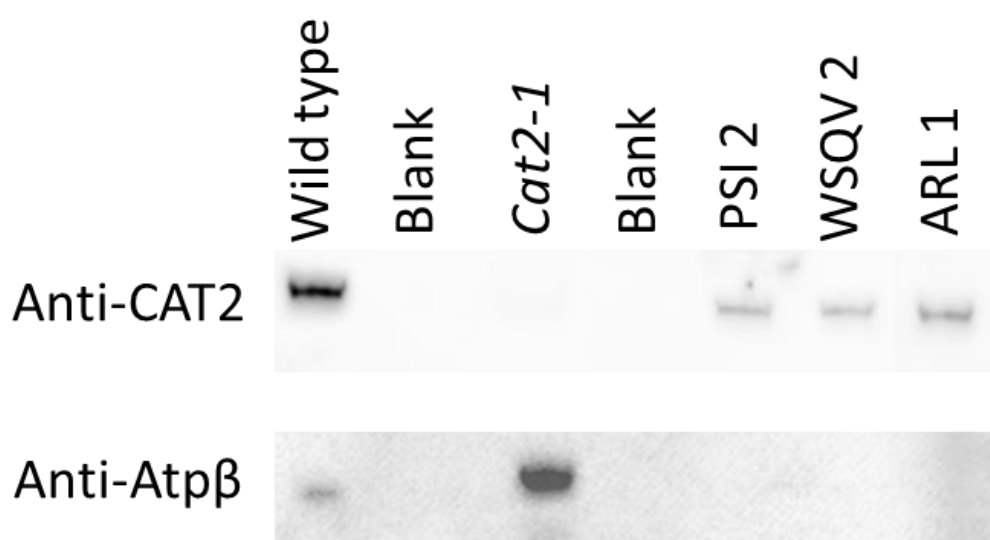


**Figure 5.7: Western blot of peak peroxisomal fractions.**

The fractions corresponding to the peroxisomes were separate by SDS-PAGE (10 µg protein per lane) and immunoblotted with a CAT2 and AtpB- antibodies (Details of antibodies are presented in Chapter 2, Table 2.2). The antibodies were detected using ECL. Atpβ (Beta subunit of ATP synthase) was used as a mitochondrial marker, whereas, the CAT2 antibody was used to detect the presence of CAT2 in all lines. Note that the peroxisome fraction of *cat2-1* mutant showed a higher degree of contamination by mitochondria as indicated by the level of cross-reaction with Atpβ antibody, which may reflect the altered density of peroxisomes lacking their most abundant protein.

### **5.2.3 Location of CAT2 variants using confocal microscopy**

The results presented so far using cell fractionation and biochemical analysis have shown that CAT2 variants were mainly targeted to peroxisomes and not mitochondria or chloroplasts.

The problems with subcellular fractionation, such as contamination with other organelles may lead to inaccurate results (Nagahashi and Baker, 1984). Therefore, it was necessary to confirm these findings by an independent technique. To this effect, the location of CAT2 variants was investigated using the self-assembling split sfGFP<sup>OPT</sup> system (Park et al., 2017) and confocal laser scanning microscopy. In this system, CAT2 variants were fused with the 11th  $\beta$ -strand of super-folder GFP (sfGFP11) and then delivered into protoplasts made from transgenic plants expressing sfGFP1-10  $\beta$ -strand (sfGFP1-10<sup>OPT</sup>) targeted to peroxisomes, cytoplasm, and nucleus. This system has been used to enhance fluorescence intensity and allow direct visualisation of proteins in plant cells (Park et al., 2017). sfGFP11 was used instead of GFP since GFP is a large protein and its tagging to CAT2 variants could potentially affect the protein assembly, targeting and folding whereas the small 13 amino acid 11th  $\beta$ -strand is the size of a small epitope tag.

#### **5.2.3.1 Self-assembling split sfGFP<sup>OPT</sup> system to monitor subcellular localisation of CAT2 variants**

To study the subcellular localisation of CAT2 variants using sfGFP1-10<sup>OPT</sup> and sfGFP11 tag (Figure 5.1), different CAT2 variants-sfGFP11 fusion constructs were generated. For this, sfGFP11 was fused at the C-terminus of CAT2 variants (Figure 5.8). As described in Chapter 2, Section 2.2.15.1, CAT2 variants were prepared to be inserted in PEP109E vector. Figure 5.9 shows the correct products sizes produced after amplification with the specific primers. Product sizes with 1499 bp, 1445 bp and 1500 bp represent CAT2PSI, CAT2WSQV and CAT2ARL, respectively (Figure 5.9). Following the digestion, ligation, and transformation (Chapter 2, Section 2.2.15.1), CAT2variants sfGFP11 were generated.

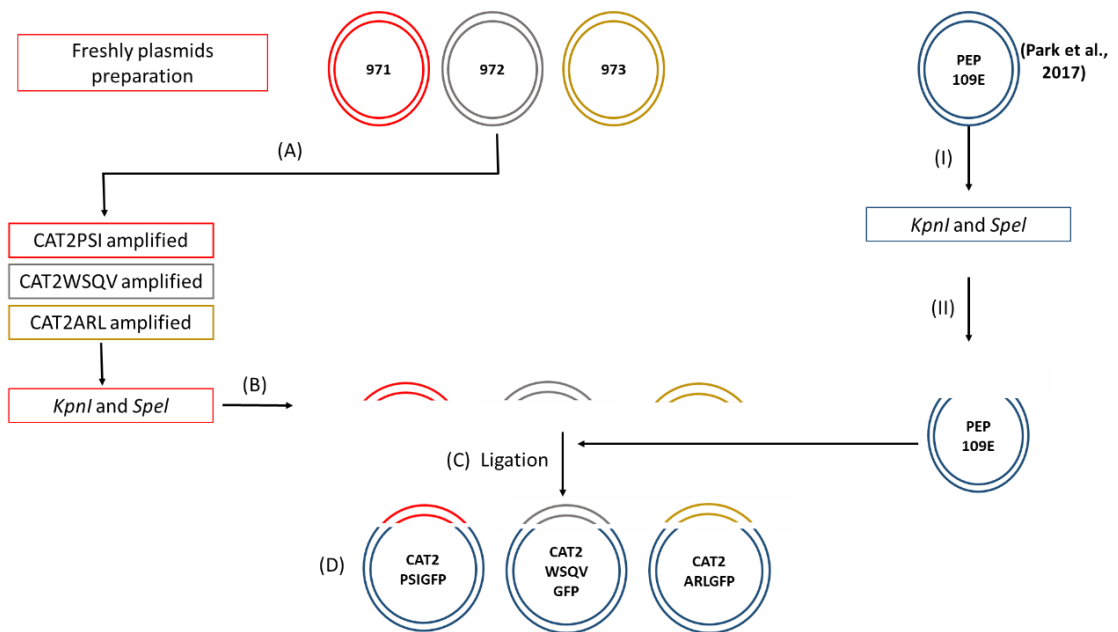


**Figure 5.8: Construction of CAT2 variants-sfGFP11.**

Fresh CAT2 plasmids (971, 972 and 973) were prepared from stock and miniprep as detailed in Chapter 2, Section 2.2.5. (A) Specific primers were designed to produce CAT2 variants. Amplified PCR products were digested with *KpnI* and *SpeI* restriction enzymes to be ligated with PEP109E. (B) PEP 109E plasmid was digested using *KpnI* and *SpeI* restriction enzymes (I and II). Vector and insert were then ligated. (D) PEP109E vector containing CAT2 variants (CAT2-PSI-GFP, CAT2-WSQV-GFP and CAT2-ARL-GFP) were sent for sequencing with specific primers. They were also amplified with CAT2F and CAT2R to confirm the presence of CAT2. All steps are explained in detail in Chapter 2, Section 2.2.15.1.

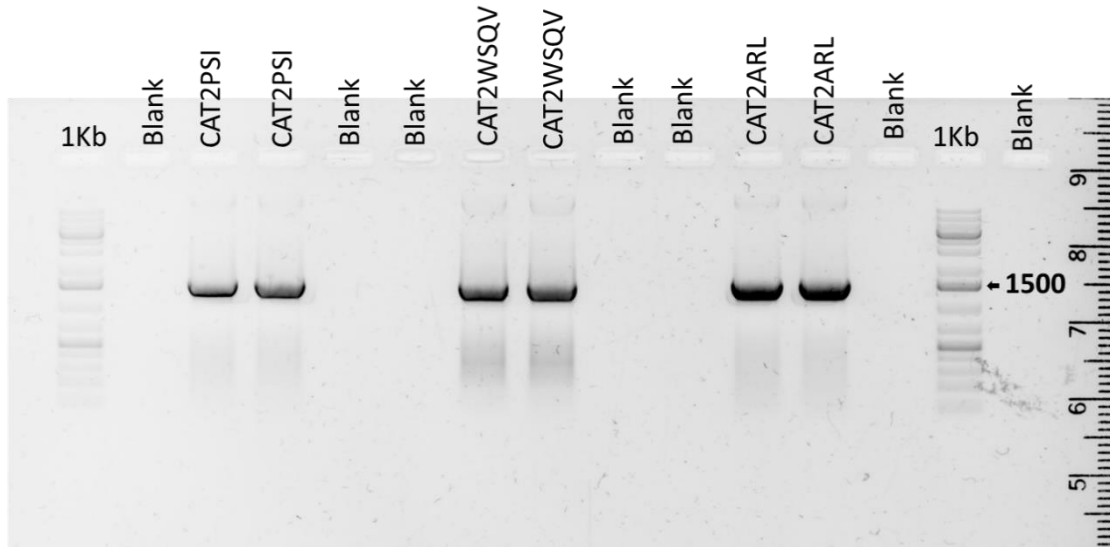


**Figure 5.9: PCR amplification of CAT2 variants to be inserted into PEP109E plasmid.**

Cat2PSIF primer was used as a forward primer with each reverse primer of cat2PSIR, cat2 WSQVR and cat2ARLR with plasmids 971, 972 and 973 as templates to generate different variants of CAT2 that contain *KpnI* and *SpeI* restriction sites. Cat2PSIF was used as a forward primer with cat2PSIR, cat2 WSQV R and cat2ARLR to generate PCR products with 1499, 1445 and 1500 bp using 971, 972 and 973 as a template. PCR products termed as CAT2PSI, CAT2WSQV and CAT2ARL.

Following transformation, plasmid DNA was extracted from putative clones and used as a template for PCR with Cat2-F and Cat2-R (Chapter 2, Table 2.3, #4 and #5 respectively) (Figure 5.10). Figure 5.10A shows that four PEP109E plasmids containing CAT2PSI (CAT2PSIGFPA, B, C and D) gave a PCR product of 293 bp. Six PEP109E vectors containing CAT2WSQV (here is called CAT2WSQVGFPA, B, C, D, E and F) were amplified with the same primers to give a 407 bp product size (Figure 5.10B). Additionally, six PEP109E vectors containing CAT2ARL (CAT2ARLGFPA, B, C, D, E and F) were amplified with the same primers to give a 293 bp product size (Figure 5.10C). They were sent for sequencing to confirm that they are all in the correct frame.

These results confirm that all plasmids are generated appropriately and can be used to study the subcellular localisation using confocal microscopy.

Plasmids maps were generated using SNAPgene software as presented in Appendix C, Section C.1.1.

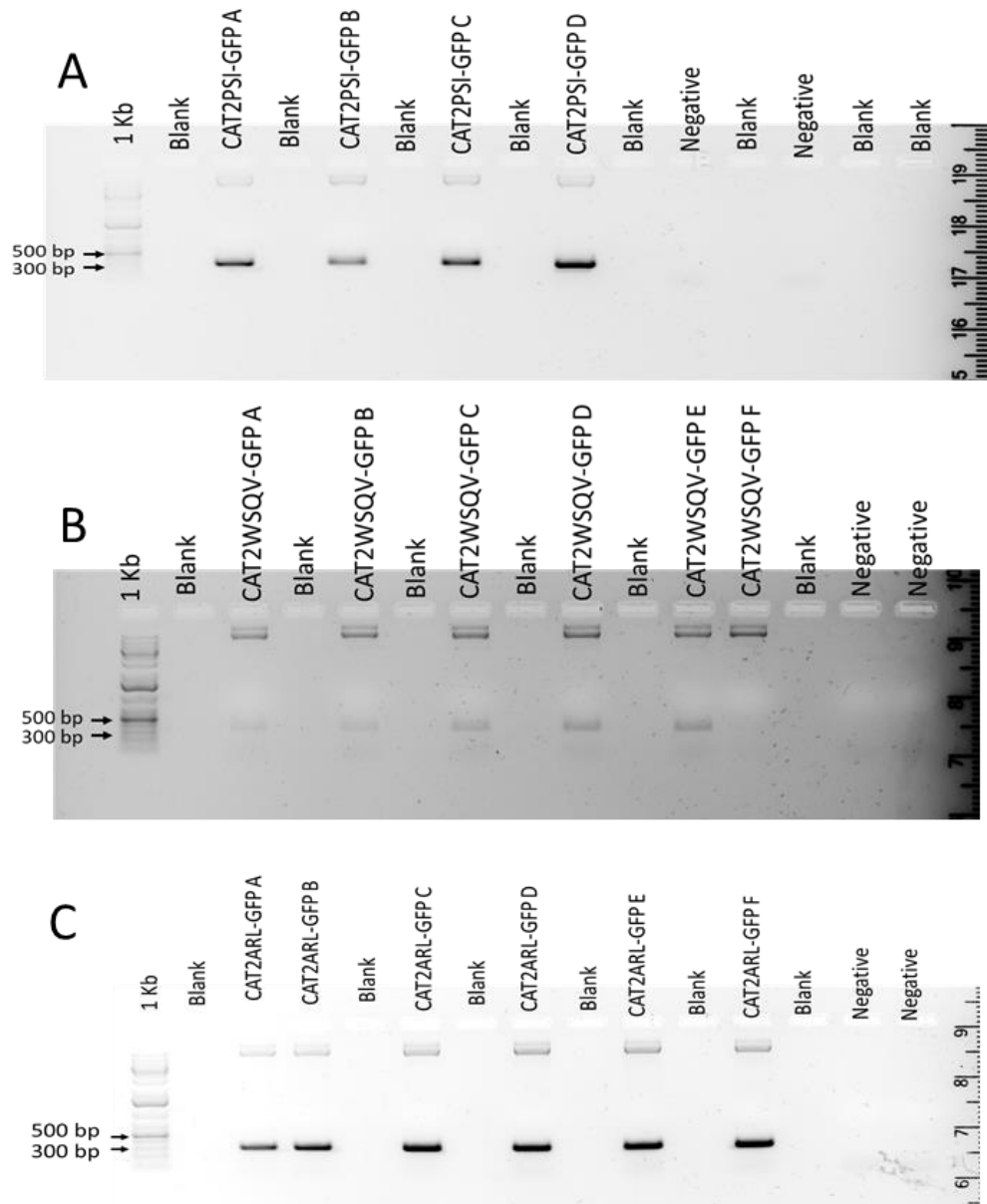


**Figure 5.10: Validation of CAT2 variants ligation into the PEP109E plasmid.**

(A) Plasmids (CAT2PSI-GFP A, B, C and D) were isolated from four positive colonies and used with CAT2F and CAT2R primers to confirm the presence of CAT2PSI fragment. The presence of a 293 bp fragment indicated correct plasmids. (B) A 407bp band confirms the presence of the desired CAT2WSQV insert in the respective vectors. Six plasmids were isolated from different colonies after transformation. (C) presence of CAT2ARL bands at 293 bp using CAT2F and CAT2R. Plasmids were isolated from positive colonies transformed with ligation products of CAT2ARL insert and PEP109E vector. A-F represents plasmids prepared from different colonies. Primer sequences can be found in Chapter 2, Table 2.3. 1kb; DNA ladder. Negative; no DNA. Blank; no sample.

### 5.2.3.2 CAT2 variants localisation using confocal microscopy

#### 5.2.3.2.1 *A. thaliana* transgenic lines expressing sfGFP1-10<sup>OPT</sup> targeted to peroxisomes

Protoplasts were isolated from 4-week-old plants expressing sfGFP1-10<sup>OPT</sup> targeted to peroxisomes (Details of growth conditions, protoplast isolation and transformation are described in Chapter 2, Section 2.2.13). Positive control previously reported by Park et al. (2017) was used where the expression of peroxisome-targeted mCherry-sfGFP11 fused with peroxisomal targeted sfGFP1-10<sup>OPT</sup> leads to sfGFP signal in the peroxisomes (A, Figures 5.11), whilst the negative control (No GFP11construct) showed no GFP signal (B, Figures 5.11). The CAT2 variants-sfGFP11 were also transfected into protoplasts made from peroxisomal sfGFP1-10<sup>OPT</sup> transgenic plants. Protoplasts were observed with LSM700 laser scanning confocal microscope after 27-39 hr incubation (Figure 5.11) using the settings described (Chapter 2, Section 2.2.13.5). Three independent experiments were conducted with the same results except for CAT2-ARL as discussed later. Number of protoplasts that show the sfGFP signal is indicated in Table 5.2.

Expression of CAT2PSI-sfGFP11 and CAT2WSQV-sfGFP11 in protoplasts isolated from peroxisomes-targeted sfGFP1-10<sup>OPT</sup> reconstituted sfGFP fluorescence signal in peroxisomes (C and D Figures 5.11), suggesting that these variants are targeted to peroxisomes. No signal was detected with CAT2-ARL (E, Figures 5.11). These findings were confirmed by scanning the same samples after 39hr incubation. Surprisingly, during the 3<sup>rd</sup> independent experiment, a fluorescent signal was detected in only two protoplast transfected with CAT2ARL-constructs (Figure 5.12, arrows), pointing to a possible peroxisomal localisation of the CAT2ARL variant. However, these do not look like typical peroxisomes and could be clusters of peroxisomes or some other compartment.

PX-sfGFP1-10<sup>OPT</sup> +

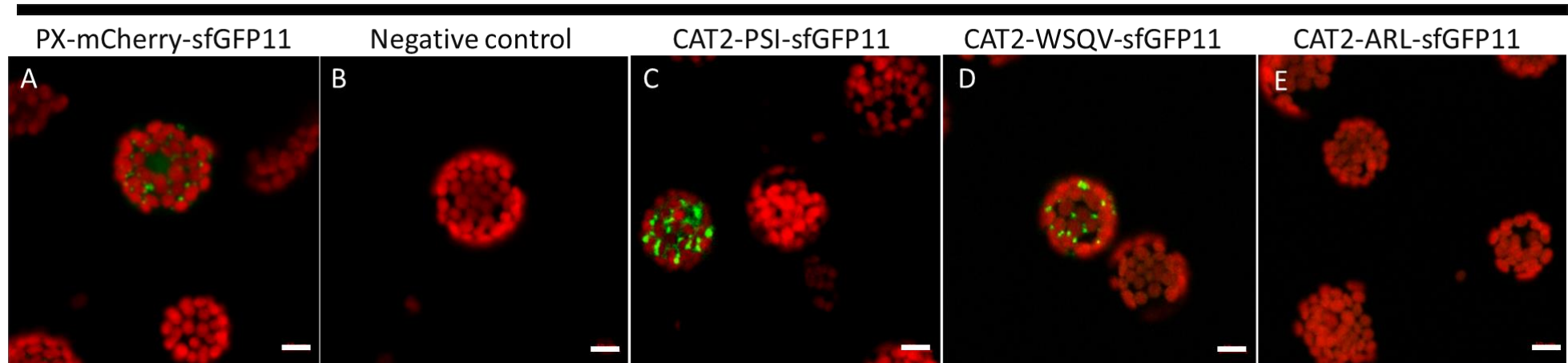


**Figure 5.11: Expression of CAT2-PSI-sfGFP11 and CAT2-WSQV-sfGFP11 in protoplasts with peroxisome targeted sfGFP1-10 leads to peroxisomal GFP fluorescence.**

Plasmids containing CAT2-variants-sfGFP11 (PSI, WSQV and ARL), peroxisome targeted-mCherry-sfGFP11 were transfected into protoplasts that were isolated from lines expressing sfGFP1-10<sup>OPT</sup> targeted to peroxisomes. (A) positive control: PX-mCherry-11 (ABRC Stock Number CD3-2434). (B) Negative control (no plasmid). (C) CAT2-PSI-sfGFP11. (D) CAT2-WSQV-sfGFP11. (E) CAT2-ARL-sfGFP11. Bars = 10  $\mu$ m. Protoplasts were incubated for 27 hr in light and scanned using confocal microscopy. Representative images reflecting the results of 3 independent experiments are shown.

PX-sfGFP1-10<sup>OPT</sup> +  
CAT2-ARL-sfGFP11

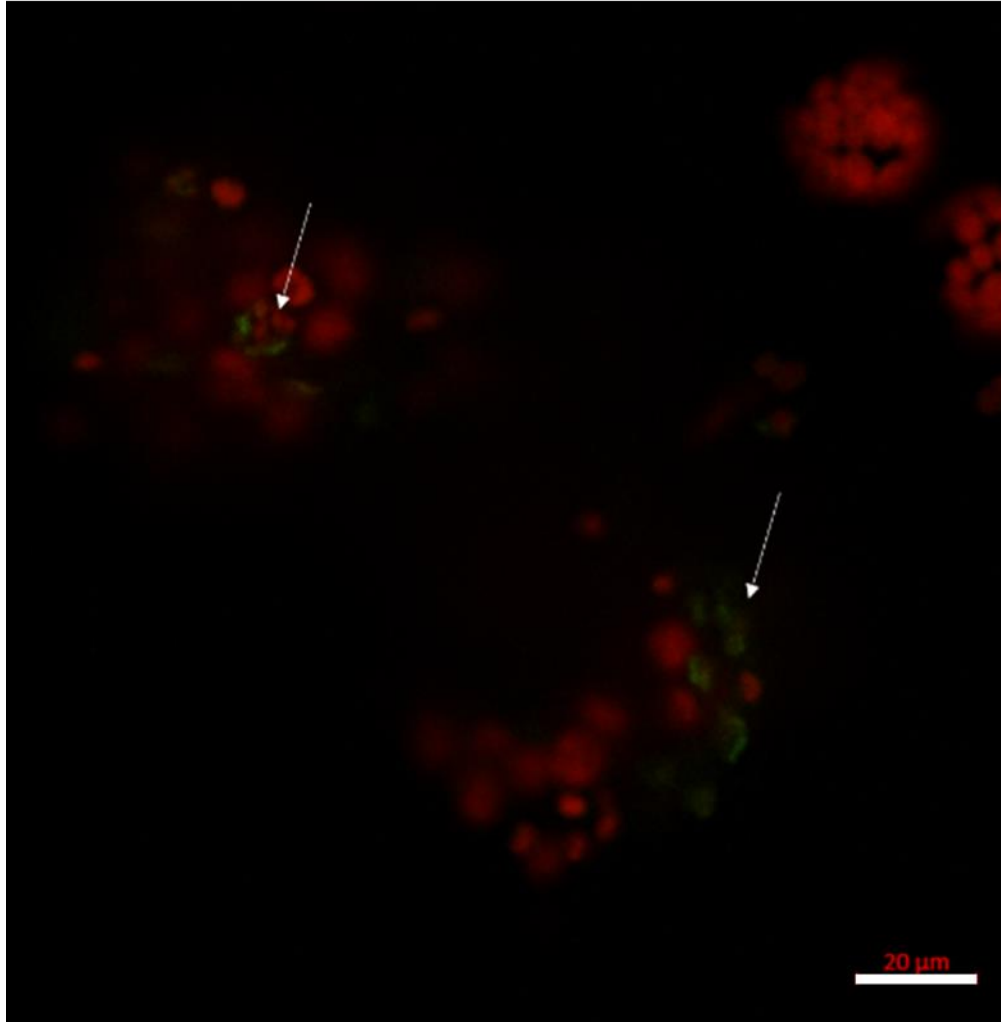


**Figure 5.12: CAT2ARL tagged with sfGFP11 is detectable in *A. thaliana* transgenic plants expressing sfGFP1-10<sup>OPT</sup> targeted to peroxisomes.** Expression of CAT2-ARL-sfGFP11 in protoplasts isolated from peroxisome-targeted sfGFP1-10<sup>OPT</sup> (PX-sfGFP1-10<sup>OPT</sup>) reconstituted faint sfGFP fluorescence signal in unidentified clustered vesicles which might have been aggregated peroxisomes. Protoplasts were incubated for 37hr in light and scanned using confocal laser scanning microscopy. Scale bar = 20 μm.

These results, taken together with the biochemical data already presented in this chapter, confirmed the targeting of CAT2 variants to peroxisomes, nevertheless, with the caveat that the sfGFP could in principle assemble in the cytosol and then be imported into the peroxisomes as shown in Park et al. (2017). If that were correct, it would be expected to see cytosolic sfGFP. Therefore, it was necessary to isolate protoplasts from the transgenic lines that are expressing sfGFP1-10<sup>OPT</sup> targeted to the cytoplasm.

#### **5.2.3.2.2 *A.thaliana* transgenic lines expressing sfGFP1-10<sup>OPT</sup> targeted to cytoplasm**

Protoplasts were prepared from lines expressing sfGFP1-10<sup>OPT</sup> targeted to the cytoplasm. CYTO-mCherry-11 (ABRC Stock Number CD3-2430) was used as a positive control (Figure 5.13A). Negative control was also used (Figure 5.13, B). CAT2 variants fused to sfGFP11 at the C-terminal region were also transfected (Figure 5.13C, D and E). This analysis showed that no fluorescence signal was detected in protoplasts transfected with three CAT2 variants. These results are really exciting as they suggest that the sfGFP fused to the CAT2 variants are assembled inside the peroxisome, not in the cytoplasm. They also suggest that the CAT2 variants might be targeted very quickly to the peroxisomes. However, these results await further investigations. Protoplasts were visualised after 30-43hr incubation using laser confocal microscopy. Results under two incubation periods were the same. Three independent experiments were performed with the same results (+ve control was used with only two independent experiments). Number of protoplasts that show the sfGFP signal can be seen in Table 5.2.

CYTO-sfGFP1-10<sup>OPT+</sup>

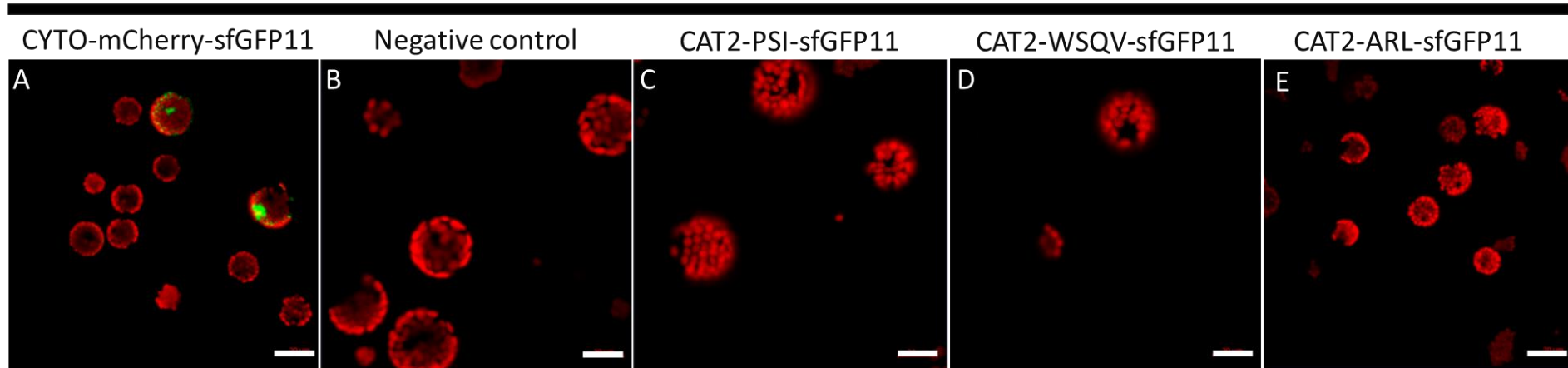


**Figure 5.13: CAT2 variants are not assembled in the cytoplasm.**

CAT2 variants tagged with sfGFP11 transfected into protoplasts of sfGFP1-10<sup>OPT</sup> targeted to the cytoplasm. (A) Positive control, CYTO-mCherry-11 (ABRC Stock Number CD3-2430). (B) Negative control (no plasmid). (C) CAT2-PSI-sfGFP11. (D) CAT2-WSQV-sfGFP11. (E) CAT2-ARL-sfGFP11. Protoplasts were incubated for 30 hr in light and scanned using confocal microscopy. Representative images reflecting the results of 2 independent experiments are shown. Bars = 20  $\mu$ m.

### 5.2.3.2.3 *A. thaliana* transgenic lines expressing sfGFP1-10<sup>OPT</sup> targeted to nucleus

Protoplasts were also isolated from leaves of *A. thaliana* transgenic lines expressing sfGFP1-10<sup>OPT</sup> targeted to the nucleus. Positive control NU-mCherry-11 (ABRC Stock Number CD3-2431) was used in this experiment (Figure 5.14A). After 29hr incubation, reconstituted sfGFP signal was observed at the nucleus in the protoplasts transfected with CAT2PSI-sfGFP11 construct (Figure 5.14C), while no signal was detectable at the protoplasts transfected with CAT2WSQV and ARL-sfGFP11 variants (Figure 5.14D and E, respectively), implying that CAT2PSI-sfGFP11 but not its variants can be imported into the nucleus. However, the number of protoplasts that show the sfGFP signal is presented in Table 5.2.

**Table 5.2: Number of protoplasts that show sfGFP signal in different compartments.**

Number of protoplasts observed with fluorescence in each organelle as shown in representative images in figures 5.11-5.14. Positive controls: PX-mCherry-11(ABRC Stock Number CD3-2434) CYTO-mCherry-11 (ABRC Stock Number CD3-2430) and NU-mCherry-11(ABRC Stock Number CD3-2431), for peroxisome, cytoplasm, and nucleus, respectively.

Plasmid	Peroxisomes	Cytoplasm	Nucleus	Unknown
Positive control	14	10	15	-
CAT2-PSI-sfGFP11	23	0	13	-
CAT2-WSQV-sfGFP11	20	0	0	-
CAT2-ARL-sfGFP11	0	0	0	2

NU-sfGFP1-10<sup>OPT+</sup>

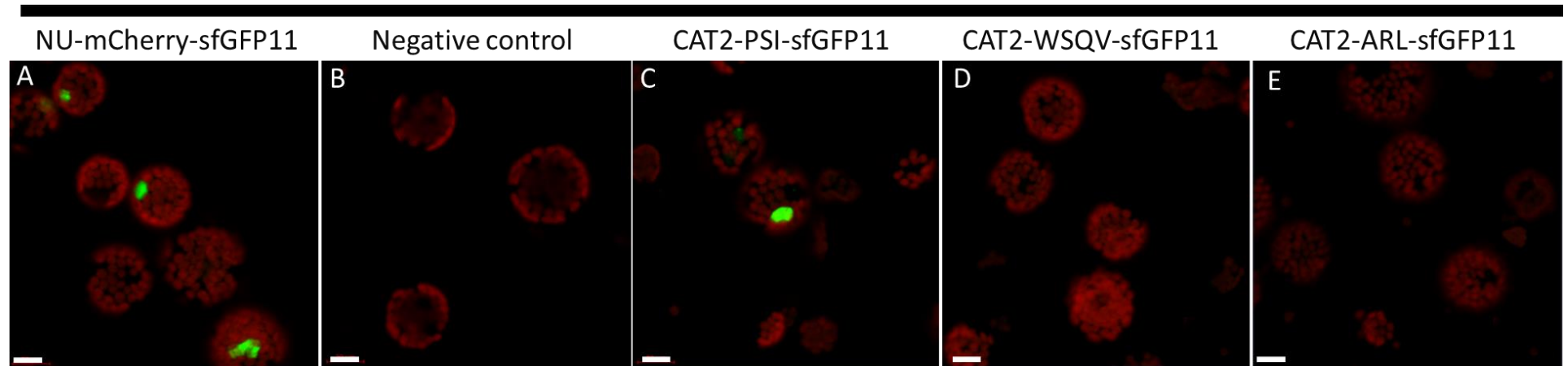


**Figure 5.14: Nuclear localisation of CAT2-PSI-sfGFP11.**

CAT2 variants-sfGFP11 were expressed into protoplasts isolated from *A. thaliana* lines expressing sfGFP1-10<sup>OPT</sup> targeted to the nucleus. NU-mCherry-11 (ABRC Stock Number CD3-2431) (A), negative control (no plasmid) (B), CAT2-PSI-sfGFP11 (C), CAT2-WSQV-sfGFP11 (D) and CAT2-ARL-sfGFP11 (E) were transferred into protoplasts of transgenic Arabidopsis expressing sfGFP1-10 targeted to nucleus. Negative control (no plasmid) (B). Bars = 20  $\mu$ m. Protoplasts were incubated for 29hr in light and scanned using confocal microscopy. Experiments were repeated twice with similar results.

### 5.3 Discussion

In this chapter, subcellular localisation of CAT2 variants was investigated using crude fractionation, percoll and sucrose density fractionation and split fluorescent protein fragments. The results from the crude fractionation supported the targeting of CAT2 variants into peroxisomes. Such findings were confirmed by percoll and sucrose density gradient analysis, as well as confocal microscopy.

Through crude fractionation, it was shown that CAT2PSI and CAT2WSQV were clearly found in the peroxisome enriched pellet, as strongly evidenced by recovering the catalase activity in P2; high catalase activity (Table 5.1). It was also shown that further analysis was required to show whether CAT2ARL present in peroxisomes or not due to the lower catalase activity in the P2 fraction (Table 5.1). The presence of these variants in the organelle pellet fraction was confirmed using Native-PAGE gel and western blotting (Figure 5.3). These results are interesting as they also supported that CAT2 is the only detectable isoform in leaf tissue whereas CAT1 and CAT3 are not detectable. Isolation of more pure peroxisome fractions confirmed that CAT2 variants were targeted to peroxisomes. Contamination with chloroplast and mitochondria was tested by chlorophyll assay and ATP $\beta$  antibody, respectively, and shown to be below detection.

By using confocal microscopy, it was demonstrated that CAT2PSI and CAT2WQSV were targeted into peroxisomes, but the situation is less clear with CAT2 ARL (Figure 5.11). Interestingly, it was found that the assembly of these variants was not in the cytoplasm (Figure 5.13). It was also found that CAT2PSI localises in nucleus. Finally, it was shown that sfGFP11 fusion at the C-terminus did not mask the peroxisomal targeting signal for PSI and WSQV but perhaps did for ARL (Figure 5.14). The implications of all of these findings will be discussed in more detail in this section.

Despite the recently suggested that the catalase localisation could be dynamic due to the interaction with various cytosolic proteins (Yang and Poovaiah, 2002; Verslues et al., 2007; Li et al., 2015; Zou et al., 2015; Zhou, Y.B. et al., 2018; Foyer et al., 2020), results presented in this chapter are generally in agreement with previous reports which showed that the plant catalases particularly *A. thaliana* catalase2 (*AtCAT2*) are localised into peroxisomes (Mullen et al., 1997; Kamada et al., 2003; Mhamdi et al., 2010b). The current study showed that fusing fluorescent tag at the C-terminal region of CAT2 did not prevent the import. Recently it was reported that *AtCAT2* was localised to the peroxisome by fusing the GFP at its C-terminus (Fujikawa et al., 2019). In contrast, it has been found that fusing the GFP at the C-terminus of a plant catalase-phenol oxidase (*AcCATPO*) from *Amaranthus cruentus* affects the localisation (Chen et al., 2017). The current study is in agreement with the findings by (Fujikawa et al., 2019).

Cellular fractionation results and fusing the sfGFP11 to the CAT2WSQV variant have shown that *AtCAT2* lacking the C-terminal 18-amino acid region (CAT2WQSV variant) is localised in peroxisomes. This provides a novel insight into targeting of the alternative splicing variants since the effect of alternative splicing on the PTS targeting signal was rarely studied. A recent study analysed the effect of alternative splicing on the PTS1 targeting signal, suggesting that alternative splicing can alter the C-terminal PTS1, affecting the subcellular localisation of the protein isoforms (An et al., 2017). However, the disparities between the current study and the previous study are (1) genes analysed in the previous study had only splicing variants encoding a C-terminal protein sequence of canonical PTS1 and have lost at least 30 amino acids. For example, *A. thaliana* thioesterase superfamily protein, *At5g48950* has two splice variants, *At5g48950.1* and *At5g48950.2*, which encodes 157 amino acids and 127 amino acids, respectively. Thus, the second variant arises from non-splicing of the last intron, which removes the last 30 amino acids. The same authors also analysed other splicing variants that were missing 100 amino acids. (2) Authors of the previous study used GFP fusion protein under 35S promoter in the presence of endogenous protein.

In contrast, the short-form of *AtCAT2* expressed as a native form in the *cat2-1* mutant. These results suggest that the last 18 amino acids are not involved in the import of *AtCAT2* to peroxisomes. Thus, CAT2 import could be carried out by contributing other amino acids distant from the C-terminal part. Acyl-CoA oxidase of *Saccharomyces cerevisiae* is targeted to peroxisomes via a non-linear sequence known as PTS3. This targeting signal is a signal patch that is composed of amino acids that are distant from each other in the primary sequence, but not in the folded protein (Kempiński et al., 2020). An additional study by Li et al. (2017) revealed that HSP17.6 contains a novel non-canonical PTS1. This PTS1 was 16 amino acids upstream from the C terminus. Therefore, *AtCAT2* could be imported to peroxisomes via another unrevealed type of targeting signal.

To gain an insight into the CAT2 variants localisation in a variety of organelles and subcellular sites, the subcellular localisation of these variants in the cytosol was also studied. Curiously, there was neither cytosolic nor peroxisome sfGFP fluorescence in transgenic *A. thaliana* plants expressing sfGFP1-10<sup>OPT</sup> targeted to the cytoplasm. These results are curious because if the expressed proteins assemble in the cytosol, it is expected to observe either cytosolic or peroxisome sfGFP if the CAT2 constructs can drag the sfGFP1-10<sup>OPT</sup> to peroxisomes. Park et al. (2017) showed that peroxisome-targeted mCherry-sfGFP11 could complement with sfGFP1-10<sup>OPT</sup> targeted to the cytoplasm in *Nicotiana benthamiana* (Park et al., 2017). In contrast, the same authors also showed that localisation to some organelles could be detected only when targeted to the corresponding organelles (Park et al., 2017). However, results presented here could also suggest that the CAT2 subunits are imported separately then assembled in peroxisomes since peroxisomes prefer the import of monomeric proteins (Freitas et al., 2011; Freitas et al., 2015). Whether this is the case for CAT2 is still unclear and further analysis are needed to solve this conundrum.

Peroxisomal localisation of CAT2ARL-sfGFP11 was observed as a weak signal presented as large dots (clusters) in only one independent experiment (Figure 5.12). Moreover, the peroxisomal signal was observed as a small dots when CAT2ARL-sfGFP11 was transfected with protoplasts made from lines

expressing sfGFP1-10<sup>OPT</sup> targeted to the nucleus (data not shown). It must be noted that only two cells showing reconstituted sfGFP signal in the peroxisome were observed in each experiment. In addition to the reasons mentioned previously about the reconstitution of the fluorescent signal in different organelles, the expression and the timing points after incubation could also affect the localisation. *Pseudomonas syringae* effectors AvrB changes its localisation from the plasma membrane to unknown vesicles at different time points after inoculation (Park et al., 2017). It has been suggested that the signal could be improved either using sfYFP1-10<sup>OPT</sup> or multimerizing sfGFP11 tag. GFP has been engineered for improved brightness (Heim and Tsien, 1996). Using tandem repeat of sfGFP11 can increase the fluorescence signal in mammalian cells and *Nicotiana benthamiana* (Kamiyama et al., 2016; Park et al., 2017).

The cellular fractionation and confocal microscopy analysis of the CAT2ARL variant localisation correlate with each other, albeit imperfectly. That this correlation is incomplete is difficult to explain. It is likely that placing the GFP11 at the C-terminus of ARL would block the interaction with classic PTS1-receptor (PEX5) which might explain the discrepancy between the cell fractionation and confocal data for ARL. Hypothetically could replacing PSI with ARL reduce the efficiency of catalase taking its 'normal' targeting pathway?

Finally, through the cellular fractionation, it was shown that CAT2 variants are found only in peroxisomes not in mitochondria or chloroplasts. However, a very interesting finding was observed through confocal microscopy where the co-expression with nuclear GFP1-10 reconstituted sfGFP in the nucleus only with CAT2PSI (Figure 5.13C). This suggests that C terminal 18 amino acid sequence allows catalase to enter the nucleus as WQSV doesn't and changing PSI to ARL also seems to prevent it. This might explain why the C terminal sequence is conserved but is not important for activity or peroxisome targeting. Even though there is no similarity between the last 18 amino acids and a classic nuclear localisation signal.

## Chapter 6 General discussion

### 6.1 Summary

Prior to the commencement of this study, the effect of C-terminal deletions of *Arabidopsis thaliana* CAT2 (*AtCAT2*) on plant physiology and biochemistry had not been studied. All previous studies focused on the effect of the C-terminal part of various plant catalase enzymes on targeting to peroxisomes using a variety of experimental systems, and obtained contradictory results depending on the precise experimental setup. In this thesis, the physiological, biochemical, and targeting consequences of introducing *AtCAT2* versions with modified C-termini under the control of the native promoter and terminator into *cat2-1* mutant background were investigated. This allows the simultaneous evaluation of targeting, activity, and function in a physiologically relevant context. My major conclusion is that under the conditions tested, the last 18 amino acids of *AtCAT2* are dispensable for targeting to peroxisomes, catalase activity and redox homeostasis. The latter was evaluated by measurements of glutathione and ascorbate and expression of redox regulated transcripts. In contrast, the last 18 amino acids has been concluded to be necessary for the nuclear localisation of CAT2 since the CATPSIsfGFP11 construct was frequently detected in the nucleus but the WQSVsfGFP11 and ARLsfGFP11 constructs never were.

Plant catalases have a non-consensus PTS1 sequence. The requirement for this sequence in peroxisomal targeting has been extensively reported in the literature (Table 6.1). However, the conclusions are contradictory, as illustrated in Table 6.1 and discussed in Chapter 1, targeting section (1.9.7). The reasons for such contradictory results may be (1) high expression levels of the constructs in the transient systems used; (2) use of heterologous systems involving genes from a different species; (3) limited experimental conditions/approaches that prevented unambiguous conclusions to be drawn, for instance, studies involving a large tag as GFP that can potentially negatively affect protein folding; (4) deletion a large part of the protein (e.g. 150 amino acids), which could also perturb protein folding.

The studies reported in this thesis were designed to avoid many of these potential problems. Therefore, transgenic lines were generated with a native expression level without using any tag that could interfere with targeting and folding, and this is the strength of this work compared to all previous studies. In this chapter, the key findings from each results chapter will be (i) summarised and (ii) considered with respect to the literature. Finally, various avenues of future research will also be discussed.

**Table 6.1: Plant catalase targeting studies.**

Reference	Key finding
Mullen et al., 1997	C-terminal tripeptide sequence is necessary for import of cottonseed catalase into tobacco BY-2 cell peroxisomes.
Kamigaki et al., 2003	C-terminal 10-amino acid region pumpkin catalase1 is not required for the import into peroxisomes using stable expression system.
Kamigaki et al., 2003	C-terminal 3-amino acid region pumpkin catalase1 is required for the import using transient expression system.
Oshima et al., 2008	Pumpkin catalase interacts with the N-terminal domain of PEX5 rather than the C-terminal domain.
Fujikawa et al., 2019	C-terminal tripeptide sequence of AtCAT2 is not important for the import but the amino acids at the positions 11 to 4, especially position 11, are necessary for import using transient expression system.

Firstly, the data presented in Chapter 3 concern the growth phenotype in each of the transgenic lines relative to the wild type and the *cat2-1* mutant. These findings allow an analysis of the physiological consequences of introducing AtCAT2 with different C-termini into the *cat2-1* mutant background. These data demonstrate that each of the AtCAT2 variants can complement the *cat2-1* mutant with regard to growth. Therefore, these findings suggest that the last 18 amino acids of the AtCAT2 sequence are not crucial for growth under long or short days under ambient CO<sub>2</sub> growth conditions. Additionally, under photorespiration-promoting conditions, the introduction of CAT2 with modified C-termini was sufficient to prevent or delay the presence of lesions on the leaves, which were observed in the *cat2-1* mutant.

The consequences of *AtCAT2* C-terminal domain modification on enzyme activity, cellular redox homeostasis and autophagy are presented in Chapter 4. This study is the first to demonstrate that CAT2 variants with modified C-termini restore the leaf catalase activity to wild type levels. Furthermore, the levels of antioxidant buffers were similar in the CAT2 variants with modified C-termini and the wild type, as was the level of expression of autophagy-marker genes. These findings confirm that the CAT2 variants that were introduced into the transgenic lines were able to restore the leaf catalase activity to wild type levels and so prevent the redox state perturbations observed in the *cat2-1* mutants.

Finally, the studies reported in Chapter 5 addressed the impacts of C-terminal domain modification on *AtCAT2* targeting. Using crude fractionation, cell fractionation and confocal microscopy using super folded split GFP, it was found that the native form and the short-form variants were correctly targeted to peroxisomes. These results suggest correct peroxisomal localisation in these variants. However, the data with regard to the peroxisomal localisation of the ARL variant are inconclusive. Using the sfGFP system, it was found that the last 18 amino acids were important for the nuclear localisation.

The main findings reported in this thesis are summarised in Table 6.2. The implications of the data are discussed in detail in the following sections.

**Table 6.2: Summary of main findings**

The main findings summarised in Section 6.1 are presented.

Ch.3	Rosette phenotype			Rosette diameter		Plant fresh weight		# of leaves		Primary root length	Chlorophyll content
	SD	LD	PC	SD	LD	SD	LD	SD	LD	LD	PC
PSI	C	C	C	C	C	C	C	C	C	C	C
WSQV	C	C	C	C	C	C	C	C	C	C	C
ARL	C	C	C	C	C	C	C	C	C	C	C*
SD: Short-day conditions			LD: Long-day conditions				PC: Photorespiratory Conditions				
C: Complement			C*: Partially complement								

Ch.4	Catalase activity		Ascorbate		Glutathione		H <sub>2</sub> O <sub>2</sub> marker genes	Autophagy Marker genes
	SD	LD	SD	LD	SD	LD	SD	SD
PSI	C	C	C	C	C	C	C	C
WSQV	C	C	C	C	C	C	C	C
ARL	C	C*	C	C	C	C	C	C

Ch.5	Crude fractionation	Cell fractionation	Split Fluorescent Protein Fragments
PSI	Targeted	Targeted	Targeted
WSQV	Targeted	Targeted	Targeted
ARL	inconclusive	Targeted	inconclusive

## **6.2 AtCAT2 lacking the last 18 amino acids produces sufficient activity to maintain growth and cellular redox homeostasis at wildtype levels.**

This study investigated the ability of CAT2 sequences with modified C-termini to complement the growth defects of the *cat2-1* mutant. The different constructs were expressed in transgenic lines and the growth phenotypes were compared to *cat2-1* mutant. The significant growth retardation caused by *cat2-1* mutation was fully rescued in the presence of CAT2 with modified C-termini.

A range of parameters associated with shoot growth were measured such as fresh rosette weight, rosette diameter and the number of leaves (Table 6.2). These data suggest that, in addition to the CAT2PSI, other CAT2 variants (CAT2WSQV and CAT2ARL) are able to recover most, if not all, the growth phenotypes of the *cat2-1* mutant (Table 6.2). These findings are a clear indication that CAT2 sequences lacking the last 18 amino acids of the C-terminus function in a similar manner to the native CAT2 isoform. It has previously been reported that CAT2 is the major leaf isoform and that CAT2 deficiency causes severe growth defects, as evidenced by studies on *cat2* mutants (Bueso et al., 2007; Queval et al., 2007; Mhamdi et al., 2010b; Gao et al., 2014; Waszczak et al., 2016; Su et al., 2018; Yang et al., 2018). However, other possibilities for growth complementation exist and these will be discussed in the sections below.

One alternative explanation for the observed growth complementation is that the expression of other catalases (i.e. CAT1 and CAT3) is increased in the transgenic lines (Frugoli et al., 1996). However, the results presented in Chapter 3 (Figures 3.8 and 3.9) demonstrate that this is not the case because no increase in the expression of other isoforms was observed in the transgenic lines. Interestingly, the levels of *CAT1* and *CAT3* transcripts were not increased even in the *cat2-1* mutants. Therefore, it is unlikely that this would explain the observed complementation data. This finding is in line with previous studies, which showed that *CAT2* is highly expressed in leaves and plays a crucial role in photorespiration.

Moreover, the functions of the photorespiratory *CAT2* cannot be replaced by the other isoforms (Frugoli et al., 1996; Zhong and McClung, 1996; Hu et al., 2010; Mhamdi et al., 2010b). Even mis-expression of *CAT2* cannot rescue the *cat2* phenotype, as was demonstrated by studies in which *CAT2* was expressed under the control of the *CAT3* promoter. No growth complementation was observed in these experiments, largely because *CAT2* and *CAT3* have different expression patterns (Hu et al., 2010). Taken together, these findings show that the introduced *CAT2* constructs can fulfil the photorespiratory *CAT* roles, leading to growth complementation.

Analysis of the expression of *CAT3*, using *CAT3* specific antibodies, provided additional evidence that *CAT3* cannot compensate for the absence of *CAT2*. The levels of *CAT3* protein were similar in all lines, including the wild type, the *cat2-1* mutants, and the transgenic lines, as determined by western blot analysis using *CAT3* specific antibodies. Similarly, no *CAT3* activity was detected by activity staining on native gels. In contrast, *CAT2* activity was readily detected using this approach. It is likely that *CAT3* activity was not observed because the activity of this form fell below the level of detection by the staining procedure and also because of *CAT2* accounts for most of the leaf activity (70-80%) (Frugoli et al., 1996; Zhong and McClung, 1996; Zimmermann et al., 2006; Queval and Noctor, 2007; Yang et al., 2018).

The importance of *CAT2* sequences with modified C-termini was also studied in roots because *CAT2* is also expressed in these organs (Mhamdi et al., 2010b); Figure 4A]. The growth of the primary root was restored to wild type levels in the three transgenic lines. In contrast, the *cat2-1* mutants exhibited a significant decrease in primary root length, a finding which was also recently reported in *cat2* mutants [(Yang et al., 2018), Figure 2a, centre]. These results also suggest that the *CAT2* lacking the last 18 amino acids produces sufficient catalase activity to maintain the root growth of the *cat2-1* mutant.

In the leaves of C3 plants such as *A. thaliana*, peroxisomal H<sub>2</sub>O<sub>2</sub> production is an inevitable consequence of photosynthesis at ambient CO<sub>2</sub> levels, as a result of flux through the photorespiratory pathway. Photorespiratory H<sub>2</sub>O<sub>2</sub> production leads to cell death in the leaves of the *cat2* mutants that lack the photorespiratory catalase form (Queval et al., 2007; Waszczak et al., 2016). In the present study, a restriction of air flow, which further decreases the CO<sub>2</sub> levels, was used to study the photorespiratory phenotype of the *cat2-1* mutants (Vanderauwera et al., 2012; Kerchev et al., 2015; Waszczak et al., 2016). The cell death phenotype of the *cat2-1* mutants that is induced by photorespiratory H<sub>2</sub>O<sub>2</sub> production in the peroxisomes, was abolished in the three transgenic lines expressing CAT2 with modified C-terminal domains.

These findings demonstrate that even under conditions of high photorespiratory flux, the C-terminal truncations are able to provide sufficient catalase activity in the appropriate cell compartments, to deal effectively with the photorespiratory H<sub>2</sub>O<sub>2</sub>, even when the C-terminus is lacking. The phenotype of wild type and CAT2PSI can fully support the phenotype observations of CAT2WSQV and CAT2ARL. Despite the observation that CAT2ARL does not completely complement the phenotype, (possible reasons for this will be discussed later, section 6.4), the expression of the different variants is sufficient to limit H<sub>2</sub>O<sub>2</sub> accumulation and its consequences. Limiting peroxisomal H<sub>2</sub>O<sub>2</sub> accumulation via expression of the CAT2 isoform is required for optimal plant growth (Vandenabeele et al., 2004; Vanderauwera et al., 2005; Queval et al., 2007; Hu et al., 2010; Mhamdi et al., 2010a; Noctor et al., 2015).

Taken together, the studies reported here using untagged constructs expressed in the *cat2-1* mutant background clearly demonstrate that the highly conserved C-terminal 18 amino acids are dispensable for growth under different environmental conditions (short / long-days and photorespiratory conditions).

The growth complementation data suggest that CAT2 with C-terminal truncations produces sufficient catalase activity to rescue the growth of the *cat2-1* mutants. Catalase activity measurements in homogenates and in organelle fractions (Chapter 4 and 5) demonstrate that the *AtCAT2* with C-terminal modifications is enzymatically active. These findings suggest that the last 18 amino acids are not essential for leaf catalase activity. Comparisons of the catalase activity of the transgenic lines with that of the *cat2-1* mutant background clearly show that catalase activity is associated with *AtCAT2* with modified C-termini. This conclusion is also supported by evidence from the in-gel activity assays, which indicate that catalase is assembled into tetramers in each transgenic line.

The catalase activity of transgenic leaves was increased to wild type levels, whereas the *cat2-1* mutant had only about 20% of the activity of the wild type plants. This evidence supports the conclusion that the CAT2 variants are enzymatically active. This conclusion is consistent with the findings of other studies showing the importance of the native *CAT2* gene in determining high leaf catalase activities (Queval et al., 2007; Du et al., 2008; Mhamdi et al., 2010b; Su et al., 2018; Yang et al., 2018). However, it is impossible to exclude the possibility that the C terminal modifications cause subtle changes in activity that cannot be detected using the experimental procedures reported here. Future studies in this require the purification of the variant enzymes and detailed kinetic analysis.

The absence of *CAT2* has been reported to cause activation of oxidative signalling, particularly under photorespiratory conditions in *A. thaliana* mutants, and in other species such as tobacco in which catalase expression has been modified (Smith et al., 1984; Willekens et al., 1997; Noctor et al., 2002b; Queval et al., 2007). Redox perturbations have been reported in the *A. thaliana cat2* mutants (Queval et al., 2007; Mhamdi et al., 2010b; Waszczak et al., 2016; Su et al., 2018). Such findings point to the main role of *CAT2* in cellular redox homeostasis. The data reported in chapter 4 demonstrate that cellular redox homeostasis was restored in the transgenic lines expressing the different CAT2 variants with modified C-termini.

The expression of AtCAT2 with modified C-termini was able to deactivate oxidative signalling, as detected by the levels of antioxidants and H<sub>2</sub>O<sub>2</sub> marker transcripts. The accumulation of H<sub>2</sub>O<sub>2</sub> in the *cat2* mutant leaves under photorespiratory conditions triggers the accumulation of glutathione (Queval et al., 2007; Chaouch et al., 2010; Hu et al., 2010). Although H<sub>2</sub>O<sub>2</sub> was not measured directly in this study, glutathione accumulation was observed in the *cat2-1* mutant leaves, together with increased levels of marker transcripts.

An increased availability of H<sub>2</sub>O<sub>2</sub> in the *cat2* mutants may induce peroxisomal aggregation, and the induction of autophagy (Shibata et al., 2013). Therefore, the expression of autophagy-marker genes was measured in this study. As presented in Chapter 4, the levels of transcripts encoding autophagy marker proteins were only increased in the *cat2-1* mutant. In contrast, the transgenic lines, expressing CAT2 without the last 18 amino acids did not show increased levels of transcripts relative to the wild type. It is possible to conclude therefore that photorespiratory H<sub>2</sub>O<sub>2</sub> does not accumulate in the peroxisomes of these lines. It was previously reported that an accumulation of H<sub>2</sub>O<sub>2</sub> in the peroxisomes leads to irreversible oxidation of the matrix proteins and defects in peroxisomal functions (Van den Bosch et al., 1992; Eastmond et al., 2000; Adham et al., 2005; Fahnenstich et al., 2008). It has also been demonstrated that autophagy plays an important role in the regulation of oxidative stress metabolism (Xiong et al., 2007; Yoshimoto et al., 2014; Yamauchi et al., 2019). The C-terminal truncations therefore prevent the accumulation of H<sub>2</sub>O<sub>2</sub> that would lead to such responses, at least under growth conditions used in this study.

It should be noted that no attempts were made to measure H<sub>2</sub>O<sub>2</sub> concentrations in this study, because of the complexities and difficulties encountered in accurately measuring H<sub>2</sub>O<sub>2</sub> (Mhamdi et al., 2010b; Chaouch et al., 2012). The presence of other antioxidant enzymes complicates the interpretation of H<sub>2</sub>O<sub>2</sub> accumulation data. Moreover, extraction techniques may not preserve oxidant levels at *in vivo* concentrations and assay methods are fraught with ambiguities (Noctor et al., 2016; Tuzet et al., 2019).

## 6.3 *At*CAT2 variants are targeted to peroxisomes

### 6.3.1 Peroxisomal localisation of *At*CAT2 short form.

Data are presented in Chapter 5 showing that the short form of *At*CAT2 is targeted to peroxisomes. These results were attained using crude and cell fractionation techniques, as well as confocal microscopy. A key question arises concerning the finding that the C terminal truncation (WSQV construct) is imported into peroxisomes. This question concerns whether catalase is “piggybacked”, into the peroxisomes by assembling with CAT1 or CAT3. Many studies have shown that proteins that lack a PTS1 can be imported into peroxisomes through a piggyback mechanism that involves interactions with the native subunits (Glover et al., 1994; Lee et al., 1997; Jung et al., 2010; Schueren et al., 2014; Thoms, 2015; Gabay-Maskit et al., 2020).

In fact, it is unlikely that the WSQV form is imported via this mechanism because: (1) the WSQV variant is expressed in the *cat2-1* mutant background preventing interaction with endogenous CAT2 subunits, (2) CAT3 is unlikely to play a role as a shuttling factor for the WSQV variant because it was not detected in the peroxisome-enriched pellet from this transgenic line (Chapter 5). CAT3 activity was not also detected in the in-gel activity assays because of its low activity. It has previously been demonstrated that *cat3* mutation leads to a 15-20% decrease in leaf catalase activity, (Mhamdi et al., 2010b; Hu et al., 2010; Su et al., 2018; Yang et al., 2018). Additionally, unlike CAT2, CAT3 is mainly expressed in the vascular tissues and in senescent leaves, while CAT1 is expressed in seeds and pollen (Willekens et al., 1995; Dat et al., 2000; Zimmermann et al., 2006; Hu et al., 2010). CAT1 cannot complement *cat2* mutations (Section 6.2). It can be therefore concluded that the formation of hetero-oligomeric proteins is a minor phenomenon.

The finding that the CAT2GFP11 construct is delivered into peroxisomes agrees with the results reported by Fujikawa et al. (2019), who showed that catalase C terminally tagged with GFP was successfully imported into peroxisomes. This result also provides further support for the conclusion that a free C terminus is not required for catalase targeting, and is consistent with the finding that the C terminus of CAT2 does not interact with PEX5 TPR domain (Oshima et al., 2008).

The classic PTS1 signal has critical hydrogen bonding interactions in the PTS1 binding pocket, with its terminal carboxylate group. Previously, it was shown that a Pumpkin catalase interacts with the N-terminal half of PEX5 (Oshima et al., 2008). These studies used yeast 2-hybrid experiments to show that the C-terminal 150 amino acids of the protein interact with 1-450 amino acids of PEX5 (Oshima et al., 2008). Moreover, it was recently shown that *Saccharomyces cerevisiae* Catalase A (Cta1p) is imported into peroxisomes without interaction with the PEX5 TPR domain (Rymer et al., 2018).

A further possibility is that *At*CAT2 might possess an internal targeting signal. Previously, it was reported that *Saccharomyces cerevisiae* Cta1p contains a second internal PTS signal that is present between residues 104-126 within the first N terminal third of the protein, and that this can direct Cta1p into the peroxisomes (Kragler et al., 1993).

Overall, previous studies have not considered the importance of the 3-dimensional (3D) structure of catalase. Although structural data are not available for *At*CAT2, a 3D model for CAT2 has been predicated using the bioinformatics tool “Phyre2” (Kelley et al., 2015). The results of this study were analysed and visualised using PyMOL and are presented in Figure 6.1. The striking feature of this model is that the C-terminal helix is extended from the structure. Therefore, removing the last 18 amino acids (red colour) might not perturb the folding of the protein.

However, some partial truncations or mutations could result in a disruption of folding. Heme binding site mutations have been reported to disrupt protein folding (Walton et al., 1995; Janošík et al., 2001; Smith et al., 2010; Williams et al., 2012a; Díaz et al., 2012).

Recently, it was demonstrated that certain amino acids (Arginine and Tyrosine) in the heme-binding sites are essential for the import of *A. thaliana* CAT2 into peroxisomes (Fujikawa et al., 2019). However, it will be necessary to determine the structural features of AtCAT2 in greater detail and to perform a comprehensive biochemical, biophysical, and structural analysis to gain further insights into these crucial issues.



**Figure 6.1: Three-dimensional structure of *A. thaliana* CAT2 (AtCAT2).**

C-terminal 18 amino acids and predicted PTS internal sequence are coloured by red, yellow, respectively. Structural representation was prepared using *PyMOL* (<http://www.pymol.org>). The 3D structure was modelled based on *bacillus pumilus* catalase (PDB code; 4QOQ). The predicted internal sequence of AtCAT2 was determined based on the sequence alignment between Cta1p and AtCAT2.

### **6.3.2 Peroxisomal targeting of CAT2ARL.**

The subcellular localisation of CAT2 variant with ARL (instead of PSI) as C-terminal tripeptide sequence was studied to gain further insights into the effects of a consensus PTS1 signal on *At*CAT2 targeting. Cell fractionation experiments revealed that this variant is targeted to the peroxisomes, a finding that suggests that replacing the -PSI sequence of *At*CAT2 with -ARL allows transport of the *At*CAT2 protein into the peroxisomes. However, in the experiments using sfGFP, the fluorescent signal was observed in clustered structures in only one independent experiment. This result contrasts with the clear observations of a peroxisomal localization in the wild type and with the C terminal truncated constructs. Therefore, these data are inconclusive and await further confirmation.

The peroxisomal localisation of CAT2ARL may indicate that replacing the non-canonical -PSI tripeptide sequence with -ARL, which is a canonical tripeptide sequence, does not disrupt the peroxisomal import of *At*CAT2. This is the first report of this type of study with plant catalases, but the findings are consistent with the results of Koepke et al., 2007, who showed that altering the non-canonical sequence of human (-KANL) catalase to the more effective SKL sequence resulted in efficient import of the proteins into peroxisomes (Koepke et al., 2007). Therefore, taken together with the previous findings (Koepke et al., 2007), the results presented here suggest that altering the non-canonical PTS1 sequence to a canonical PTS1 sequence allows efficient import of plant, and mammalian catalases into peroxisomes.

These findings may also shed some light on the binding affinity of the PEX5 receptor. Interestingly, two previous studies showed that the canonical PTS1 sequence binds strongly to PEX5 receptor (Koepke et al., 2007; Williams et al., 2012a). Indeed, several studies have also shown that the PTS1 consensus sequence binds PEX5 with a higher affinity than the non-consensus PTS1 signals that were tested (Gatto et al., 2003; Maynard et al., 2004; Ghosh and Berg, 2010). As mammalian and yeast catalases also contain non-canonical PTS1 sequences, it is possible to speculate that the peptide containing -ARL has a higher binding affinity for PEX5 relative to the non-canonical PTS1 sequence (-PSI) and -WSQV.

Future investigations of the binding affinity of the peptides-PEX5 interactions must be undertaken to demonstrate this point. In such studies, PSI, ARL, WSQV and the last 18 amino acids must be synthesised and attached to a fluorescent label by conjugation to the lissamine rhodamine B sulfonyl chloride, as previously described (Gatto et al., 2003). The interactions can then be quantified using receptor-based fluorescence anisotropy involving changes in the lissamine-tagged peptide upon the addition of the PEX5. Unpublished data from previous student who tested the ability of peptides corresponding to CAT2 terminus to interact in vitro with recombinant PEX5 and could not detect an interaction (N. Skoulding, 2011 PhD thesis University of Leeds) but it would be interesting to repeat this with the WQSV and ARL variants described in this thesis.

#### **6.4 CAT2ARL behaves differently under certain conditions.**

Further studies were undertaken involving the transfer of transgenic lines that had been grown under short-day conditions to long-day conditions (16hr photoperiod), for one week. In these studies, the transgenic lines that contained CAT2ARL exhibited a slight decrease in catalase activity. Moreover, under conditions that enhance the photorespiratory flux (24hr photoperiod), the chlorophyll content of the CAT2ARL leaves was also decreased. It should be noted that both catalase activity and chlorophyll content were significantly increased in the CAT2ARL leaves relative to the *cat2-1* mutant. This is an interesting finding because this variant must be experiencing some degree of oxidative stress under these conditions. Further analysis is required to understand the mechanisms involved. The duration of the photoperiod influences the cell death phenotype and gene expression in the *cat2* mutants (Queval et al., 2007). Consequently, growing plants under long-day conditions and/or photorespiratory conditions for more than one week is needed to further examine the interactions between catalase activity, H<sub>2</sub>O<sub>2</sub>-marker gene expression level and cell death. Studying subcellular localisation could also be interesting. Indeed, the import of the three CAT2 could be suppressed under oxidative stress. Recently, it has been shown that catalase import is suppressed by exposure to oxidative stress in several different species [Reviewed in (Fujiki and Bassik, 2021; Foyer et al., 2020)].

Such responses could be linked to PEX14 phosphorylation (Okumoto et al., 2020). However, the regulatory mechanisms involved are largely unknown.

## **6.5 CAT2 variants are assembled within peroxisomes.**

The data presented here show that up to 18 amino acids can be removed from the C terminus without disturbing AtCAT2 assembly. Using an sfGFP system with confocal microscopy, it was found that the expression of CAT2sfGFP11 variants with cytoplasmic-targeted sfGFP1-10<sup>OPT</sup> could not reconstitute an sfGFP signal in the cytoplasm relative to the positive control. This finding suggests that the assembly of the CAT2 variants occurs in the peroxisomes rather than in the cytoplasm. Therefore, the CAT2 variants may be imported into peroxisomes as monomers.

Despite the fact that there is no previous evidence that plant catalases may be imported into peroxisomes as monomers, there is no reason to believe that peroxisomes could not import monomeric proteins (Lazarow and De Duve, 1973; Waterham et al., 1993; Crookes and Olsen, 1998; Stewart et al., 2001; Faber et al., 2002; Freitas et al., 2011; Freitas et al., 2015).

The data presented here are consistent with previous observations that suggest that rat liver catalase oligomerisation occurs in peroxisomes (Lazarow and De Duve, 1973). Such observations were extended by Freitas and co-workers, who showed that mammalian PEX5 is capable of binding to monomeric catalase (Freitas et al., 2011). PEX5 is responsible for transporting catalase into the peroxisomes.

Monomeric import has also been reported for other proteins in various organisms. For example, mammalian acyl-CoA oxidase 1 (ACOX1) and urate oxidase (UOX) were shown to be imported into peroxisomes as monomers (Lazarow and De Duve, 1973; Freitas et al., 2015). Crookes and Olsen (1998) showed that monomeric pumpkin isocitrate lyase is imported more efficiently than oligomeric isocitrate lyase (Crookes and Olsen, 1998). It was also demonstrated that alcohol oxidase (AO) octamers were not present in the cytosol of *Candida boidinii* cells (Waterham et al., 1993; Stewart et al., 2001). Later, Faber et al. (2002) showed that yeast *Hansenula polymorpha* PEX5

binds monomeric AO (Faber et al., 2002), providing an explanation for the monomeric AO importing into peroxisomes.

In contrast to these reports, some studies have shown that most peroxisomal proteins oligomerise in the cytosol (Glover et al., 1994; McNew and Goodman, 1994; Lee et al., 1997; Yang et al., 2001; Titorenko et al., 2002; Madrid et al., 2004; Moscicka et al., 2007; Otera and Fujiki, 2012; Schueren et al., 2014). For example, gel permeation chromatography was used to show that the *Leishmania donovani* PEX5 binds cargo as a tetramer (Madrid et al., 2004), while electron microscopy studies revealed similar findings in *Hansenula polymorpha* (Moscicka et al., 2007). However, it remains to be established whether these contradictory findings truly represent disparities in the architecture of PEX5 between organisms, or whether they simply result from variations in the experimental conditions used.

The experimental conditions may result, for example, in premature oligomerisation of proteins or/and titration of the cytosolic receptors PEX5 or exceeding the capacity of folding factors like NO CATALASE ACTIVITY1 (NCA1). Such anomalies have demonstrated in an *in vivo* system for targeting priority to the peroxisomal matrix [(Rosenthal et al., 2020) and reviewed in (Bürgi et al., 2021)]. If the PEX5-cargo proteins are expressed at low levels, the targeting will not be affected whereas high expression levels can create competition with other PEX5-cargo proteins. In consequence, peroxisomal targeting will occur only for proteins with high targeting priority (i.e. when high levels of protein are expressed) (Rosenthal et al., 2020).

It is striking that the studies (see Table 6.1) that used transient expression systems, where copy number and expression levels were high report that the C-terminus is necessary for import, whereas this is not the case in the present study (Table 6.1). This finding could suggest the presence of two pathways, one which has a limited capacity and is dependent on folded catalase interacting with the N terminus of PEX5, and one in which correct folding is prevented either by mutation or overexpression, which then involves interactions with the TPR domain as illustrated in Figure 6.2.

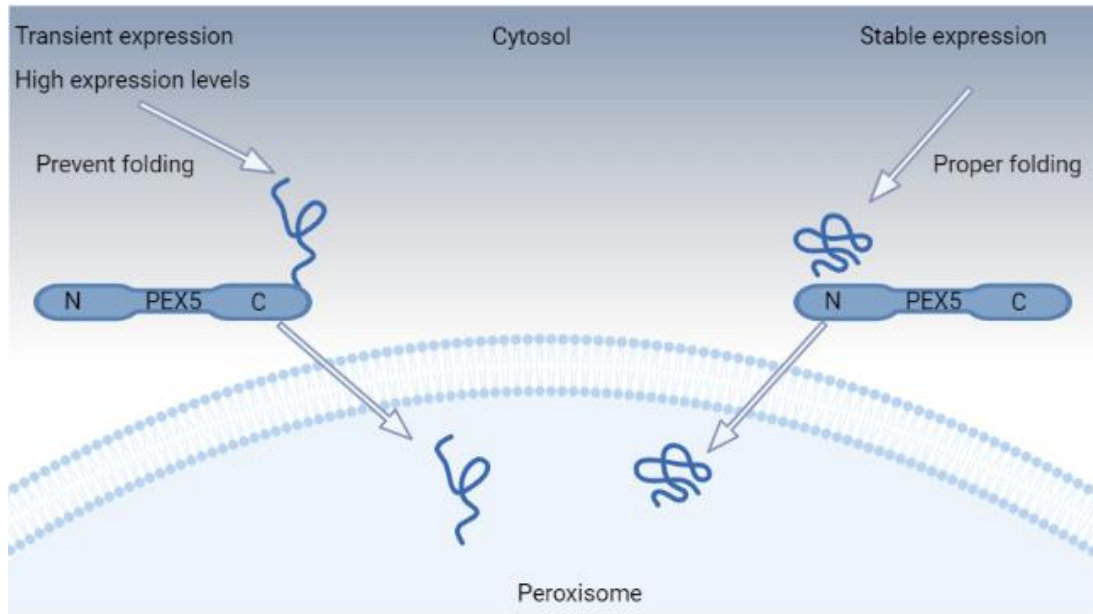


**Figure 6.2: Proposed model of two targeting pathways**

### **6.6 If not targeting or activity, what is the function of the conserved C terminus?**

Questions remain concerning the importance of the plant catalase C-terminal sequence. Using the sfGFP system, it was shown that *AtCAT2* is imported into the nucleus. As the WQSV variant was not, this strongly suggests nuclear localisation of *AtCAT2* is controlled by the presence of the last 18 amino acids. Therefore, this is the first evidence that *AtCAT2* import to the nucleus without the action of the effector proteins. Previously, it was shown that pathogen effectors recruit catalase to the nucleus. The *Phytophthora sojae* effectors PsCRN63 and PsCRN115 (for crinkling and necrosis inducing proteins) both interact with catalase (CAT1) from *Nicotiana benthamiana* and soybean (*Glycine max*) and traffic it into the nucleus (Zhang et al., 2015). It was also reported that *Cucumber mosaic virus* 2b protein interacts directly with *A. thaliana* catalase 3 (CAT3) which will be then recruited to the plant nucleus (Inaba et al., 2011).

The last 18 amino acids could be also important in regulation of activity or localisation, particularly because post-translational modifications (PMTs) have been previously reported in this region.

For example, a single acetylation site motif has been identified (K481; ...DKSLGQ(K)LASRLNVRPSI....) (Liu et al., 2018). Protein phosphorylation (S491;...DKSLGQKLASRLNVRP(S)I...) has also been reported (Umezawa et al., 2013; Bhaskara et al., 2017). However, it is still unclear whether these modifications have a functional significance. It should also be noted that these data come from large scale proteomic data sets. Nevertheless, such observations merit further investigation particularly because it is known that PTMs affect catalase activity (Zhou, H. et al., 2018; Sandalio et al., 2019; Palma et al., 2020). It is interesting to note that both K481 and S491 have been implicated by mutation/deletion in previous studies suggesting that this region is important for targeting. Thus, these PTMs may fine tune activity and/or localisation.

## 6.7 Conclusions

In conclusion, the transgenic lines prepared and characterised in this study have provided new insights into the roles of C-terminal modifications of catalase on plant physiology, biochemistry, and subcellular localisation. This research sought to integrate morphological, biochemical, and targeting data to evaluate the effect of C-terminal truncations in a physiologically-relevant context. The results presented in this thesis demonstrate that the last 18 amino acids of *AtCAT2* are dispensable for catalase activity, cellular redox homeostasis and peroxisomal targeting. Based on these findings, it is possible to conclude that the *AtCAT2* C-terminal domain is not essential for growth, enzyme activity or targeting. But, it is essential to direct the protein into the nucleus. However, it is possible to speculate that this region could potentially play an important role in the regulation of the activity of the enzyme. Nevertheless, further work is needed to elucidate this possibility. Finally, the possibility of the presence of two targeting pathways has been postulated in this discussion. This concept may allow interpretation of the seemingly contradictory results reported in the literature.

## 6.8 Future directions

The studies reported in this thesis were carefully designed to express native proteins at physiological levels in a completely homologous system. While piggyback import is highly unlikely, this phenomenon cannot be completely excluded and so analysis is required to determine the impact of piggyback import. In this study, the peroxisome-targeted sfGFP1-10<sup>OPT</sup> [(Park et al., 2017), Supplemental Table 1] and CAT2WSQV-sfGFP11 plasmids had to be transfected into protoplasts isolated from the *cat2-1* or *cat2cat3* mutants. Since the protoplasts obtained in these procedure for use in the sfGFP system, are mainly derived from mesophyll cells, it might be interesting to measure the CAT2/CAT3 protein ratios in the protoplasts to determine the extent to which CAT3 is present and therefore a piggybacking mechanism is possible in this system.

The evidence derived from this study is consistent with the proposal that AtCAT2 monomers can be imported into peroxisomes for assembly. It would be interesting to determine whether PEX5 displays any preferences for the monomeric and/or tetrameric forms of AtCAT2. Thus, the preparation of monomeric and tetrameric versions of AtCAT2 using a reticulocyte lysate based *in vitro* translation system will be carried out in the future in order to characterise the interactions between the different AtCAT2 versions and PEX5. Knowing how PEX5 interacts with AtCAT2 is crucial for our understanding of the sorting pathway of AtCAT2.

In the current study, catalase activity was only measured in crude homogenates and organelle fractions. To test if the C terminus has any influence on the kinetics of the catalase, it will be necessary to measure the activity of the purified protein.

The leaves of the CAT2ARL lines had low levels of chlorophyll. Thus, further characterisation of the ARL lines is required for example with regard to stress tolerance. A chlorophyll fluorescence imaging system could be used to measure parameters such as photosystem II (PSII) maximum efficiency ( $F_v'/F_m'$ ) in the wild type, *cat2-1* mutant and transgenic lines under photorespiratory and other conditions.

The quantum efficiency of PSII is likely to be much lower in the *cat2-1* mutants than the wild type. It may be that the PSI and WSQV transgenic lines have similar values to the wild type for parameters such as  $F_v'/F_m'$  values, whereas ARL may have lower  $F_v'/F_m'$  values than the wild type.

## References

**Adams, E., Miyazaki, T., Watanabe, S., Ohkama-Ohtsu, N., Seo, M. and Shin, R.** (2020). Glutathione and its biosynthetic intermediates alleviate cesium stress in Arabidopsis. *Frontiers in Plant Science*. **10**, p1711.

**Adham, A.R., Zolman, B.K., Millius, A. and Bartel, B.** (2005). Mutations in Arabidopsis acyl-CoA oxidase genes reveal distinct and overlapping roles in  $\beta$ -oxidation. *The Plant Journal*. **41**(6), pp.859-874.

**Aebi, H., Jeunet, F., Richterich, R., Suter, H., Bütler, R., Frei, J. and Marti, H.** (1962). Observations in two Swiss families with acatalasia. *Enzymologia biologica et clinica*. **2**, pp.1-22.

**Agne, B., Meindl, N.M., Niederhoff, K., Einwächter, H., Rehling, P., Sickmann, A., Meyer, H.E., Girzalsky, W. and Kunau, W.H.** (2003). Pex8p: an intraperoxisomal organizer of the peroxisomal import machinery. *Molecular cell*. **11**(3), pp.635-646.

**Akram, N.A., Shafiq, F. and Ashraf, M.** (2017). Ascorbic acid-a potential oxidant scavenger and its role in plant development and abiotic stress tolerance. *Frontiers in plant science*. **8**, p613.

**Al Saryi, N.A., Hutchinson, J.D., Al-Hejjaj, M.Y., Sedelnikova, S., Baker, P. and Hettema, E.H.** (2017). Pnc1 piggy-back import into peroxisomes relies on Gpd1 homodimerisation. *Scientific reports*. **7**(1), pp.1-12.

**Alfonso-Prieto, M., Biarnés, X., Vidossich, P. and Rovira, C.** (2009). The molecular mechanism of the catalase reaction. *Journal of the American Chemical Society*. **131**(33), pp.11751-11761.

**An, C., Gao, Y., Li, J., Liu, X., Gao, F. and Gao, H.** (2017). Alternative splicing affects the targeting sequence of peroxisome proteins in Arabidopsis. *Plant Cell Reports*. pp.1-10.

**Apanasets, O., Grou, C.P., Van Veldhoven, P.P., Brees, C., Wang, B., Nordgren, M., Dodt, G., Azevedo, J.E. and Fransen, M.** (2014). PEX5, the shuttling import receptor for peroxisomal matrix proteins, is a redox-sensitive protein. *Traffic*. **15**(1), pp.94-103.

**Apel, K. and Hirt, H.** (2004). Reactive oxygen species: metabolism, oxidative stress, and signal transduction. *Annu. Rev. Plant Biol.* **55**, pp.373-399.

**Asada, K.** (1999). The water-water cycle in chloroplasts: scavenging of active oxygens and dissipation of excess photons. *Annual review of plant biology*. **50**(1), pp.601-639.

**Avin-Wittenberg, T. and Fernie, A.R.** (2014). At long last: evidence for pexophagy in plants. *Molecular plant*. **7**(8), pp.1257-1260.

**Baker, A.** (1996). Biogenesis of plant peroxisomes. *Membranes: Specialized Function in Plants*. pp.421-440.

**Baker, A. and Graham, I.A.** 2013. *Plant peroxisomes: biochemistry, cell biology and biotechnological applications*. Springer Science & Business Media.

**Baker, A., Graham, I.A., Holdsworth, M., Smith, S.M. and Theodoulou, F.L.** (2006). Chewing the fat:  $\beta$ -oxidation in signalling and development. *Trends in plant science*. **11**(3), pp.124-132.

**Ball, L., Accotto, G.P., Bechtold, U., Creissen, G., Funck, D., Jimenez, A., Kular, B., Leyland, N., Mejia-Carranza, J. and Reynolds, H.** (2004). Evidence for a direct link between glutathione biosynthesis and stress defense gene expression in Arabidopsis. *The Plant Cell*. **16**(9), pp.2448-2462.

**Bartel, B., Farmer, L.M., Rinaldi, M.A., Young, P.G., Danan, C.H. and Burkhart, S.E.** (2014). Mutation of the Arabidopsis LON2 peroxisomal protease enhances pexophagy. *Autophagy*. **10**(3), pp.518-519.

**Barth, C., Moeder, W., Klessig, D.F. and Conklin, P.L.** (2004). The timing of senescence and response to pathogens is altered in the ascorbate-deficient Arabidopsis mutant vitamin c-1. *Plant Physiology*. **134**(4), pp.1784-1792.

**Bassham, D.C.** (2007). Plant autophagy—more than a starvation response. *Current opinion in plant biology*. **10**(6), pp.587-593.

**Bassham, D.C., Laporte, M., Marty, F., Moriyasu, Y., Ohsumi, Y., Olsen, L.J. and Yoshimoto, K.** (2006). Autophagy in development and stress responses of plants. *Autophagy*. **2**(1), pp.2-11.

**Baune, M.-C., Lansing, H., Fischer, K., Meyer, T., Charton, L., Linka, N. and von Schaewen, A.** (2020). The Arabidopsis Plastidial Glucose-6-phosphate Transporter GPT1 is Dually Targeted to Peroxisomes via the Endoplasmic Reticulum. *The Plant Cell*. **32**(5), pp.1703-1726.

**Baureder, M., Barane, E. and Hederstedt, L.** (2014). In vitro assembly of catalase. *Journal of Biological Chemistry*. **289**(41), pp.28411-28420.

**Baxter, A., Mittler, R. and Suzuki, N.** (2014). ROS as key players in plant stress signalling. *Journal of experimental botany*. **65**(5), pp.1229-1240.

**Beevers, H.** (1979). Microbodies in higher plants. *Annual Review of Plant Physiology*. **30**(1), pp.159-193.

**Bhaskara, G.B., Wen, T.N., Nguyen, T.T. and Verslues, P.E.** (2017). Protein phosphatase 2Cs and microtubule-associated stress protein 1 control microtubule stability, plant growth, and drought response. *The Plant Cell*. **29**(1), pp.169-191.

**Bick, J.A., Setterdahl, A.T., Knaff, D.B., Chen, Y., Pitcher, L.H., Zilinskas, B.A. and Leustek, T.** (2001). Regulation of the plant-type 5'-adenylyl sulfate reductase by oxidative stress. *Biochemistry*. **40**(30), pp.9040-9048.

**Blomster, T., Salojärvi, J., Sipari, N., Brosché, M., Ahlfors, R., Keinänen, M., Overmyer, K. and Kangasjärvi, J.** (2011). Apoplastic reactive oxygen species transiently decrease auxin signaling and cause stress-induced morphogenic response in Arabidopsis. *Plant Physiology*. **157**(4), pp.1866-1883.

**Boisson-Dernier, A., Frietsch, S., Kim, T.H., Dizon, M.B. and Schroeder, J.I.** (2008). The peroxin loss-of-function mutation abstinence by mutual consent disrupts male-female gametophyte recognition. *Current Biology*. **18**(1), pp.63-68.

**Breidenbach, R. and Beevers, H.** (1967). Association of the glyoxylate cycle enzymes in a novel subcellular particle from castor bean endosperm. *Biochemical and biophysical research communications*. **27**(4), pp.462-469.

**Brocard, C. and Hartig, A.** (2006). Peroxisome targeting signal 1: is it really a simple tripeptide? *Biochimica et Biophysica Acta (BBA)-Molecular Cell Research*. **1763**(12), pp.1565-1573.

**Brown, L.A. and Baker, A.** (2003). Peroxisome biogenesis and the role of protein import. *Journal of cellular and molecular medicine*. **7**(4), pp.388-400.

**Brown, L.A. and Baker, A.** (2008). Shuttles and cycles: transport of proteins into the peroxisome matrix. *Molecular membrane biology*. **25**(5), pp.363-375.

**Brugna, M., Tasse, L. and Hederstedt, L.** (2010). In vivo production of catalase containing haem analogues. *The FEBS journal*. **277**(12), pp.2663-2672.

**Bueso, E., Alejandro, S., Carbonell, P., Perez-Amador, M.A., Fayos, J., Bellés, J.M., Rodriguez, P.L. and Serrano, R.** (2007). The lithium tolerance of the *Arabidopsis* *cat2* mutant reveals a cross-talk between oxidative stress and ethylene. *The Plant Journal*. **52**(6), pp.1052-1065.

**Bürgi, J., Ekal, L. and Wilmanns, M.** (2021). Versatile allosteric properties in Pex5-like tetratricopeptide repeat proteins to induce diverse downstream function. *Traffic*. pp.1-13.

**Burkhart, S.E., Lingard, M.J. and Bartel, B.** (2013). Genetic dissection of peroxisome-associated matrix protein degradation in *Arabidopsis thaliana*. *Genetics*. **193**(1), pp.125-141.

**Busch, F.A.** (2020). Photorespiration in the context of Rubisco biochemistry, CO<sub>2</sub> diffusion and metabolism. *The Plant Journal*. **101**(4), pp.919-939.

**Cabantous, S., Nguyen, H.B., Pedelacq, J.D., Koraïchi, F., Chaudhary, A., Ganguly, K., Lockard, M.A., Favre, G., Terwilliger, T.C. and Waldo, G.S.** (2013). A new protein-protein interaction sensor based on tripartite split-GFP association. *Scientific reports*. **3**, p2854.

**Cabantous, S., Terwilliger, T.C. and Waldo, G.S.** (2005). Protein tagging and detection with engineered self-assembling fragments of green fluorescent protein. *Nature biotechnology*. **23**(1), pp.102-107.

**Cairns, N.G., Pasternak, M., Wachter, A., Cobbett, C.S. and Meyer, A.J.** (2006). Maturation of *Arabidopsis* seeds is dependent on glutathione biosynthesis within the embryo. *Plant Physiology*. **141**(2), pp.446-455.

**Cao, C., Leng, Y. and Kufe, D.** (2003). Catalase activity is regulated by c-Abl and Arg in the oxidative stress response. *Journal of Biological Chemistry*. **278**(32), pp.29667-29675.

**Carpena, X., Soriano, M., Klotz, M.G., Duckworth, H.W., Donald, L.J., Melik-Adamyán, W., Fita, I. and Loewen, P.C.** (2003). Structure of the clade 1 catalase, CatF of *Pseudomonas syringae*, at 1.8 Å resolution. *Proteins: structure, function, and bioinformatics*. **50**(3), pp.423-436.

**Cavalier-Smith, T.** (1987). The origin of eukaryote and archaeobacterial cells. *Ann. NY Acad. Sci.* **503**, pp.7-54.

**Chalfie, M., Tu, Y., Euskirchen, G., Ward, W.W. and Prasher, D.C.** (1994). Green fluorescent protein as a marker for gene expression. *Science*. **263**(5148), pp.802-805.

**Chamnongpol, S., Willekens, H., Moeder, W., Langebartels, C., Sandermann, H., Van Montagu, M., Inzé, D. and Van Camp, W.** (1998). Defense activation and enhanced pathogen tolerance induced by H<sub>2</sub>O<sub>2</sub> in transgenic tobacco. *Proceedings of the National Academy of Sciences*. **95**(10), pp.5818-5823.

**Chaouch, S., Queval, G. and Noctor, G.** (2012). AtRbohF is a crucial modulator of defence-associated metabolism and a key actor in the interplay between intracellular oxidative stress and pathogenesis responses in Arabidopsis. *The Plant Journal*. **69**(4), pp.613-627.

**Chaouch, S., Queval, G., Vanderauwera, S., Mhamdi, A., Vandenborgh, M., Langlois-Meurinne, M., Van Breusegem, F., Saindrenan, P. and Noctor, G.** (2010). Peroxisomal hydrogen peroxide is coupled to biotic defense responses by ISOCHORISMATE SYNTHASE1 in a daylength-related manner. *Plant Physiology*. **153**(4), pp.1692-1705.

**Chelikani, P., Carpena, X., Fita, I. and Loewen, P.C.** (2003). An electrical potential in the access channel of catalases enhances catalysis. *Journal of Biological Chemistry*. **278**(33), pp.31290-31296.

**Chelikani, P., Fita, I. and Loewen, P.** (2004). Diversity of structures and properties among catalases. *Cellular and molecular life sciences*. **61**(2), pp.192-208.

**Chen, N., Teng, X.L. and Xiao, X.G.** (2017). Subcellular localization of a plant catalase-phenol oxidase, AcCATPO, from Amaranthus and identification of a non-canonical peroxisome targeting signal. *Frontiers in Plant Science*. **8**, p1345.

**Cobbett, C.S., May, M.J., Howden, R. and Rolls, B.** (1998). The glutathione-deficient, cadmium-sensitive mutant, cad2-1, of Arabidopsis thaliana is deficient in  $\gamma$ -glutamylcysteine synthetase. *The Plant Journal*. **16**(1), pp.73-78.

**Conklin, P. and Barth, C.** (2004). Ascorbic acid, a familiar small molecule intertwined in the response of plants to ozone, pathogens, and the onset of senescence. *Plant, Cell & Environment*. **27**(8), pp.959-970.

**Conklin, P.L., Pallanca, J.E., Last, R.L. and Smirnoff, N.** (1997). L-ascorbic acid metabolism in the ascorbate-deficient Arabidopsis mutant vtc1. *Plant Physiology*. **115**(3), pp.1277-1285.

**Conklin, P.L., Williams, E.H. and Last, R.L.** (1996). Environmental stress sensitivity of an ascorbic acid-deficient Arabidopsis mutant. *Proceedings of the National Academy of Sciences*. **93**(18), pp.9970-9974.

**Considine, M.J., Diaz-Vivancos, P., Kerchev, P., Signorelli, S., Agudelo-Romero, P., Gibbs, D.J. and Foyer, C.H.** (2017). Learning to breathe: developmental phase transitions in oxygen status. *Trends in plant science*. **22**(2), pp.140-153.

**Cooper, T. and Beevers, H.** (1969). Mitochondria and glyoxysomes from castor bean endosperm enzyme constituents and catalytic capacity. *Journal of Biological Chemistry*. **244**(13), pp.3507-3513.

**Crookes, W.J. and Olsen, L.J.** (1998). The effects of chaperones and the influence of protein assembly on peroxisomal protein import. *Journal of Biological Chemistry*. **273**(27), pp.17236-17242.

**Crooks, G.E., Hon, G., Chandonia, J.M. and Brenner, S.E.** (2004). WebLogo: a sequence logo generator. *Genome research*. **14**(6), pp.1188-1190.

**Cross, L.L., Ebeed, H.T. and Baker, A.** (2016). Peroxisome biogenesis, protein targeting mechanisms and PEX gene functions in plants. *Biochimica et Biophysica Acta (BBA)-Molecular Cell Research*. **1863**(5), pp.850-862.

**Dat, J., Vandenabeele, S., Vranová, E., Van Montagu, M., Inzé, D. and Van Breusegem, F.** (2000). Dual action of the active oxygen species during plant stress responses. *Cellular and Molecular Life Sciences CMLS*. **57**(5), pp.779-795.

**Davey, M.W., Montagu, M.V., Inze, D., Sanmartin, M., Kanellis, A., Smirnoff, N., Benzie, I.J.J., Strain, J.J., Favell, D. and Fletcher, J.** (2000). Plant L-ascorbic acid: chemistry, function, metabolism, bioavailability and effects of processing. *Journal of the Science of Food and Agriculture*. **80**(7), pp.825-860.

**Davletova, S., Rizhsky, L., Liang, H., Shengqiang, Z., Oliver, D.J., Coutu, J., Shulaev, V., Schlauch, K. and Mittler, R.** (2005). Cytosolic ascorbate peroxidase 1 is a central component of the reactive oxygen gene network of Arabidopsis. *The Plant Cell*. **17**(1), pp.268-281.

**De Duve and Baudhuin, P.** (1966). Peroxisomes (microbodies and related particles). *Physiological reviews*. **46**(2), pp.323-357.

**De Marcos Lousa, C., Dietrich, D., Johnson, B., Baldwin, S., Holdsworth, M., Theodoulou, F.L. and Baker, A.** (2009). The NBDs that wouldn't die: A cautionary tale of the use of isolated nucleotide binding domains of ABC transporters. *Communicative & integrative biology*. **2**(2), pp.97-99.

**Del Buono, D., Terzano, R., Panfili, I. and Bartucca, M.L.** (2020). Phytoremediation and detoxification of xenobiotics in plants: herbicide-safeners as a tool to improve plant efficiency in the remediation of polluted environments. A mini-review. *International Journal of Phytoremediation*. **22**(8), pp.789-803.

**Del Río, L.A.** (2015). ROS and RNS in plant physiology: an overview. *Journal of Experimental Botany*. **66**(10), pp.2827-2837.

**Del Río, L.A., Corpas, F.J., Sandalio, L.M., Palma, J.M., Gómez, M. and Barroso, J.B.** (2002). Reactive oxygen species, antioxidant systems and nitric oxide in peroxisomes. *Journal of Experimental Botany*. **53**(372), pp.1255-1272.

**Del Río, L.A. and López-Huertas, E.** (2016). ROS generation in peroxisomes and its role in cell signaling. *Plant and Cell Physiology*. **57**(7), pp.1364-1376.

**Del Río, L.A., Pastori, G.M., Palma, J.M., Sandalio, L.M., Sevilla, F., Corpas, F.J., Jiménez, A., López-Huertas, E. and Hernández, J.A.** (1998). The activated oxygen role of peroxisomes in senescence. *Plant Physiology*. **116**(4), pp.1195-1200.

**Díaz, A., Loewen, P.C., Fita, I. and Carpena, X.** (2012). Thirty years of heme catalases structural biology. *Archives of biochemistry and biophysics*. **525**(2), pp.102-110.

**Didion, T. and Roggenkamp, R.** (1992). Targeting signal of the peroxisomal catalase in the methylotrophic yeast *Hansenula polymorpha*. *FEBS letters*. **303**(2-3), pp.113-116.

**Ding, M., Clayton, C. and Soldati, D.** (2000). *Toxoplasma gondii* catalase: are there peroxisomes in toxoplasma? *Journal of cell science*. **113**(13), pp.2409-2419.

**Dodt, G., Warren, D., Becker, E., Rehling, P. and Gould, S.J.** (2001). Domain mapping of human PEX5 reveals functional and structural similarities to *Saccharomyces cerevisiae* Pex18p and Pex21p. *Journal of Biological Chemistry*. **276**(45), pp.41769-41781.

**Drory, A. and Woodson, W.R.** (1992). Molecular cloning and nucleotide sequence of a cDNA encoding catalase from tomato. *Plant physiology*. **100**(3), p1605.

**Drumm, H., Falk, H., Moller, J. and Mohr, H.** (1970). The development of catalase in the mustard seedling. *Cytobiologie*. **2**(3), pp.335-340.

**Du, Y.Y., Wang, P.C., Chen, J. and Song, C.P.** (2008). Comprehensive functional analysis of the catalase gene family in *Arabidopsis thaliana*. *Journal of Integrative Plant Biology*. **50**(10), pp.1318-1326.

**Eastmond, P., Hooks, M. and Graham, I.** 2000. The *Arabidopsis* acyl-CoA oxidase gene family. *Biochemical Society Transactions*. **28**, pp.755-757.

**Eastmond, P.J.** (2006). SUGAR-DEPENDENT1 encodes a patatin domain triacylglycerol lipase that initiates storage oil breakdown in germinating *Arabidopsis* seeds. *The Plant Cell*. **18**(3), pp.665-675.

**Eckert, J. and Erdmann, R.** (2003). Peroxisome biogenesis. *Reviews of physiology, biochemistry and pharmacology*. Springer, pp.75-121.

**Edwards, K., Johnstone, C. and Thompson, C.** (1991). A simple and rapid method for the preparation of plant genomic DNA for PCR analysis. *Nucleic acids research*. **19**(6), p1349.

**Effelsberg, D., Cruz-Zaragoza, L.D., Schliebs, W. and Erdmann, R.** (2016). Pex9p is a new yeast peroxisomal import receptor for PTS1-containing proteins. *Journal of cell science*. **129**(21), pp.4057-4066.

**Effelsberg, D., Cruz-Zaragoza, L.D., Tonillo, J., Schliebs, W. and Erdmann, R.** (2015). Role of Pex21p for piggyback import of Gpd1p and Pnc1p into peroxisomes of *Saccharomyces cerevisiae*. *Journal of Biological Chemistry*. **290**(42), pp.25333-25342.

**El Magraoui, F., Bäumer, B.E., Platta, H.W., Baumann, J.S., Girzalsky, W. and Erdmann, R.** (2012). The RING-type ubiquitin ligases Pex2p, Pex10p and Pex12p form a heteromeric complex that displays enhanced activity in an ubiquitin conjugating enzyme-selective manner. *The FEBS journal*. **279**(11), pp.2060-2070.

**Esaka, M., Yamada, N., Kitabayashi, M., Setoguchi, Y., Tsugeki, R., Kondo, M. and Nishimura, M.** (1997). cDNA cloning and differential gene expression of three catalases in pumpkin. *Plant molecular biology*. **33**(1), pp.141-155.

**Eskling, M., Arvidsson, P.O. and Åkerlund, H.E.** (1997). The xanthophyll cycle, its regulation and components. *Physiologia Plantarum*. **100**(4), pp.806-816.

**Faber, K.N., Van Dijk, R., Keizer-Gunnink, I., Koek, A., Van Der Klei, I.J. and Veenhuis, M.** (2002). Import of assembled PTS1 proteins into peroxisomes of the yeast *Hansenula polymorpha*: yes and no! *Biochimica et Biophysica Acta (BBA)-Molecular Cell Research*. **1591**(1-3), pp.157-162.

**Fahnenstich, H., Scarpeci, T.E., Valle, E.M., Flügge, U.I. and Maurino, V.G.** (2008). Generation of hydrogen peroxide in chloroplasts of *Arabidopsis* overexpressing glycolate oxidase as an inducible system to study oxidative stress. *Plant Physiology*. **148**(2), pp.719-729.

**Falter, C., Thu, N.B.A., Pokhrel, S. and Reumann, S.** (2019). New guidelines for fluorophore application in peroxisome targeting analyses in transient plant expression systems. *Journal of integrative plant biology*. **61**(7), pp.884-899.

**Fan, J., Quan, S., Orth, T., Awai, C., Chory, J. and Hu, J.** (2005). The *Arabidopsis* PEX12 gene is required for peroxisome biogenesis and is essential for development. *Plant Physiology*. **139**(1), pp.231-239.

**Fang, Y., Morrell, J.C., Jones, J.M. and Gould, S.J.** (2004). PEX3 functions as a PEX19 docking factor in the import of class I peroxisomal membrane proteins. *The Journal of cell biology*. **164**(6), pp.863-875.

**Farmer, L.M., Rinaldi, M.A., Young, P.G., Danan, C.H., Burkhart, S.E. and Bartel, B.** (2013). Disrupting autophagy restores peroxisome function to an *Arabidopsis* lon2 mutant and reveals a role for the LON2 protease in peroxisomal matrix protein degradation. *The Plant Cell*. **25**(10), pp.4085-4100.

**Feinstein, R.N.** (1970). Acatalasemia in the mouse and other species. *Biochemical genetics*. **4**(1), pp.135-155.

**Fenech, M., Amaya, I., Valpuesta, V. and Botella, M.A.** (2019). Vitamin C content in fruits: Biosynthesis and regulation. *Frontiers in plant science*. **9**, p2006.

**Fidaleo, M.** (2010). Peroxisomes and peroxisomal disorders: the main facts. *Experimental and toxicologic pathology*. **62**(6), pp.615-625.

**Fita, I., Silva, A.M., Murthy, M. and Rossmann, M.G.** (1986). The refined structure of beef liver catalase at 2.5 Å resolution. *Acta Crystallographica Section B: Structural Science*. **42**(5), pp.497-515.

**Fodor, K., Wolf, J., Erdmann, R., Schliebs, W. and Wilmanns, M.** (2012). Molecular requirements for peroxisomal targeting of alanine-glyoxylate aminotransferase as an essential determinant in primary hyperoxaluria type 1. *PLoS Biol.* **10**(4), pe1001309.

**Fodor, K., Wolf, J., Reglinski, K., Passon, D.M., Lou, Y., Schliebs, W., Erdmann, R. and Wilmanns, M.** (2015). Ligand-Induced Compaction of the PEX5 Receptor-Binding Cavity Impacts Protein Import Efficiency into Peroxisomes. *Traffic*. **16**(1), pp.85-98.

**Footitt, S., Slocombe, S.P., Lerner, V., Kurup, S., Wu, Y., Larson, T., Graham, I., Baker, A. and Holdsworth, M.** (2002). Control of germination and lipid mobilization by COMATOSE, the Arabidopsis homologue of human ALDP. *The EMBO Journal*. **21**(12), pp.2912-2922.

**Foyer, C.H.** (1997). Oxygen metabolism and electron transport in photosynthesis. *Oxidative stress and the molecular biology of antioxidant defences*. pp.587-621.

**Foyer, C.H.** (2018). Reactive oxygen species, oxidative signaling and the regulation of photosynthesis. *Environmental and experimental botany*. **154**, pp.134-142.

**Foyer, C.H., Baker, A., Wright, M., Sparkes, I.A., Mhamdi, A., Schippers, J.H. and Van Breusegem, F.** (2020). On the move: redox-dependent protein relocation in plants. *Journal of experimental botany*. **71**(2), pp.620-631.

**Foyer, C.H., Bloom, A.J., Queval, G. and Noctor, G.** (2009). Photorespiratory metabolism: genes, mutants, energetics, and redox signaling. *Annual review of plant biology*. **60**, pp.455-484.

**Foyer, C.H. and Halliwell, B.** (1976). The presence of glutathione and glutathione reductase in chloroplasts: a proposed role in ascorbic acid metabolism. *Planta*. **133**(1), pp.21-25.

**Foyer, C.H. and Noctor, G.** (2003). Redox sensing and signalling associated with reactive oxygen in chloroplasts, peroxisomes and mitochondria. *Physiologia plantarum*. **119**(3), pp.355-364.

**Foyer, C.H. and Noctor, G.** (2005). Oxidant and antioxidant signalling in plants: a re-evaluation of the concept of oxidative stress in a physiological context. *Plant, Cell & Environment*. **28**(8), pp.1056-1071.

**Foyer, C.H. and Noctor, G.** (2009). Redox regulation in photosynthetic organisms: signaling, acclimation, and practical implications. *Antioxidants & redox signaling*. **11**(4), pp.861-905.

**Foyer, C.H. and Noctor, G.** (2011). Ascorbate and glutathione: the heart of the redox hub. *Plant physiology*. **155**(1), pp.2-18.

**Foyer, C.H. and Noctor, G.** 2013. Redox signaling in plants. *Antioxidants. Redox signaling*. **18**, pp.2087-2090.

**Foyer, C.H. and Noctor, G.** (2015). Defining robust redox signalling within the context of the plant cell. *Plant, cell & environment*. **38**(2), pp.239-239.

**Foyer, C.H. and Shigeoka, S.** (2011). Understanding oxidative stress and antioxidant functions to enhance photosynthesis. *Plant physiology*. **155**(1), pp.93-100.

**Francisco, T., Rodrigues, T.A., Dias, A.F., Barros-Barbosa, A., Bicho, D. and Azevedo, J.E.** (2017). Protein transport into peroxisomes: Knowns and unknowns. *BioEssays*. **39**(10), p1700047.

**Francisco, T., Rodrigues, T.A., Pinto, M.P., Carvalho, A.F., Azevedo, J.E. and Grou, C.P.** (2014). Ubiquitin in the peroxisomal protein import pathway. *Biochimie*. **98**, pp.29-35.

**Freitas, M.O., Francisco, T., Rodrigues, T.A., Alencastre, I.S., Pinto, M.P., Grou, C.P., Carvalho, A.F., Fransen, M., Sá-Miranda, C. and Azevedo, J.E.** (2011). PEX5 protein binds monomeric catalase blocking its tetramerization and releases it upon binding the N-terminal domain of PEX14. *Journal of Biological Chemistry*. **286**(47), pp.40509-40519.

**Freitas, M.O., Francisco, T., Rodrigues, T.A., Lismont, C., Domingues, P., Pinto, M.P., Grou, C.P., Fransen, M. and Azevedo, J.E.** (2015). The peroxisomal protein import machinery displays a preference for monomeric substrates. *Open biology*. **5**(4), p140236.

**Frugoli, J.A., Zhong, H.H., Nuccio, M.L., McCourt, P., McPeck, M.A., Thomas, T.L. and McClung, C.R.** (1996). Catalase is encoded by a multigene family in *Arabidopsis thaliana* (L.) Heynh. *Plant Physiology*. **112**(1), pp.327-336.

**Fujikawa, Y., Suekawa, M., Endo, S., Fukami, Y., Mano, S., Nishimura, M. and Esaka, M.** (2019). Effect of mutation of C-terminal and heme binding region of *Arabidopsis* catalase on the import to peroxisomes. *Bioscience, biotechnology, and biochemistry*. **83**(2), pp.322-325.

**Fujiki, Y., Abe, Y., Imoto, Y., Tanaka, A.J., Okumoto, K., Honsho, M., Tamura, S., Miyata, N., Yamashita, T. and Chung, W.K.** (2020). Recent insights into peroxisome biogenesis and associated diseases. *Journal of cell science*. **133**(9).

**Fujiki, Y. and Bassik, M.C.** (2021). A New Paradigm in Catalase Research. *Trends in Cell Biology*. pp.1-3.

**Fujiki, Y., Okumoto, K., Mukai, S., Honsho, M. and Tamura, S.** (2014). Peroxisome biogenesis in mammalian cells. *Frontiers in physiology*. **5**, p307.

**Fukamatsu, Y., Yabe, N. and Hasunuma, K.** (2003). *Arabidopsis* NDK1 is a component of ROS signaling by interacting with three catalases. *Plant and Cell Physiology*. **44**(10), pp.982-989.

**Gabay-Maskit, S., Cruz-Zaragoza, L.D., Shai, N., Eisenstein, M., Bibi, C., Cohen, N., Hansen, T., Yifrach, E., Harpaz, N. and Belostotsky, R.** (2020). A piggybacking mechanism enables peroxisomal localization of the glyoxylate cycle enzyme Mdh2 in yeast. *Journal of cell science*. **133**(24).

**Gao, X., YUAN, H.M., HU, Y.Q., Li, J. and LU, Y.T.** (2014). Mutation of *Arabidopsis* CATALASE2 results in hyponastic leaves by changes of auxin levels. *Plant, cell & environment*. **37**(1), pp.175-188.

**García-Quirós, E., Alché, J.d.D., Karpinska, B. and Foyer, C.H.** (2020). Glutathione redox state plays a key role in flower development and pollen vigour. *Journal of Experimental Botany*. **71**(2), pp.730-741.

**Gatto, G.J., Geisbrecht, B.V., Gould, S.J. and Berg, J.M.** (2002). Peroxisomal targeting signal-1 recognition by the TPR domains of human PEX5. *Nature Structural & Molecular Biology*. **9**(10), pp.788-788.

**Gatto, G.J., Maynard, E.L., Guerrerio, A.L., Geisbrecht, B.V., Gould, S.J. and Berg, J.M.** (2003). Correlating structure and affinity for PEX5: PTS1 complexes. *Biochemistry*. **42**(6), pp.1660-1666.

**Ghosh, D. and Berg, J.M.** (2010). A proteome-wide perspective on peroxisome targeting signal 1 (PTS1)-Pex5p affinities. *Journal of the American Chemical Society*. **132**(11), pp.3973-3979.

**Gigolashvili, T. and Kopriva, S.** (2014). Transporters in plant sulfur metabolism. *Frontiers in Plant Science*. **5**, p442.

**Gill, S.S. and Tuteja, N.** (2010). Reactive oxygen species and antioxidant machinery in abiotic stress tolerance in crop plants. *Plant Physiology and Biochemistry*. **48**(12), pp.909-930.

**Girzalsky, W., Saffian, D. and Erdmann, R.** (2010). Peroxisomal protein translocation. *Biochimica et Biophysica Acta (BBA)-Molecular Cell Research*. **1803**(6), pp.724-731.

**Glorieux, C. and Calderon, P.B.** (2017). Catalase, a remarkable enzyme: targeting the oldest antioxidant enzyme to find a new cancer treatment approach. *Biological chemistry*. **398**(10), pp.1095-1108.

**Glover, J.R., Andrews, D.W. and Rachubinski, R.A.** (1994). *Saccharomyces cerevisiae* peroxisomal thiolase is imported as a dimer. *Proceedings of the National Academy of Sciences*. **91**(22), pp.10541-10545.

**Goepfert, S., Vidoudez, C., Rezzonico, E., Hiltunen, J.K. and Poirier, Y.** (2005). Molecular identification and characterization of the Arabidopsis  $\Delta 3$ ,  $\Delta 5$ ,  $\Delta 2$ , 4-dienoyl-coenzyme A isomerase, a peroxisomal enzyme participating in the  $\beta$ -oxidation cycle of unsaturated fatty acids. *Plant physiology*. **138**(4), pp.1947-1956.

**Goldberg, I. and Hochman, A.** (1989). Three different types of catalases in *Klebsiella pneumoniae*. *Archives of biochemistry and biophysics*. **268**(1), pp.124-128.

**Goldman, B.M. and Blobel, G.** (1978). Biogenesis of peroxisomes: intracellular site of synthesis of catalase and uricase. *Proceedings of the National Academy of Sciences*. **75**(10), pp.5066-5070.

**Gómez, L.D., Vanacker, H., Buchner, P., Noctor, G. and Foyer, C.H.** (2004). Intercellular distribution of glutathione synthesis in maize leaves and its response to short-term chilling. *Plant Physiology*. **134**(4), pp.1662-1671.

**González, E.** (1991). The C-terminal domain of plant catalases Implications for a glyoxysomal targeting sequence. *European journal of biochemistry*. **199**(1), pp.211-215.

**Goto, S., Mano, S., Nakamori, C. and Nishimura, M.** (2011). Arabidopsis ABERRANT PEROXISOME MORPHOLOGY9 is a peroxin that recruits the PEX1-PEX6 complex to peroxisomes. *The Plant Cell*. **23**(4), pp.1573-1587.

**Gould, S.J., Keller, G.A., Hosken, N., Wilkinson, J. and Subramani, S.** (1989). A conserved tripeptide sorts proteins to peroxisomes. *The Journal of cell biology*. **108**(5), pp.1657-1664.

**Goyal, M.M. and Basak, A.** (2010). Human catalase: looking for complete identity. *Protein & cell*. **1**(10), pp.888-897.

**Graham, I.A.** (2008). Seed storage oil mobilization. *Annu. Rev. Plant Biol.* **59**, pp.115-142.

**Grill, E., Löffler, S., Winnacker, E.-L. and Zenk, M.H.** (1989). Phytochelatins, the heavy-metal-binding peptides of plants, are synthesized from glutathione by a specific  $\gamma$ -glutamylcysteine dipeptidyl transpeptidase (phytochelatin synthase). *Proceedings of the National Academy of Sciences*. **86**(18), pp.6838-6842.

**Grou, C.P., Pinto, M.P., Mendes, A.V., Domingues, P. and Azevedo, J.E.** (2015). The de novo synthesis of ubiquitin: identification of deubiquitinases acting on ubiquitin precursors. *Scientific reports*. **5**, p12836.

**Guan, L. and Scandalios, J.G.** (1995). Developmentally related responses of maize catalase genes to salicylic acid. *Proceedings of the National Academy of Sciences*. **92**(13), pp.5930-5934.

**Guan, L. and Scandalios, J.G.** (1996). Molecular evolution of maize catalases and their relationship to other eukaryotic and prokaryotic catalases. *Journal of molecular evolution*. **42**(5), pp.570-579.

**Gupta, A.S., Alscher, R.G. and McCune, D.** (1991). Response of photosynthesis and cellular antioxidants to ozone in Populus leaves. *Plant Physiology*. **96**(2), pp.650-655.

**Hackenberg, T., Juul, T., Auzina, A., Gwiżdż, S., Małolepszy, A., Van Der Kelen, K., Dam, S., Bressendorff, S., Lorentzen, A. and Roepstorff, P.** (2013). Catalase and NO CATALASE ACTIVITY1 promote autophagy-dependent cell death in Arabidopsis. *The Plant Cell*. **25**(11), pp.4616-4626.

**Hajra, A.K. and Wu, D.** (1985). Preparative isolation of peroxisomes from liver and kidney using metrizamide density gradient centrifugation in a vertical rotor. *Analytical biochemistry*. **148**(1), pp.233-244.

**Halliwell, B.** (2006). Reactive species and antioxidants. Redox biology is a fundamental theme of aerobic life. *Plant physiology*. **141**(2), pp.312-322.

**Halliwell, B. and Foyer, C.** (1978). Properties and physiological function of a glutathione reductase purified from spinach leaves by affinity chromatography. *Planta*. **139**(1), pp.9-17.

**Hasanuzzaman, M., Nahar, K., Anee, T.I. and Fujita, M.** (2017). Glutathione in plants: biosynthesis and physiological role in environmental stress tolerance. *Physiology and Molecular Biology of Plants*. **23**(2), pp.249-268.

**Hawkins, J., Mahony, D., Maetschke, S., Wakabayashi, M., Teasdale, R.D. and Bodén, M.** (2007). Identifying novel peroxisomal proteins. *Proteins: Structure, Function, and Bioinformatics*. **69**(3), pp.606-616.

**Hayashi, M., Aoki, M., Kondo, M. and Nishimura, M.** (1997). Changes in targeting efficiencies of proteins to plant microbodies caused by amino acid substitutions in the carboxy-terminal tripeptide. *Plant and cell physiology*. **38**(6), pp.759-768.

**Hayashi, M. and Nishimura, M.** (2006). Arabidopsis thaliana—a model organism to study plant peroxisomes. *Biochimica et Biophysica Acta (BBA)-Molecular Cell Research*. **1763**(12), pp.1382-1391.

**Hayashi, M., Nito, K., Takei-Hoshi, R., Yagi, M., Kondo, M., Suenaga, A., Yamaya, T. and Nishimura, M.** (2002). Ped3p is a peroxisomal ATP-binding cassette transporter that might supply substrates for fatty acid  $\beta$ -oxidation. *Plant and Cell Physiology*. **43**(1), pp.1-11.

**Hayashi, M., Toriyama, K., Kondo, M. and Nishimura, M.** (1998). 2, 4-Dichlorophenoxybutyric acid-resistant mutants of Arabidopsis have defects in glyoxysomal fatty acid  $\beta$ -oxidation. *The Plant Cell*. **10**(2), pp.183-195.

**Heiland, I. and Erdmann, R.** (2005). Biogenesis of peroxisomes: topogenesis of the peroxisomal membrane and matrix proteins. *The FEBS journal*. **272**(10), pp.2362-2372.

**Heim, R. and Tsien, R.Y.** (1996). Engineering green fluorescent protein for improved brightness, longer wavelengths and fluorescence resonance energy transfer. *Current biology*. **6**(2), pp.178-182.

**Helm, M., Lück, C., Prestele, J., Hierl, G., Huesgen, P.F., Fröhlich, T., Arnold, G.J., Adamska, I., Görg, A. and Lottspeich, F.** (2007). Dual specificities of the glyoxysomal/peroxisomal processing protease Deg15 in higher plants. *Proceedings of the National Academy of Sciences*. **104**(27), pp.11501-11506.

**Herschbach, C. and Rennenberg, H.** (1994). Influence of glutathione (GSH) on net uptake of sulphate and sulphate transport in tobacco plants. *Journal of Experimental Botany*. **45**(8), pp.1069-1076.

**Hieta, R. and Myllyharju, J.** (2002). Cloning and characterization of a low molecular weight prolyl 4-hydroxylase from *Arabidopsis thaliana* effective hydroxylation of proline-rich, collagen-like, and hypoxia-inducible transcription factor  $\alpha$ -like peptides. *Journal of Biological Chemistry*. **277**(26), pp.23965-23971.

**Ho, Y.S., Xiong, Y., Ma, W., Spector, A. and Ho, D.S.** (2004). Mice lacking catalase develop normally but show differential sensitivity to oxidant tissue injury. *Journal of Biological Chemistry*. **279**(31), pp.32804-32812.

**Holroyd, C. and Erdmann, R.** (2001). Protein translocation machineries of peroxisomes. *FEBS letters*. **501**(1), pp.6-10.

**Horemans, N., Foyer, C.H. and Asard, H.** (2000). Transport and action of ascorbate at the plant plasma membrane. *Trends in plant science*. **5**(6), pp.263-267.

**Horiguchi, H., Yurimoto, H., Goh, T.K., Nakagawa, T., Kato, N. and Sakai, Y.** (2001). Peroxisomal catalase in the methylotrophic yeast *Candida boidinii*: transport efficiency and metabolic significance. *Journal of bacteriology*. **183**(21), pp.6372-6383.

**Houben, M. and Van de Poel, B.** (2019). 1-Aminocyclopropane-1-carboxylic acid oxidase (ACO): the enzyme that makes the plant hormone ethylene. *Frontiers in plant science*. **10**, p695.

**Hu, J., Baker, A., Bartel, B., Linka, N., Mullen, R.T., Reumann, S. and Zolman, B.K.** (2012). Plant peroxisomes: biogenesis and function. *The Plant Cell*. **24**(6), pp.2279-2303.

**Hu, L., Yang, Y., Jiang, L. and Liu, S.** (2016). The catalase gene family in cucumber: genome-wide identification and organization. *Genetics and molecular biology*. **39**(3), pp.408-415.

**Hu, Y.Q., Liu, S., YUAN, H.M., Li, J., YAN, D.W., ZHANG, J.F. and LU, Y.T.** (2010). Functional comparison of catalase genes in the elimination of photorespiratory H<sub>2</sub>O<sub>2</sub> using promoter-and 3'-untranslated region exchange experiments in the Arabidopsis cat2 photorespiratory mutant. *Plant, cell & environment*. **33**(10), pp.1656-1670.

**Hua, R., Gidda, S.K., Aranovich, A., Mullen, R.T. and Kim, P.K.** (2015). Multiple domains in PEX16 mediate its trafficking and recruitment of peroxisomal proteins to the ER. *Traffic*. **16**(8), pp.832-852.

**Hutton, D. and Stumpf, P.** (1969). Fat metabolism in higher plants. XXXVII. Characterization of the  $\beta$ -oxidation systems from maturing and germinating castor bean seeds. *Plant Physiology*. **44**(4), pp.508-516.

**Inaba, J.i., Kim, B.M., Shimura, H. and Masuta, C.** (2011). Virus-induced necrosis is a consequence of direct protein-protein interaction between a viral RNA-silencing suppressor and a host catalase. *Plant Physiology*. **156**(4), pp.2026-2036.

**Islinger, M., Li, K.W., Seitz, J., Völkl, A. and Lüers, G.H.** (2009). Hitchhiking of Cu/Zn superoxide dismutase to peroxisomes—evidence for a natural piggyback import mechanism in mammals. *Traffic*. **10**(11), pp.1711-1721.

**Jamet, A., Sigaud, S., Van de Sype, G., Puppo, A. and Hérouart, D.** (2003). Expression of the bacterial catalase genes during Sinorhizobium meliloti-Medicago sativa symbiosis and their crucial role during the infection process. *Molecular plant-microbe interactions*. **16**(3), pp.217-225.

**Janošík, M., Oliveriusová, J., Janošíková, B., Sokolová, J., Kraus, E., Kraus, J.P. and Kožich, V.** (2001). Impaired heme binding and aggregation of mutant cystathionine  $\beta$ -synthase subunits in homocystinuria. *The American Journal of Human Genetics*. **68**(6), pp.1506-1513.

**Jansen, R.L., Molina, C.S., van den Noort, M., Devos, D.P. and van der Klei, I.J.** (2020). Comparative genomics of peroxisome biogenesis proteins: making sense of the PEX mess. *bioRxiv*.

**Jiménez, A., Hernández, J.A., Pastori, G., del Río, L.A. and Sevilla, F.** (1998). Role of the ascorbate-glutathione cycle of mitochondria and peroxisomes in the senescence of pea leaves. *Plant physiology*. **118**(4), pp.1327-1335.

**Jones, J.M., Morrell, J.C. and Gould, S.J.** (2004). PEX19 is a predominantly cytosolic chaperone and import receptor for class 1 peroxisomal membrane proteins. *Journal of Cell Biology*. **164**(1), pp.57-67.

**Joo, J., Lee, Y.H. and Song, S.I.** (2014). Rice CatA, CatB, and CatC are involved in environmental stress response, root growth, and photorespiration, respectively. *Journal of Plant Biology*. **57**(6), pp.375-382.

**Jung, S., Marelli, M., Rachubinski, R.A., Goodlett, D.R. and Aitchison, J.D.** (2010). Dynamic changes in the subcellular distribution of Gpd1p in response to cell stress. *Journal of Biological Chemistry*. **285**(9), pp.6739-6749.

**Kamada, T., Nito, K., Hayashi, H., Mano, S., Hayashi, M. and Nishimura, M.** (2003). Functional differentiation of peroxisomes revealed by expression profiles of peroxisomal genes in *Arabidopsis thaliana*. *Plant and Cell Physiology*. **44**(12), pp.1275-1289.

**Kamigaki, A., Mano, S., Terauchi, K., Nishi, Y., Tachibe-Kinoshita, Y., Nito, K., Kondo, M., Hayashi, M., Nishimura, M. and Esaka, M.** (2003). Identification of peroxisomal targeting signal of pumpkin catalase and the binding analysis with PTS1 receptor. *The Plant Journal*. **33**(1), pp.161-175.

**Kamiyama, D., Sekine, S., Barsi-Rhyne, B., Hu, J., Chen, B., Gilbert, L.A., Ishikawa, H., Leonetti, M.D., Marshall, W.F. and Weissman, J.S.** (2016). Versatile protein tagging in cells with split fluorescent protein. *Nature communications*. **7**(1), pp.1-9.

**Kao, Y.-T., Gonzalez, K.L. and Bartel, B.** (2018). Peroxisome function, biogenesis, and dynamics in plants. *Plant Physiology*. **176**(1), pp.162-177.

**Karakus, Y.Y.** (2020). Typical Catalases: Function and Structure. *Glutathione Peroxidase in Health and Disease*. IntechOpen.

**Kärkönen, A. and Kuchitsu, K.** (2015). Reactive oxygen species in cell wall metabolism and development in plants. *Phytochemistry*. **112**, pp.22-32.

**Kataya, A.R., Heidari, B., Hagen, L., Kommedal, R., Slupphaug, G. and Lillo, C.** (2015). Protein phosphatase 2A holoenzyme is targeted to peroxisomes by piggybacking and positively affects peroxisomal  $\beta$ -oxidation. *Plant physiology*. **167**(2), pp.493-506.

**Kato, A., Hayashi, M., Kondo, M. and Nishimura, M.** (1996). Targeting and processing of a chimeric protein with the N-terminal presequence of the precursor to glyoxysomal citrate synthase. *The Plant Cell*. **8**(9), pp.1601-1611.

**Kato, S., Ueno, T., Fukuzumi, S. and Watanabe, Y.** (2004). Catalase Reaction by Myoglobin Mutants and Native Catalase mechanistics investigation by kinetic isotope effect. *Journal of Biological Chemistry*. **279**(50), pp.52376-52381.

**Kaur, N., Reumann, S. and Hu, J.** (2009). Peroxisome biogenesis and function. *The Arabidopsis book/American Society of Plant Biologists*. **7**.

**Kelley, L.A., Mezulis, S., Yates, C.M., Wass, M.N. and Sternberg, M.J.** (2015). The Phyre2 web portal for protein modeling, prediction and analysis. *Nature protocols*. **10**(6), pp.845-858.

**Kempiński, B., Chełstowska, A., Poznański, J., Król, K., Rymer, Ł., Frydzińska, Z., Girzalsky, W., Skoneczna, A., Erdmann, R. and Skoneczny, M.** (2020). The Peroxisomal Targeting Signal 3 (PTS3) of the Budding Yeast Acyl-CoA Oxidase Is a Signal Patch. *Frontiers in Cell and Developmental Biology*. **8**, p198.

**Kendall, A.C., Keys, A.J., Turner, J.C., Lea, P.J. and Mifflin, B.J.** (1983). The isolation and characterisation of a catalase-deficient mutant of barley (*Hordeum vulgare* L.). *Planta*. **159**(6), pp.505-511.

**Kerchev, P., Mühlenbock, P., Denecker, J., Morreel, K., Hoeberichts, F.A., Van Der Kelen, K., Vandorpe, M., Nguyen, L., Audenaert, D. and Van Breusegem, F.** (2015). Activation of auxin signalling counteracts photorespiratory H<sub>2</sub>O<sub>2</sub>-dependent cell death. *Plant, cell & environment*. **38**(2), pp.253-265.

**Kim, J., Lee, H., Lee, H.N., Kim, S.-H., Shin, K.D. and Chung, T.** (2013). Autophagy-related proteins are required for degradation of peroxisomes in *Arabidopsis* hypocotyls during seedling growth. *The Plant Cell*. **25**(12), pp.4956-4966.

**Kim, P. and Hettema, E.** (2015). Multiple pathways for protein transport to peroxisomes. *Journal of molecular biology*. **427**(6), pp.1176-1190.

**Kirkman, H.N., Rolfo, M., Ferraris, A.M. and Gaetani, G.F.** (1999). Mechanisms of protection of catalase by NADPH Kinetics and stoichiometry. *Journal of Biological Chemistry*. **274**(20), pp.13908-13914.

**Kivirikko, K.I. and Pihlajaniemi, T.** (1998). Collagen hydroxylases and the protein disulfide isomerase subunit of prolyl 4-hydroxylases. *Advances in enzymology and related areas of molecular biology*. **72**, pp.325-398.

**Klapheck, S.** (1988). Homogluthathione: isolation, quantification and occurrence in legumes. *Physiologia Plantarum*. **74**(4), pp.727-732.

**Klapheck, S., Chrost, B., Starke, J. and Zimmermann, H.** (1992).  $\gamma$ -Glutamylcysteinylserine—a new homologue of glutathione in plants of the family Poaceae. *Botanica Acta*. **105**(3), pp.174-179.

**Klotz, M.G., Klassen, G.R. and Loewen, P.C.** (1997). Phylogenetic relationships among prokaryotic and eukaryotic catalases. *Molecular Biology and Evolution*. **14**(9), pp.951-958.

**Koepke, J.I., Nakrieko, K.A., Wood, C.S., Boucher, K.K., Terlecky, L.J., Walton, P.A. and Terlecky, S.R.** (2007). Restoration of peroxisomal catalase import in a model of human cellular aging. *Traffic*. **8**(11), pp.1590-1600.

**Koller, A., Snyder, W.B., Faber, K.N., Wenzel, T.J., Rangell, L., Keller, G.A. and Subramani, S.** (1999). Pex22p of *Pichia pastoris*, essential for peroxisomal matrix protein import, anchors the ubiquitin-conjugating enzyme, Pex4p, on the peroxisomal membrane. *The Journal of cell biology*. **146**(1), pp.99-112.

**Koller, A., Spong, A., Lüers, G. and Subramani, S.** (1999). Analysis of the peroxisomal acyl-CoA oxidase gene product from *Pichia pastoris* and determination of its targeting signal. *Yeast*. **15**(11), pp.1035-1044.

**Kragler, F., Langeder, A., Raupachova, J., Binder, M. and Hartig, A.** (1993). Two independent peroxisomal targeting signals in catalase A of *Saccharomyces cerevisiae*. *The Journal of Cell Biology*. **120**(3), pp.665-673.

**Kunze, M., Kragler, F., Binder, M., Hartig, A. and Gurvitz, A.** (2002). Targeting of malate synthase 1 to the peroxisomes of *Saccharomyces cerevisiae* cells depends on growth on oleic acid medium. *European journal of biochemistry*. **269**(3), pp.915-922.

**Kurochkin, I.V., Mizuno, Y., Konagaya, A., Sakaki, Y., Schönbach, C. and Okazaki, Y.** (2007). Novel peroxisomal protease Tysnd1 processes PTS1- and PTS2-containing enzymes involved in  $\beta$ -oxidation of fatty acids. *The EMBO Journal*. **26**(3), pp.835-845.

**Lametschwandtner, G., Brocard, C., Fransen, M., Van Veldhoven, P., Berger, J. and Hartig, A.** (1998). The difference in recognition of terminal tripeptides as peroxisomal targeting signal 1 between yeast and human is due to different affinities of their receptor Pex5p to the cognate signal and to residues adjacent to it. *Journal of Biological Chemistry*. **273**(50), pp.33635-33643.

**Lamoureux, G.L. and Rusness, D.G.** (1993). Glutathione in the metabolism and detoxification of xenobiotics in plants. *Sulfur Nutrition and Assimilation in Higher Plants. The Hague, The Netherlands: SPB Academic Publishing.* pp.221-237.

**Lappartient, A.G. and Touraine, B.** (1996). Demand-driven control of root ATP sulfurylase activity and SO<sub>4</sub><sup>2-</sup>-uptake in intact canola (the role of phloem-translocated glutathione). *Plant Physiology.* **111**(1), pp.147-157.

**Lazarow, P.B.** (2003). Peroxisome biogenesis: advances and conundrums. *Current opinion in cell biology.* **15**(4), pp.489-497.

**Lazarow, P.B. and De Duve, C.** (1973). The synthesis and turnover of rat liver peroxisomes. *The Journal of cell biology.* **59**(2), pp.507-524.

**Lazarow, P.B. and Fujiki, Y.** (1985). Biogenesis of peroxisomes. *Annual review of cell biology.* **1**(1), pp.489-530.

**Lee, J.R., Jang, H.H., Park, J.H., Jung, J.H., Lee, S.S., Park, S.K., Chi, Y.H., Moon, J.C., Lee, Y.M. and Kim, S.Y.** (2006). Cloning of two splice variants of the rice PTS1 receptor, OsPex5pL and OsPex5pS, and their functional characterization using pex5-deficient yeast and Arabidopsis. *The Plant Journal.* **47**(3), pp.457-466.

**Lee, M.S., Mullen, R.T. and Trelease, R.N.** (1997). Oilseed isocitrate lyases lacking their essential type 1 peroxisomal targeting signal are piggybacked to glyoxysomes. *The Plant Cell.* **9**(2), pp.185-197.

**Leonetti, M.D., Sekine, S., Kamiyama, D., Weissman, J.S. and Huang, B.** (2016). A scalable strategy for high-throughput GFP tagging of endogenous human proteins. *Proceedings of the National Academy of Sciences.* **113**(25), pp.E3501-E3508.

**Li, F. and Vierstra, R.D.** (2012). Autophagy: a multifaceted intracellular system for bulk and selective recycling. *Trends in plant science.* **17**(9), pp.526-537.

**Li, G., Li, J., Hao, R. and Guo, Y.** (2017). Activation of catalase activity by a peroxisome-localized small heat shock protein Hsp17. 6CII. *Journal of Genetics and Genomics.* **44**(8), pp.395-404.

**Li, J., Liu, J., Wang, G., Cha, J.-Y., Li, G., Chen, S., Li, Z., Guo, J., Zhang, C. and Yang, Y.** (2015). A chaperone function of NO CATALASE ACTIVITY1 is required to maintain catalase activity and for multiple stress responses in Arabidopsis. *The Plant Cell*. **27**(3), pp.908-925.

**Li, X., Yang, Q., Tu, H., Lim, Z. and Pan, S.Q.** (2014). Direct visualization of A grobacterium-delivered V ir E 2 in recipient cells. *The Plant Journal*. **77**(3), pp.487-495.

**Li, Y., Chen, L., Mu, J. and Zuo, J.** (2013). LESION SIMULATING DISEASE1 interacts with catalases to regulate hypersensitive cell death in Arabidopsis. *Plant physiology*. **163**(2), pp.1059-1070.

**Lingner, T., Kataya, A.R., Antonicelli, G.E., Benichou, A., Nilssen, K., Chen, X.-Y., Siemsen, T., Morgenstern, B., Meinicke, P. and Reumann, S.** (2011). Identification of novel plant peroxisomal targeting signals by a combination of machine learning methods and in vivo subcellular targeting analyses. *The Plant Cell*. **23**(4), pp.1556-1572.

**Liu, S., Yu, F., Yang, Z., Wang, T., Xiong, H., Chang, C., Yu, W. and Li, N.** (2018). Establishment of dimethyl labeling-based quantitative Acetylproteomics in Arabidopsis. *Molecular & Cellular Proteomics*. **17**(5), pp.1010-1027.

**Liu, W.C., Han, T.T., Yuan, H.M., Yu, Z.D., Zhang, L.Y., Zhang, B.L., Zhai, S., Zheng, S.Q. and Lu, Y.T.** (2017). CATALASE2 functions for seedling postgerminative growth by scavenging H<sub>2</sub>O<sub>2</sub> and stimulating ACX2/3 activity in Arabidopsis. *Plant, cell & environment*. **40**(11), pp.2720-2728.

**Loew, O.** (1900). A new enzyme of general occurrence in organisms. *Science*. **11**, pp.701-702.

**Lousa, C.D.M., van Roermund, C.W., Postis, V.L., Dietrich, D., Kerr, I.D., Wanders, R.J., Baldwin, S.A., Baker, A. and Theodoulou, F.L.** (2013). Intrinsic acyl-CoA thioesterase activity of a peroxisomal ATP binding cassette transporter is required for transport and metabolism of fatty acids. *Proceedings of the National Academy of Sciences*. **110**(4), pp.1279-1284.

**Madrid, K.P., De Crescenzo, G., Wang, S. and Jardim, A.** (2004). Modulation of the Leishmania donovani peroxin 5 quaternary structure by peroxisomal targeting signal 1 ligands. *Molecular and cellular biology*. **24**(17), pp.7331-7344.

**Marquez, Y., Brown, J.W., Simpson, C., Barta, A. and Kalyna, M.** (2012). Transcriptome survey reveals increased complexity of the alternative splicing landscape in Arabidopsis. *Genome research*. **22**(6), pp.1184-1195.

**Marrs, K.A.** (1996). The functions and regulation of glutathione S-transferases in plants. *Annual review of plant biology*. **47**(1), pp.127-158.

**Marshall, R.S. and Vierstra, R.D.** (2018). Autophagy: the master of bulk and selective recycling. *Annual Review of Plant Biology*. **69**, pp.173-208.

**Mathioudakis, M.M., Veiga, R.S., Canto, T., Medina, V., Mossialos, D., Makris, A.M. and Livieratos, I.** (2013). P epino mosaic virus triple gene block protein 1 (TGBp1) interacts with and increases tomato catalase 1 activity to enhance virus accumulation. *Molecular Plant Pathology*. **14**(6), pp.589-601.

**May, M.J., Hammond-Kosack, K.E. and Jones, J.D.** (1996). Involvement of reactive oxygen species, glutathione metabolism, and lipid peroxidation in the Cf-gene-dependent defense response of tomato cotyledons induced by race-specific elicitors of *Cladosporium fulvum*. *Plant Physiology*. **110**(4), pp.1367-1379.

**Maynard, E.L., Gatto Jr, G.J. and Berg, J.M.** (2004). Pex5p binding affinities for canonical and noncanonical PTS1 peptides. *Proteins: Structure, Function, and Bioinformatics*. **55**(4), pp.856-861.

**McClung, C.R.** (1997). Regulation of catalases in Arabidopsis. *Free Radical Biology and Medicine*. **23**(3), pp.489-496.

**McNew, J.A. and Goodman, J.M.** (1994). An oligomeric protein is imported into peroxisomes in vivo. *The Journal of cell biology*. **127**(5), pp.1245-1257.

**Mehlhorn, H., Lelandais, M., Korth, H. and Foyer, C.** (1996). Ascorbate is the natural substrate for plant peroxidases. *FEBS letters*. **378**(3), pp.203-206.

**Meinecke, M., Cizmowski, C., Schliebs, W., Krüger, V., Beck, S., Wagner, R. and Erdmann, R.** (2010). The peroxisomal importomer constitutes a large and highly dynamic pore. *Nature Cell Biology*. **12**(3), p273.

**Meister, A.** (1988). Glutathione metabolism and its selective modification. *Journal of biological chemistry*. **263**(33), pp.17205-17208.

**Melik-Adamyán, W.R., Barynin, V.V., Vagin, A.A., Borisov, V.V., Vainshtein, B.K., Fita, I., Murthy, M.R. and Rossmann, M.G.** (1986). Comparison of beef liver and *Penicillium vitale* catalases. *Journal of molecular biology*. **188**(1), pp.63-72.

**Meuwly, P., Thibault, P. and Rauser, W.E.** (1993).  $\gamma$ -Glutamylcysteinylglutamic acid—a new homologue of glutathione in maize seedlings exposed to cadmium. *FEBS letters*. **336**(3), pp.472-476.

**Mhamdi, A., Hager, J., Chaouch, S., Queval, G., Han, Y., Taconnat, L., Saindrenan, P., Gouia, H., Issakidis-Bourguet, E. and Renou, J.P.** (2010a). Arabidopsis GLUTATHIONE REDUCTASE1 plays a crucial role in leaf responses to intracellular hydrogen peroxide and in ensuring appropriate gene expression through both salicylic acid and jasmonic acid signaling pathways. *Plant physiology*. **153**(3), pp.1144-1160.

**Mhamdi, A., Noctor, G. and Baker, A.** (2012). Plant catalases: peroxisomal redox guardians. *Archives of Biochemistry and Biophysics*. **525**(2), pp.181-194.

**Mhamdi, A., Queval, G., Chaouch, S., Vanderauwera, S., Van Breusegem, F. and Noctor, G.** (2010b). Catalase function in plants: a focus on Arabidopsis mutants as stress-mimic models. *Journal of Experimental Botany*. **61**(15), pp.4197-4220.

**Michels, P.A.** (1988). Compartmentation of glycolysis in trypanosomes: a potential target for new trypanocidal drugs. *Biology of the Cell*. **64**(2), pp.157-164.

**Mignolet-Spruyt, L., Xu, E., Idänheimo, N., Hoerberichts, F.A., Mühlenbock, P., Brosché, M., Van Breusegem, F. and Kangasjärvi, J.** (2016). Spreading the news: subcellular and organellar reactive oxygen species production and signalling. *Journal of experimental botany*. **67**(13), pp.3831-3844.

**Milla, M.A.R., Maurer, A., Huete, A.R. and Gustafson, J.P.** (2003). Glutathione peroxidase genes in Arabidopsis are ubiquitous and regulated by abiotic stresses through diverse signaling pathways. *The Plant Journal*. **36**(5), pp.602-615.

**Mittler, R.** (2017). ROS are good. *Trends in plant science*. **22**(1), pp.11-19.

**Mittler, R. and Zilinskas, B.** (1992). Molecular cloning and characterization of a gene encoding pea cytosolic ascorbate peroxidase. *Journal of Biological Chemistry*. **267**(30), pp.21802-21807.

**Moscicka, K.B., Klompaker, S.H., Wang, D., van der Klei, I.J. and Boekema, E.J.** (2007). The Hansenula polymorpha peroxisomal targeting signal 1 receptor, Pex5p, functions as a tetramer. *FEBS letters*. **581**(9), pp.1758-1762.

**Mou, Z., Fan, W. and Dong, X.** (2003). Inducers of plant systemic acquired resistance regulate NPR1 function through redox changes. *Cell*. **113**(7), pp.935-944.

**Mullen, R.T., Lee, M.S. and Trelease, R.N.** (1997). Identification of the peroxisomal targeting signal for cottonseed catalase. *The Plant Journal*. **12**(2), pp.313-322.

**Mullen, R.T. and Trelease, R.N.** (2006). The ER-peroxisome connection in plants: development of the "ER semi-autonomous peroxisome maturation and replication" model for plant peroxisome biogenesis. *Biochimica et Biophysica Acta (BBA)-Molecular Cell Research*. **1763**(12), pp.1655-1668.

**Mulvey, M.R., Switala, J., Borys, A. and Loewen, P.C.** (1990). Regulation of transcription of katE and katF in Escherichia coli. *Journal of Bacteriology*. **172**(12), pp.6713-6720.

**Nagahashi, G. and Baker, A.F.** (1984).  $\beta$ -Glucosidase activity in corn roots: Problems in subcellular fractionation. *Plant physiology*. **76**(4), pp.861-864.

**Nagai, T., Ibata, K., Park, E.S., Kubota, M., Mikoshiba, K. and Miyawaki, A.** (2002). A variant of yellow fluorescent protein with fast and efficient maturation for cell-biological applications. *Nature biotechnology*. **20**(1), pp.87-90.

**Nakano, Y. and Asada, K.** (1987). Purification of ascorbate peroxidase in spinach chloroplasts; its inactivation in ascorbate-depleted medium and reactivation by monodehydroascorbate radical. *Plant and cell physiology*. **28**(1), pp.131-140.

**Nicholls, P.** (2012). Classical catalase: ancient and modern. *Archives of biochemistry and biophysics*. **525**(2), pp.95-101.

**Nicholls, P., Fita, I. and Loewen, P.C.** (2000). Enzymology and structure of catalases. *Advances in Inorganic Chemistry*. **51**, pp.51-106.

**Nito, K., Hayashi, M. and Nishimura, M.** (2002). Direct interaction and determination of binding domains among peroxisomal import factors in Arabidopsis thaliana. *Plant and Cell Physiology*. **43**(4), pp.355-366.

**Noctor, G. and Foyer, C.H.** (1998). Ascorbate and glutathione: keeping active oxygen under control. *Annual review of plant biology*. **49**(1), pp.249-279.

**Noctor, G. and Foyer, C.H.** (2016). Intracellular redox compartmentation and ROS-related communication in regulation and signaling. *Plant physiology*. **171**(3), pp.1581-1592.

**Noctor, G., Gomez, L., Vanacker, H. and Foyer, C.H.** (2002a). Interactions between biosynthesis, compartmentation and transport in the control of glutathione homeostasis and signalling. *Journal of experimental botany*. **53**(372), pp.1283-1304.

**Noctor, G., Lelarge-Trouverie, C. and Mhamdi, A.** (2015). The metabolomics of oxidative stress. *Phytochemistry*. **112**, pp.33-53.

**Noctor, G., Mhamdi, A., Chaouch, S., Han, Y., Neukermans, J., MARQUEZ-GARCIA, B., Queval, G. and Foyer, C.H.** (2012). Glutathione in plants: an integrated overview. *Plant, Cell & Environment*. **35**(2), pp.454-484.

**Noctor, G., Mhamdi, A. and Foyer, C.H.** (2016). Oxidative stress and antioxidative systems: recipes for successful data collection and interpretation. *Plant, cell & environment*. **39**(5), pp.1140-1160.

**Noctor, G., Queval, G., Mhamdi, A., Chaouch, S. and Foyer, C.H.** (2011). Glutathione. *The arabidopsis book*. **9**(1), pp.1-32.

**Noctor, G., Reichheld, J.P. and Foyer, C.H.** 2017. ROS-related redox regulation and signaling in plants. In: *Seminars in Cell & Developmental Biology*: Elsevier.

**Noctor, G., Veljovic-Jovanovic, S., Driscoll, S., Novitskaya, L. and Foyer, C.H.** (2002b). Drought and oxidative load in the leaves of C3 plants: a predominant role for photorespiration? *Annals of Botany*. **89**(7), pp.841-850.

**Nötzel, C., Lingner, T., Klingenberg, H. and Thoms, S.** (2016). Identification of new fungal peroxisomal matrix proteins and revision of the PTS1 consensus. *Traffic*. **17**(10), pp.1110-1124.

**Novikoff, A.B. and Goldfischer, S.** (1969). Visualization of peroxisomes (microbodies) and mitochondria with diaminobenzidine. *Journal of Histochemistry & Cytochemistry*. **17**(10), pp.675-680.

**Nyathi, Y. and Baker, A.** (2006). Plant peroxisomes as a source of signalling molecules. *Biochimica et Biophysica Acta (BBA)-Molecular Cell Research*. **1763**(12), pp.1478-1495.

**Okumoto, K., El Shermely, M., Natsui, M., Kosako, H., Natsuyama, R., Marutani, T. and Fujiki, Y.** (2020). The peroxisome counteracts oxidative stresses by suppressing catalase import via Pex14 phosphorylation. *Elife*. **9**, pe55896.

**Opperdoes, F.R., Baudhuin, P., Coppens, I., De Roe, C., Edwards, S.W., Weijers, P.J. and Misset, O.** (1984). Purification, morphometric analysis, and characterization of the glycosomes (microbodies) of the protozoan hemoflagellate *Trypanosoma brucei*. *The Journal of cell biology*. **98**(4), pp.1178-1184.

**Orendi, G., Zimmermann, P., Baar, C. and Zentgraf, U.** (2001). Loss of stress-induced expression of catalase3 during leaf senescence in *Arabidopsis thaliana* is restricted to oxidative stress. *Plant Science*. **161**(2), pp.301-314.

**Oshima, Y., Kamigaki, A., Nakamori, C., Mano, S., Hayashi, M., Nishimura, M. and Esaka, M.** (2008). Plant catalase is imported into peroxisomes by Pex5p but is distinct from typical PTS1 import. *Plant and cell physiology*. **49**(4), pp.671-677.

**Otera, H. and Fujiki, Y.** (2012). Pex5p imports folded tetrameric catalase by interaction with Pex13p. *Traffic*. **13**(10), pp.1364-1377.

**Otter, T. and Polle, A.** (1994). The influence of apoplastic ascorbate on the activities of cell wall-associated peroxidase and NADH oxidase in needles of Norway spruce (*Picea abies* L.). *Plant and Cell Physiology*. **35**(8), pp.1231-1238.

**Overmyer, K., Brosché, M., Pellinen, R., Kuitinen, T., Tuominen, H., Ahlfors, R., Keinänen, M., Saarma, M., Scheel, D. and Kangasjärvi, J.** (2005). Ozone-induced programmed cell death in the *Arabidopsis* radical-induced cell death1 mutant. *Plant Physiology*. **137**(3), pp.1092-1104.

**Padh, H.** (1990). Cellular functions of ascorbic acid. *Biochemistry and Cell Biology*. **68**(10), pp.1166-1173.

**Palm, G.J., Zdanov, A., Gaitanaris, G.A., Stauber, R., Pavlakis, G.N. and Wlodawer, A.** (1997). The structural basis for spectral variations in green fluorescent protein. *Nature structural biology*. **4**(5), pp.361-365.

**Palma, J.M., Mateos, R.M., López-Jaramillo, J., Rodríguez-Ruiz, M., González-Gordo, S., Lechuga-Sancho, A.M. and Corpas, F.J.** (2020). Plant catalases as NO and H<sub>2</sub>S targets. *Redox biology*. p101525.

**Pan, R. and Hu, J.** (2017). Sequence and biochemical analysis of Arabidopsis SP1 protein, a regulator of organelle biogenesis. *Communicative & integrative biology*. **10**(4), pe1338991.

**Pan, R., Liu, J., Wang, S. and Hu, J.** (2020). Peroxisomes: versatile organelles with diverse roles in plants. *New Phytologist*. **225**(4), pp.1410-1427.

**Park, E., Lee, H.Y., Woo, J., Choi, D. and Dinesh-Kumar, S.P.** (2017). Spatiotemporal monitoring of *Pseudomonas syringae* effectors via type III secretion using split fluorescent protein fragments. *The Plant Cell*. **29**(7), pp.1571-1584.

**Pavet, V., Olmos, E., Kiddle, G., Mowla, S., Kumar, S., Antoniow, J., Alvarez, M.E. and Foyer, C.H.** (2005). Ascorbic acid deficiency activates cell death and disease resistance responses in Arabidopsis. *Plant Physiology*. **139**(3), pp.1291-1303.

**Pena-Soler, E., Vega, M.C., Wilmanns, M. and Williams, C.** (2011). Structural features of peroxisomal catalase from the yeast *Hansenula polymorpha*. *Acta Crystallographica Section D: Biological Crystallography*. **67**(8), pp.690-698.

**Petriv, I. and Rachubinski, R.A.** (2004). Lack of peroxisomal catalase causes a progeric phenotype in *Caenorhabditis elegans*. *Journal of Biological Chemistry*. **279**(19), pp.19996-20001.

**Petrova, V.Y., Drescher, D., Kujumdzieva, A.V. and Schmitt, M.J.** (2004). Dual targeting of yeast catalase A to peroxisomes and mitochondria. *Biochemical Journal*. **380**(2), pp.393-400.

**Platta, H.W., El Magraoui, F., Bäumer, B.E., Schlee, D., Girzalsky, W. and Erdmann, R.** (2009). Pex2 and pex12 function as protein-ubiquitin ligases in peroxisomal protein import. *Molecular and cellular biology*. **29**(20), pp.5505-5516.

**Platta, H.W. and Erdmann, R.** (2007). Peroxisomal dynamics. *Trends in cell biology*. **17**(10), pp.474-484.

**Platta, H.W., Grunau, S., Rosenkranz, K., Girzalsky, W. and Erdmann, R.** (2005). Functional role of the AAA peroxins in dislocation of the cycling PTS1 receptor back to the cytosol. *Nature cell biology*. **7**(8), pp.817-822.

**Platta, H.W., Hagen, S., Reidick, C. and Erdmann, R.** (2014). The peroxisomal receptor dislocation pathway: to the exportomer and beyond. *Biochimie*. **98**, pp.16-28.

**Pracharoenwattana, I., Cornah, J.E. and Smith, S.M.** (2007). Arabidopsis peroxisomal malate dehydrogenase functions in  $\beta$ -oxidation but not in the glyoxylate cycle. *The plant journal*. **50**(3), pp.381-390.

**Prakash, K., Prajapati, S., Ahmad, A., Jain, S. and Bhakuni, V.** (2002). Unique oligomeric intermediates of bovine liver catalase. *Protein Science*. **11**(1), pp.46-57.

**Purdue, P.E. and Lazarow, P.B.** (1996). Targeting of human catalase to peroxisomes is dependent upon a novel COOH-terminal peroxisomal targeting sequence. *The Journal of cell biology*. **134**(4), pp.849-862.

**Putnam, C.D., Arvai, A.S., Bourne, Y. and Tainer, J.A.** (2000). Active and inhibited human catalase structures: ligand and NADPH binding and catalytic mechanism. *Journal of molecular biology*. **296**(1), pp.295-309.

**Qi, H., Xia, F.N. and Xiao, S.** (2020). Autophagy in plants: Physiological roles and post-translational regulation. *Journal of Integrative Plant Biology*. **63**, pp.161-179.

**Quan, F., Korneluk, R., Tropak, M. and Gravel, R.** (1986). Isolation and characterization of the human catalase gene. *Nucleic Acids Research*. **14**(13), pp.5321-5335.

**Queval, G., Issakidis-Bourguet, E., Hoerberichts, F.A., Vandorpe, M., Gakiere, B., Vanacker, H., Miginiac-Maslow, M., Van Breusegem, F. and Noctor, G.** (2007). Conditional oxidative stress responses in the Arabidopsis photorespiratory mutant *cat2* demonstrate that redox state is a key modulator of daylength-dependent gene expression, and define photoperiod as a crucial factor in the regulation of H<sub>2</sub>O<sub>2</sub>-induced cell death. *The Plant Journal*. **52**(4), pp.640-657.

**Queval, G. and Noctor, G.** (2007). A plate reader method for the measurement of NAD, NADP, glutathione, and ascorbate in tissue extracts: application to redox profiling during Arabidopsis rosette development. *Analytical biochemistry*. **363**(1), pp.58-69.

**Rabinowitz, J.D. and White, E.** (2010). Autophagy and metabolism. *Science*. **330**(6009), pp.1344-1348.

**Radi, R., Turrens, J.F., Chang, L.Y., Bush, K.M., Crapo, J.D. and Freeman, B.A.** (1991). Detection of catalase in rat heart mitochondria. *Journal of Biological Chemistry*. **266**(32), pp.22028-22034.

**Rahantaniaina, M.S., Li, S., Chatel-Innocenti, G., Tuzet, A., Mhamdi, A., Vanacker, H. and Noctor, G.** (2017). Glutathione oxidation in response to intracellular H<sub>2</sub>O<sub>2</sub>: key but overlapping roles for dehydroascorbate reductases. *Plant signaling & behavior*. **12**(8), pe1356531.

**Rasool, B., Karpinska, B., Pascual, J., Kangasjärvi, S. and Foyer, C.H.** (2020). Catalase, glutathione, and protein phosphatase 2A-dependent organellar redox signalling regulate aphid fecundity under moderate and high irradiance. *Plant, Cell & Environment*. **43**(1), pp.209-222.

**Rausser, W.E.** (1987). Changes in glutathione content of maize seedlings exposed to cadmium. *Plant Science*. **51**(2-3), pp.171-175.

**Rayapuram, N. and Subramani, S.** (2006). The importomer—a peroxisomal membrane complex involved in protein translocation into the peroxisome matrix. *Biochimica et Biophysica Acta (BBA)-Molecular Cell Research*. **1763**(12), pp.1613-1619.

**Reid, T.J., Murthy, M., Sicignano, A., Tanaka, N., Musick, W. and Rossmann, M.** (1981). Structure and heme environment of beef liver catalase at 2.5 Å resolution. *Proceedings of the National Academy of Sciences*. **78**(8), pp.4767-4771.

**Reumann, S., Babujee, L., Ma, C., Wienkoop, S., Siemsen, T., Antonicelli, G.E., Rasche, N., Lüder, F., Weckwerth, W. and Jahn, O.** (2007). Proteome analysis of Arabidopsis leaf peroxisomes reveals novel targeting peptides, metabolic pathways, and defense mechanisms. *The Plant Cell*. **19**(10), pp.3170-3193.

**Reumann, S. and Bartel, B.** (2016). Plant peroxisomes: recent discoveries in functional complexity, organelle homeostasis, and morphological dynamics. *Current opinion in plant biology*. **34**, pp.17-26.

**Reumann, S., Chowdhary, G. and Lingner, T.** (2016). Characterization, prediction and evolution of plant peroxisomal targeting signals type 1 (PTS1s). *Biochimica et Biophysica Acta (BBA)-Molecular Cell Research*. **1863**(5), pp.790-803.

**Reumann, S. and Lisik, P.** (2017). Isolation of Arabidopsis leaf peroxisomes and the peroxisomal membrane. *Isolation of Plant Organelles and Structures*. Springer, pp.97-112.

**Reumann, S., Ma, C., Lemke, S. and Babujee, L.** (2004). AraPeroX. A database of putative Arabidopsis proteins from plant peroxisomes. *Plant physiology*. **136**(1), pp.2587-2608.

**Reumann, S. and Singhal, R.** (2014). Isolation of leaf peroxisomes from Arabidopsis for organelle proteome analyses. *Plant Proteomics*. Springer, pp.541-552.

**Rhodin, J.** (1954). Correlation of ultrastructural organization and function in normal and experimentally changed proximal convoluted tubule cells of the mouse kidney. *Doctoral Thesis., Karolinska Institutet, Stockholm, Aktiebolaget Godvil*. **1**.

**Rosenthal, M., Metz-Raz, E., Bürgi, J., Yifrach, E., Drwesh, L., Fadel, A., Peleg, Y., Rapaport, D., Wilmanns, M. and Barkai, N.** (2020). Uncovering targeting priority to yeast peroxisomes using an in-cell competition assay. *Proceedings of the National Academy of Sciences*. **117**(35), pp.21432-21440.

**Ruis, H.** (1979). The biosynthesis of catalase. *Canadian journal of biochemistry*. **57**(9), pp.1122-1130.

**Rymer, Ł., Kempniński, B., Chelstowska, A. and Skoneczny, M.** (2018). The budding yeast Pex5p receptor directs Fox2p and Cta1p into peroxisomes via its N-terminal region near the FxxxW domain. *J Cell Sci*. **131**(17), p.jcs216986.

**Saffian, D., Grimm, I., Girzalsky, W. and Erdmann, R.** (2012). ATP-dependent assembly of the heteromeric Pex1p–Pex6p-complex of the peroxisomal matrix protein import machinery. *Journal of structural biology*. **179**(2), pp.126-132.

**Sandalio, L.M., Gotor, C., Romero, L.C. and Romero-Puertas, M.C.** (2019). Multilevel regulation of peroxisomal proteome by post-translational modifications. *International journal of molecular sciences*. **20**(19), p4881.

**Sandalio, L.M., Peláez-Vico, M.A., Molina-Moya, E. and Romero-Puertas, M.C.** (2021). Peroxisomes as Redox-Signaling Nodes in Intracellular Communication and Stress Responses. *Plant Physiology*.

**Scandalios, J.G.** (1965). Subunit dissociation and recombination of catalase isozymes. *Proceedings of the National Academy of Sciences*. **53**(5), pp.1035-1040.

**Scandalios, J.G., Guan, L. and Polidoros, A.N.** (1997). Catalases in plants: gene structure, properties, regulation, and expression. *Cold Spring Harbor Monograph Series*. **34**, pp.343-406.

**Scandalios, J.G., Tong, W.F. and Roupakias, D.G.** (1980). Cat3, a third gene locus coding for a tissue-specific catalase in maize: genetics, intracellular location, and some biochemical properties. *Molecular and General Genetics MGG*. **179**(1), pp.33-41.

**Scheller, H.V., Huang, B., Hatch, E. and Goldsbrough, P.B.** (1987). Phytochelatin synthesis and glutathione levels in response to heavy metals in tomato cells. *Plant Physiology*. **85**(4), pp.1031-1035.

**Schmidt, M., Dehne, S. and Feierabend, J.** (2002). Post-transcriptional mechanisms control catalase synthesis during its light-induced turnover in rye leaves through the availability of the hemin cofactor and reversible changes of the translation efficiency of mRNA. *The Plant Journal*. **31**(5), pp.601-613.

**Schönbein, C.** (1863). Chemische Mittheilungen. *Journal fuer praktische Chemie*. **89**(1), pp.1-38.

**Schopfer, P.** (1996). Hydrogen peroxide-mediated cell-wall stiffening in vitro in maize coleoptiles. *Planta*. **199**(1), pp.43-49.

**Schroeder, W., Shelton, J.R., Shelton, J.B., Robberson, B. and Apell, G.** (1969). The amino acid sequence of bovine liver catalase: a preliminary report. *Archives of biochemistry and biophysics*. **131**(2), pp.653-655.

**Schueren, F., Lingner, T., George, R., Hofhuis, J., Dickel, C., Gärtner, J. and Thoms, S.** (2014). Peroxisomal lactate dehydrogenase is generated by translational readthrough in mammals. *Elife*. **3**, pe03640.

**Schuhmann, H., Huesgen, P.F., Gietl, C. and Adamska, I.** (2008). The DEG15 serine protease cleaves peroxisomal targeting signal 2-containing proteins in Arabidopsis. *Plant physiology*. **148**(4), pp.1847-1856.

**Schumann, U., Wanner, G., Veenhuis, M., Schmid, M. and Gietl, C.** (2003). AthPEX10, a nuclear gene essential for peroxisome and storage organelle formation during Arabidopsis embryogenesis. *Proceedings of the National Academy of Sciences*. **100**(16), pp.9626-9631.

**Sewelam, N., Kazan, K., Hüdig, M., Maurino, V.G. and Schenk, P.M.** (2019). The AtHSP17. 4C1 Gene Expression Is Mediated by Diverse Signals that Link Biotic and Abiotic Stress Factors with ROS and Can Be a Useful Molecular Marker for Oxidative Stress. *International journal of molecular sciences*. **20**(13), p3201.

**Sharma, P., Jha, A.B., Dubey, R.S. and Pessarakli, M.** (2012). Reactive oxygen species, oxidative damage, and antioxidative defense mechanism in plants under stressful conditions. *Journal of botany*. **2012**, pp.1-27.

**Shibata, M., Oikawa, K., Yoshimoto, K., Kondo, M., Mano, S., Yamada, K., Hayashi, M., Sakamoto, W., Ohsumi, Y. and Nishimura, M.** (2013). Highly oxidized peroxisomes are selectively degraded via autophagy in Arabidopsis. *The Plant Cell*. **25**(12), pp.4967-4983.

**Sievers, F., Wilm, A., Dineen, D., Gibson, T.J., Karplus, K., Li, W., Lopez, R., McWilliam, H., Remmert, M. and Söding, J.** (2011). Fast, scalable generation of high-quality protein multiple sequence alignments using Clustal Omega. *Molecular systems biology*. **7**(1), p539.

**Singh, I.** (1996). Mammalian peroxisomes: metabolism of oxygen and reactive oxygen species. *Annals of the New York Academy of Sciences*. **804**(1), pp.612-627.

**Skadsen, R.W., Schulze-Lefert, P. and Herbst, J.M.** (1995). Molecular cloning, characterization and expression analysis of two catalase isozyme genes in barley. *Plant Molecular Biology*. **29**(5), pp.1005-1014.

**Skoulding, N.S., Chowdhary, G., Deus, M.J., Baker, A., Reumann, S. and Warriner, S.L.** (2015). Experimental validation of plant peroxisomal targeting prediction algorithms by systematic comparison of in vivo import efficiency and in vitro PTS1 binding affinity. *Journal of molecular biology*. **427**(5), pp.1085-1101.

**Smirnoff, N.** (2000). Ascorbate biosynthesis and function in photoprotection. *Philosophical transactions of the royal society of London. Series b: Biological Sciences*. **355**(1402), pp.1455-1464.

**Smirnoff, N., Conklin, P.L. and Loewus, F.A.** (2001). Biosynthesis of ascorbic acid in plants: a renaissance. *Annual review of plant biology*. **52**(1), pp.437-467.

**Smith, I., Kendall, A., Keys, A., Turner, J. and Lea, P.** (1984). Increased levels of glutathione in a catalase-deficient mutant of barley (*Hordeum vulgare* L.). *Plant Science Letters*. **37**(1-2), pp.29-33.

**Smith, I., Kendall, A., Keys, A., Turner, J. and Lea, P.** (1985). The regulation of the biosynthesis of glutathione in leaves of barley (*Hordeum vulgare* L.). *Plant Science*. **41**(1), pp.11-17.

**Smith, J.J. and Aitchison, J.D.** (2013). Peroxisomes take shape. *Nature reviews Molecular cell biology*. **14**(12), pp.803-817.

**Smith, J.J., Ververidis, P. and John, P.** (1992). Characterization of the ethylene-forming enzyme partially purified from melon. *Phytochemistry*. **31**(5), pp.1485-1494.

**Smith, L.J., Kahraman, A. and Thornton, J.M.** (2010). Heme proteins—diversity in structural characteristics, function, and folding. *Proteins: structure, function, and bioinformatics*. **78**(10), pp.2349-2368.

**Spadaro, D., Yun, B.W., Spoel, S.H., Chu, C., Wang, Y.Q. and Loake, G.J.** (2010). The redox switch: dynamic regulation of protein function by cysteine modifications. *Physiologia plantarum*. **138**(4), pp.360-371.

**Sparkes, I.A., Brandizzi, F., Slocombe, S.P., El-Shami, M., Hawes, C. and Baker, A.** (2003). An *Arabidopsis* pex10 null mutant is embryo lethal, implicating peroxisomes in an essential role during plant embryogenesis. *Plant physiology*. **133**(4), pp.1809-1819.

**Sparkes, I.A., Hawes, C. and Baker, A.** (2005). AtPEX2 and AtPEX10 are targeted to peroxisomes independently of known endoplasmic reticulum trafficking routes. *Plant physiology*. **139**(2), pp.690-700.

**Stanley, W.A., Pursiainen, N.V., Garman, E.F., Juffer, A.H., Wilmanns, M. and Kursula, P.** (2007). A previously unobserved conformation for the human Pex5p receptor suggests roles for intrinsic flexibility and rigid domain motions in ligand binding. *BMC structural biology*. **7**(1), pp.1-12.

**Stern, K.G.** (1937). Spectroscopy of catalase. *The Journal of general physiology*. **20**(4), pp.631-648.

**Stewart, M.Q., Esposito, R.D., Gowani, J. and Goodman, J.M.** (2001). Alcohol oxidase and dihydroxyacetone synthase, the abundant peroxisomal proteins of methylotrophic yeasts, assemble in different cellular compartments. *Journal of cell science*. **114**(15), pp.2863-2868.

**Su, T., Li, X., Yang, M., Shao, Q., Zhao, Y., Ma, C. and Wang, P.** (2020). Autophagy: An Intracellular Degradation Pathway Regulating Plant Survival and Stress Response. *Frontiers in Plant Science*. **11**, p164.

- Su, T., Wang, P., Li, H., Zhao, Y., Lu, Y., Dai, P., Ren, T., Wang, X., Li, X. and Shao, Q.** (2018). The Arabidopsis catalase triple mutant reveals important roles of catalases and peroxisome-derived signaling in plant development. *Journal of integrative plant biology*. **60**(7), pp.591-607.
- Sumner, J.B. and Dounce, A.L.** (1937). Crystalline catalase. *Journal of Biological Chemistry*. **121**(2), pp.417-424.
- Sumner, J.B. and Gralén, N.** (1938). The molecular weight of crystalline catalase. *Journal of Biological Chemistry*. **125**(1), pp.33-36.
- Sun, W., Bernard, C., Van De Cotte, B., Van Montagu, M. and Verbruggen, N.** (2001). At-HSP17. 6A, encoding a small heat-shock protein in Arabidopsis, can enhance osmotolerance upon overexpression. *The Plant Journal*. **27**(5), pp.407-415.
- Sun, W., Van Montagu, M. and Verbruggen, N.** (2002). Small heat shock proteins and stress tolerance in plants. *Biochimica et Biophysica Acta (BBA)-Gene Structure and Expression*. **1577**(1), pp.1-9.
- Swinkels, B.W., Gould, S.J., Bodnar, A.G., Rachubinski, R.A. and Subramani, S.** (1991). A novel, cleavable peroxisomal targeting signal at the amino-terminus of the rat 3-ketoacyl-CoA thiolase. *The EMBO Journal*. **10**(11), pp.3255-3262.
- Takahama, U.** (1993). Regulation of peroxidase-dependent oxidation of phenolics by ascorbic acid: different effects of ascorbic acid on the oxidation of coniferyl alcohol by the apoplastic soluble and cell wall-bound peroxidases from epicotyls of *Vigna angularis*. *Plant and cell physiology*. **34**(6), pp.809-817.
- Takahara, S.** (1948). Clinical and experimental studies on the odontogenous progressive necrotic otitis due to lack of blood catalase. *J. Otorhinol. Soc. Jpn.* **51**, pp.163-164.
- Taub, J., Lau, J.F., Ma, C., Hahn, J.H., Hoque, R., Rothblatt, J. and Chalfie, M.** (1999). A cytosolic catalase is needed to extend adult lifespan in *C. elegans* daf-C and clk-1 mutants. *Nature*. **399**(6732), pp.162-166.
- Tenberge, K.B. and Eising, R.** (1995). Immunogold labelling indicates high catalase concentrations in amorphous and crystalline inclusions of sunflower (*Helianthus annuus* L.) peroxisomes. *The Histochemical Journal*. **27**(3), pp.184-195.

**Thénard, L.J.** (1818). Observations sur des nouvelles combinaisons entre l'oxygène et divers acides. *Ann. Chim. Phys.* **8**, pp.306-312.

**Thoms, S.** (2015). Import of proteins into peroxisomes: piggybacking to a new home away from home. *Open biology.* **5**(11), p150148.

**Titorenko, V.I. and Mullen, R.T.** (2006). Peroxisome biogenesis: the peroxisomal endomembrane system and the role of the ER. *The Journal of cell biology.* **174**(1), pp.11-17.

**Titorenko, V.I., Nicaud, J.M., Wang, H., Chan, H. and Rachubinski, R.A.** (2002). Acyl-CoA oxidase is imported as a heteropentameric, cofactor-containing complex into peroxisomes of *Yarrowia lipolytica*. *The Journal of cell biology.* **156**(3), pp.481-494.

**Togo, S.H., Maebuchi, M., Yokota, S., Bun-Ya, M., Kawahara, A. and Kamiryo, T.** (2000). Immunological detection of alkaline-diaminobenzidine-negative peroxisomes of the nematode *Caenorhabditis elegans*: Purification and unique pH optima of peroxisomal catalase. *European journal of biochemistry.* **267**(5), pp.1307-1312.

**Turek, I., Wheeler, J., Bartels, S., Szczurek, J., Wang, Y.H., Taylor, P., Gehring, C. and Irving, H.** (2020). A natriuretic peptide from *Arabidopsis thaliana* (AtPNP-A) can modulate catalase 2 activity. *Scientific reports.* **10**(1), pp.1-14.

**Tuzet, A., Rahantaniaina, M.S. and Noctor, G.** (2019). Analyzing the Function of Catalase and the Ascorbate–Glutathione Pathway in H<sub>2</sub>O<sub>2</sub> Processing: Insights from an Experimentally Constrained Kinetic Model. *Antioxidants & redox signaling.* **30**(9), pp.1238-1268.

**Umezawa, T., Sugiyama, N., Takahashi, F., Anderson, J.C., Ishihama, Y., Peck, S.C. and Shinozaki, K.** (2013). Genetics and phosphoproteomics reveal a protein phosphorylation network in the abscisic acid signaling pathway in *Arabidopsis thaliana*. *Science signaling.* **6**(270), prs8.

**Valpuesta, V. and Botella, M.A.** (2004). Biosynthesis of L-ascorbic acid in plants: new pathways for an old antioxidant. *Trends in plant science.* **9**(12), pp.573-577.

**Van den Bosch, H., Schutgens, R., Wanders, R. and Tager, J.** (1992). Biochemistry of peroxisomes. *Annual review of biochemistry.* **61**(1), pp.157-197.

**van Doorn, W.G. and Papini, A.** (2013). Ultrastructure of autophagy in plant cells: a review. *Autophagy*. **9**(12), pp.1922-1936.

**Van Engelenburg, S.B. and Palmer, A.E.** (2010). Imaging type-III secretion reveals dynamics and spatial segregation of Salmonella effectors. *Nature methods*. **7**(4), pp.325-330.

**Vanacker, H., Carver, T.L. and Foyer, C.H.** (2000). Early H<sub>2</sub>O<sub>2</sub> accumulation in mesophyll cells leads to induction of glutathione during the hyper-sensitive response in the barley-powdery mildew interaction. *Plant Physiology*. **123**(4), pp.1289-1300.

**Vandenabeele, S., Vanderauwera, S., Vuylsteke, M., Rombauts, S., Langebartels, C., Seidlitz, H.K., Zabeau, M., Van Montagu, M., Inzé, D. and Van Breusegem, F.** (2004). Catalase deficiency drastically affects gene expression induced by high light in *Arabidopsis thaliana*. *The Plant Journal*. **39**(1), pp.45-58.

**Vanderauwera, S., Vandenbroucke, K., Inzé, A., Van De Cotte, B., Mühlenbock, P., De Rycke, R., Naouar, N., Van Gaever, T., Van Montagu, M.C. and Van Breusegem, F.** (2012). AtWRKY15 perturbation abolishes the mitochondrial stress response that steers osmotic stress tolerance in *Arabidopsis*. *Proceedings of the National Academy of Sciences*. **109**(49), pp.20113-20118.

**Vanderauwera, S., Zimmermann, P., Rombauts, S., Vandenabeele, S., Langebartels, C., Gruissem, W., Inzé, D. and Van Breusegem, F.** (2005). Genome-wide analysis of hydrogen peroxide-regulated gene expression in *Arabidopsis* reveals a high light-induced transcriptional cluster involved in anthocyanin biosynthesis. *Plant Physiology*. **139**(2), pp.806-821.

**Veenhuis, M., Douma, A., Harder, W. and Osumi, M.** (1983). Degradation and turnover of peroxisomes in the yeast *Hansenula polymorpha* induced by selective inactivation of peroxisomal enzymes. *Archives of microbiology*. **134**(3), pp.193-203.

**Veljovic-Jovanovic, S.D., Pignocchi, C., Noctor, G. and Foyer, C.H.** (2001). Low ascorbic acid in the vtc-1 mutant of *Arabidopsis* is associated with decreased growth and intracellular redistribution of the antioxidant system. *Plant Physiology*. **127**(2), pp.426-435.

**Verslues, P.E., Batelli, G., Grillo, S., Agius, F., Kim, Y.-S., Zhu, J., Agarwal, M., Katiyar-Agarwal, S. and Zhu, J.-K.** (2007). Interaction of SOS2 with nucleoside diphosphate kinase 2 and catalases reveals a point of connection between salt stress and H<sub>2</sub>O<sub>2</sub> signaling in *Arabidopsis thaliana*. *Molecular and cellular biology*. **27**(22), pp.7771-7780.

**Vigil, E.L.** (1970). Cytochemical and developmental changes in microbodies (glyoxysomes) and related organelles of castor bean endosperm. *The Journal of cell biology*. **46**(3), pp.435-454.

**Vlad, F., Spano, T., Vlad, D., Daher, F.B., Ouelhadj, A., Fragkostefanakis, S. and Kalaitzis, P.** (2007). Involvement of Arabidopsis prolyl 4 hydroxylases in hypoxia, anoxia and mechanical wounding. *Plant Signaling & Behavior*. **2**(5), pp.368-369.

**von Ossowski, I., Hausner, G. and Loewen, P.C.** (1993). Molecular evolutionary analysis based on the amino acid sequence of catalase. *Journal of molecular evolution*. **37**(1), pp.71-76.

**Walter, T. and Erdmann, R.** (2019). Current advances in protein import into peroxisomes. *The protein journal*. **38**(3), pp.351-362.

**Walton, P.A., Brees, C., Lismont, C., Apanasets, O. and Fransen, M.** (2017). The peroxisomal import receptor PEX5 functions as a stress sensor, retaining catalase in the cytosol in times of oxidative stress. *Biochimica et Biophysica Acta (BBA)-Molecular Cell Research*. **1864**(10), pp.1833-1843.

**Walton, P.A., Hill, P. and Subramani, S.** (1995). Import of stably folded proteins into peroxisomes. *Molecular biology of the cell*. **6**(6), pp.675-683.

**Wanders, R.J. and Waterham, H.R.** (2006). Peroxisomal disorders: the single peroxisomal enzyme deficiencies. *Biochimica et Biophysica Acta (BBA)-Molecular Cell Research*. **1763**(12), pp.1707-1720.

**Wang, P., Du, Y., Li, Y., Ren, D. and Song, C.P.** (2010). Hydrogen peroxide-mediated activation of MAP kinase 6 modulates nitric oxide biosynthesis and signal transduction in Arabidopsis. *The Plant Cell*. **22**(9), pp.2981-2998.

**Warburg, O.** (1923). Über die antikatalytische Wirkung der Blausäure. *Biochem. Z.* **136**, pp.266-277.

**Waszczak, C., Akter, S., Jacques, S., Huang, J., Messens, J. and Van Breusegem, F.** (2015). Oxidative post-translational modifications of cysteine residues in plant signal transduction. *Journal of experimental botany*. **66**(10), pp.2923-2934.

**Waszczak, C., Carmody, M. and Kangasjärvi, J.** (2018). Reactive oxygen species in plant signaling. *Annual review of plant biology*. **69**, pp.209-236.

**Waszczak, C., Kerchev, P.I., Mühlenbock, P., Hoerberichts, F.A., Van Der Kelen, K., Mhamdi, A., Willems, P., Denecker, J., Kumpf, R.P., Noctor, G., Messens, J. and Van Breusegem, F.** (2016). SHORT-ROOT deficiency alleviates the cell death phenotype of the Arabidopsis catalase2 mutant under photorespiration-promoting conditions. *The Plant Cell*. **28**(8), pp.1844-1859.

**Waterham, H.R., Titorenko, V.I., Swaving, G.J., Harder, W. and Veenhuis, M.** (1993). Peroxisomes in the methylotrophic yeast *Hansenula polymorpha* do not necessarily derive from pre-existing organelles. *The EMBO journal*. **12**(12), pp.4785-4794.

**Welinder, K.G.** (1992). Superfamily of plant, fungal and bacterial peroxidases. *Current Opinion in Structural Biology*. **2**(3), pp.388-393.

**Weydert, C.J. and Cullen, J.J.** (2010). Measurement of superoxide dismutase, catalase and glutathione peroxidase in cultured cells and tissue. *Nature protocols*. **5**(1), pp.51-66.

**Wheeler, G.L., Jones, M.A. and Smirnoff, N.** (1998). The biosynthetic pathway of vitamin C in higher plants. *Nature*. **393**(6683), pp.365-369.

**Whittaker, J.W.** (2012). Non-heme manganese catalase—the ‘other’catalase. *Archives of biochemistry and biophysics*. **525**(2), pp.111-120.

**Willekens, H., Chamnongpol, S., Davey, M., Schraudner, M., Langebartels, C., Van Montagu, M., Inzé, D. and Van Camp, W.** (1997). Catalase is a sink for H<sub>2</sub>O<sub>2</sub> and is indispensable for stress defence in C<sub>3</sub> plants. *The EMBO journal*. **16**(16), pp.4806-4816.

**Willekens, H., Inzé, D., Van Montagu, M. and van Camp, W.** (1995). Catalases in plants. *Molecular Breeding*. **1**(3), pp.207-228.

**Willekens, H., Langebartels, C., Tire, C., Van Montagu, M., Inze, D. and Van Camp, W.** (1994a). Differential expression of catalase genes in *Nicotiana glauca* (L.). *Proceedings of the National Academy of Sciences*. **91**(22), pp.10450-10454.

**Willekens, H., Villarroel, R., Van Montagu, M., Inzé, D. and Van Camp, W.** (1994b). Molecular identification of catalases from *Nicotiana glauca* (L.). *Febs Letters*. **352**(1), pp.79-83.

**Williams, C., Aksam, E.B., Gunkel, K., Veenhuis, M. and van der Klei, I.J.** (2012a). The relevance of the non-canonical PTS1 of peroxisomal catalase. *Biochimica et Biophysica Acta (BBA)-Molecular Cell Research*. **1823**(7), pp.1133-1141.

**Williams, C., van den Berg, M., Geers, E. and Distel, B.** (2008). Pex10p functions as an E3 ligase for the Ubc4p-dependent ubiquitination of Pex5p. *Biochemical and biophysical research communications*. **374**(4), pp.620-624.

**Williams, C., Van Den Berg, M., Panjkar, S., Stanley, W.A., Distel, B. and Wilmanns, M.** (2012b). Insights into ubiquitin-conjugating enzyme/co-activator interactions from the structure of the Pex4p: Pex22p complex. *The EMBO journal*. **31**(2), pp.391-402.

**Williams, C., van den Berg, M., Sprenger, R.R. and Distel, B.** (2007). A conserved cysteine is essential for Pex4p-dependent ubiquitination of the peroxisomal import receptor Pex5p. *Journal of Biological Chemistry*. **282**(31), pp.22534-22543.

**Wojtaszek, P., Smith, C.G. and Bolwell, G.P.** (1999). Ultrastructural localisation and further biochemical characterisation of prolyl 4-hydroxylase from *Phaseolus vulgaris*: comparative analysis. *The international journal of biochemistry & cell biology*. **31**(3-4), pp.463-477.

**Wolucka, B.A. and Van Montagu, M.** (2003). GDP-mannose 3', 5'-epimerase forms GDP-L-gulose, a putative intermediate for the de novo biosynthesis of vitamin C in plants. *Journal of Biological Chemistry*. **278**(48), pp.47483-47490.

**Wu, F.H., Shen, S.C., Lee, L.Y., Lee, S.H., Chan, M.T. and Lin, C.S.** (2009). Tape-Arabidopsis Sandwich-a simpler Arabidopsis protoplast isolation method. *Plant methods*. **5**(1), p16.

**Xiong, Y., Contento, A.L., Nguyen, P.Q. and Bassham, D.C.** (2007). Degradation of oxidized proteins by autophagy during oxidative stress in Arabidopsis. *Plant physiology*. **143**(1), pp.291-299.

**Yamauchi, S., Mano, S., Oikawa, K., Hikino, K., Teshima, K.M., Kimori, Y., Nishimura, M., Shimazaki, K.i. and Takemiya, A.** (2019). Autophagy controls reactive oxygen species homeostasis in guard cells that is essential for stomatal opening. *Proceedings of the National Academy of Sciences*. **116**(38), pp.19187-19192.

**Yang, T. and Poovaiah, B.** (2002). Hydrogen peroxide homeostasis: activation of plant catalase by calcium/calmodulin. *Proceedings of the National Academy of Sciences*. **99**(6), pp.4097-4102.

**Yang, X., Purdue, P.E. and Lazarow, P.B.** (2001). Eci1p uses a PTS1 to enter peroxisomes: either its own or that of a partner, Dci1p. *European journal of cell biology*. **80**(2), pp.126-138.

**Yang, Z., Mhamdi, A. and Noctor, G.** (2018). Analysis of catalase mutants underscores the essential role of CATALASE2 for plant growth and day length-dependent oxidative signalling. *Plant, cell & environment*. **42**(2), pp.688-700.

**Yoshimoto, K., Jikumaru, Y., Kamiya, Y., Kusano, M., Consonni, C., Panstruga, R., Ohsumi, Y. and Shirasu, K.** (2009). Autophagy negatively regulates cell death by controlling NPR1-dependent salicylic acid signaling during senescence and the innate immune response in Arabidopsis. *The Plant Cell*. **21**(9), pp.2914-2927.

**Yoshimoto, K. and Ohsumi, Y.** (2018). Unveiling the molecular mechanisms of plant autophagy—from autophagosomes to vacuoles in plants. *Plant and Cell Physiology*. **59**(7), pp.1337-1344.

**Yoshimoto, K., Shibata, M., Kondo, M., Oikawa, K., Sato, M., Toyooka, K., Shirasu, K., Nishimura, M. and Ohsumi, Y.** (2014a). Organ-specific quality control of plant peroxisomes is mediated by autophagy. *Journal of cell science*. **127**(6), pp.1161-1168.

**Yoshimoto, K., Shibata, M., Kondo, M., Oikawa, K., Sato, M., Toyooka, K., Shirasu, K., Nishimura, M. and Ohsumi, Y.** (2014b). Quality control of plant peroxisomes in organ specific manner via autophagy. *J Cell Sci*. **127**(2014), pp.1161-1168.

**Young, P.G. and Bartel, B.** (2016). Pexophagy and peroxisomal protein turnover in plants. *Biochimica et Biophysica Acta (BBA)-Molecular Cell Research*. **1863**(5), pp.999-1005.

**Yu, M., Lamattina, L., Spoel, S.H. and Loake, G.J.** (2014). Nitric oxide function in plant biology: a redox cue in deconvolution. *New Phytologist*. **202**(4), pp.1142-1156.

**Yuan, H.M., Liu, W.C. and Lu, Y.T.** (2017). CATALASE2 coordinates SA-mediated repression of both auxin accumulation and JA biosynthesis in plant defenses. *Cell Host & Microbe*. **21**(2), pp.143-155.

**Yuzugullu, Y., Trinh, C.H., Smith, M.A., Pearson, A.R., Phillips, S.E., Sutay Kocabas, D., Bakir, U., Ogel, Z.B. and McPherson, M.J.** (2013). Structure, recombinant expression and mutagenesis studies of the catalase with oxidase activity from *Scytalidium thermophilum*. *Acta Crystallographica Section D: Biological Crystallography*. **69**(3), pp.398-408.

**Zamocky, M., Furtmüller, P.G. and Obinger, C.** (2008). Evolution of catalases from bacteria to humans. *Antioxidants & redox signaling*. **10**(9), pp.1527-1548.

**Zámocký, M., Furtmüller, P.G. and Obinger, C.** (2010). Evolution of structure and function of Class I peroxidases. *Archives of Biochemistry and Biophysics*. **500**(1), pp.45-57.

**Zámocký, M., Gasselhuber, B., Furtmüller, P.G. and Obinger, C.** (2012). Molecular evolution of hydrogen peroxide degrading enzymes. *Archives of biochemistry and biophysics*. **525**(2), pp.131-144.

**Zámocký, M. and Koller, F.** (1999). Understanding the structure and function of catalases: clues from molecular evolution and in vitro mutagenesis. *Progress in biophysics and molecular biology*. **72**(1), pp.19-66.

**Žárský, V. and Tachezy, J.** (2015). Evolutionary loss of peroxisomes—not limited to parasites. *Biology direct*. **10**(1), pp.1-10.

**Zhang, M., Li, Q., Liu, T., Liu, L., Shen, D., Zhu, Y., Liu, P., Zhou, J.M. and Dou, D.** (2015). Two cytoplasmic effectors of *Phytophthora sojae* regulate plant cell death via interactions with plant catalases. *Plant physiology*. **167**(1), pp.164-175.

**Zhong, H.H. and McClung, C.R.** (1996). The circadian clock gates expression of two *Arabidopsis* catalase genes to distinct and opposite circadian phases. *Molecular and General Genetics MGG*. **251**(2), pp.196-203.

**Zhong, H.H., Young, J.C., Pease, E.A., Hangarter, R.P. and McClung, C.R.** (1994). Interactions between light and the circadian clock in the regulation of CAT2 expression in *Arabidopsis*. *Plant Physiology*. **104**(3), pp.889-898.

**Zhou, H., Finkemeier, I., Guan, W., Tossounian, M.A., Wei, B., Young, D., Huang, J., Messens, J., Yang, X. and Zhu, J.** (2018). Oxidative stress-triggered interactions between the succinyl- and acetyl-proteomes of rice leaves. *Plant, cell & environment*. **41**(5), pp.1139-1153.

**Zhou, Y.B., Liu, C., Tang, D.Y., Yan, L., Wang, D., Yang, Y.Z., Gui, J.S., Zhao, X.Y., Li, L.G. and Tang, X.D.** (2018). The receptor-like cytoplasmic kinase STRK1 phosphorylates and activates CatC, thereby regulating H<sub>2</sub>O<sub>2</sub> homeostasis and improving salt tolerance in rice. *The Plant Cell*. **30**(5), pp.1100-1118.

**Zhou, Z. and Kang, Y.J.** (2000). Cellular and subcellular localization of catalase in the heart of transgenic mice. *Journal of Histochemistry & Cytochemistry*. **48**(5), pp.585-594.

**Zimmermann, P., Heinlein, C., Orendi, G. and Zentgraf, U.** (2006). Senescence-specific regulation of catalases in *Arabidopsis thaliana* (L.) Heynh. *Plant, cell & environment*. **29**(6), pp.1049-1060.

**Zolman, B.K., Monroe-Augustus, M., Silva, I.D. and Bartel, B.** (2005). Identification and functional characterization of *Arabidopsis* PEROXIN4 and the interacting protein PEROXIN22. *The Plant Cell*. **17**(12), pp.3422-3435.

**Zou, J.J., Li, X.D., Ratnasekera, D., Wang, C., Liu, W.X., Song, L.F., Zhang, W.Z. and Wu, W.H.** (2015). *Arabidopsis* CALCIUM-DEPENDENT PROTEIN KINASE8 and CATALASE3 function in abscisic acid-mediated signaling and H<sub>2</sub>O<sub>2</sub> homeostasis in stomatal guard cells under drought stress. *The Plant Cell*. **27**(5), pp.1445-1460.

## Appendix A

### A.1 Selection of T<sub>1</sub> and T<sub>2</sub> generation of PSI, WSQV and ARL on hygromycin plates

#### A.1.1 Selection of hygromycin-resistant transformants

As can be seen in (Figure A1) the hygromycin resistant seedlings had long hypocotyls and closed cotyledons, whereas, the hygromycin sensitive seedlings had short hypocotyls and open cotyledons.

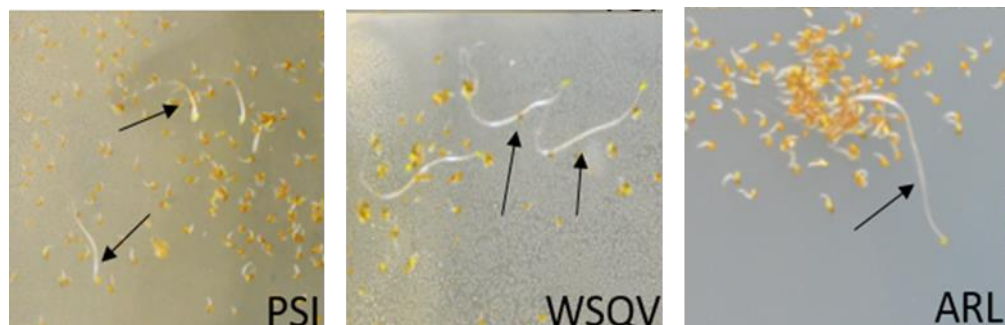


**Figure A1: Selection of transformants on hygromycin plates.**

Hygromycin resistant seedlings had long hypocotyls and closed cotyledons (arrows), however, sensitive seedlings had very short hypocotyls and open cotyledons.

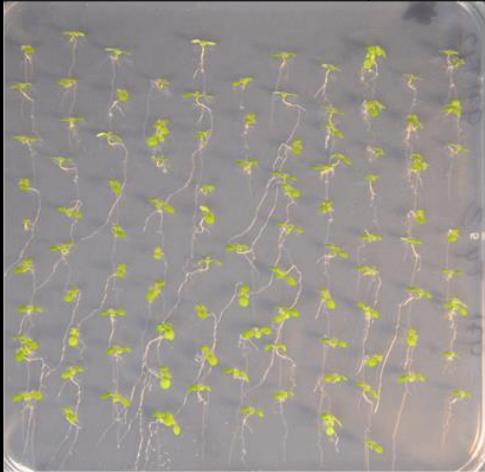
#### A.1.2 First independent line generation

One line (First independent line) for each PSI, WSQV and ARL had been selected and taken to T<sub>3</sub> prior to the start of this project. 100 seeds of selected T<sub>3</sub> lines were checked for resistant and sensitive as shown in Figure A2.

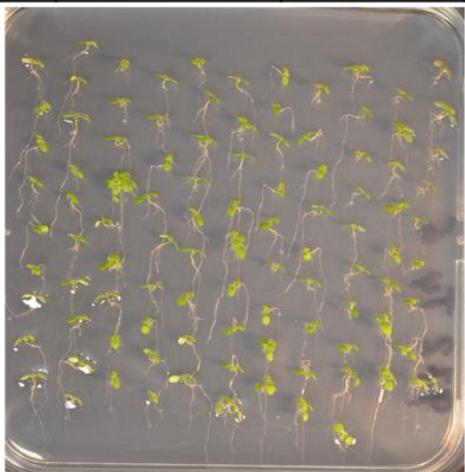
As can be seen in Figure A2, the number of resistant and sensitive seedlings were counted to check the homozygosity. PSI T<sub>3</sub> plant #2 and WSQV T<sub>3</sub> plant #6 (highlighted red) were homozygous and taken forward for further study. Genotyping result of PSI and WSQV is shown in Figure A3. For product sized, see Chapter 3, Section 3.2.

T3 generation	Number of sensitive	Number of resistant	Non-germinating
PSI T <sub>3</sub> plant # 3	20	79	1
<b>PSI T<sub>3</sub> plant # 2</b>	-	<b>100</b>	-
PSI T <sub>4</sub> plant # 1	24	71	5
<b>WSQV T<sub>3</sub> plant # 6</b>	-	<b>100</b>	-
WSQV T <sub>3</sub> plant # 2	-	100	-
WSQV T <sub>3</sub> plant # 9	-	100	-



**PSI T<sub>3</sub> plant # 2**



**WSQV T<sub>3</sub> plant # 6**

**Figure A2: First independent line selection.**

Sensitive and resistance seedling were counted after sowing on ½ MS containing hygromycin.

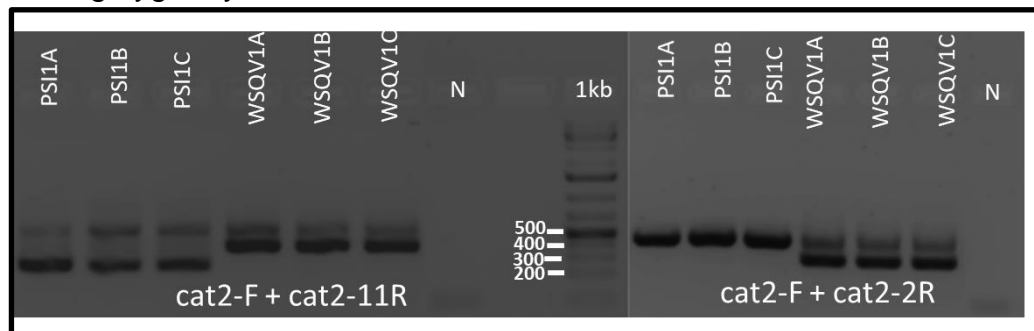


**Figure A3: First independent line genotyping.**

Presence of transgene was confirmed using PCR amplification with specific primers. N, negative control (No DNA). Expected bands: DNA from PSI lines with Cat2-F and cat2-11R primer pair; 563bp (Genomic) and 259bp (cDNA). Same primer pair with DNA from WSQV lines; 563bp (Genomic) and 373bp (cDNA). On the other hand, cat2-F and cat2-2R with PSI lines DNA; 466bp (Genomic). WSQV lines DNA with the same primer give 2 bands: 466bp (Genomic) and 276bp (cDNA). Three DNA samples were prepared from 3 independent plants of each line. DNA was isolated from three different samples of each genotype.

### A.1.3 Second independent line generation

Regarding the 2<sup>nd</sup> and 3<sup>rd</sup> independent lines, T2 seeds (T1 generation) were selected on hygromycin to get 2 independent lines for each (to get more lines with 3:1 segregation ratio). The number of hygromycin sensitive and resistant were counted. 10 resistant seedlings of each line which showed a 3:1 ratio were transplanted to soil (Figure A4). T3 seeds were then checked for homozygosity (Figure A5). Homozygous lines which were used for the analysis were also checked using PCR. The result of this line is presented in Chapter 3 (Figure 3.6). Expected band sizes are also presented in Chapter 3 (Table 3.2).

T2 generation	Number of sensitive	Number of resistant	Non-germinating
PSI T <sub>2</sub> plant # 6	23	77	0
WSQV T <sub>2</sub> plant # 4	18	73	0
ARL T <sub>2</sub> plant # 1	21	71	0

PSI T<sub>2</sub> plant # 6      WSQV T<sub>2</sub> plant # 4      ARL T<sub>2</sub> plant # 1

**Figure A4: Antibiotic selection of T2 generation.**

100 seeds of T1 generation of each line were sown on ½ MS media containing hygromycin to find a plate with a 3:1 ratio of resistant plants. Upper table shows the lines which are segregating 3:1 after screening. The screening plates are shown (Bottom).

T3 generation	Number of sensitive	Number of resistant	Non-germinating
PSI T <sub>2</sub> plant # 6 T <sub>3</sub> plant # 6	0	42	8
WSQV T <sub>2</sub> plant # 4 T <sub>3</sub> plant # 4	0	50	0
ARL T <sub>2</sub> plant # 1 T <sub>3</sub> plant # 1	0	50	0

**PSI T<sub>2</sub> plant # 6  
T<sub>3</sub> plant # 6**

**WSQV T<sub>2</sub> plant # 4  
T<sub>3</sub> plant # 4**

**ARL T<sub>2</sub> plant # 1  
T<sub>3</sub> plant # 1**

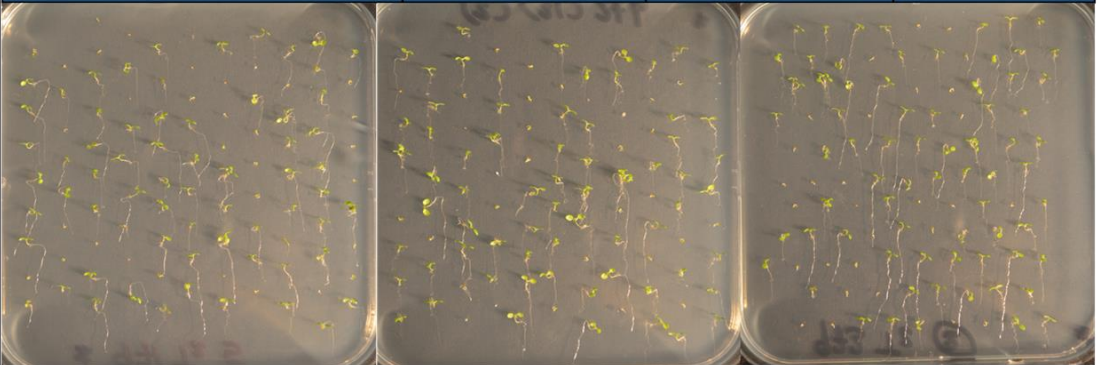
**Figure A5: Antibiotic selection of T3 generation.**

50 seeds of T<sub>2</sub> generation of each line were sown on ½ MS media containing hygromycin to find a plate with a 100% resistant plants. Upper table shows the homozygous lines (100 % resistant). The screening plates are shown (Bottom).

### A.1.4 Third independent line generation

The 3<sup>rd</sup> independent line, 3:1 ratio selection, homozygosity screening and presence of transgene by PCR are shown in Figure A.6,7 and 8.

T2 generation	Number of sensitive	Number of resistant	Non-germinating
PSI T <sub>2</sub> plant # 5	27	69	0
WSQV T <sub>2</sub> plant # 2	30	70	0
ARL T <sub>2</sub> plant # 3	23	73	0

PSI T<sub>2</sub> plant # 5      WSQV T<sub>2</sub> plant # 2      ARL T<sub>2</sub> plant # 3

**Figure A6: Third independent line T2 selection.**

100 seeds of T1 generation of each line were sown on ½ MS media containing hygromycin to find a plate with a 3:1 ratio of resistant plants. Upper table shows the lines which are segregating 3:1 after screening. The screening plates are shown (Bottom).

T3 generation	Number of sensitive	Number of resistant	Non-germinating
PSI T <sub>2</sub> plant # 5 T <sub>3</sub> plant # 3	0	50	0
WSQV T <sub>2</sub> plant # 2 T <sub>3</sub> plant # 3	0	50	0
ARL T <sub>2</sub> plant # 3 T <sub>3</sub> plant # 5	0	50	0

PSI T<sub>2</sub> plant # 5  
T<sub>3</sub> plant # 3

WSQV T<sub>2</sub> plant # 2  
T<sub>3</sub> plant # 7

ARL T<sub>2</sub> plant # 3  
T<sub>3</sub> plant # 5

**Figure A 7: Third independent line T3 generation.**

50 seeds of T<sub>2</sub> generation of each line were sown on ½ MS media containing hygromycin to find a plate with a 100% resistant plants. Upper table shows the homozygous lines (100 % resistant). The screening plates are shown (Bottom).

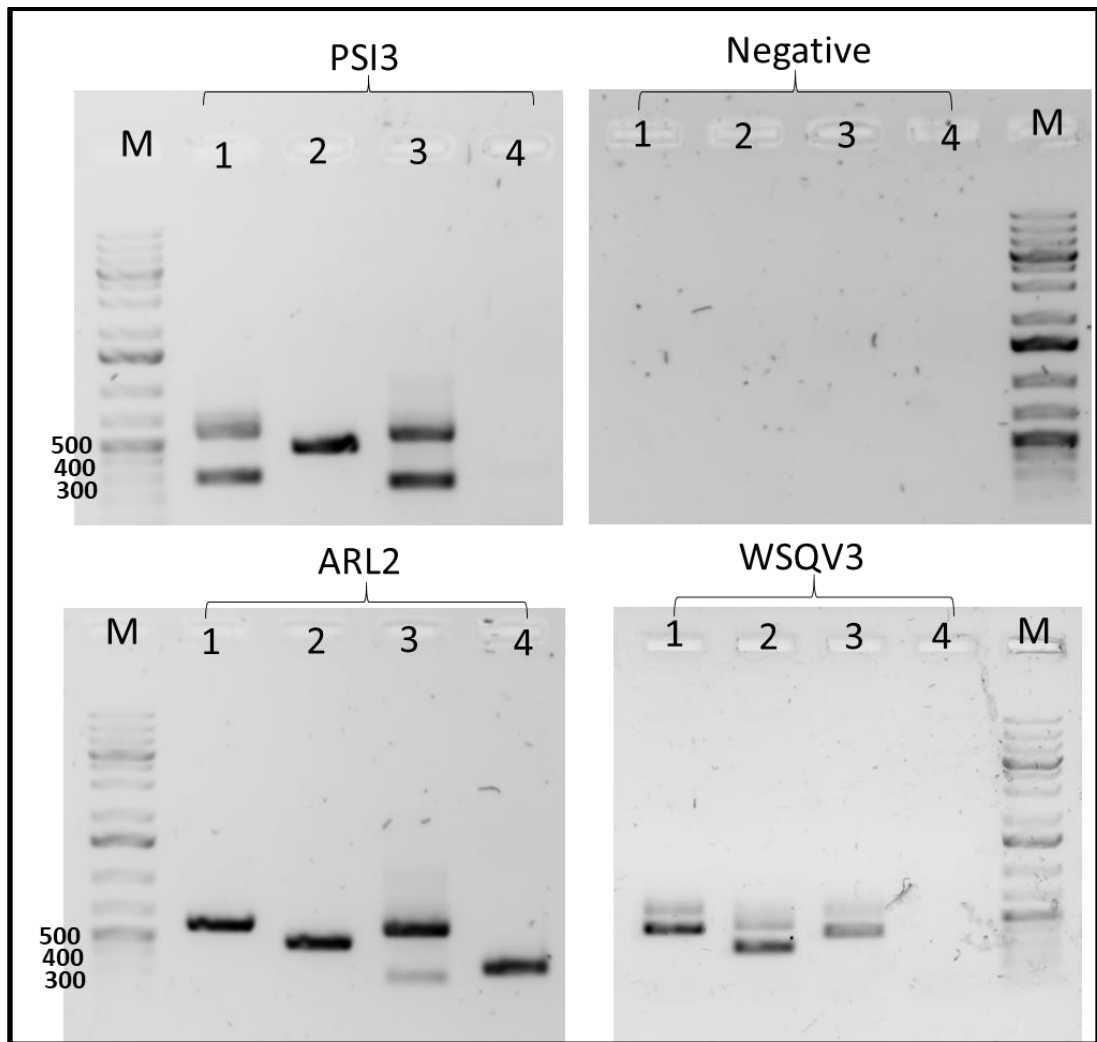


**Figure A8: Third independent line genotyping1.**

1% of agarose gel electrophoresis of PCR products of genomic DNA of PSI, WSQV and ARL plants. 1kb ladder was used in this gel (M), the numbers represent the primer pair (1-4). Negative: negative control (no DNA). Primer details and the expected bands are presented in chapter 3 (Table 3.2). All bands indicated correct size expect for ARL DNA with primer pair 1. Results repeated twice with same results. Amplification of ARL DNA using primer pair 1 was also repeated and shown in Figure A9.

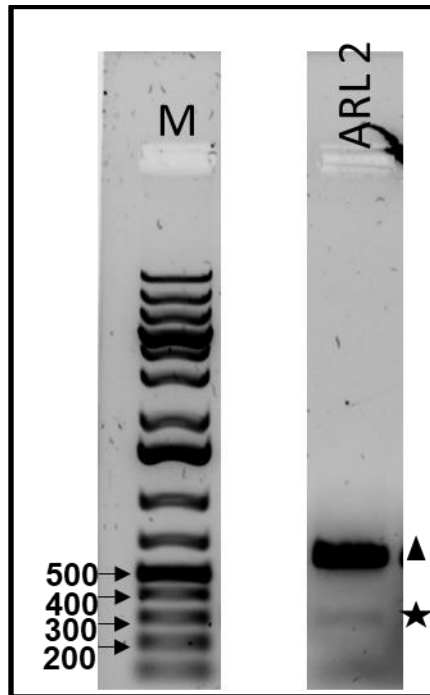


**Figure A9: ARL 2<sup>nd</sup> independent line DNA amplification using cat2-F and cat2-R primer pair.**

Two bands are produced as a result of the amplification of ARL DNA using primer pair 1 (see Chapter 3, Table 3.2). Details of the primer sequences used can be found in Chapter 2, Table 2.2. The presence of a 597bp and 293bp fragments are shown as triangle and star, respectively.

## A.2 RNA quality

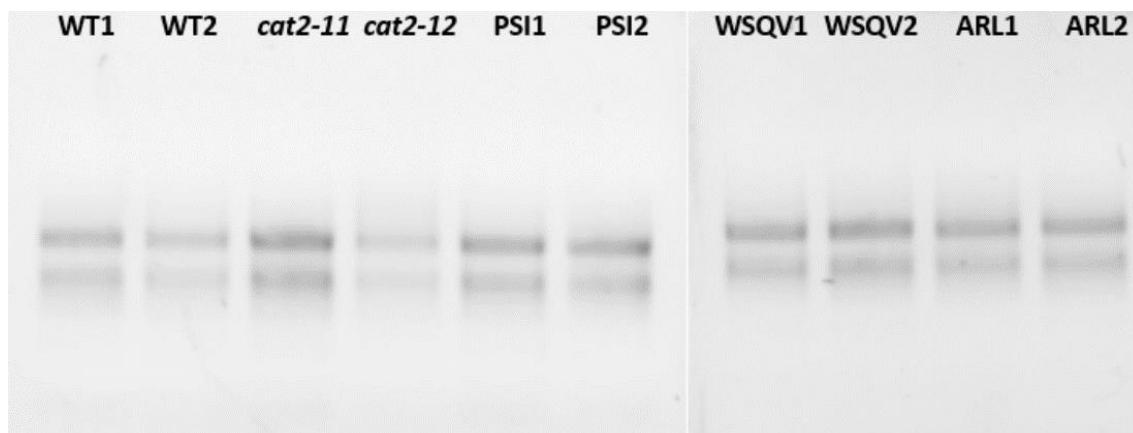


**Figure A10: RNA quality assessment using agarose gel electrophoresis.**

Example of 1% agarose gel electrophoresis for RNA quality check on samples from the qPCR analysis. Total RNA was prepared from 4-week-old leaves of wild type, *cat2-1* mutant, PSI, WSQV, ARL. RNA was extracted from two plants per each genotype. Second independent line of PSI and WSQV, as well as first independent line of ARL were used. Samples show 28S (upper) and 18S (lower) bands.

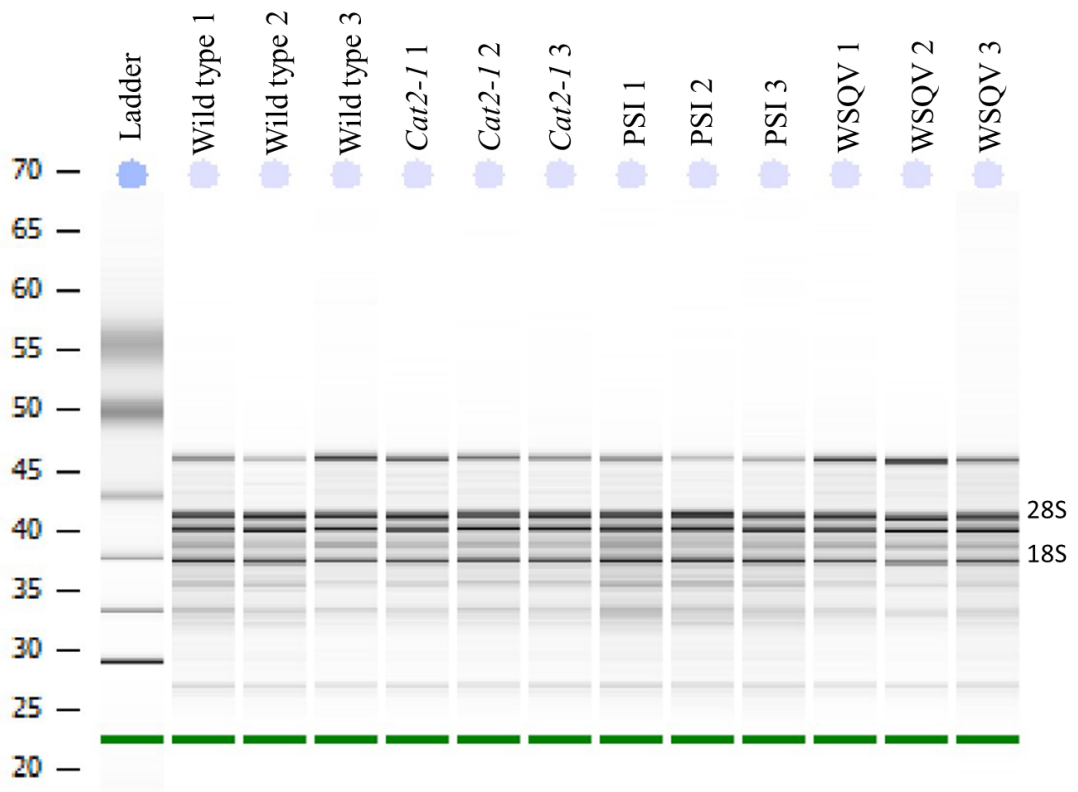
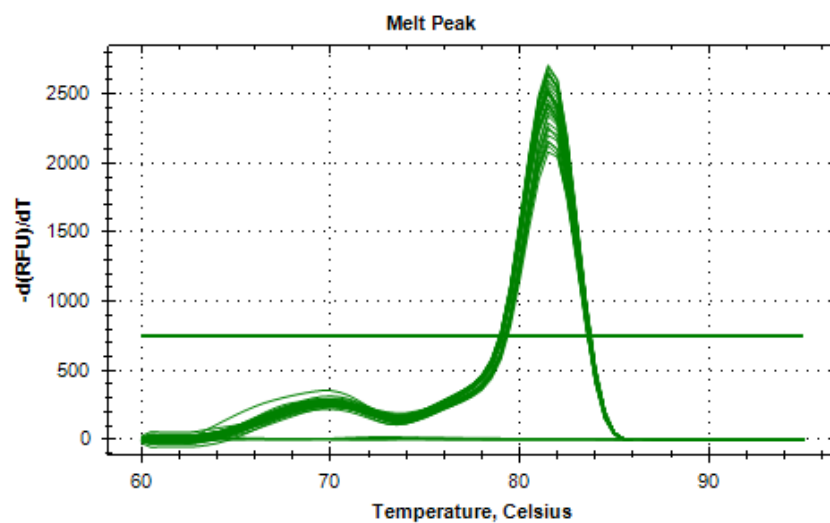


**Figure A11: Agilent bioanalyzer digital gel image of total RNA.**

The image shows a total RNA total RNA from 4 weeks leaves of wild type, *cat2-1* mutant, PSI and WSQV. Three RNA samples were prepared from each samples. The 28S and 18S ribosomal RNA bands are observed for all samples. First independent lines of PSI and WSQV were used.

### A.3 Representative image of melting curve for qRT-PCR analysis

Melting curve of *ACTIN2* control *ACTIN2* used in RT-qPCR analysis.



#### A.4 Semi-quantitative result of 1<sup>st</sup> independent line

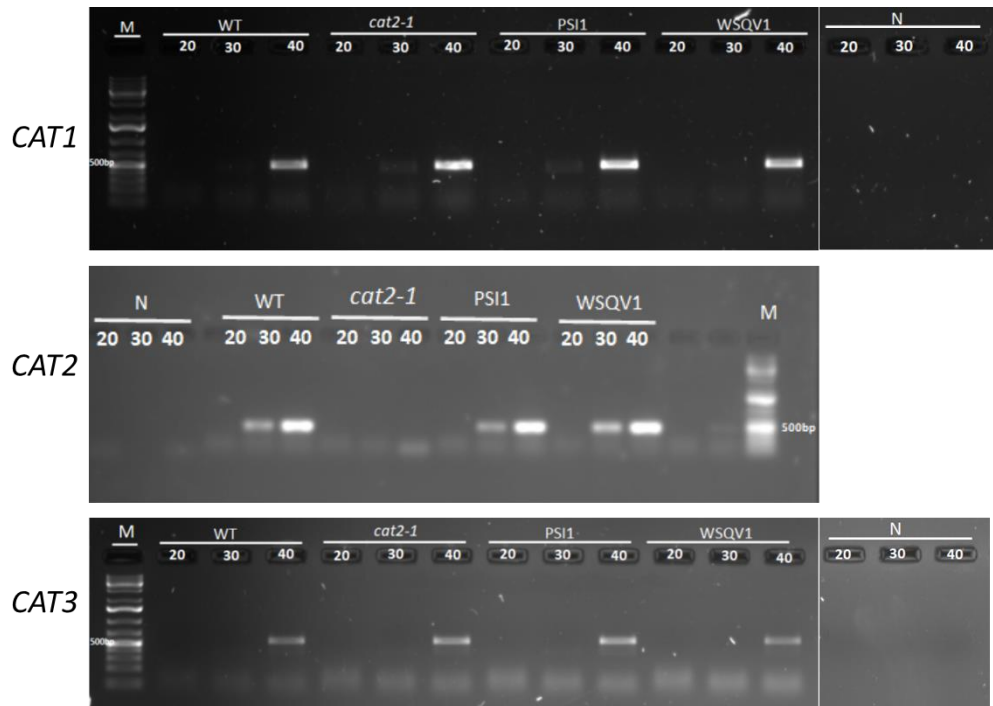


**Figure A 12: A representative image of semi-quantitative RT- PCR of *CAT1*, *CAT2* and *CAT3* expression levels.**

Total RNA was isolated from wild type, *cat2-1*, PSI1, WSQV1 and reverse transcribed to cDNA. Cat1 primer pair should be specific for *CAT1* and amplify cDNA with product size 487bp respectively. Cat2 primer pair should be specific for *CAT2* and amplify cDNA with product size 483bp respectively. Cat3 primer pair should be specific for *CAT3* and amplify cDNA with product size 532bp respectively. N; negative control.

## A.5 Expression level of catalase genes in 2<sup>nd</sup> independent line using RT-PCR

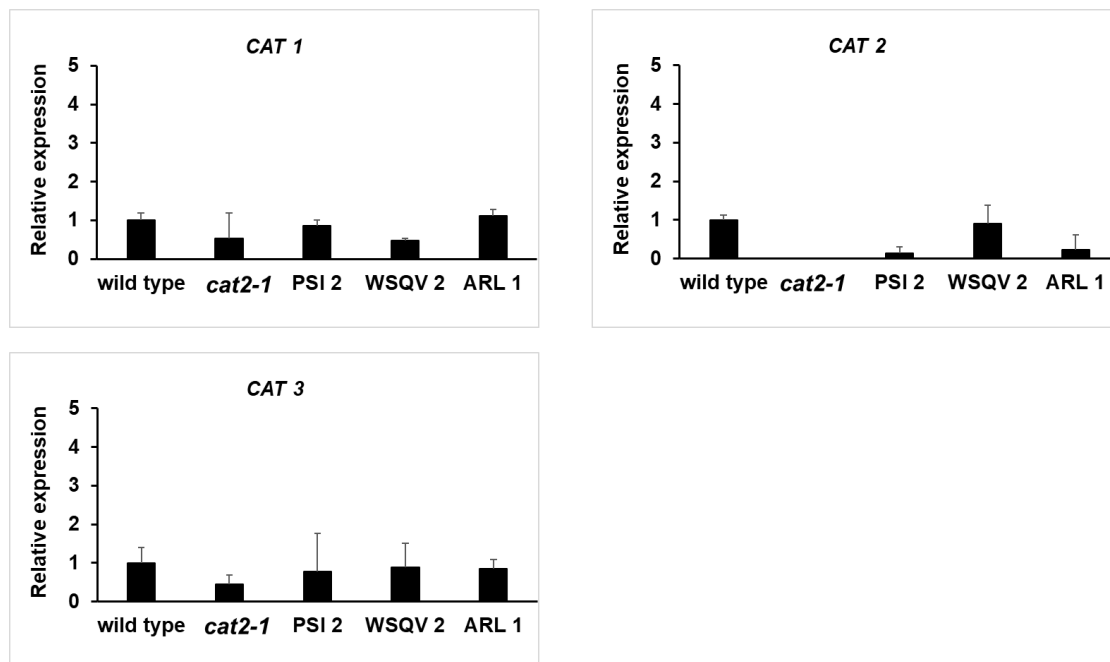


**Figure A 13: Catalase genes expression level**

RT-qPCR was performed using gene-specific primers (see chapter 2 Table 2.3) and cDNA obtained from duplicate RNA extracts of plants grown under short-day conditions for 4 weeks. Independent lines of transgenic lines are numbered; 1<sup>st</sup> independent line of ARL and 2<sup>nd</sup> independent lines of PSI and WSQV. Wild type and *cat2-1* mutant grown in parallel with the transgenic lines. The expression level was quantified by RT-qPCR and are relative to *ACTIN 2*.

## Appendix B

### B.1 Morphological characterization of transgenic lines using wild type and *cat2-1* mutant as a control.

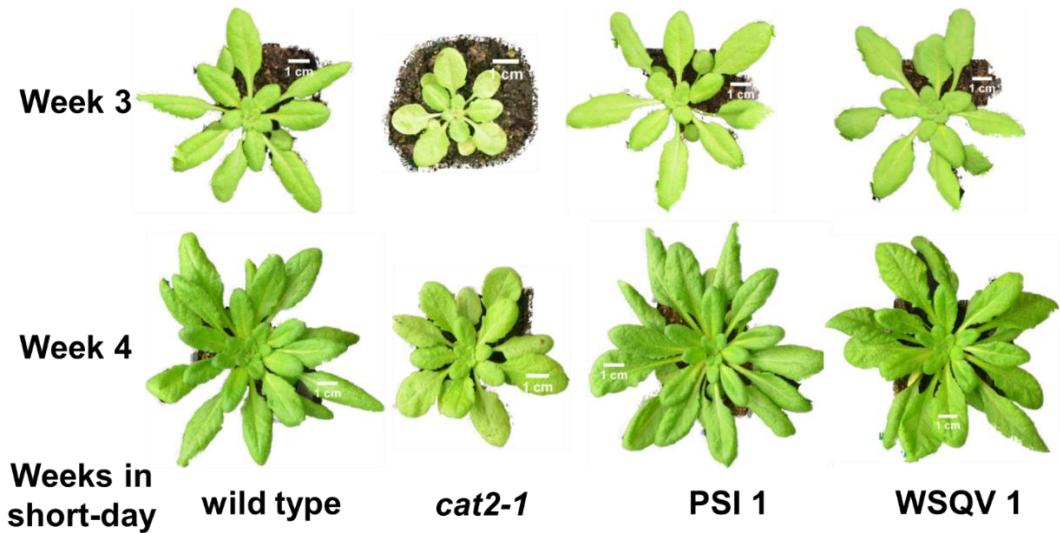


**Figure B1: Whole plant phenotypes of first independent line of transgenic plants (PSI and WSQV).**

5- and 6-week-old (31 and 38 days after sowing, respectively) plants grown under short-day conditions (8 h light/16 h dark) for 3 and 4 weeks. Wild type and *cat2-1* mutant were grown in parallel with the transgenic plants. All plants photographed at same magnification. Scale bars represent 1 cm. Images were taken for 30 plant per genotype.

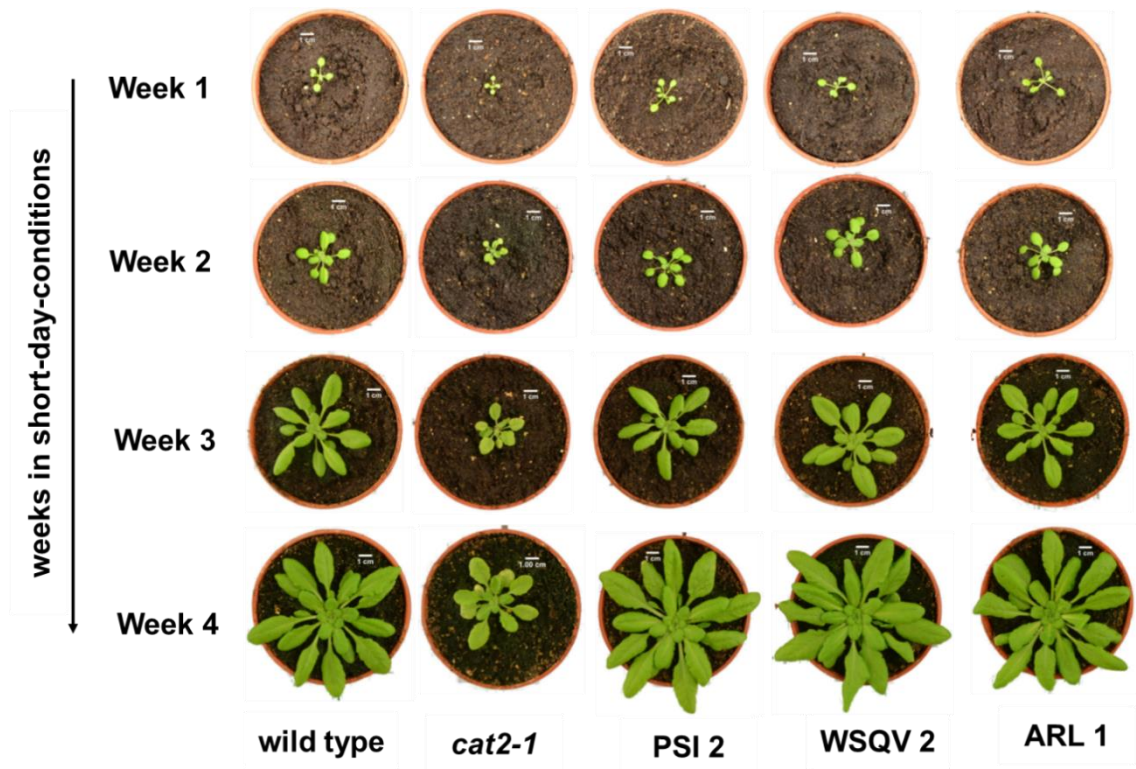


**Figure B2: Morphological characterisation of the transgenic lines.**

2-3-4- and 5 -week-old plants grown under short-day conditions for 4 weeks. Scale bars represent 1cm. All plants photographed at same magnification. PSI2; 2<sup>nd</sup> independent line of PSI, WSQV2; 2<sup>nd</sup> independent line of WSQV, ARL1; 1<sup>st</sup> independent line of ARL.

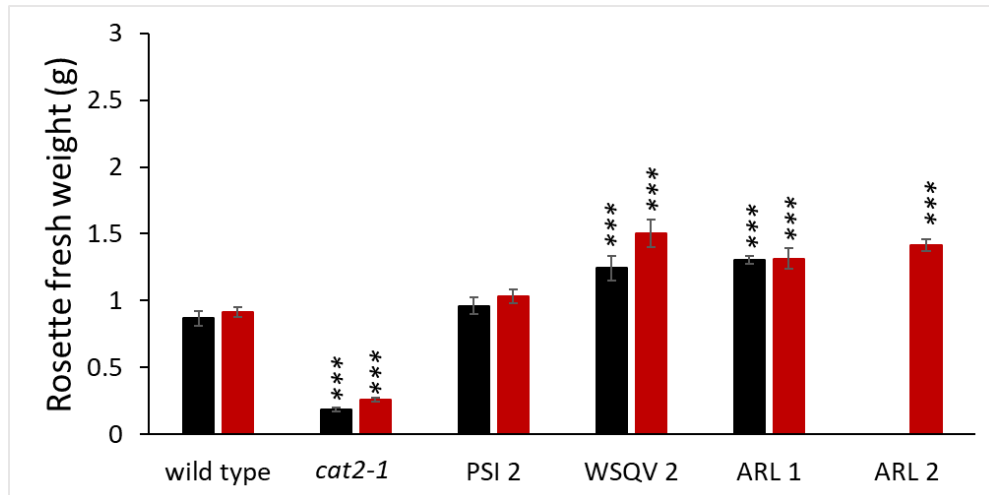
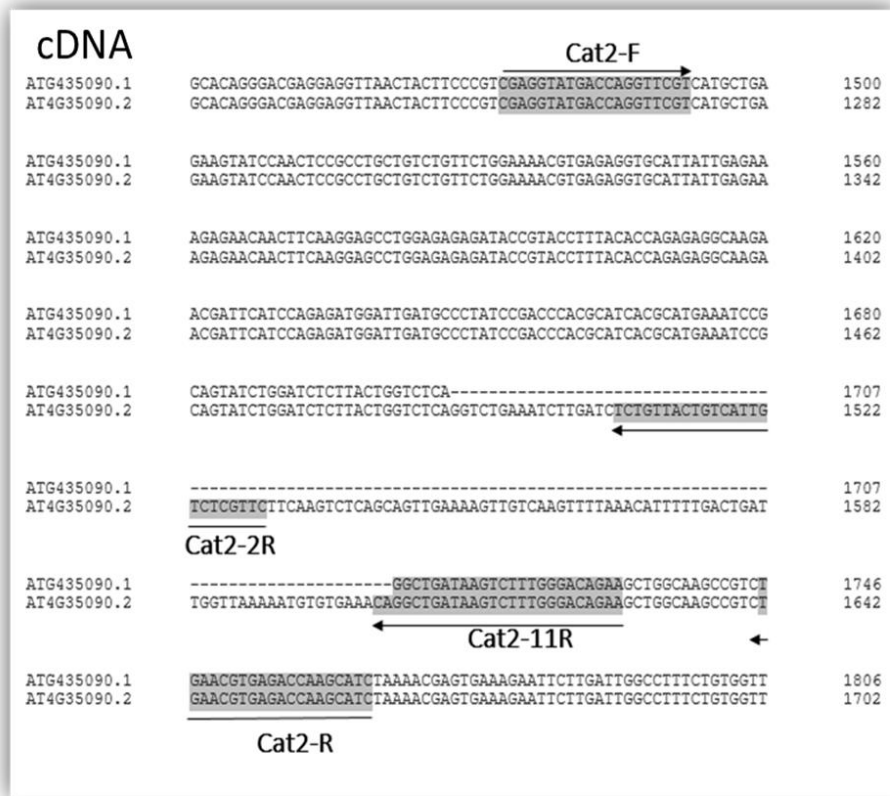


**Figure B3: Rosette fresh weight of wild type, *cat2-1* and transgenic lines grown in short-day conditions for 4 weeks.**

Rosette fresh weight was measured for different lines grown for 4 weeks under short-day conditions (8hr light). \*\*\*  $P < 0.001$  in significance given from analysis student's *t* test between (wild-type, *cat2-1* mutant) and (wild type and transgenic lines). First independent lines of ARL was grown at the same time with the 2<sup>nd</sup> independent lines of PSI and WSQV (Black). Results were also repeated (Red) as the 2<sup>nd</sup> independent line of ARL was also grown in this set of experiment (Red). Means are average of 6 plants per each genotype per experiment. Plants were repeated twice to confirm the result of rosette fresh weight presented in Chapter 3, Figure 3.13.



B



C

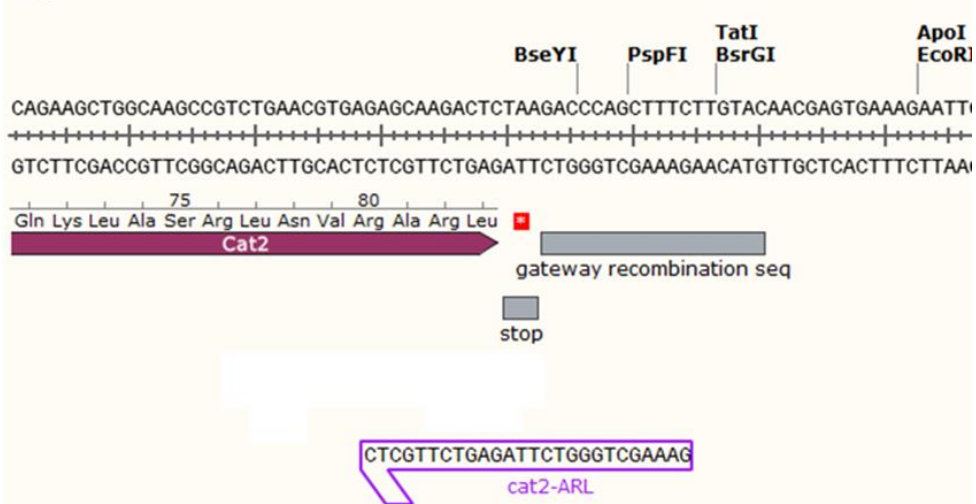


**Figure B 4: Diagram showing the primers used (highlighted), genomic DNA sequence of the *CAT2* gene and the expected product size. (A and B) Sequence alignment of the transcripts of both variants of *CAT2* gene and the binding sites of *CAT2* splice variant specific primers. (C) Shows the engineered C terminal sequence of the ARL construct and the binding site of the *cat2-ARL* specific visualised using the Snap gene program. The small grey box indicates stop codon while the large one represents the gateway recombination sequence.**

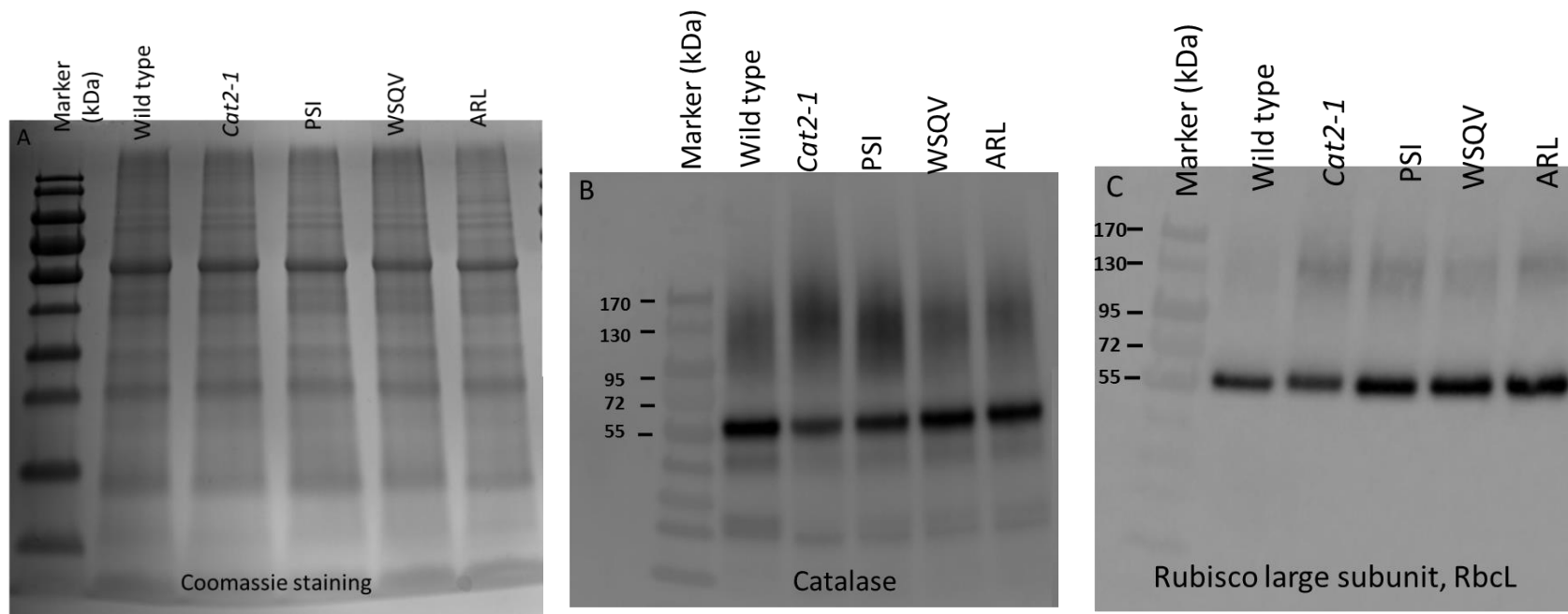


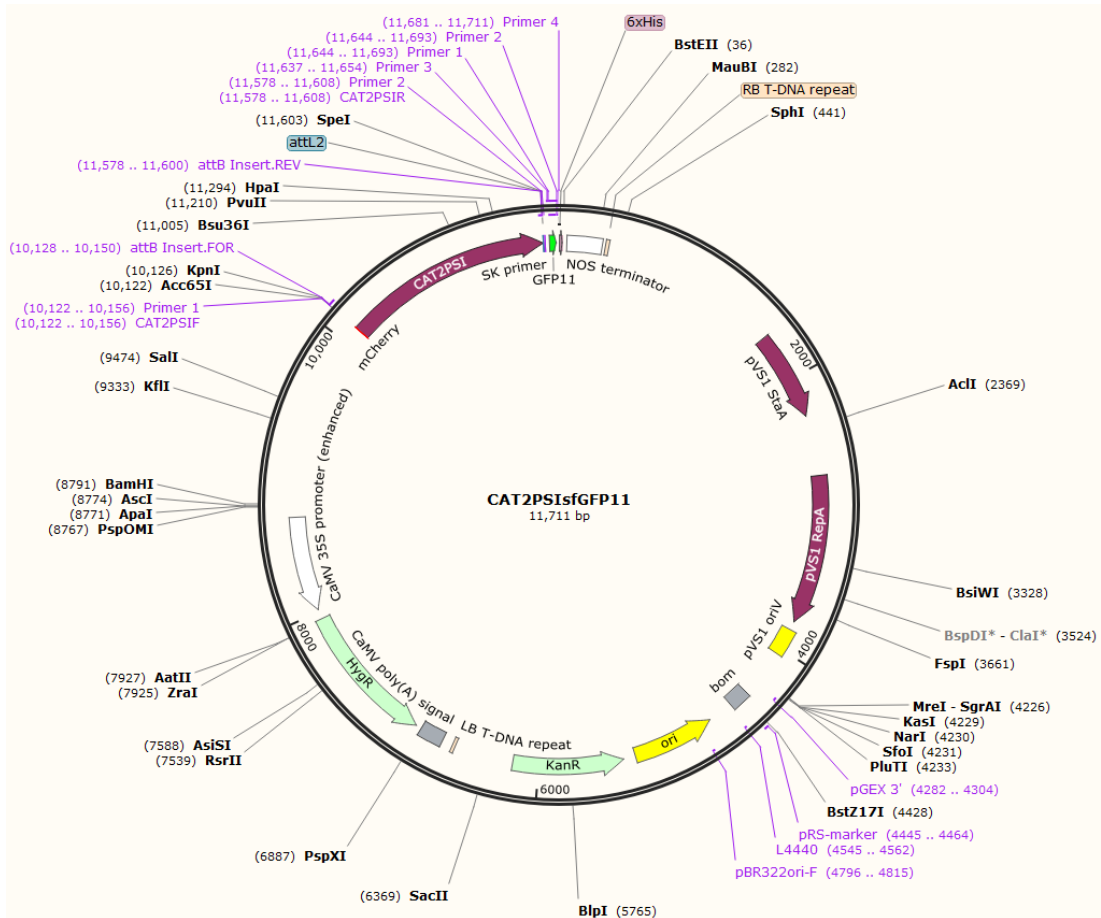
**Figure B 5: Agrisera catalase antibody (AS09501) also recognises rubisco**

Total protein (10 ug) was extracted from leaf tissues (100 mg) of 4-week-old wild type, *cat2-1* mutant, PSI, WSQV and ARL and separated on SDS-PAGE for 60 min at 100V. Three gels were prepared and used for analysis: First, one of the gels was used for Coomassie blue staining to visualise proteins and used as a loading control (A). The second and third gels were transferred on nitrocellulose membrane and used for western blot analysis. Blots were incubated overnight at four °C using 3% BSA as a blocking reagent. 3%BSA was discarded and blots were then incubated with antibodies against catalase(B) and rubisco (C). Blots were washed and then incubated with Goat-anti rabbit secondary antibody. Antibodies details were presented in Chapter 2 (Table). Blots were then washed, developed, and pictured. Molecular mass markers are indicated on the left. Note that the band observed with the anti-catalase antibody in the *cat2-1* mutant is of similar intensity to all the other lines despite the fact that CAT2 contributes ~80% of catalase activity in leaves and on native gels the CAT2 tetrameric band is absent in this mutant (Figures 4.1 and 4.3).

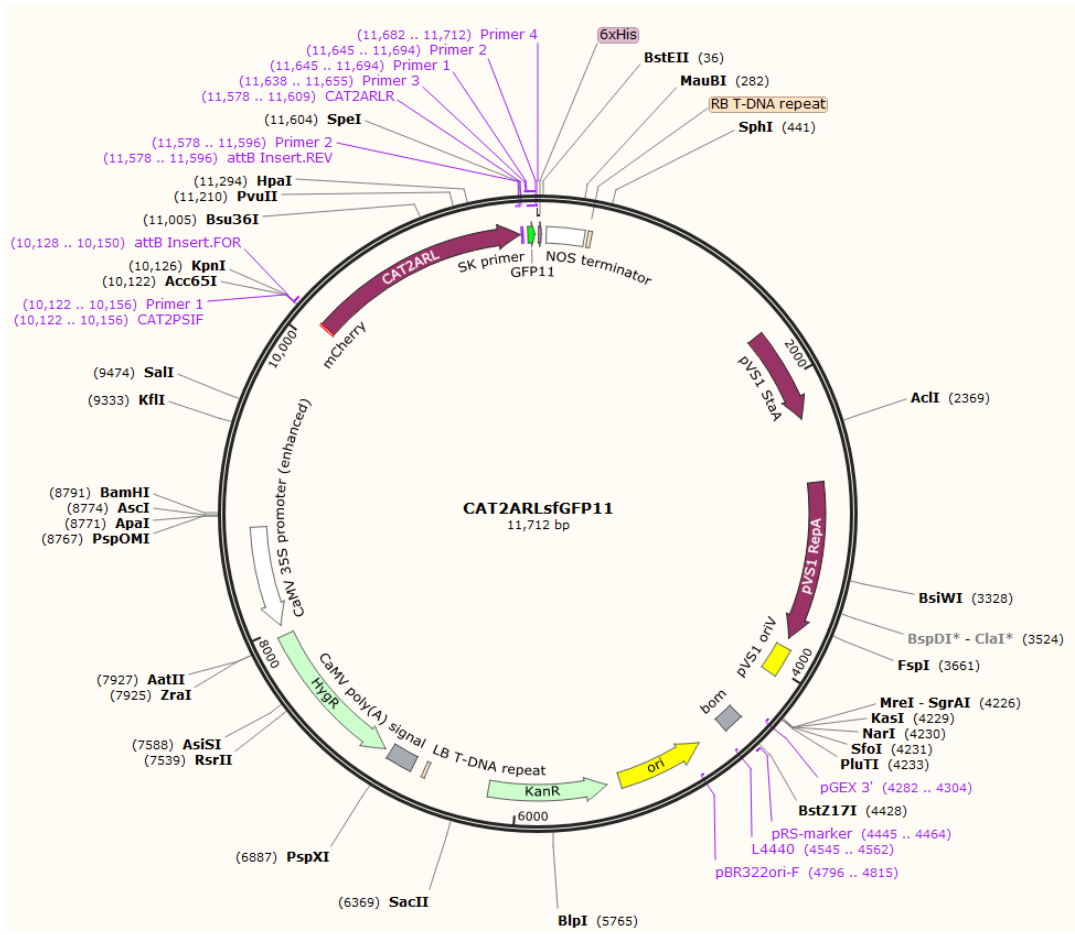
# Appendix C

## C.1 Vector maps

### C.1.1 CAT2variants-sfGFP11







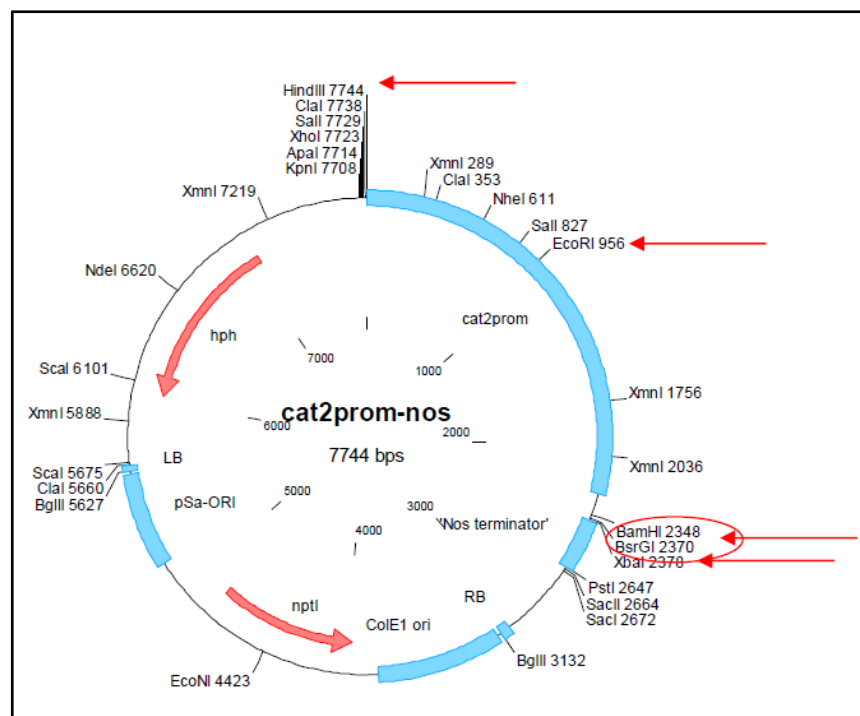
### C.1.2 Construction of CAT2 variants under the CAT2 promoter (by Dr Elena Zubko).

2.4kb genomic DNA upstream of the CAT2 gene was amplified with primers

Cat2prom-R –5' tccctctagaattgtacaAGGGTTTACCTTGTAAGGAT3'

Cat2prom-F – 5'AGATTGAATTGGATCATATA3'

The lower-case sequence in Cat2promR contains restriction sites *Bsr*GI and *Xba*I. The sequence of the potential promoter region also contains *Hind*III at the 5' end. The PCR product was cut with *Xba*I and *Hind*III and cloned into pGreen0179 +NosT to generate cat2prom-nos.



The corresponding CAT2 variants were excised from 957, 959 and 962 as *Bam*HI and *Bsr*GI fragments (ca 1.5 kb) and cloned into *Bam*HI and *Bsr*GI digested *cat2prom-nos* (glycerols 968 [cat2promCAT2PSI nos],969 [cat2pro-CATSWQSVnos],970[cat2proCAT2ARL-nos]).

Finally, the native 3'UTR was placed in front of the Nos terminator . Primers to amplify 3'UTR regions of both spliced forms:

PSI-3UTR-F – ccctactgtacaACGAGTGAAAGAATTCTTGATTGG

PSI-3UTR-R - cctagtctaga GCAGACTAAAAATCACGTCTT

WSQV-3UTR-F- ccctactgtacaCTGAAATCTTGATCTCTGTTACTG

WSQV-3UTR-R- cctagtctagaTGTCAAAACCAAGTTTATTTTC

Both sets of primers had *BsrGI* and *XbaI* sites designed in. PCR products and vectors 968,969,970 were digested with *XbaI* and *BsrGI*. Vector 968 and vector 970 were ligated with 3'UTR-PSI to give the final plasmids 971 [cat2promoter-CAT2-PSI-3'UTR-nos in pGreen0179] and 973 [cat2promoter-CAT2-ARL-3'UTR-nos in pGreen 0179]. Vector 969 was ligated with 3'UTRWSQV to give vector 972 [cat2promoter-CAT2-WSQV-3'UTR-nos in pGreen0179].

